The Dissertation Committee for Melissa Mary Donahue Certifies that this is the approved version of the following Dissertation:

Controlling Trace Impurities in a Dividing Wall Distillation Column

Committee:

Michael Baldea, Supervisor

Robert Bruce Eldridge, Co-Supervisor

Thomas F. Edgar

Gary T. Rochelle

James J. Downs

Controlling Trace Impurities in a Dividing Wall Distillation Column

by Melissa Mary Donahue

Dissertation

Presented to the Faculty of the Graduate School of

The University of Texas at Austin

in Partial Fulfillment

of the Requirements

for the Degree of

Doctor of Philosophy

The University of Texas at Austin

December 2018

Dedication

To my family

Acknowledgements

This dissertation would not be possible without the help and guidance of many people. I would first like to thank my advisor, Dr. Bruce Eldridge. Bruce has been an excellent mentor. He has a passion for teaching and truly cares about his students. Bruce's words of encouragement, unique emailing style, and dry sense of humor have made my graduate school experience enjoyable. Bruce and his wife Kathleen are incredibly kind and welcoming people who have enriched my time in grad school. I would be remiss if I did not mention Beau puppy, the happy and loveable Labrador retriever who is a central figure to the Eldridge group.

In addition, I would like to thank my co-advisor Dr. Michael Baldea for his assistance in this work. His help with and input into my manuscripts was invaluable. Thank you also for your patience and understanding and for including me in Baldea group events such as your holiday party.

I will forever be grateful to Eastman Chemical Company and Emerson Process Management for providing the funds for this research and to all of the people at those companies who have made this project possible. I am very fortunate to have had the opportunity to complete two internships while in graduate school: one at Eastman Chemical Company and the other at Emerson Process Management. My summer internships gave me invaluable industrial experience that not only shaped the direction of my project but also who I am as an engineer today. Through these collaborations, I have had the opportunity to work with many talented and wonderful people. Thank you to Mark Nixon, Terry Blevins, Dr. Willy Wojsznis, Dr. Noel Bell, and Tinh Phan at Emerson Process Management. You have all been extremely helpful in donating and troubleshooting equipment for my project. Thank you to Terry and Willy for teaching me how to operate our DeltaV™ system and for occasionally buying this poor grad student food from UT Commons. Thank you also for the opportunity to travel to and present at multiple Emerson Exchange Conferences.

At Eastman Chemical Company, I would like to thank Dr. Jim Downs, Dr. Ernie Vogel, Dr. Scott Owens, Dr. Steve Miller, Thomas Lamp, and the rest of the Advanced Controls and Technology group. Jim has played a very large role in this project, and for that, I am very thankful. I appreciate the time you have taken to answer all of my questions, to provide feedback, to serve as a committee member, and to teach me about distillation control. Thank you to Jim and Ernie for their help with my model. It was always nice to catch up with both of you at TWCCC. Scott has been the ultimate example of a former Eldridge group member giving back. I definitely owe him a beer or two for all of the assistance he has provided over the years.

Thank you also to my committee members Dr. Edgar and Dr. Rochelle for their time and feedback. I would also like to thank Mark Pilling for his willingness to always help with any of my packing and mixing questions.

Having the opportunity to work on an experimental unit the size of our column would not be possible without the Separations Research Program (SRP). I would like to thank Robert Montgomery, Steve Briggs, and Henry Bautiste for their help in installing and operating equipment. I would also like to thank Jarett Spinhirne and Neil Crane for their help with the gas chromatogram. I would also like to thank Dr. Frank Seibert for his continuous support and teaching. Though a Houston-area sports fan, Frank worked night shift on my campaign, helped me with the gas chromatogram when I feared all was lost, and taught me the importance of the Seibert rule. Thank you also to the additional staff that have helped me while at UT: Susan Tedter, Lauren Murrah, Terri Mulvey, Susan McCoy, the Steve Orwick, and Denzil Smith.

My time in the Eldridge group has been remarkable in part due to my great labmates: Dr. Bailee Roach, Jeff Weinfeld, Mikey Phan, and Luke McFarlan. I've enjoyed getting to know all of you and sharing plenty of laughs along the way. You've all inspired me to be a better engineer, and I look forward to hearing about your future accomplishments. When I first joined the then all-female Eldridge group, Bailee welcomed me and taught me about dividing wall columns and the pilot column that she helped build. I enjoyed learning beside her and am forever grateful for her help. Jeff later joined the

group and increased the number of New England sports fans. Jeff has provided many entertaining comments during his time in our group. I would also like to thank Jeff for my undisputed Intramural Championship. Mikey has been nothing but helpful from his first day when I made him move a table within five minutes of meeting him to his night shift during my pilot campaign to his assistance with HEEDS. He has also stepped up the Eldridge group food game, which is always appreciated. Luke had the daunting task of sharing an office me as a young grad student as I was preparing for graduation. I hope I didn't scare him too badly. I enjoyed sharing an office with him, especially since both of us were constantly eating. I would also like to thank Johannes Voggenreiter whose quick wit provided endless entertainment. Finally, I would also like to thank my undergraduate assistants Joseph Jakubowski and Scott Gentry.

I would like to thank the members of the Baldea and Edgar groups with whom I worked over the years: Dr. Cara Touretzky, Dr. Siyun Wang, Dr. Richard Pattison, Dr. Conan Park, Dr. Corey James, Dr. Abby Ondeck, Dr. Ankur Kumar, Dr. Ray Wang, Dr. Matt Walters, Joannah Otashu, Hari Ganesh, Lingqing, Jodie Simkoff, Calvin Tsay, Morgan Kelley, and many more. Though I did not get to see you as much because of my work at Pickle, I've enjoyed sharing my experimental work with you and our many coffee runs.

Graduate school is difficult for more reasons than just research, and I would like to thank all of the people who supported me along the way both near and far. There are too many people to list individually, and for that, I am grateful. I've made great friendships during my time in Austin through the department, intramural sports, and dodgeball. My friends and former teammates from UMass are like a second family to me. Your continuous support, sense of humor, and love mean the world to me. Special thanks goes to Wendy, Nicole, Matteen, Mike, Amy, and Dong-yeop. Most importantly, thank you to my parents and family who, even if they never quite understood my research, always lent a supportive ear and encouraged me to pursue my goals.

Abstract

Controlling Trace Impurities in a Dividing Wall Distillation Column

Melissa Mary Donahue, Ph. D.

The University of Texas at Austin, 2018

Supervisor: Michael Baldea

Co-Supervisor: Robert Bruce Eldridge

Dividing wall distillation columns (DWCs) separate a feed mixture into three pure product streams using one column shell. Though attractive due to capital and operational savings, DWCs have yet to gain widespread industrial acceptance. One notable concern is controllability. The research within this document examines a four component feed mixture to evaluate the operational flexibility of a fixed-design DWC through experimental and simulation-based studies. A pilot DWC was successfully controlled at multiple operating points, and a dynamic model was developed to reflect the pilot dividing wall column.

As a form of process intensification, DWCs have a higher risk for controller interaction making conventional PID control potentially inadequate. This work successfully used two PID temperature controllers to maintain the column at steady state, transition the column between steady states, and reject feed disturbances without controller interaction. These controller pairings were determined using conventional controller design techniques. Therefore, for this chemical system and column design, traditional approaches to distillation control are sufficient to handle the intensified nature of DWCs.

Because more components are present in DWCs in larger amounts, there is concern that temperature control will no longer imply composition control. Temperature control proved successful in this study. Controlling two temperatures maintained column operation

against feed disturbances. In addition, prefractionator temperature correlated well with reboiler duty for multiple feed qualities therefore serving as a promising control variable though more disturbances such as feed composition should be examined. The minimum energy controller was not tested experimentally. A steady state model with heat transfer matching the pilot data was scaled to the size of an industrial tower and used to generate a minimum energy response surface for different vapor and liquid split values.

In summary, this research investigated the operational flexibility of a fixed-design DWC using a four component mixture, tested the ability of conventional distillation control design techniques to determine control structures for a DWC, and created a minimum energy operating surface that could be used to examine control structures. A technique to determine the overall heat transfer coefficients was developed, and the model closely matched experimental steady state data.

Table of Contents

List of Tables

List of Figures

Chapter 1: Introduction

SUMMARY OF WORK

The research discussed in the following dissertation focuses on the control of a dividing wall distillation column, a multicomponent separation technology that incorporates process intensification and advanced process integration concepts. Through experimental work and modeling efforts, this work has shown that the control of dividing wall columns is very similar to that of traditional distillation columns. For particular feed mixtures and column designs, a simple and yet effective control strategy can be determined using standard controller design tools.

Using the pilot DWC at UT's Pickle Research Campus, this research tested a four component feed mixture to evaluate the operational flexibility of a fixed-design DWC. The fourth component served as a trace component not only mirroring industrial operations where isolating a contaminant or side reaction product is sometimes necessary but also providing the flexibility to change the operating objectives of the DWC. The trace component was moved between product streams to create different steady state operating points, and a control configuration was determined for each steady state using traditional controller design tools. As product compositions changed between operating points so did sensitive regions within the column and therefore the resulting control structure. In addition to steady state operation and transitioning the column between operating points, the control configurations were tested with a series of feed disturbances. The column successfully rejected these disturbances. Although numerous studies have successfully used model predictive control and other advanced techniques to control dividing wall columns,[1–4] this work focuses on decentralized control structures because they remain the most widely used in industry. In addition, for practical implementation, it may be preferable to only use the level of complication that is necessary as dividing wall columns themselves are quite complicated.

Finally, this research also examines the minimum energy operation of a dividing wall column. An experimentally-validated steady state model is scaled to an industrial size and used to generate a response surface showing minimum energy operation for various combinations of liquid and vapor splits. Multiple candidate control variables are examined.

MOTIVATION

Distillation Control

Before discussing the current progress and challenges of controlling dividing wall distillation columns, the control of traditional distillation columns must be reviewed. Dividing wall columns are an extension of traditional distillation columns. Therefore, understanding the fundamentals of distillation control will elucidate some of the issues and concerns facing dividing wall columns. The control of distillation columns has been extensively researched, and the following is only a summary. There are many books and papers in which more information can be found.[5–7]

With over 40,000 distillation columns operated around the world, distillation is the most commonly used separations technique for multicomponent mixtures.[8] As with any piece of process equipment, the control of distillation columns is necessary to ensure safe and optimal operation. Successful control of a distillation column is two-fold: one is to ensure column stability and the second is to ensure product purity through composition or temperature control.

Column stability is maintained through constant pressure and constant inventory levels. The controllers for these should be designed before temperature or composition controllers. Column pressure is typically controlled with the condenser duty through varying the heat transfer rate in the condenser. This could be a valve or fan on the media side of the condenser or changing the effective surface area on the process side of a flooded condenser.[6] For traditional distillation columns, inventory control denotes controlling the column level (or reboiler if kettle reboiler is used) and the reflux drum level.[5] Though in

theory these could be controlled with any available valve, the desire to reduce lag time and therefore improve process dynamics has led to the convention of controlling a level by using one of the nearest manipulated variables. This leaves the column level to be typically controlled by either the heat duty to the column or the bottoms flow and the reflux drum to be typically controlled by either the overhead reflux flow or the distillate flow. The choice in level control manipulated variable is not trivial. The variables used for level control will impact how flow disturbances are rejected and will not be available for composition or temperature control. Furthermore, most distillation columns are located in a refinery, chemical plant, or other complex processing plant and are often part of a series of distillation columns. In these settings, plantwide implications should strongly be considered as the ability of a column to dampen or reject disturbances will impact downstream operations.[5]

Composition or temperature control is used to maintain product purities. Composition control is typically achieved by maintaining the composition of the impurity. However, composition analyzers are expensive and have large residence times. For cheaper and faster control, temperatures are often used instead. In a distillation column, temperatures are reflective of composition. Therefore, maintaining the position of the temperature profile will achieve indirect composition control. A good candidate control temperature must be sensitive to the paired manipulated variable, exhibit minimum interaction with other controllers in the system, and be reflective of product compositions. Temperatures at the ends of the column must be avoided as these will often be insensitive to changes in manipulated variables. Likewise, temperatures which naturally fluctuate with stable operation must be avoided. Numerous techniques can be used to determine the best location for control temperatures. These include singular value decomposition, the slope criterion, and sensitivity criterion.[9]

In addition to the type of measurement and the location within the column, the associated manipulated variables and the number of composition or temperature controllers must be determined. Understanding the different impacts of the internal and external flows

of a distillation column is key in gaining insight into choices in manipulated variables for temperature or composition control. Changes in external flows (distillate or bottoms) have large effects on the product compositions. However, due to material balance constraints, changes in external flows purifying one end of the column while negatively impacting the purity of the other end. The result is the temperature profile shifting up or down the column. Changes in internal flows have a smaller but faster impact on the column. Because the energy balance must remain closed, changes in internal flows will purify both components. The result is a sharpening of the temperature profile.

For economic reasons, controlling both ends of the column is beneficial. Doing so ensures that both components meet their purity restrictions without excess energy consumption resulting from excess reflux or boilup. The practice of controlling purities at both ends of the column is known as dual composition or two-point temperature control. However, due to the previously mentioned effects of the manipulated variables on the energy and material balances, interaction between controllers can lead to stability and dynamic issues for dual composition control configurations. Tools such as relative gain array (RGA) analysis and frequency-dependent RGA have been successfully employed to screen pairings for interaction. In some cases, the energy savings of two-point temperature control may not be worth the dynamic concerns or the increased cost and complexity of instrumentation. A ratio between the reflux or heat input and the feed while controlling one product purity will successfully reject throughput disturbances. This configuration is particularly beneficial when the cost of energy is low.

With all of these factors to consider, it becomes clear that there is no “best” control configuration for traditional distillation columns. Different feed systems, column conditions, and equipment design pose a different set of challenges. Control engineers must rely on process knowledge, an understanding of the control system objectives, and dynamic considerations to determine the proper control configuration. Algorithms and tools have been developed to assist in this process, many of them steady state-based.

Advanced multivariate controllers such as Model Predictive Control (MPC) are often used on distillation columns. In MPC, rather than pairing one controlled variable with one manipulated variable, multiple manipulated variables are used to control multiple controlled variables.

Dividing Wall Columns

Dividing wall distillation columns are more complicated than the traditional distillation columns because of their higher degree of thermal integration and reduced size. With dividing wall columns, a multicomponent separation that is usually done using two distillation columns in sequence is performed with one shell. This saves on capital expenditure and reduces space requirements. A wall is placed in the column to physically separate product and feed streams therefore reducing remixing and increasing thermal efficiency. The wall can be placed almost anywhere in the column, favoring the product or feed side or the top or bottom of the column. In addition, the wall can be insulated or non-insulated.[10–13] Additionally, numerous studies have examined dividing wall columns with additional product streams or more than one wall.[14,15,15,16]

A dividing wall column behaves as a series of binary separations. In a DWC whose wall is in the vertical middle of the column, the focus of this dissertation, the first separation occurs in the prefractionator, or feed side of the wall, between the heaviest and lightest components. The three component feed enters the prefractionator, and a sharp separation between highest and lowest boiling components occurs. The lowest boiling component moves above the wall, and the highest boiling component moves under the wall. Historically, in optimal operation, a fraction of the middle boiling component moves both above and below the wall. In the rectifying section and the upper portion of the mainfractionator, or side product side of the wall, the lowest and middle boiling components are separated. Finally, in the lower portion of the mainfractionator and the stripping section, the heaviest and middle boiling components are separated.[17]

Control of Dividing Wall Columns

Because of their intensified nature, there are numerous concerns regarding the controllability of dividing wall columns. Compared to two distillation columns operating in sequence, dividing wall columns have less degrees of freedom meaning fewer choices in manipulated variables. Additionally, due to their smaller size, dividing wall columns have a higher potential for controller interaction and nonlinear behavior. As previously discussed, controller interaction is a concern for binary distillation columns having two temperature controllers. A dividing wall column has three products meaning that there is the potential for three temperature controllers. If two temperature controllers can cause stability and dynamic concerns, then three temperature controllers will most certainly do the same. This work successfully uses two temperature controllers to maintain three product compositions. Many studies have avoided the issue of controller interaction by overdesigning their columns. However, this is not an optimal solution because this increases capital costs. Though distillation is a nonlinear process, many design tools based on linear systems have been developed to determine control pairings. The limitations of these tools in their applicability to DWCs is a major focus of this dissertation. If PID control proves ineffective in controlling for the degree of interaction and nonlinear behavior present in dividing wall columns, more advanced control may be necessary. Finally, temperature control may not be sufficient for dividing wall columns. Temperature control works on a traditional distillation column because temperatures are reflective of composition. However, there are more components present in larger amounts in dividing wall columns. Therefore, a single temperature may not reflect a single composition. If this is the case, temperature difference control or composition control may be necessary.

Currently, there is a lack of available dividing wall column dynamic models in the open literature. Furthermore, since very few of these available models are verified with experimental data, the assumptions or degree of model complexity best suited to represent dividing wall columns are unclear. Accurate models must be developed before the process

industry will widely adopt DWCs as dynamic models are used to test candidate control strategies and to determine optimal locations for temperature or composition control.

Dividing Wall Columns and Minimum Energy

Dividing wall columns have been reported to reduce energy consumption by 30-50% when compared to traditional distillation trains. This level of energy savings is a huge driving force for the adoption of DWCs. However, with the steady state multiplicity of DWCs, energy savings is not guaranteed. The optimal reboiler duty changes with operation and disturbances and can be difficult to predict and measure. Therefore, controls play a key role in realizing the energy savings promised by DWCs. A variety of control schemes have been proposed to maintain optimal operation. However, most of this work has been done on simplified models that do not include wall heat transfer.

SUMMARY

In summary, this research investigated the operational flexibility of a fixed-design DWC using a four component mixture, validated a model using pilot plant data, tested the ability of conventional distillation control design techniques to determine control structures for a DWC, and created a minimum energy operating surface. Together, this shows that, for this chemical system, a dividing wall column is controllable and conventional controller design tools do not break down due to the intensified nature of the process. By studying a chemical mixture for which experimental studies have not been reported in the open literature, this work adds to the otherwise limited number of experimental dividing wall column studies. In addition, this work explores the management of trace components within a dividing wall column, something that has not been reported in the open literature before.

Chapter 2: Literature Review[1]

INTRODUCTION

Distillation is the most commonly used technique for the separation of multicomponent mixtures in the chemical manufacturing industries. In 2010, there were over 40,000 distillation columns reported in operation around the world.[8] Distillation is, however, an energy intensive process, representing more than 40 percent of the total energy consumption in the refining and chemical manufacturing industries.[18] Possible solutions to these large energy demands include the use of thermally-coupled distillation columns and dividing wall columns, multicomponent separation technologies with lower capital and operating costs than conventional multicomponent distillation sequences.

Traditionally, ternary separations are performed in a train of two distillation columns, using either the direct sequence (where the most volatile component is separated first) or the indirect sequence (where the least volatile component is separated first). While effective, using a train of distillation columns incurs the cost and space of multiple column shells, reboilers, and condensers. Moreover, it is thermodynamically inefficient: remixing effects caused by thermal inefficiencies in conventional multicomponent distillation sequences increase energy demands and therefore operating cost.[18]

Thermally-integrated distillation columns offer lower energy requirements and less capital expenditure than traditional distillation trains. The Dutch inventor Antoine Johan Brugma first introduced the idea of a prefractionator column in 1936, receiving a Dutch patent in 1936 and a US patent in 1942.[19] Brugma's process included multiple designs, but each design included multiple column shells in series each with their own reboiler and condenser. The first column split the lightest and heaviest components leaving the closer boiling components to be separated in downstream columns. Brugma's design will be

1 Work originally published in Donahue, M. M.; Roach, B. J.; Downs, J. J.; Blevins, T.; Baldea, M.; Eldridge, R. B. Dividing Wall Column Control: Common Practices and Key Findings. Chemical Engineering and Processing: Process Intensification 2016, 107, 106–115. Melissa Mary Donahue wrote the literature review paper and did the necessary background research.

further referred to as the prefractionator arrangement in this work. Petlyuk and coworkers further expanded upon this concept to create a thermally-coupled unit in which the prefractionator has no reboiler or condenser.[20–22] In 1949, Wright introduced the dividing wall column (DWC) as an alternative distillation scheme that allowed one column shell to produce three pure product streams while only requiring one reboiler and one condenser.[23] Though pre-dating Petyluk's column, a DWC is a fully coupled realization of the Petyluk column. Petlyuk's design is often referred to as either the Petlyuk column or the thermally-coupled column. This work will use "thermally-coupled" to refer to Petyluk's design where the prefractionator and mainfractionator are separate shells and "dividing wall column" when the mainfractionator and prefractionator are integrated into one shell. Wright's design consisted of a conventional trayed column shell that contained a vertical wall partitioning the feed and side product streams. In a DWC, the feed enters on the prefractionator, or prefrac, side of the wall, and the side product is removed on the mainfractionator, or mainfrac, (i.e., the opposite) side of the wall. Similar to conventional distillation, the light and heavy components are removed as distillate and bottoms products, respectively (Figure 2-1). Unlike conventional distillation, the rectifying section liquid is collected at the top of the wall and split as reflux between the prefractionator and mainfractionator sides of the wall. Optimizing the reflux flow rate/liquid split fraction is key to obtaining significant energy savings in DWC operations.[24–26]

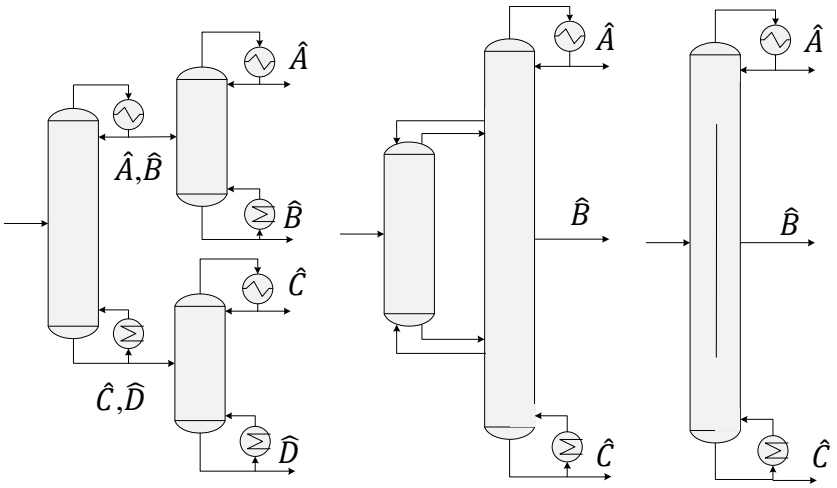

Figure 2-1 – Brugma's prefractionator design (left), thermally-coupled column (center), and dividing wall column (right)

The energy and capital savings (the latter derived from reducing the equipment number and corresponding material and labor costs) promised by using a dividing wall column render it an attractive separation technology for the chemical and refining industries. Several industrial implementations have been reported in the open literature. For example, BASF of Germany operates more than 100 DWCs around the world and is building as many as 10 per year.[26,27] ExxonMobil has also demonstrated successful implementation of DWCs. The company's Fawley Refinery near Southampton, England retrofitted a trayed xylenes column and achieved more than 50 percent energy savings.[28] ExxonMobil operates a second xylenes recovery DWC at their Port Jerome refinery and a benzene-toluene-xylene DWC in Rotterdam.[27] The applicability of DWCs extends to azeotropic[29], extractive [29,30], and reactive distillation.[31–34] Germany's Uhde GmbH has commercialized an extractive DWC process which was reported to save approximately 20 percent in both capital and energy costs.[27] The DWC ideas and principles were further expanded to include four-product separations; this setup, known as the Kaibel column, has two product sidestreams.[14,15,35–37]

Despite these successes, DWCs still represent a minor proportion of distillation trains currently in operation in the chemical and petrochemical industries and have yet to gain wide industry acceptance. Controllability concerns, originating in their intensified nature, represent a significant hurdle in the widespread implementation of DWCs. Intensified processes, such as dividing wall columns, are considered more difficult to control than their conventional counterparts due to: i) the loss of degrees of freedom due to carrying out multiple conventional unit operations in a single physical device, ii) the nonlinear behavior caused by interactions between these operations/phenomena, and iii) faster time constants due to the smaller physical size.[38] DWC control entails stable operation, upholding product specifications in the face of disturbances, and maintaining energy efficiency using the available manipulated variables. Successful control has been demonstrated in the open literature using several control configurations, varying from multi-loop linear control to advanced control strategies, confirming that that DWCs are indeed controllable in practical settings.

However, individual DWC studies are often difficult to compare due to differences in modeling approaches, feedstock selection, disturbances tested, and product specifications. To ensure a meaningful analysis, this literature review is organized by process objectives. Control structures are presented in a way that highlights connections between process objectives and control strategy selection.

- Minimize energy consumption: Minimum energy operation while maintaining product specifications is arguably the most significant process objective of a DWC. This review begins with a discussion on minimum energy operation and the control structures proposed to ensure operation within this regime.
- Achieve separation performance: Control strategies are organized by feed stock as a means to include any inherent design considerations that could potentially impact control decisions.

Control strategies are summarized, and reported performance is discussed. A particular emphasis is given to experimental studies. Beyond design decisions incorporated in feedstock selection, little focus within this review is given to the design of DWCs. Although DWCs are the main focus, work regarding thermally-coupled columns is included in this review. Thermally-coupled and dividing wall columns are often seen as thermodynamically equivalent. However, in a DWC, the prefractionator and mainfractionator are physically in the same shell, inviting the potential for wall effects and for heat to be transferred across the dividing wall.[10,34,39–43] Numerous studies have shown that the impact of this wall transfer decreases as the column diameter grows.[40,44] Therefore, for larger column diameters, thermally-coupled and dividing wall columns can be viewed as one and the same.

OVERVIEW OF DWC DEGREES OF FREEDOM

Dividing wall columns have a unique set of degrees of freedom that can be used to meet their control objectives of stability, product composition specifications, and energy minimization.

Figure 2-2 provides a schematic of a standard dividing wall column with labeled process flows. As in the case of a traditional distillation column with a side stream, DWC degrees of freedom include reflux (L), distillate (D), side stream (S), bottoms (B), vapor boilup (V) or reboiler duty (Q_R), and condenser duty (Q_C). The condenser duty is typically used to maintain column pressure, and the five remaining degrees of freedom are used to control product compositions and holdups in the reflux drum and reboiler. The reflux and distillate can be combined as a reflux ratio (r=L/D). For consistency, in this work compositions are denoted by two sets of letters separated by a comma. The first specifies the stream (D, S, or B), and the second specifies the component ($\hat{A}$,$\hat{B}$, or $\hat{C}$ for light, middle, and heavy components, respectively).

The dividing wall of DWCs creates an additional degree of freedom that can be used for control. This additional degree of freedom is associated with the liquid split at the

top of the wall (β_L). In published reports, the liquid split is controlled by either i.) a specially designed tray to operate at a fixed liquid split, ii) collecting the entire amount of liquid from the upper part of the column using a special tray ("trapout tray") or ii) via an electromagnetic funnel. The total trapout tray collects all of the liquid from the rectifying section of the column and physically removes it from the column. This liquid may then be placed in an external tank whose level is minimized to the extent that control can be managed. The liquid is returned to the column via dedicated lines and control valves according to the desired liquid split. An electromagnetic funnel collects the liquid at the top of the wall just like a total trapout tray. However, the funnel is controlled by two electromagnets whose cycling time determines the flow of liquid to the two sides of the dividing wall, thereby leading to a periodic disturbance in the column operations.

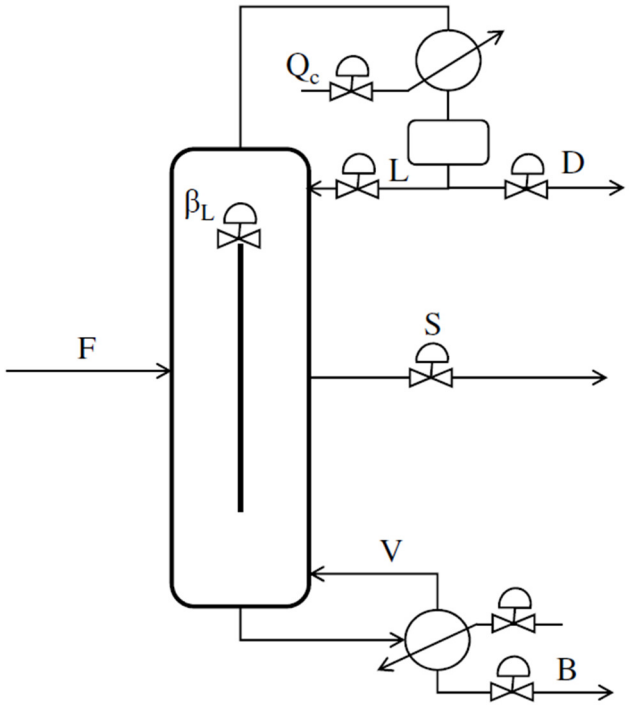

Figure 2-2 – Diagram of DWC with degrees of freedom labeled

At the bottom of the wall, the vapor is split to both sides of the wall according to the vapor split ratio (β_V). However, the vapor split is not a degree of freedom because it cannot be easily controlled. Though some success has been shown on a pilot scale Kaibel column[45], controlling the vapor split in an industrial-sized column may be impractical or not cost effective. Instead, β_V is determined by the wall placement or the condition of equal pressure drop on both sides of the wall.[26,40,46] Although this review will discuss DWCs with the wall placed in the horizontal and vertical center of the column, such as in Figure 2-2, it should be noted that DWCs may have off-center wall placement, i.e. the wall may be placed closer to the feed or side product side or closer to the rectifying or stripping section (upper or lower dividing wall). Although upper and lower dividing wall configurations require lower investment costs when compared to conventional distillation trains, Kaibel highlights that there are no energy savings due to the entropy of mixing on the feed plate.[47]

MINIMUM ENERGY OPERATION AND CONTROL

The reboiler with its associated heat duty is the largest heat sink for both dividing wall and traditional distillation columns. Unlike direct and indirect distillation trains, thermally-coupled and DWCs generally only use one reboiler, though there is a possibility of side reboilers. When compared to reboiler energy requirements to complete the same separation using traditional distillation trains, thermally-coupled columns and DWCs have been reported to require less energy, regardless of the choice in chemical system.[39,48,49] However, the reported optimal feed conditions and associated energy savings vary. Reported energy savings are in the range of thirty to fifty percent.[18,24,25,49] For some chemical systems, thermally-coupled and dividing wall columns are best when the intermediate component feed fraction is small.[24,50] While for other chemical systems, dividing wall and thermally-coupled columns provide significant savings when there is a moderate to high intermediate feed fractions.[18,24,51] Nevertheless, due to process nonlinearity, minimum energy operation of dividing wall columns is not always ensured. Controls play a key role in realizing the energy savings promised by DWCs.

Given that the reboiler is the dominant energy sink, the energy use optimization of DWCs is generally simplified to consider only the minimum boilup rate, V_{min}, or the boilup to feed ratio, V/F, the latter accounting for throughput. The optimal V_{min} cannot be guaranteed in open-loop operation; amongst others,

- operation is infeasible at low boilup rates, i.e. for $< V_{min}$
- the optimal value of V_{min} changes with operation, and an appropriate model and measurement of disturbances would be needed to regularly recalculate V_{min}
- actual measurement of V is generally difficult and inaccurate[17]

Therefore, closed-loop control is needed to remain close to minimum energy operation. The liquid split at the top of the wall is often considered the available control parameter that influences energy consumption. The vapor split at the bottom of the wall also impacts the internal traffic of the column and therefore the column energy consumption. However, as noted by many authors, controlling the vapor split in actual operation is difficult and impractical.[17,39,52]

Before discussing closed-loop control configurations that minimize energy usage, it is important to characterize optimal operation as this process knowledge will inform control objectives.

Process nonlinearities: steady state multiplicity and infeasible operating regions

The key impact of the liquid split on energy efficiency of DWCs has prompted further analysis of its relationship to other operating parameters, in particular vapor boilup. Chavez et al. found multiple steady states for a thermally-coupled column through numerical simulation.[53] These steady states featured the same feed composition, product specifications, and reflux flow but different internal flows due to different liquid and vapor split values. It was found that the system exhibits a single steady state once the reflux ratio reaches a minimum value and that the simulation did not converge below this threshold. Wolff and Skogestad[54] confirmed these findings, showing that multiple boilup values can produce the same products for the same liquid split. Additional infeasible operating points

were identified in the case of increasing the side product purity via a dedicated control loop specifying the ratio of side product impurities.

Further exploring the effect of the liquid split on the optimum boilup, Halvorsen and Skogestad provided a graphical analysis, representing the steady-state optimal boilup surface as a function of liquid and vapor splits for various feed conditions.[17] The results show that the surface is quite narrow and strongly depends on disturbances and design parameters. For example, the surface is shaped like the hull of a ship for a partly vaporized feed and forms a near-vertical wall near the optimum operating regime for saturated liquid feeds. For cases with a saturated liquid feed, even slight changes in the internal splits could lead to nonconvergent solutions. Multiple steady-state solutions were identified for subcooled feeds.

Together, these studies show that energy efficient operation of a DWC is only possible for specific design and process conditions due to the nonlinearity of a dividing wall column. Process nonlinearity leads to multiple steady-states that differ in the liquid or vapor splits and therefore energy usage. Although this new steady state will provide sufficient separation to meet product specifications, an increased energy requirement may classify it as a sub-optimal column operating point. The effect of vapor split in influencing multiple steady-states stresses the importance of wall placement in the design phase. The effect of the liquid split in transitioning to new steady states directly affects operation and control choices for a DWC. For a DWC with limited purpose, designed to operate at a single steady state, or with a large amount of heat integration, process nonlinearity may not need to be accounted for in control and dynamic modeling, provided a lower energy steady state is selected. However, process nonlinearity suggests the need for nonlinear optimization and control for DWCs operated in a transient fashion and/or employed for separating several different feed systems.

Steady state optimal operating point

Before discussing closed-loop control configurations that minimize energy usage, it is important to characterize optimal operation as this process knowledge will inform control objectives.

Numerous authors have examined methods for determining the minimum energy usage of thermally-coupled columns, the thermodynamic equivalent to a DWC.[24,55–59] The Underwood equations[24,51,55,57–59] or a similar approach[56] can be used to determine the analytical expressions for a column's required minimum energy in relation to the recovery of intermediate component. Here, recovery is defined as the fraction of middle boiling component at the top of the first column of the thermally-coupled system in relation to the middle boiling component feed flow. Most studies using the Underwood equations have been done using an infinite stage thermally-coupled column with a saturated liquid, three component feed and a sharp split[24,55,58] However, work has been done to include any number of middle components[59] and various column arrangements.[57] Fidkowski and Krolikowski[58] found that there was a region of middle boiling component recovery where the minimum energy usage was constant.

Recognizing that a component recovery is difficult to measure and control in operation, Christiansen and Skogestad[52] examined the minimum energy requirement in relation to the mole fraction or distillate flow leaving the prefractionator. Through explicit expressions and numerical solutions, the authors found that the region of relatively constant minimum energy previously discovered by Fidkowski and Krolikowski[58] corresponded to the fractional recovery of the middle boiling component between the "preferred split" in the prefractionator and a "balanced main column" (rectifying, stripping and mainfractionator section of DWC or the second column in the thermally-coupled sequence). The "preferred split" is the minimum energy operation that is "naturally preferred" in a ternary column with two product streams, which in this case is the prefractionator. Characteristics of the preferred separation include a top product with no heavy boiling component, a bottoms product with no light boiling component, and the

intermediate component pinched at the feed.[52,60] When examining just the prefractionator column, there is a sharp minimum at the distillate flow or middle boiling component recovery corresponding to the preferred separation.[52] The job of the main column, or the parts of the DWC excluding the prefractionator, is to perform two separations: separating $\hat{A}$ from $\hat{B}$ (rectifying and upper mainfractionator section) and $\hat{B}$ from $\hat{C}$ (lower mainfractionator and stripping section). The required energy usage in this column is the maximum energy demand for the two separations.[25,52,55,60] A balanced column is when these energy demands are equal and corresponds to the overall minimum energy of the main column.[25,52] Ehlers et al.[39] used the same variable; however, the authors renamed it the component split. The authors used an equilibrium model with and without heat transfer across the wall to study an ideal system with a saturated liquid feed. Rather than finding a flat minimum where the energy could be minimized for a range of component split values, the authors found a sharp minimum at 0.5 meaning that energy in the DWC could be minimized when the middle boiling component was split equally above and below the wall. The authors also found that including heat transfer across the dividing wall will not change the overall minimum energy demand by more or less than the heat flow through the wall.

Christiansen and Skogestad[52] found that the region of constant Vmin was "relatively flat" for the prefractionator arrangement with the preferred separation having slightly more optimum energy usage while this region was completely flat for finite stage thermally-coupled columns both for sharp and non-sharp (lower side product purity) splits. This was shown for multiple feed systems and feed compositions though each feed system still had a relatively large amount of intermediate component.

Halvorsen and Skogestad[17] further expanded this work by creating a solution surface of a finite and an infinitely staged thermally-coupled column by plotting the energy demand as function of vapor and liquid ratios. The results of earlier researchers regarding the optimal composition profiles and the flat region between the preferred split for the prefractionator and the balanced split for the main column still held true. However, for the chemical system studied, the optimum of the solution surface could at times be very

narrow. Small changes or uncertainty in the liquid or vapor ratios could lead to 10 to 30 percent increases in energy usage. Consistent with earlier work[52], changing the feed liquid fraction favorably extended the "flat" minimum energy region. Though adding more heat in the feed may not be as efficient, the ability to extend the solution surface by changing the feed quality negates the necessity to manipulate both the vapor and liquid splits to maintain minimum energy operation.

In summary, dividing wall and thermally-coupled columns are at minimum energy operation when the recovery of the middle boiling component is between the preferred split for the prefractionator and the balanced main column. Minimum energy operation is often characterized by minimum amount of heavy boiling component leaving the top of the prefractionator, minimum amount of light boiling component leaving the bottom of the prefractionator, and a middle boiling component pinch zone at the feed. The flatness of this minimum energy region and therefore the ability of the column to maintain minimum energy operation in the face of disturbances and uncertainty depends upon the chemical system separated, the feed quality, the vapor split, and the liquid split.

Controlling for minimum energy

Measuring the component split is not a trivial task. However, its value can be inferred from composition or temperature measurements, e.g., from a prefrac temperature measurement. Noting that at least 1-point control was needed to maintain optimum operation and that the vapor split is difficult to change during operation, Christiansen and Skogestad[52] suggested controlling one end of the prefractionator with the liquid split and overpurifying the other end. Which end to control and which end to overpurify depended upon which intermediate component fractional recovery was greater and in turn which separation in the main column required more energy. When the $\hat{B}$,$\hat{C}$ separation is more difficult in the main column (termed "lower feed controls"), the authors recommend maintaining a composition at the top of the prefractionator and overpurifying the bottom of the prefractionator by minimizing the $\hat{A}$ component leaving the bottom of the

prefractionator. When the $\hat{A}$,$\hat{B}$ separation is more difficult in the main column (termed "upper feed controls"), the authors recommend maintaining a composition at the bottom of the prefractionator and overpurifying the top by minimizing the $\hat{C}$ component leaving the top of the prefractionator. Overpurifying one end of the prefractionator does not result in a significant increase in energy. However, control may be more difficult when the upper feed controls because the liquid split will be controlling a composition at the opposite end of the prefractionator.

Implementing this strategy has led to success. Controlling an upper prefractionator temperature with the liquid split on a pilot-scale column led to 24 to 41 percent energy savings when compared to a conventional distillation sequence.[39] Moreover, the same study reported that improper values of the liquid split can result in energy demands that are twice to three times as large as those of conventional distillation sequences operating at the same capacity. A similar strategy was used by Ling and Luyben, who studied using a composition[61] or a temperature[62] control loop for a stage at the top of the prefrac section using the liquid split as a manipulated variable to maintain minimum energy operation. However, in this case the control objective was to achieve a specified (constant, minimal) heavy component concentration at the top of wall rather than to maintain a constant component split. This study confirmed that manipulating the liquid split to maintain a low composition of the heavy component at the top of the wall correlates to minimum energy consumption, and that the optimal value of the liquid split changes with feed composition but not feed flow rates. The side draw stream in the system considered was entirely liquid. In this case, liquid impurities from the top of wall affect the side stream composition more than vapor impurities from below the wall. However, the side streams of DWCs may be chosen to be in the vapor phase or may be drawn as a liquid/vapor mixture. It is not clear whether the decision to control the heavy component concentration at the top of the wall would lead to minimal energy consumption in these latter cases. It should be noted that while the overall purity of the side product can be controlled, there are not enough degrees

of freedom to specify particular values or ratios of light and heavy impurities in the side product. Halvorsen and Skogestad investigated a fourth composition controller that specified the ratio of side product impurities and found that it lead to infeasible operating regions and resulted in higher energy usage.[54]

Conversely, Halvorsen and Skogestad[17] evaluated five candidate variables for self-optimizing control: the main column temperature profile position, the temperature profile symmetry, the prefractionator impurity outflows, the prefractionator flow split, and the prefractionator temperature difference. Similar to[61], it was found that the heavy component concentration at the top of the prefractionator has close to ideal properties of a self-optimizing variable, with the disadvantage that implementing self-optimizing control may require one or more composition controllers. Further studies in this direction sought to identify combinations of controlled variables that can fulfill the self-optimizing control role.[63] Controlling the resulting variable combinations yielded good resilience to disturbances but proved to be sensitive to measurement errors;[64] furthermore, such variable combinations are not physically meaningful and therefore likely difficult to understand by operators.

The above studies highlight the importance of control to maintain proper energy minimization of DWCs. While energy savings have been reported using the liquid split as a control parameter in a temperature control strategy, a self-optimizing control variable that maintains near-optimal operation without the need to reoptimize when the system is perturbed by disturbances remains an open research area.

DWC BENCHMARK MIXTURES

Overall, similar systems are explored in the DWC control literature, but numerous control structures have been investigated (Table 2-1). In order to provide a better understanding of the selection of control structures, control studies are organized according to feedstock: presenting structures based on desired chemical separation inherently accounts for design choices and process limitations.

Benzene, toluene, xylene (BTX) mixtures

The control of BTX DWCs has been studied extensively via simulation. Control approaches range from conventional multi-loop temperature and composition PID controllers, with and without energy minimization loops, to optimization-based multivariable control structures such as Model Predictive Control. Although the best PID structure is unclear, advanced control techniques have demonstrated faster and tighter control than their PID counterparts. Though their implementation requires more effort, advanced control techniques provide better control because they account for the strong interactions between process variables that arise due to process intensification.

Table 2-1. Summary of DWC control structures available in the open literature, organized by chemical system. TC denotes temperature control, and CC denotes composition control. The normalized boiling point temperatures are the normal boiling points in °F normalized by the boiling point of the middle component. The n-hexanol/n-octanol/n-decanol and butanol/pentanol/hexanol systems were converted to mole percent from weight percent. Sim. denotes simulation-based studies, and exp. denotes experimental studies.

Chemical System	Normalized Boiling Point (°F/ °F)	Feed Composition	Control Structure	Reference	Method
benzene toluene xylene	0.76 1 1.23	equimolar	3 and 4-pt CC	[65,66]	sim.
			MPC	[3]	sim.
		30/30/40 mole %	4-pt TC and CC	[61,62]	sim.
			temperature difference	[62]	sim.
			MPC	[4]	sim.
n-hexanol n-octanol n-decanol	0.82 1 1.16	41/32/27 mole %	4-pt TC	[46]	exp.
			MPC	[1]	exp.
methanol iso-propanol butanol	0.82 1 1.18	equimolar	2-pt TC	[67]	exp.
butanol pentanol hexanol	0.87 1 1.13	18/70/12 mole %	3-pt PID TC MPC	[68]	exp.
ethanol propanol n-butanol	0.84 1 1.18	equimolar	3-pt TC	[54, 69]	sim.
			4-pt TC	[54,70]	sim.
		20/60/20 mole %	3-pt TC	[32]	sim.
methanol ethanol propanol	0.86 1 1.2	20/60/20 mole %	3-pt TC	[32]	sim.
		N/A	4-pt CC	[61]	sim.
n-pentane n-hexane n-heptane	0.62 1 1.34	40/20/40 mole %	2-pt TC	[71]	sim.
		33/33/33 mole %			
		20/60/20 mole %			
n-butane i-pentane n-pentane	0.38 1 1.18	40/20/40 mole %	2-pt TC	[71]	sim.
		33/33/33 mole %			
		20/60/20 mole %			
i-pentane n-pentane n-hexane	0.85 1 1.61	40/20/40 mole %	2-pt TC	[71]	sim.
		33/33/33 mole %			
		20/60/20 mole %			

Composition control with linear multi-loop controllers

Ling and Luyben studied the control of a 30/30/40 mole percent BTX mixture in a DWC.[61] The column was modeled as a pressure-driven system using a set of interconnected conventional distillation column models. Four PID composition controllers were used to maintain the top (benzene), side (toluene), and bottom (xylene) product compositions and minimize energy consumption. The four-point structure comprised the following controller pairings $X_{D,\hat{B}}$ - L (for reflux ratios < 3), $X_{S,\hat{C}}$ - S, and $X_{B,\hat{B}}$ - V, or DB/LSV[2] (Figure 2-3). A fourth control loop maintaining the composition of the heavy component at the top of wall by manipulating the liquid split (β_L) was used to minimize energy consumption. The four-point structure was tested against feed flow disturbances and showed good performance. It was found that the addition of feedforward controllers for the reboiler duty and reflux reduced settling time without resulting in any product deviations.

Kiss and Rewagad further explored the concept of four-point PID composition control to include alternate controller pairings.[65] Examining composition control and inventory control of an equimolar BTX system, the authors studied the DB/LSV, LB/DSV, DV/LSB, and LV/DSB configurations (Table 2-2). Responses to 10 percent feed flow and composition disturbances were compared using Integral Absolute Error (IAE), and structure stability was compared using a frequency-dependent Relative Gain Array (RGA). DB/LSV and LB/DSV had lower IAE values than other structures, and DB/LSV had the lowest RGA numbers, suggesting weaker interactions and stable control.

[2] The following notation is used to distinguish three-point temperature/composition control configurations: the first two letters note the manipulated variable for the reflux drum and the column level, respectively, and the following three letters denote the top, middle, and bottom compositions, respectively.

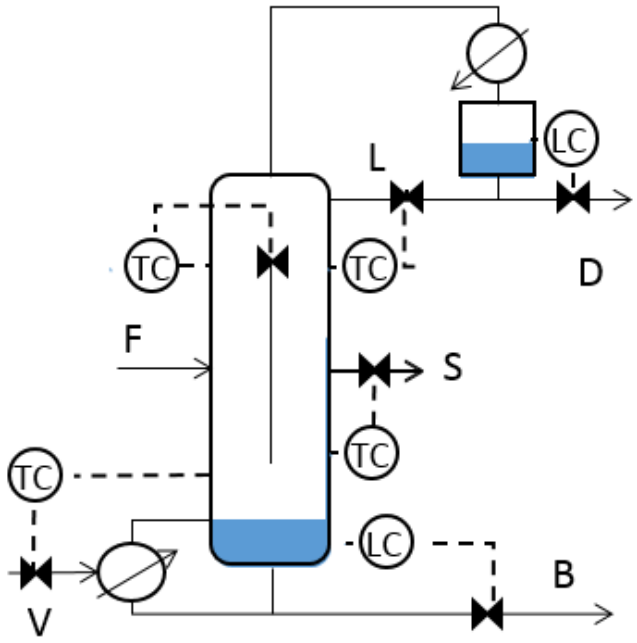

Figure 2-3 – DB/LSV structure showing the distillate and bottoms streams used for level control and the reflux, side stream, and steam used for composition/temperature control. These pairings switch to form the other three structures LB/DSV, LV/DSB, and DV/LSB. The fourth temperature controller controls the prefrac temperature with the liquid split at the top of the wall and is the same for all four structures.

Table 2-2. 4-Point Multiloop Control Structures

	Loop manipulated based on control selection			
Independent Loop	DB/LSV	DV/LSB	LV/DSB	LB/DSV
Accumulator Level	Distillate		Reflux	
Top Temperature	Reflux		Distillate	
Bottom Level	Bottoms	Steam		Bottoms
Bottom Temperature	Steam	Bottoms		Steam

A similar analysis was conducted by Koko and Barakat on an equimolar BTX system.[66] Simplified material and energy balances used for the column trays resulted in a non-linear dynamic model that was then linearized. Proportional level controllers and

proportional-integral composition controllers were used to test the four candidate control strategies: DB/LSV, DV/LSB, LB/DSV, and LV/DSB. However, an energy minimization loop was not implemented. RGA analysis suggested that LB/DSV and DV/LSB had the least loop interactions. Disturbance testing of +10 percent feed flow and -10 percent feed quality of the two structures suggested LB/DSV to be the better structure with faster settling times. These results are in partial agreement with the findings of Kiss and Rewagad[65] who also identified LB/DSV as a better candidate structure regarding disturbance rejection. However, Kiss and Rewagad ultimately found DB/LSV to be the best structure. It is unclear if the type of control loops, choice of model format, or different column designs are responsible for the discrepancy.

Temperature control with multi-loop PID

Online composition controllers are often expensive, require maintenance, and can cause long time delays; these reasons have motivated carrying out studies of DWC control based on temperature, rather than composition measurements. Ling and Luyben provided a direct extension of their previous work[61] using temperature controllers in the place of the composition controllers, and maintaining the same model and feed composition.[62] The authors compared four-point temperature control and temperature difference control in the presence of 10 percent feed flow and composition disturbances. Sensitivity analysis and singular value decomposition (SVD) were used to determine tray locations for both temperature control structures. The absolute temperature control approach was found to handle feed flow disturbances well but not disturbances in feed composition. Conversely, the temperature difference approach handled both disturbances well because of its ability to handle column temperature deviations and pressure disturbances. The temperature difference between two trays does not significantly change for feed disturbances, and since temperature difference control maintains temperature deviations rather than absolute temperatures, setpoints do not have to change with feed composition disturbances. In addition, tray pressures change with changes in liquid and vapor flow rates. Differential

temperature control accounts for this to an extent because both temperatures are affected by pressure in the same manner.

Model predictive control (MPC)

MPC offers numerous advantages over multi-loop PID control structures, including the ability to handle constraints on inputs, states and outputs and to coordinate optimum setpoint and control calculations. These features, along with the ability to capture dynamic and static interactions in the process, make MPC an attractive control strategy for DWCs, where process intensification leads to variable interactions. In general, dynamic simulations comparing MPC to PID controller performance for a BTX DWC show that MPC results in tighter and faster control.

Dohare et al. compared the performance of a 3x3 (3 control variables x 3 manipulated variables) MPC to Ling and Luyben's PID absolute temperature control structure on a simulated 30/30/40 mole percent BTX system.[4,62] The three temperatures controlled via MPC were the uppermost rectifying temperature, the side stream temperature, and the bottom stage temperature in the stripping section, and the manipulated variables were L, S, and V. The MPC exhibited good performance in the face of 10 percent feed flow and composition disturbances and liquid split setpoint changes. MPC showed shorter settling times and smaller offsets than PID control. For example, MPC had one-fourth of the settling time of PID control for changes in benzene feed composition.

Rewagad and Kiss compared the performance of a 6x6 (6 controlled variables x 6 manipulated variables) MPC to the DB/LSV PID control of their earlier paper for an equimolar BTX system.[3,65] The controlled variables for the MPC were $X_{D,\hat{A}}$, $X_{S,\hat{B}}$, $X_{B,\hat{C}}$, the heavy component at the top of the prefrac, and the liquid holdups in the reboiler and the reflux tank. The manipulated variables included D, B, L, S, V, and β_L. A simplified MPC where the holdups were controlled through PID level control was also considered. The high-dimensional MPC model was derived from the linearization of the non-linear distillation column model. The three control structures were tested against disturbances of

10 percent increases in feed flow and in benzene feed composition. The product purity setpoints were also varied. The DB/LSV multi-loop configuration outperformed MPC in the face of benzene feed composition disturbances, but MPC performed consistently well overall. The IAE for MPC was the lowest. The combined MPC and PID structure performed similarly to the larger MPC. Therefore, either would be favorable in practice. Because the linear and non-linear dynamic models matched closely in open loop responses and the authors considered a narrow operating range, non-linear MPC is not expected to provide significant advantages in this case. The authors note that the major drawback of MPC is its "burden of implementation" where the controller's performance is dependent upon the efficiency of optimization algorithms, the computational capacity of the hardware and the complexity of the model.[3] Nevertheless, note that successful industrial implementations of MPC with far larger numbers of inputs and outputs have been reported in the literature. Hence MPC applications are well within reach from a technical perspective as long as the economic motivation is sufficiently strong.

Further applications of advanced control strategies

Frequency-domain multi-variable techniques have been tested and show improvements in performance over multi-loop controllers.[8] However, these techniques require high order controllers (in this case, greater than or equal to 25) which makes their implementation difficult and unlikely to be widely used in industrial practice.

Alcohol mixtures

Numerous theoretical and experimental studies have examined the separation alcohol systems using DWCs.

Experimental studies

While experimental studies are in general lacking from the DWC open literature, their significance cannot be underestimated in the progress towards a complete

understanding of the process. Although differing in chemical systems and column design (Table 2-3) the experimental studies reviewed in this work show that three or more temperature controllers are needed for successful operation in the presence of disturbances. In addition, these studies confirm that MPC provides tighter control and shorter settling times over PID.

n-hexanol, n-octanol, and n-decanol

Fieg et al. conducted a multitude of studies on the industrially-relevant mixture of n-hexanol, n-octanol, and n-decanol in both a pilot plant and simulation environment. The experimental system comprised a stainless steel column that was 11 meter tall and 68 millimeters in diameter with a welded wall in the center.[46] The column used a total condenser and electrical flange reboiler and was operated under vacuum using a rotary vane vacuum pump. Montz structured packing provided 20 theoretical stages in the column, and there were three temperature transmitters per element of packing. Two pressure differentials and thirty six temperatures were measured along the column. Stable operation was ensured by pressure control using a magnetic valve and level control of the reflux drum and reboiler using the reflux (for reflux ratios > 3.3) and bottoms streams, respectively. Product samples were analyzed through gas chromatography (GC), and the liquid split at the top of the wall was controlled using an electromagnetic funnel. A companion mathematical model was developed and validated for multiple operating conditions and disturbances.[43,72]

Relying on the same experimental setup and model, Buck et al. used an equal weight percent feed mixture to develop a systematic procedure for the design and analysis of decentralized control structures for dividing wall columns.[46] Three-point and four-point temperature control structures with and without automatic set point adaption were compared using sensitivity analysis, RGA, and experimental studies. The set point adaption was carried out using a linear function that captured setpoint dependence on the feed flow and composition. The fourth temperature controller manipulated the liquid split to ensure energy optimal operation. Temperature measurement locations and loop pairings were

determined using the slope criterion and sensitivity analysis on the experimentally validated mathematical model. The resulting pairings were $T_{rectifying}$ - D, $T_{stripping}$ - S, $T_{lower\ prefrac}$ - V, and $T_{upper\ mainfrac}$ - β_L. RGA analysis of the four-point temperature control structure showed interactions between the heat duty and the liquid split. Therefore, an alternative four-point structure where these pairings were switched was also studied. Simulation was used to test the four control structures against disturbances of a 10 percent increase in feed flow and 10 percent increases in the weight percent of each component. For feed composition disturbances, the three-point structure performed poorly in regards to purity and heat duty. The structure with setpoint adaptation performed slightly better (however, the fact that it required online feed flow and composition measurements and its increased implementation effort make it less attractive for industry). Due to its superior performance, the four-point structure was tested on the pilot scale column against feed flow and composition disturbances. For a 15 percent increase in feed flow, the controls returned the column to stable operation within an hour with minimum overshoot.

Linear MPC was employed on the same feed system that was used for decentralized control studies.[1] The manipulated variables for the MPC were D, S, V, and β_L, and the controlled variables for the MPC were the same: $T_{rectifying}$, $T_{stripping}$, $T_{lower\ prefrac}$, and $T_{upper\ mainfrac}$. Once again, temperature locations were selected by slope and sensitivity criterion. A linear model was built by performing system identification on the rigorous mathematical model, and the tuning parameters for the MPC were also chosen based on simulations. The MPC was tested experimentally and demonstrated successful control against feed disturbances including a 15 percent increase in flow and 20 percent increase in octanol composition. There were negligible oscillations and little overshoot as temperatures were kept constant and product purities stayed within specs.

Table 2-3. Experimental Studies

Chemical System	Normal BP (°F)	Column Diameter	Theoretical Stages	Control Structure	Disturbances		Reference
					Feed Flow	Feed Composition	
n-Hexanol n-Octanol n-Decanol	315 383 444.2	68 mm	20	$T_{rectifying} - D$ $T_{stripping} - S$ $T_{prefrac} - V$ $T_{mainfrac}$ - β_L MPC	Successfully ±15%	Successfully +20% $X_{\hat{B}}$	1,46
Methanol Iso-propanol Butanol	148.5 180.7 243.3	305 mm	32	$T_{14} - L$ $T_{28} - V$ $T_{14} - ML$ T_{28} - V	N/A	$X_{D,\hat{A}}$ offset for $\Delta X_{F,\hat{B}}$	67,73
Butanol Pentanol Hexanol	243.3 280 315	40 mm wall, 55 mm otherwise	N/A	$T_{prefrac} - r$ $T_{mainfrac} - \beta_L$ MPC	ΔT = 6-8 K for -20% F ΔT = 2-3 K for -20% F	ΔT = 4-6 K for $\uparrow X_{F,\hat{B}}$ ΔT < 2 K for $\uparrow X_{F,\hat{B}}$	68

Methanol, iso-propanol, and butanol

Mutalib et al. tested an equimolar mixture of methanol, iso-propanol, and butanol on an experimental column and compared the results to a dynamic simulation.[67] The experimental DWC was 10.97 meter tall with a 0.305 meter diameter and structured packing. The liquid split was imposed using a total trapout tray, and the wall was positioned closer to the feed side of the column. The ratio of cross sectional area of the products side to the feed side was 1.29. Products were recycled to a feed tank, and a portion of the side product was recycled to the column as a middle reflux (ML). Temperature was used to infer product compositions that were analyzed via GC.

The authors employed a two-point temperature control strategy. Locations for temperature measurements were determined two ways: SVD and column temperature profile analysis, in which only the product side of the dividing wall was studied. Temperatures were paired with two of the three remaining degrees of freedom to form the structures L/V, ML/V, and L/ML. Only L/V and ML/V were used for analysis due to temperature measurement locations. RGA analysis for both structures showed values close to one for the chosen loops. The dynamic simulation and the pilot plant showed stable responses and little interaction in the face of feed composition changes. Both cases demonstrated stable control of bottom and middle purities but large offsets in the top product purity. Steady-state studies of the same column resulted in side product purities inferior to design specifications. The authors suggested over-refluxing to avoid adding additional temperature controllers, a strategy that proved to be successful in simulation studies.

Butanol, pentanol, hexanol

Adrian et al. investigated a 15/70/15 weight percent butanol/pentanol/hexanol mixture using a pilot scale column to compare decentralized control and MPC.[68] The pilot column was 11.5 meters tall and well insulated. The divided section was 40 millimeters in diameter and consisted of two independent columns in parallel. The upper and lower sections of the column had a diameter of 55 millimeters.

The PID pairings were $T_{upper\ prefrac}$ - L, $T_{upper\ mainfrac}$ - β_L, and $T_{stripping}$ - S. It was found that without including feed to reboiler feedforward control in the multi-loop structure, feed disturbances caused the heavy component to move up the column and increase stage temperatures. The manipulated variables for MPC were V, β_L, S, and the reflux ratio. The MPC model was obtained using system identification techniques similar to.[1] Though MPC required approximately three times the implementation effort, MPC outperformed PID in regards to settling time and minimizing offsets from feed flow and composition disturbances.

Simulation studies

Ethanol, propanol, n-butanol

Wolff and Skogestad compared the performance of three-point and four-point composition control of an equimolar ethanol, propanol, and butanol mixture in a thermally-coupled column.[54] RGA was used to determine the control loop pairing, suggesting the DB/LSV as the most appropriate pairing from a steady-state analysis point of view. The fourth composition loop was used to control the ratio of impurities in the side stream by manipulating the liquid split. Simulations of the three-point structure indicated the column handled feed flow and composition disturbances well. Some setpoint changes in product purities resulted in infeasible operation (as explained above), which could also be (in part) due to improper staging. Setpoint changes with the four-point control structure proved infeasible. A change in sidedraw setpoint resulted in unstable operation with the reflux and boilup reaching their imposed constraints, again, as explained above. For this reason, the authors advised against controlling the side draw impurity concentration of a thermally-coupled column but noted the need to adjust the liquid and vapor splits to optimize energy usage. Steady state RGA also suggested an alternative pairing of side product flow with bottoms composition. This alternative pairing was a result of changes in the sidedraw flow primarily impacting the lower part of the column. Though analysis of the closed loop disturbance gain suggested this alternative pairing was equally feasible, the alternative

structure failed to reject feed flow and composition disturbances when tested using nonlinear simulations in SPEEDUP.

Dwivedi et al. modeled a hypothetical, equimolar mixture with relative volatilites close to those of ethanol, propanol, and n-butanol (4.2:2.1:1).[70] Four alternate control structures, all with L/V composition control, were compared. The differences between the structures are summarized in Table 2-4. The structures that over-purified one of the products (CS2 and CS4) only resulted in minor increases in energy usage. All structures were subjected to 20 percent changes in feed flow and six composition changes. All structures handled feed flow changes well. CS1 resulted in poor control in the face of feed composition disturbances, and CS3, which was based on Ling and Luyben[61], failed when a feed disturbance made $\hat{A}/\hat{B}$ the difficult split. The structures that over-purified one product operated best in the face of disturbances, with CS2 using slightly less energy. However, the over-purifying structures manipulated the vapor split, which is not feasible in actual operation. Therefore, the authors suggested linear or nonlinear MPC for future work.

Qian et al. studied the temperature control of an equimolar mixture of ethanol, n-propanol, and n-butanol.[69] The authors compared temperature control schemes in which the liquid and vapor splits were constant, the liquid split was used to control a temperature in the prefractionator, and the vapor split controlled a temperature in the prefractionator. In all schemes, the reboiler duty was constant. All control schemes were able to reject feed flow disturbances. Although the structure with the changing liquid split better maintained product purities in response to ±20 % changes in vapor split than the fixed ratio structure, the prefractionator temperature did not correlate well with composition.

Ignat and Woinaroschy studied a 0.2/0.6/0.2 mole fraction mixture of ethanol, 1-propanol, and 1-butanol using three-point temperature control to infer compositions.[32] The structures LB/DSV and LB/DVS performed well in the face of 10 percent feed flow and feed composition disturbances.

Table 2-4. Third composition controller for three-point composition control of Dwivedi et al.[70]

β_V manipulated	CS1	$(X_{S,\hat{A}} + X_{S,\hat{C}})$ - S
	CS2	$X_{S,\hat{C}}$ - S Max select for V: $X_{D,\hat{B}}$ or $X_{S,\hat{A}}$
β_V fixed	CS3	$X_{S,\hat{C}}$ - S
	CS4	Max select for V: $X_{lowerprefrac,\hat{A}}$, $X_{S,\hat{A}}$, or $X_{B,\hat{B}}$

Methanol, ethanol, propanol

In addition to their ethanol, 1-propanol, and 1-butanol studies, Ignat and Woinaroschy studied a 0.2/0.6/0.2 mole fraction mixture of methanol, ethanol, 1-propanol.[32] The same controller pairings were used, but the design of the column differed in number of trays and location of streams. This system was controllable and performed well against 10 percent feed flow and feed composition disturbances.

Ling and Luyben also studied a mixture of methanol, ethanol, and propanol using the DB/LSV composition control structure, with a fourth loop for energy minimization. The good control performance suggests that the DB/LSV setup is amenable for implementation in DWCs separating a variety of systems.[61]

Other hydrocarbon mixtures

Kim et al. investigated the relationship between two-point temperature control structure, feed composition, and ease of separability index for three hydrocarbon systems.[71] The three ternary mixtures examined were n-pentane/n-hexane/n-heptane, n-butane/i-pentane/n-pentane, and i-pentane/n-pentane/n-hexane. Each system differs in ease of separability index (ESI), where

$$ESI = \frac{\alpha_{\hat{A}-\hat{B}}}{\alpha_{\hat{B}-\hat{C}}} \quad \textbf{(2-1)}$$

and α denotes the relative volatility between two components. Each system was studied at three different compositions: 0.4/0.2/0.4, 0.33/0.33/0.33, and 0.2/0.6/0.2 mole fraction light/middle/heavy. The optimum column design for each system was determined first

using steady-state simulations. Multiloop PID structures were implemented on each system. Holdups in the reflux drum and reboiler were controlled using the distillate and bottoms, respectively. Two-point temperature control using either the reflux, side draw rate, or boilup as manipulated variables was investigated. Temperature locations were determined using steady-state analysis tools including SVD, RGA, condition number, and steady-state gain. The control structures were tested against 10 percent feed flow rate disturbances and compared on the basis of settling times and integrals of absolute error. It was found that the choice of best control structure was related to the mixture's ESI rather than feed composition. The L/S structure performed best for large ESI values and ESI values equal to one. On the other hand, the V/S structure performed best for small ESI values. The L/S structure for a 0.2/0.6/0.2 mole fraction mixture of n-pentane, n-hexane, and n-heptane was compared with the L/S/V structure from Kiss and Bildea that was tested on the same feed mixture.[26] The two-point structure had shorter settling times and lower integrated errors because it lacked the interactions that were present in the three-point structure. However, intuitively, the three-point structure produced less offset in side product composition.

Ideal components

Serra et al. used an ideal system with constant relative volatility (α = 1:2.15:4.65) to examine the controllability and operation of a DWC.[74] Several combinations of inventory and three-point composition control were studied using linear analysis tools such as RGA,SVD, condition number, and the Morari resiliency index (MRI). LV/DSB had the largest stability margin and demonstrated the best control.

DISCUSSION, CONCLUSIONS, AND FUTURE WORK

Summary of findings

This review examined the control of DWCs. Important contributions to the field include the characterization of minimal energy operation by defining the split of middle-

boiling component around the dividing wall.[17,39] This can be done by controlling a prefrac temperature above the feed using the liquid split or by minimizing the heavy component concentration at the top of the wall using the same manipulated variable.[3,61,62]

Four-point temperature or composition control structures with three loops controlling (directly or inferentially) product compositions and one loop minimizing energy use were shown to be successful in controlling DWCs for separating BTX and alcohol systems in simulation and experimental environments.[3,61,62,66,72] Conversely, four-point composition control structures proved infeasible in the available literature studies.[17]

Three-point temperature control was shown to perform well for mixtures of hydrocarbons[71] and alcohols[32]. Intuitively, two-point temperature control demonstrated shorter settling times and lower integrated error than three-point control but did not provide good control of the side product composition in the face of feed disturbances. Finally, there is a general agreement that MPC provides tighter and faster control than multi-loop linear structures.[1,3,4,68]

Conclusions

The results available in the open literature indicate that DWCs are controllable, provided that the control structure is chosen appropriately. Choosing the correct control structure, however, is not straightforward. Numerous choices exist (Table 2-1). Among the questions to be answered: Which streams should be used for inventory control vs. composition control? Should composition control or temperature control be used? Are advanced control structures necessary? How can minimum energy consumption be ensured given steady-state multiplicity?

While a plethora of tools such as SVD and RGA are available and have been used to determine loop pairings, the results are far from general, and confirm the need for further investigation. Moreover, most structures investigated handle feed flow disturbances well either by manipulating all product streams or by using feedforward controllers. Maintaining product compositions in the face of feed composition disturbances proves

more challenging. While MPC and other advanced control algorithms have shown the greatest success in handling feed composition and feed flow disturbances, their extra complexity and implementation effort may detract from their added benefit.

Overall, the DWC control literature is centered on a small number of prototype mixtures to separate yet reports on a surprisingly broad array of control structures and strategies. The formulation of a transparent framework for connecting DWC design and operational objectives to control structure selection remains an open research question.

Firstly, further work is required to ensure minimum energy use during operation. First, several disparate choices of control loops for minimizing energy consumption have been proposed. While effective, it is not yet clear how the setpoints of these loops are to be determined quickly and efficiently in an industrial environment, preferably without performing elaborate and time consuming nonlinear optimization calculations on a complex first-principles process model.

Second, the importance of experimental data cannot be overstated. Experimental data from pilot plant studies are the key to fully understanding process interactions and process sensitivities. The experimental data available in the open literature are limited in many ways. Often, only one decentralized structure is tested on a particular column. When two or more control structures are compared, it is not easy to determine whether the differences in performance are truly the merit of the control structure choices or the consequence of design decisions or changes in process hardware (e.g., packing) performance. Future work thus must focus on more extensive experimental studies. Besides investigating multiple PID structures and generating advanced control models based on experimental data, these studies should take into consideration process factors, including, e.g. packing performance and constraints such as column flooding and weeping.

As in the case of binary distillation, there is no one control structure that suits all DWCs. Instead, the appropriate control structure must be chosen based on process objectives and design limitations. However, the available literature does not provide a complete assessment of all conditions that may be encountered in practice. This review

organizes structures according to feedstock in hopes of incorporating any inherent design choices that could potentially impact control decisions. However, due to differences in modeling approaches, feedstocks, and product specifications, separate studies are difficult to compare. A rigorous process for determining control structure based on process characteristics and operating objectives is still needed. The work highlighted in the following chapters shows that SVD and RGA are a set of tools that can successfully screen control structures for DWCs. A two-point temperature control structure is developed to successfully maintain steady state, reject disturbances, and transition the column between steady states without issues arising from controller interaction. Of course, it should be noted that the resulting temperature control approach should not be used for all DWCs. Rather, through the inclusion of trace components, this work shows that column sensitivities and the resulting control structure change as process conditions change. Furthermore, this work adds to the currently limited available experimental research.

Chapter 3: Dynamic Model

As highlighted in the literature review, there is a lack of available dynamic models for dividing wall columns. The assumptions and modeling approaches employed for the study of dynamic DWCs vary greatly. Very few of these models are verified with experimental data, so it is unclear what approach, assumptions, or model complexity is best suited to represent dividing wall columns. If dividing wall columns are to gain widespread industrial acceptance, they need to be accurately modeled. Furthermore, the column dynamics must be accurately captured in order to design successful control structures to handle column disturbances and changes in operation.

Among the questions to be asked is: Does a conventional stage-to-stage dynamic distillation model represent actual column dynamic behavior or does the intensified nature of the process introduce process nonlinearity that isn't captured in traditional modeling? In addition, it must be investigated if any unusual dynamic behavior comes about when transitioning from one steady state to another. This unusual dynamic behavior must not only be accounted for in the design of control systems but will affect the model and optimization choices for columns operated in a transient fashion and/or employed for separating several different feed streams.

MODEL STRUCTURE

Unless otherwise specified, the modeling efforts referenced in this work are from a dynamic model using Eastman proprietary software. Because the software does not have a distillation or dividing wall column block, the column was modeled as a series of flash tanks assembled to match the pilot plant dividing wall column described in Chapter 5. Because the pilot column was packed, the staging in the model was determined using the manufacturer's HETP value and the height of packing in the column. Six flash tanks were located both above and below the wall, and twelve flash tanks were on either side of the wall. Though there are 24 theoretical stages and a reboiler, the flash tanks were numbered such that more flash tanks could be easily added. Therefore, a stage's number does not

always represent the number of stages from the top of the column. The numbering and location of stages is shown in Table 3-1. The prefractionator stages and mainfractionator stages have been denoted with A and B, respectively. In addition to 24 theoretical stages, the model also included a total condenser, a reflux drum, a top of the wall tank, a side product tank, and a reboiler (Figure 3-4). The model also had heaters on the overhead reflux, prefrac reflux, mainfrac reflux, sidedraw reflux, and feed streams so that the temperatures of these streams could be matched to the pilot data.

Table 3-1. Stage Numbering in Dynamic Model

Column Section	Stage Number
Rectifying	1 – 6
Upper Prefrac	A11 – A16
Lower Prefrac	A21 – A26
Upper Mainfrac	B11 – B16
Lower Mainfrac	B21 – B26
Stripping	31 – 36

The conventional MESH equations for equilibrium stage models were used. This includes a system of ordinary differential equations to describe heat and material balances and algebraic equations to predict the physical properties and vapor-liquid equilibrium. The Wilson equation was used. The parameters for which came from a proprietary databank. Though different from the Non-random Two Liquid model used in the Aspen Plus® model (Chapter 6 and previous studies[40]), the models were compared, and good agreement was found.

Each flash tank had a level controller to control the liquid flow leaving the tank and a pressure controller to control the vapor flow leaving the tank. For initial simulations (Chapter 4), a pressure drop of 0.5 mmHg/stage was used in the model. This was later modified using pilot data and the Stichlmair correlation (Chapter 6). Though the vapor split

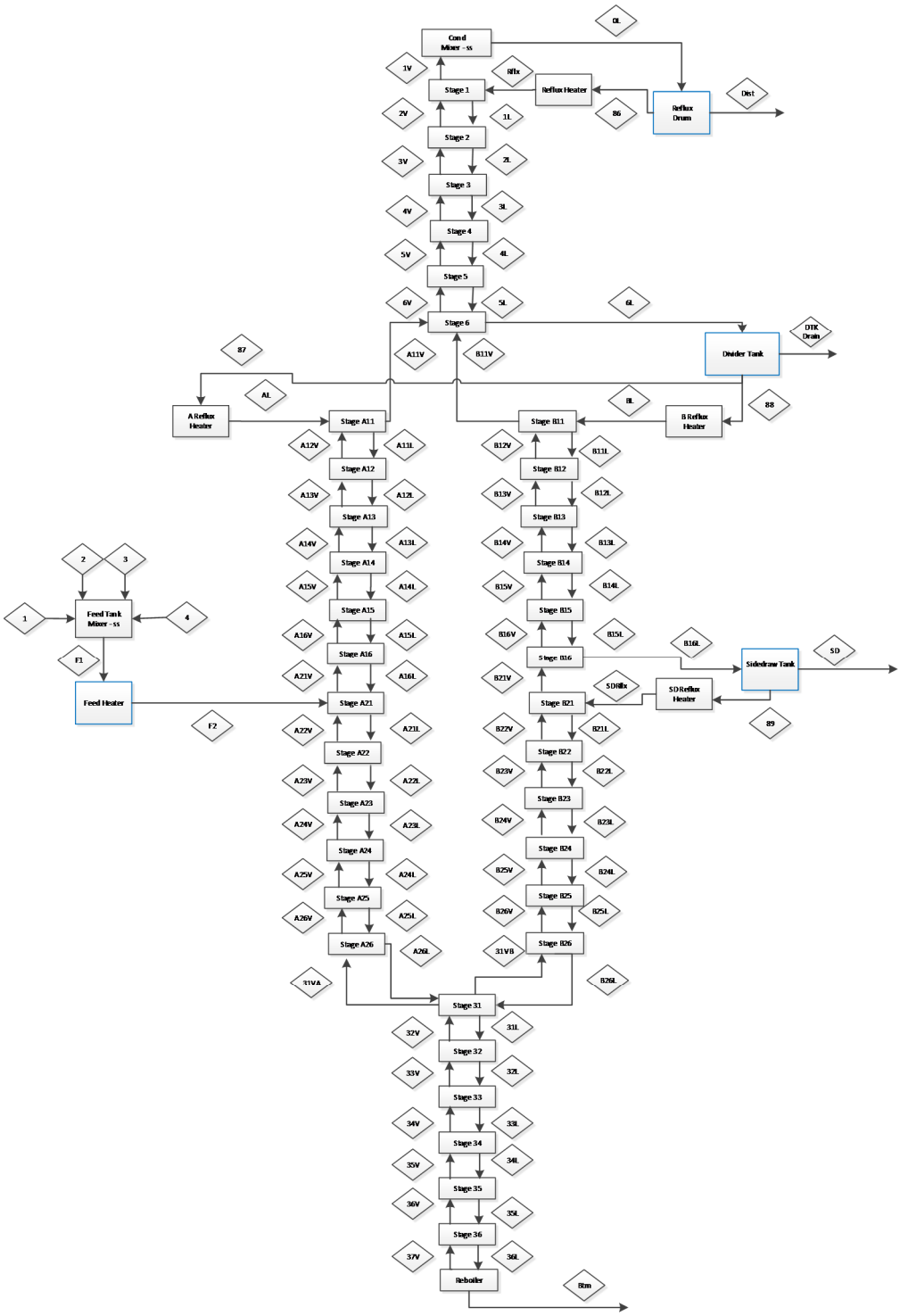

Figure 3-4 – Dynamic Model Structure

at the base of the column could be adjusted in the model, a vapor split equal to the area ratio resulting from the wall placement was assumed due to previous experimental findings.[40] The wall split was defined as ratio of the prefrac reflux to the mainfrac reflux (Equation 3-1). The value of the wall split was varied between case studies, and the procedure for determining the optimal wall split is highlighted in Chapter 4.

$$\text{Wall Split} = \frac{\text{Prefrac Reflux}}{\text{Mainfrac Reflux}} \quad \textbf{(3-1)}$$

HOLDUP CALCULATIONS

The dynamic model was modified to match the residence times and holdups of the pilot plant. Vessel volumes and holdups are summarized in Table 3-2. The holdup in the reboiler was calculated using the reboiler mechanical dimensions (Figure B-1) assuming an operating level approximately just above the height of the weir. Because the number of ¾'' 2-pass tubes was unknown, the tube volume was calculated using 40 percent volume of a 6 inch diameter cylinder. The volume within the column sump and the 2 inch pipe to the reboiler was determined using the totalizer associated with the bottoms flow meter while draining water from the unit. This volume is 7 gallons and is included in the reboiler hold ups in Table 3-2. Table 3-3 details the reboiler calculations.

Table 3-2. Vessel volumes and operating levels

Vessel	Total Volume (gallons)	Approx. Operating Level (in)	Operating Liquid Hold up (gallons)
Reflux Drum	10	8	2
Top of Wall Tank	23	8	5
Side Product Tank	23	8	5
Reboiler	38	3	25

Table 3-3. Reboiler holdups

Void Volume (gal)	22
Tube Volume (gal)	4
Reboiler Volume (gal)	18
Column Sump & Line to Reboiler (gal)	7
Total Volume (gal)	25

The holdups of the individual flash tanks were calculated to match the typical 5 percent holdup in Mellapak 500Y. These calculations resulted in full circular sections with 0.05 gallon holdup and half circle sections on either side of the wall with 0.025 gallon holdup on each stage. The Stichlmair model predicted roughly three to five percent holdup per stage. However, these small values caused numerical issues with the model sampling time and tank residence times. Therefore, the holdups per stage were increased to 0.2 gallons in full sections and 0.1 gallons in half sections. Tank volumes were also adjusted such that the liquid holdup would still resembled 3 to 5 percent of the total volume and that the ratio of liquid to vapor residence times would remain the same.

HEAT TRANSFER CALCULATIONS

Although the dividing wall pilot column was insulated with two inch thick foam glass insulation, there was still heat transfer to the environment due to the high surface area to volume ratio. This loss of energy caused rising vapor traffic to condense therefore creating an internal reflux. Evidence for this increased liquid traffic includes the overhead reflux flow being less than the total of the reflux flows on either side of the wall. In addition to heat transfer to the environment, there was also heat transfer through the uninsulated dividing wall. Composition differences on either side of the wall resulted in a temperature difference across it. Although the temperatures on either side of the wall were predominantly determined by composition and would not fully equilibrate, the difference in temperature drives heat transfer. Although not fully understood, heat transfer through a dividing wall has been noted in the literature.[10,34,39,41,42,72]

This heat transfer both to the environment and through the wall were incorporated into a dynamic dividing wall column model through heat transfer coefficients. A heat transfer coefficient through the wall and a heat transfer coefficient to the atmosphere as well as ambient temperature were specified by the user, and the model calculated a heat loss per stage. Of course, since

$$Q = UA(T - T_{ref}) \quad \textbf{(3-2)}$$

an area must be assumed. A fully wetted area for heat transfer was assumed. Therefore, the area could be calculated based on stage geometry. Heat transfer through the condenser and reboiler were not considered because appropriate areas were difficult to assume. The stage areas and calculations are further explained in the following subsections and summarized in Table 3-4.

For the work in Chapter 4, the heat transfer coefficients were obtained from previous work validating experimental data for a cyclohexane, toluene, m-xylene system.[40] The heat transfer coefficient to the atmosphere was 8.00 BTU/(hrft^2°F), and the heat transfer coefficient through the wall was 52.80 BTU/(hrft^2°F). After the pilot campaign, heat transfer coefficients which more accurately captured the run conditions were obtained. The procedure for determining these is described in Chapter 6.

Heat transfer to the atmosphere

For the full circular sections in the rectifying and stripping sections, the area was calculated from the lateral surface area of a cylinder whose height was equivalent to the packing's HETP and whose diameter was equivalent to the internal diameter of a schedule 40 six inch diameter pipe (Full Circle Area). The internal diameter was chosen because the temperature readings available measured the temperature of the process fluid inside the tower. For the sections along the wall, this area was halved since the packing is semi cylindrical in shape (Half Circle Area). Distributors and chimney trays were assumed to have no heat transfer. The reference temperature used was ambient temperature.

Heat transfer through the wall

The area for the heat transfer through the wall was calculated using a rectangle whose height was equivalent to the packing's HETP and whose width was equivalent to the internal diameter of a schedule 40 six inch diameter pipe (Wall Area). The temperature difference across the wall was calculated from the simulated temperature of the equivalently numbered stage on the other side of the wall.

Table 3-4: Dimensions and area calculations used for calculating heat transfer per stage

Parameter	Value
Schedule 40 6 inch Inner Diameter	6.07 inches
Height Equivalent to Theoretical Plate (HETP)	9.5 inches
Full Circle Area	1.258 ft^2
Half Circle Area	0.629 ft^2
Wall Area	0.40 ft^2

Chapter 4: Designing Controller Pairings

MOTIVATION

As previously noted, successful control of dividing wall columns has been demonstrated in the open literature using several control configurations, varying from multi-loop linear control to advanced control strategies. However, there is a shortage of experimentally-validated studies, and a comprehensive framework which can be used for designing control structures for dividing wall columns is lacking. Some studies have used dividing wall columns as a test ground for particular control algorithms without consideration for the best or most practical way to control the column while others have used over simplified models or various feed systems that make comparison difficult. Furthermore, many of these studies examine high purity products in overdesigned columns. These works still provide insightful information about column operation, and the authors stress that their goal is not to consider investment tradeoffs in the design of columns. However, overdesigned columns are easier to operate from a controls perspective. To a certain extent, the "plane flies itself" and the full impact of process intensification on control system performance is not seen. If one desires to truly reap the benefits of energy and capital savings promised by DWCs, columns will have to be built with closer to the minimum number of stages. Less stages leads to less physical distance between control temperatures and a higher potential for controller interaction. Whether or not overdesigning columns with the associated increased capital expenditure is simply better for research or is necessary for alleviating controller issues is a remaining question regarding DWCs. Finally, although numerous works have successfully used model predictive control for dividing wall columns,[1,3,4] this work examines decentralized control structures because PID controllers remain the most widely used in industry.[65] In addition, for practical implementation, it may be preferred to only use the level of complication that is necessary.

Though most agree that DWCs are controllable, the available literature can at times present conflicting results and a "best" strategy does not seem clear. A similar problem once faced the field of traditional distillation control. The control of traditional distillation

columns has been extensively studied and a brief review here would not do the field justice.[5–7,75–78] However, the recurring issues of choice in level control strategy and choice in number of compositions or temperatures to control led to the declaration that there is no universal "best" control structure for distillation. Instead, there is a set of developed tools that can be used to analyze alternative configurations.[76] A few studies have employed these tools to design control pairings for DWCs. However, these works only focus on a handful of chemical systems, and not all of these works are experimentally validated.

This chapter highlights the testing of conventional tools to design control structures for a dividing wall column. By studying a chemical mixture for which experimental studies have not been reported in the open literature, this work adds to the otherwise limited number of experimental dividing wall column studies. In addition, this work explores the management of trace components within a dividing wall column, something that has not been reported in the open literature. Mixtures fed to industrial distillation columns often include trace components, additional components whose presence in the feed is very small and are not high value products. Nevertheless, the ability of a column to isolate these trace components or move them around the column is an important part of successful distillation operation. Trace components are industrially relevant, and proving that DWCs can control for trace components is an important step towards their widespread acceptance in industry. Case studies are explored in which the trace component is a part of different product streams, and a decentralized control structure is designed for each case using conventional tools. The performance of the resulting control structures was verified on the pilot scale column and is discussed in subsequent chapters (Chapter 5).

FEED SYSTEM

The feed system was chosen as a psuedo benzene-toluene-xylene system, an industrially relevant system on which many simulation-based DWC control studies have been performed.[3,4,61,62,65,66] Given the physical constraints of the pilot plant (column design, available theoretical stages, utilities), the fourth component in this mixture had to have a

higher volatility than cyclohexane. Toluene was chosen to be the trace component because a middle boiling trace component is more difficult to control and allows for greater operating flexibility.

Table 4-1. Chemical System Abbreviations and Relative Volatilities

Chemical	Abbreviation	α_{imX}	α_{ij}
2-methylpentane	2MP	8.65	1.65
Cyclohexane	C6	5.24	1.84
Toluene	Tol	2.85	2.85
m-Xylene	mX	1	

STEADY STATE CASES

Four steady state case studies were chosen to be studied: a three component case where no trace component was present, a case with the trace component in the bottoms product, a case with the trace component in the side product along with the cyclohexane, and a case where the trace component was isolated as the side product and the cyclohexane was moved to the distillate product. For the reader's convenience, this document will employ a shorthand method to refer to each case. The cases are named following the convention of [distillate, side, bottoms] where the comma separates the components in the different product locations, and a forward slash separates chemicals in the same product stream. Case [2MP, C6, Tol/mX] where the toluene trace component is in the bottoms product is used in this chapter as an example. Matrices and information for all other cases can be found in Appendix A.

Before control pairings could be determined, steady state targets had to be chosen. This was done using the model highlighted in Chapter 3. Steady state targets included product compositions, the liquid split at the top of the wall, and the reboiler duty and resulting reflux flow rates. Because the separation had to be feasible for the pilot column, the design of which was already fixed, the steady state target product purities were not high

(i.e. < 99 wt %). Although other published experimental studies had higher purities for all product streams, (Mutalib et al.'s 98.5 mole percent methanol/isopropanol/butanol system[67] and Niggemann et al.'s 99 weight percent n-hexanol/n-octanol/n-decanol[72]), lower product purity targets, such as the 97 weight percent distillate seen below, challenge the control system to maintain the desired separation without relying on overdesigning the column. To ensure that the desired product distribution was obtained, the recovery of toluene trace component was defined (Equation 4-1) and set to the desired value.

$$\text{recovery} = \frac{S^{*}X_{S,\,Tol}}{F^{*}X_{F,\,Tol}} \qquad \textbf{(4-1)}$$

All simulations were done with 80°F ambient temperature, a bubble point feed, a 70°F overhead reflux temperature, and 15°F subcooling in all other reflux flows. As explained in Chapter 3, the heat transfer coefficient to the atmosphere was 8.00 BTU/(hrft^2°F), and the heat transfer coefficient through the wall was 52.80 BTU/(hrft^2°F). These were taken from previous studies on a similar chemical system. [40]

Case Study [2MP, C6, Tol/mX]

Steady state flows and compositions for the case of toluene in the bottoms product are shown in Table 4-2. The toluene trace component compositions are highlighted in blue. Because the 2-methylpentane and cyclohexane separation is more difficult than the cyclohexane and toluene separation, a 3.00 weight percent cyclohexane impurity was chosen in the distillate product, and a 2.50 weight percent 2-methylpentane impurity was chosen in the side product. The wall ratio was set such that these targets were possible. The steam flow was determined by the 3 percent recovery of toluene in the side product (97 percent recovery of toluene in the bottoms product). The temperature profile for this case is shown in Figure 4-. The profile is steepest in the stripping section where the toluene and cyclohexane are separated and relatively flat through the dividing wall. A slight temperature gradient is seen in the rectifying section and upper portions of the dividing wall.

Table 4-2. Base Case Conditions

Stream Name	Total Mass Flow (lbm/hr)	Temperature (°F)	Composition (wt %)			
			2MP	C6	Tol	mX
Feed	50.00	195.00	32.00	32.00	**4.00**	32.00
Distillate	16.09	90.00	97.00	3.00	**0.00**	0.00
Reflux	226.27	70.00	97.00	3.00	**0.00**	0.00
Prefrac Reflux	166.15	165.00	48.71	51.28	**0.01**	0.00
Mainfrac Reflux	159.10	165.00	48.71	51.28	**0.01**	0.00
Side Product	15.90	195.70	2.50	97.12	**0.38**	0.00
Side Reflux	170.98	180.00	2.50	97.12	**0.38**	0.00
Bottoms	18.01	290.03	0.00	0.41	**10.77**	88.82
Steam (KBTU/hr)	76.10					

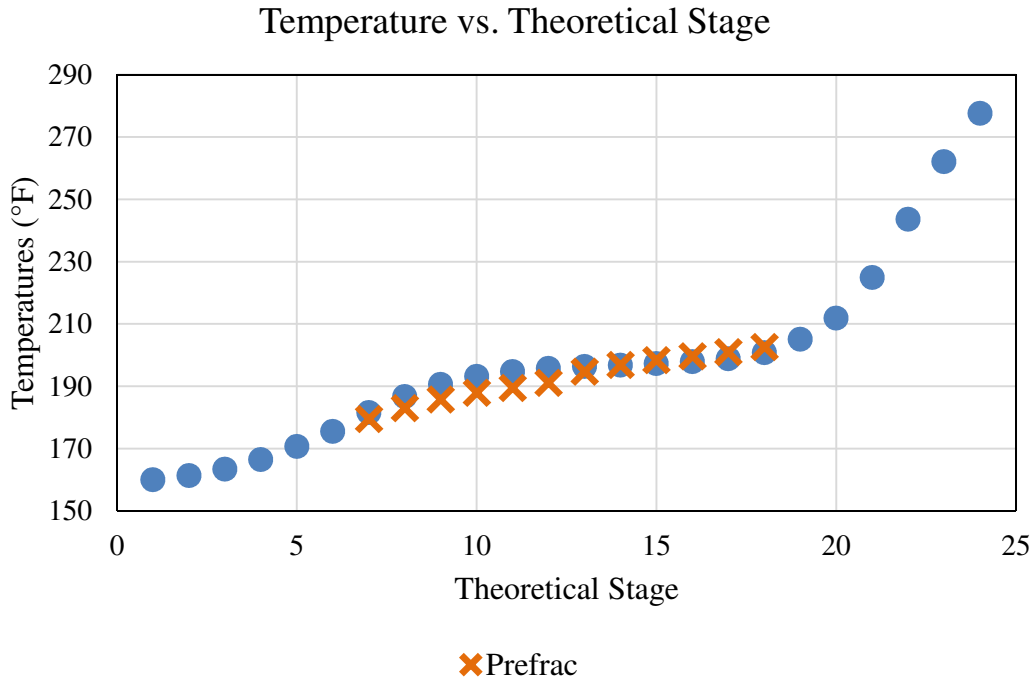

Figure 4-1 – Temperature profile for [2MP, C6, Tol/mX]. Heat transfer to the environment and through the wall is included in the model.

LEVEL CONTROL STRATEGY

Before temperature or composition control pairings were determined, a level control structure was chosen. Level control is an important part of distillation control. Controlling column and tank levels stabilizes column inventory and helps to reject disturbances. Furthermore, the choice in level control pairings impacts temperature or composition control as the degrees of freedom used for level control cannot be used for temperature or composition control. Different flows have different impacts on column compositions. Due to material balance constraints, changes product flows have a larger impact on compositions than changes in internal flows (reflux flows and vapor). Changes in product flows have a slower time constant and purify one product at the expense of another. On the other hand, changes in internal flows have a faster time constant and have the ability to make both products purer simultaneously.[76] Therefore, the choice in level control structure is important.

Many choices for level control exist. In distillation columns, the column level is typically controlled with either the heat duty/steam flow to the column or the bottoms flow. The overhead reflux accumulator level is typically controlled by either manipulating the overhead reflux flow or the distillate flow. Level is easier to control with larger flows. Therefore, for reflux ratios greater than three, accumulator level is often controlled with the reflux flow.

However, these approaches are best when considering a single distillation column. Few distillation columns in fact serve as stand-along unit operations. Distillation columns are usually a part of large chemical plants with a variety of unit operations and a large number of control loops. Rules and control structures that are effective from a unit operations perspective may lose their effectiveness when seen from a plant-wide perspective because the dynamic characteristics of a plant are different from those of a single unit operation.[79] Because of this, product flows were used for level control (i.e. column level with bottoms flow and accumulator level with distillate). The dividing wall column at UT Austin has additional tanks for the side product and the top of the wall liquid

split. These tanks are not standard for dividing wall columns and add additional level control loops to the process. For all cases except the case of an isolated trace impurity side product, the side tank level was controlled with the side product flow (Figure 4-2). For case [2MP/C6, Tol, mX], the trace impurity flow was too small to provide stable control. Therefore, the side tank level was controlled with the side reflux (Figure A-13). This configuration more accurately resembles an industrial column where there would not be a side product tank. The top of the wall tank used ratio control so that the wall split (Equation 3-1) could be manipulated separately and maintained. The top of the wall tank level controller manipulated the prefrac reflux, and the mainfrac reflux was set by the wall split ratio and the prefrac reflux.

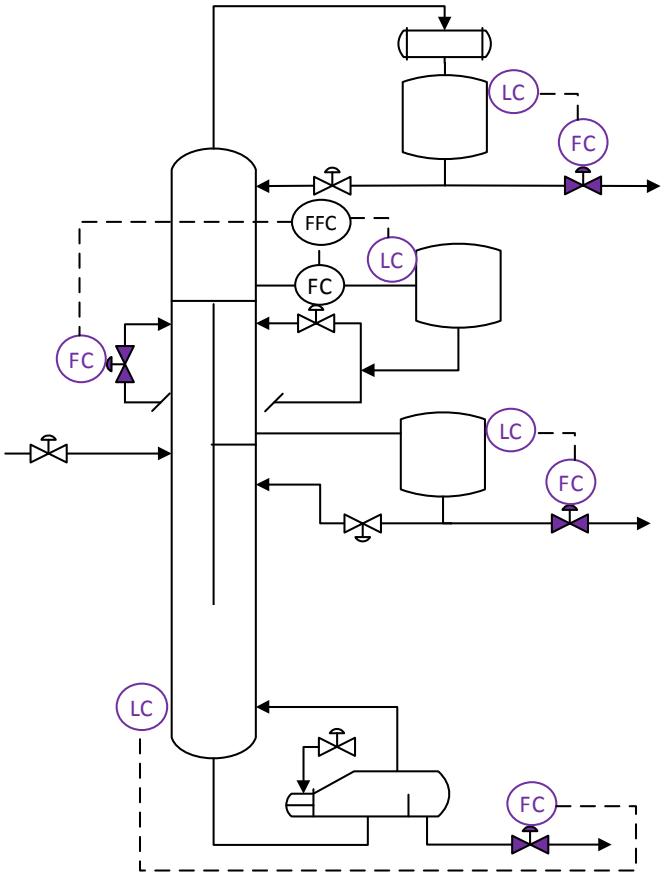

Figure 4-2 – Level Control used for all cases except [2MP/C6, Tol, mX]

SINGULAR VALUE DECOMPOSITION AND RELATIVE GAIN ARRAY

Singular value decomposition (SVD) and relative gain array (RGA) analysis are steady state based techniques that are used to determine and to test controller pairings on traditional distillation columns. These techniques have been previously applied to dividing wall and thermally-coupled columns.[46,54,62,65,67,71,74] SVD and RGA were used to determine temperature control structures in this work. Composition control was also tested, and the results can be found in Appendix A. Temperature control was ultimately chosen to be implemented on the pilot column because the lower residence times and lower cost of temperature sensors make temperature control more favorable. Before detailing how SVD and RGA were used in this work, a brief explanation of the two tools is given.

Background

Sensor sensitivity is key for control of a distillation column. Control sensors must be responsive enough that they respond to changes in valve actuation without requiring large movements in valve position but also must not be too sensitive that the manipulated variables overcompensate and steady state is never achieved. When more than one controller is present, ideal sensor locations must exhibit the appropriate sensitivity while also not interacting with other sensors. This particularly becomes a problem in distillation temperature control because the temperatures that exhibit the least amount of interaction (i.e. the ends of the column) have the least sensitivity due to relatively constant product purity while the temperatures with the most sensitivity (i.e. near separation point in column) are typically located closer to one another.[5] Numerous methods and tools have been developed to determine the optimal temperature locations for control.[9] Some of these methods rely on the steady state gain matrix, a matrix which shows how control sensors respond at steady state to changes in particular valves.

SVD is a mathematical algorithm that is useful in analyzing the multivariable nature of the gain matrix. SVD determines the rank and condition of a matrix and geometrically maps its strengths and weaknesses. SVD has numerous applications and is well

documented.[80–82] The discussion below will focus on how SVD relates to distillation control and the physical insight it provides.[5,83]

SVD decomposes the gain matrix into three matrices (Equation 4-2) where K is the gain matrix, U is an orthonormal matrix whose columns are termed the left singular vectors, V is an orthonormal matrix whose columns are termed the right singular vectors, and Σ is a diagonal matrix of scalars or singular values.

$$K = U\Sigma V^T \tag{4-2}$$

U is a measure of sensor sensitivity. The left singular vectors of the U matrix represent an orthogonal coordinate system showing the most sensitive combination of tray temperatures in the column. The first left singular vector (U_1) represents the easiest direction in which the system can be changed, followed by U_2, etc. The principal component of the U_1 vector is the most sensitive temperature location, principal component of U_2 is the second most, etc. Though by definition the U vectors are non-interacting, the principal components of each U vector may still exhibit interaction though less interaction than other choices. V is the analogous matrix for the manipulated variables. The first right singular vector (V_1) represents the combination of control inputs which have the largest effect on the system, followed by V_2, etc. The singular values (σ_1, σ_2, etc.) of the diagonal matrix Σ provide the ideal decoupled gain of the open loop process. The condition number (CN) can be calculated from the ratio of singular values (Equation 4-3).

$$CN = \frac{\sigma_{max}}{\sigma_{min}} \tag{4-3}$$

The condition number represents the ratio of the system's maximum and minimum open-loop, decoupled gains. A large condition number indicates impractical control. Typically, condition numbers larger than 100 should be avoided though there is no specific cutoff.[5] The condition number shown in Equation 4-3 represents the full multivariable control problem. However, the condition number can also be calculated for simpler cases with less controlled and manipulated variables. In these cases, the condition number shows how much more difficult control becomes as more variables are added.

Though SVD can be used to determine control pairings, this work uses RGA. This method uses the concept of relative gains to both measure process interactions and to determine the most effective pairing of manipulated and controlled variables. The relative gain (λ_{ij}) between a controlled and manipulated variable expresses the ratio of open-loop to closed-loop gain. The relative gains of a system can be arranged into a matrix or array. For a 2x2 system, the relative gain array can be calculated as follows:

$$\Lambda = \begin{bmatrix} \lambda & 1-\lambda \\ 1-\lambda & \lambda \end{bmatrix} \quad \textbf{(4-4)}$$

where

$$\lambda = \frac{1}{1 - \frac{K_{12}K_{21}}{K_{11}K_{22}}} \quad \textbf{(4-5)}$$

and K_{ij} denotes the steady state gain between the output i and the input j. The calculation of relative gain elements becomes more complex as the system size grows. Relative gains with a positive relative gain close to 1 are good for control.[84]

Procedure

A gain matrix was generated for SVD by making small changes (± 0.1 %) in one of the four available manipulated variables (reflux, wall split, side reflux/side product, and steam to reboiler) while keeping the other three variables fixed. The recorded temperature changes were then normalized by the normalized change in manipulated variable (change in manipulated variable divided by initial condition or ± 0.001). The changes in column temperatures were recorded for both the increase and decrease in manipulated variable and averaged. The averaged values became the columns of the gain matrix. Note that the prefractionator temperature changes were not recorded separately from the mainfractionator as was done in other works.[46,62] There was one gain matrix that included all stages and had 36 rows and 4 columns. The gain matrix was decomposed using

MATLAB®'s SVD program. The most sensitive temperatures were identified from the principal components of the matrix of left singular values. The maximum absolute values of the U vectors were chosen as the principal components. These are circled for the reader's convenience (Equation A-14). A similar procedure was followed for the V matrix. Once the most sensitive inputs and outputs were identified, RGA was used to identify the pairing with the least amount of interaction.[5]

Results

Overall, SVD and RGA performed well and did not break-down due to the intensified nature of the dividing wall columns. The combination of SVD and RGA produced a two-point temperature control structure for each case, and the resulting control structures are shown in Figure 4-3. The same control structure was found for three of the four cases. This control structure included a stripping temperature controlled by the steam and a rectifying temperature controlled by the reflux. The specific location of the stripping section temperature changed between cases due to changes in the overall temperature profile in the column. However, all three of these cases are characterized by relatively flat temperature profiles across the wall section leading to sensitive temperatures clustering at the top of the wall and at the base of the column. Case [2MP, C6, Tol/mX] is shown below as an example. A different control structure was suggested for the fourth case. The different level control structure and different product distribution for the isolated trace component case lead to different valves and temperatures being identified as sensitive. Sensitivities and resulting control pairings are dependent upon process conditions. The results for the original model of case [2MP/C6, Tol, mX] are shown in Appendix A. However, an SVD and RGA analysis was performed again after the model was refined to better match the conditions seen on the pilot plant (Chapter 5 and Chapter 6). This resulted in a different control structure, and those results are shown below. The SVD matrices for these cases as well as the results for all other case studies can be found in Appendix A. Composition control was also examined and can be found in Appendix A.

Case study [2MP, C6, Tol/mX]

For case [2MP, C6, Tol/mX], SVD and RGA produces a 2-point temperature control strategy that looks promising. The two temperatures are located in the stripping and rectifying sections, which is fitting given the flat temperature profile across the wall section. It's unclear if three temperatures could be controlled as temperature changes clustered at the top of the wall and at the base of the column. This temperature control pairing is very similar to that used on conventional binary distillation columns using dual end temperature control.[6,75,77]

SVD resulted in the condition numbers shown in Table 4-3. Since a high condition number suggests poor control, it can be concluded that this case is best suited for two temperature controllers and not four.

Table 4-3. Condition Numbers for Temperature SVD of case [2MP, C6, Tol/mX]

System Size	Condition Number
4 x 4	140.32
3 x 3	52.43
2 x 2	36.32

A plot of the left singular values can be used to identify temperatures that are good candidates for control (Figure 4-4, (A-14). While T33 and T35 appear to be the most sensitive temperatures due to their large peaks, these two temperatures are located relatively close to one another. Their proximity makes controlling them simultaneously difficult. T6 appears as a potential alternative candidate for control due to its peak and distance from T33 and T35. Temperatures appear to cluster at the top of the wall on either side and at the base of the column. Therefore, finding third and fourth temperatures for control proves difficult.

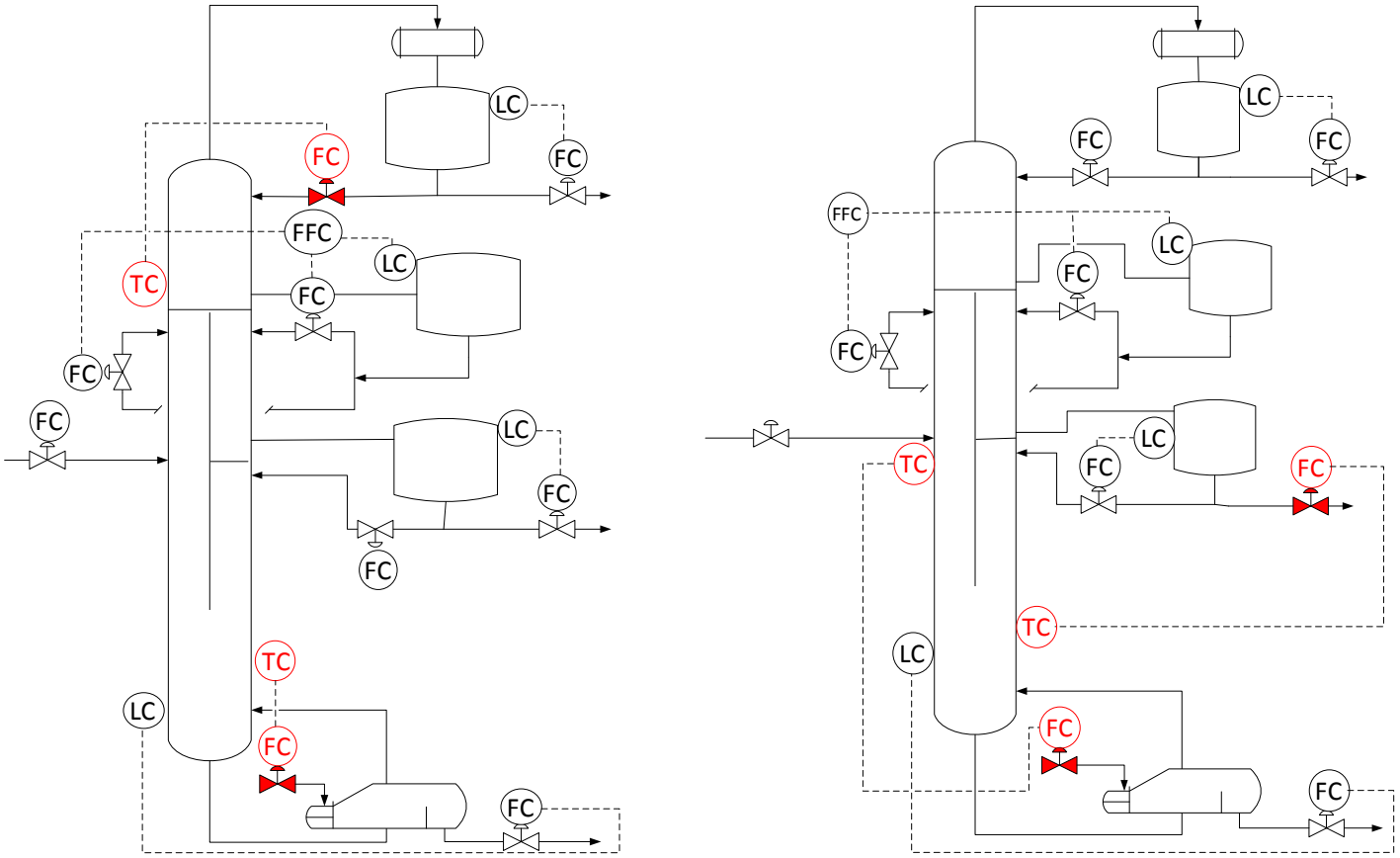

Figure 4-3 – Temperature control structure predicted for cases [2MP, C6, mX], [2MP, C6, Tol/mX], and [2MP, C6/Tol, mX] (left) and that for case [2MP/C6, Tol, mX] (right)

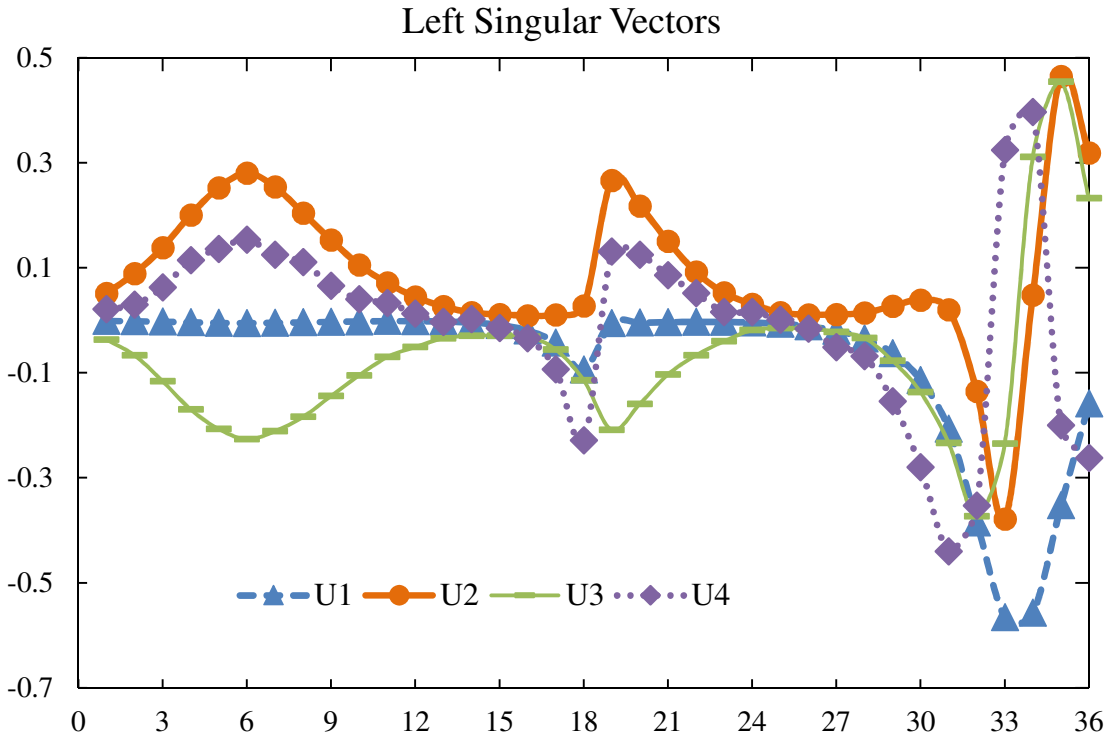

Figure 4-4 – Graphical representation of the four columns of the U matrix. Note that 1-6 are the rectifying temperatures, 7-18 are the prefrac temperatures, 19-30 are the mainfrac temperatures, and 31-36 are the stripping temperatures.

Plotting the difference of the absolute values of the first and second left singular vectors allows sensitivity and interaction to be seen on the same plot.[83] Figure 4-5 suggests stage 6 and stage 22 (T6 and T34 in the model) are the best for control. The sensitivities of T33 and T35 resulted in the temperatures between them being the best for control.

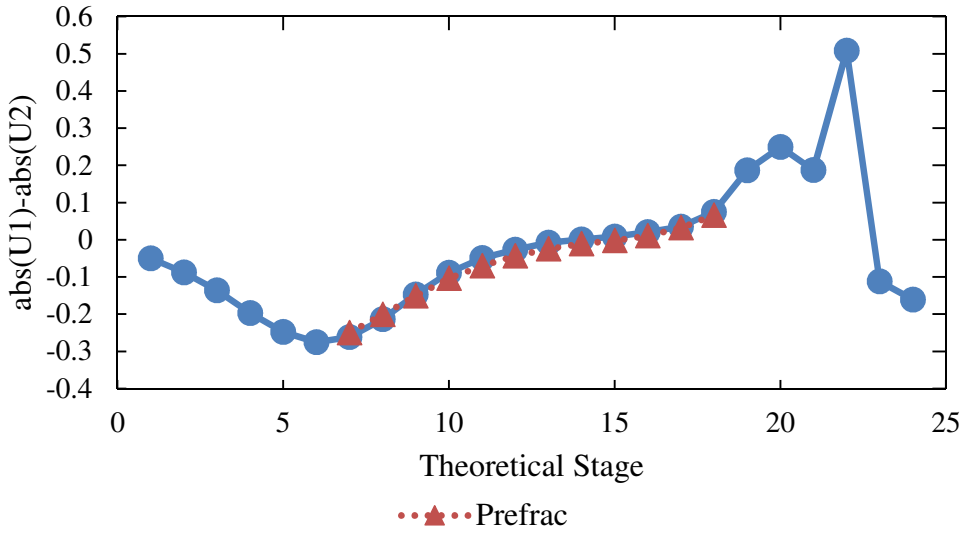

Figure 4-5 – abs(U1) – abs(U2) vs. Theoretical Stage

Extending this idea to the difference of the absolute values of the first three left singular vectors, highlights Stage 23 (T35) as a candidate control temperature in addition to the temperatures that appeared in Figure 4-5 (Figure 4-6). However, the close proximity of T34 and T35 may make them difficult to control simultaneously.

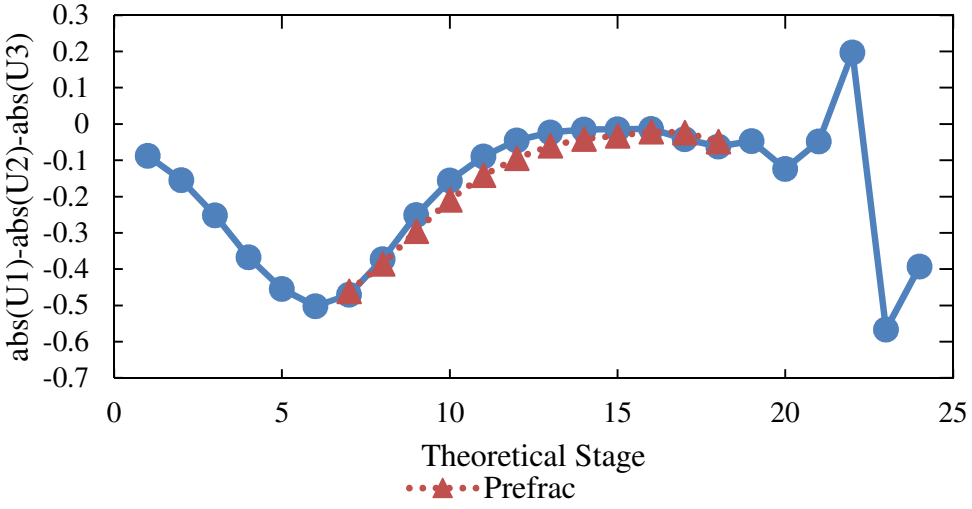

Figure 4-6 – abs(U1) – abs(U2) – abs(U3) vs. Theoretical Stage

The matrix of right singular values (Equation A-14) gives the most sensitive manipulated variables. In order of most to least sensitive, sensitive inputs are steam, wall split, sidedraw reflux, and overhead reflux. However, overhead reflux and wall split have similar values. Both of these inputs are compared in RGA analysis (Equation 4-6). RGA analysis shows that reflux is the better manipulated variable for temperature control. Using reflux results in values that are closer to 1 and pairings that would result in smaller time constants due to the smaller distance between controlled variables and manipulated variables.

$$\Lambda = \begin{matrix} \\ T_{Stripping} \\ T_{Rectifying} \end{matrix} \begin{matrix} \textit{Steam} & \textit{Wall Ratio} \\ \begin{bmatrix} 0.190 & 0.810 \\ 0.810 & 0.190 \end{bmatrix} \end{matrix} \tag{4-6}$$

$$\Lambda = \begin{matrix} \\ T_{Stripping} \\ T_{Rectifying} \end{matrix} \begin{matrix} \textit{Steam} & \textit{Reflux} \\ \begin{bmatrix} 0.995 & 0.005 \\ 0.005 & 0.995 \end{bmatrix} \end{matrix} \tag{4-7}$$

RGA analysis for a 3x3 system produces a feasible though highly interactive control structure (Equation 4-8). The rectifying temperature once again pairs nicely with the reflux. While the pairing of the lower stripping section temperature with steam and higher stripping section temperature with wall split makes sense, the larger RGA values for these pairings suggests a high degree of interaction, as expected. This structure would need to be further tested with disturbances in order to determine its feasibility.

$$\Lambda = \begin{matrix} \\ T_{Lower\ Stripping} \\ T_{Rectifying} \\ T_{Upper\ Stripping} \end{matrix} \begin{matrix} \textit{Steam} & \textit{Reflux} & \textit{Wall Split} \\ \begin{bmatrix} -3.7083 & -0.0269 & 4.7352 \\ 0.0031 & 0.9974 & -0.0005 \\ 4.7052 & 0.0294 & -3.7346 \end{bmatrix} \end{matrix} \tag{4-8}$$

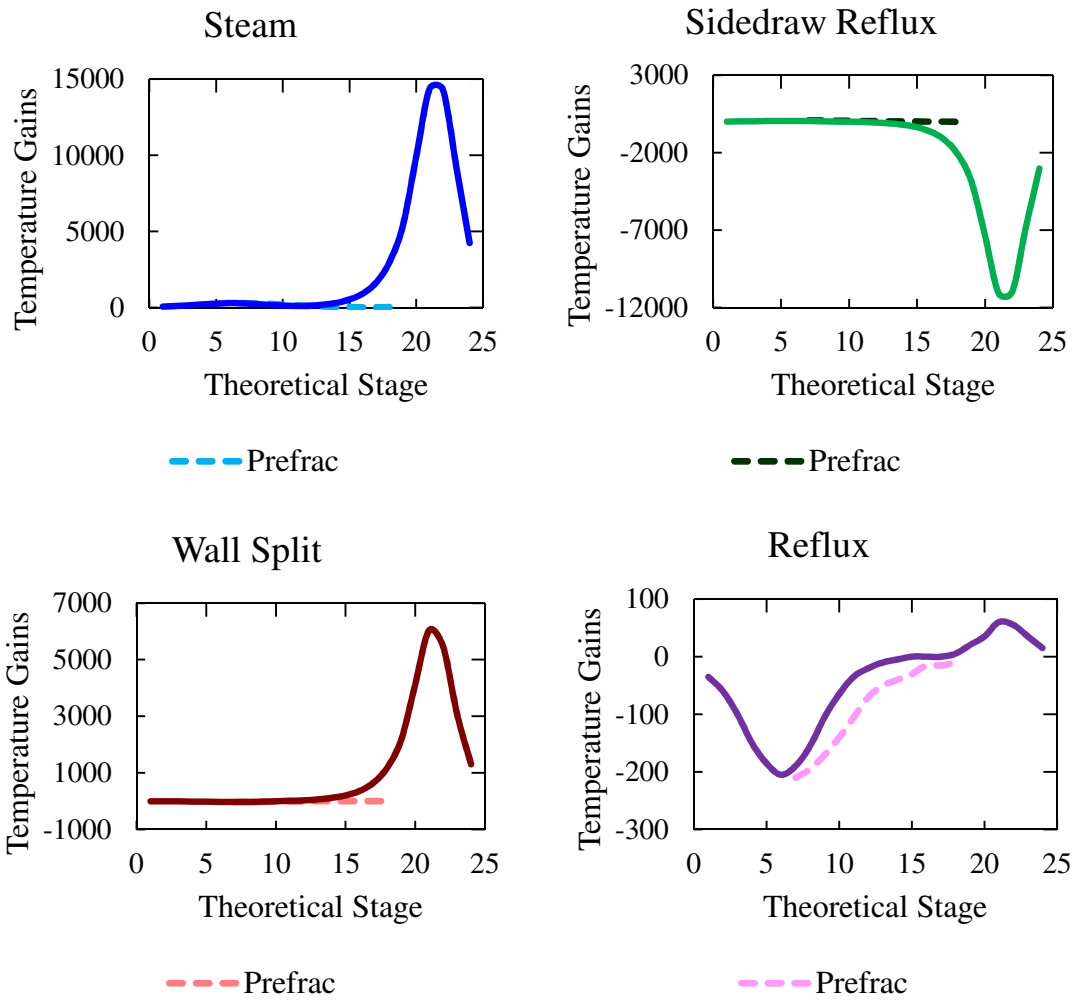

Figure 4-7 – Change in temperature over normalized change in manipulated variable for steam, wall split, sidedraw reflux, and reflux.

Figure 4-7 shows the changes in stage temperatures divided by the normalized change in manipulated variable. These are the columns of the gain matrix that were used for SVD. Temperatures at the base of the column change in response to changes in all manipulated variables. For the steam, sidedraw reflux, and wall split, the temperatures in the base change orders of magnitude more than the other temperatures in the column which

explains why two stripping section temperatures were shown to be the most sensitive. Figure 4-8 further confirms why reflux is a better manipulated variable than wall split for control of a rectifying temperature. Overhead reflux is the only variable that has a large impact on the temperatures in the rectifying section of the column. In order for open-loop impact of the other variables to be seen, the axes must be greatly adjusted. Even then the steam has a larger impact than the wall split, which explains the pairing seen in the RGA.

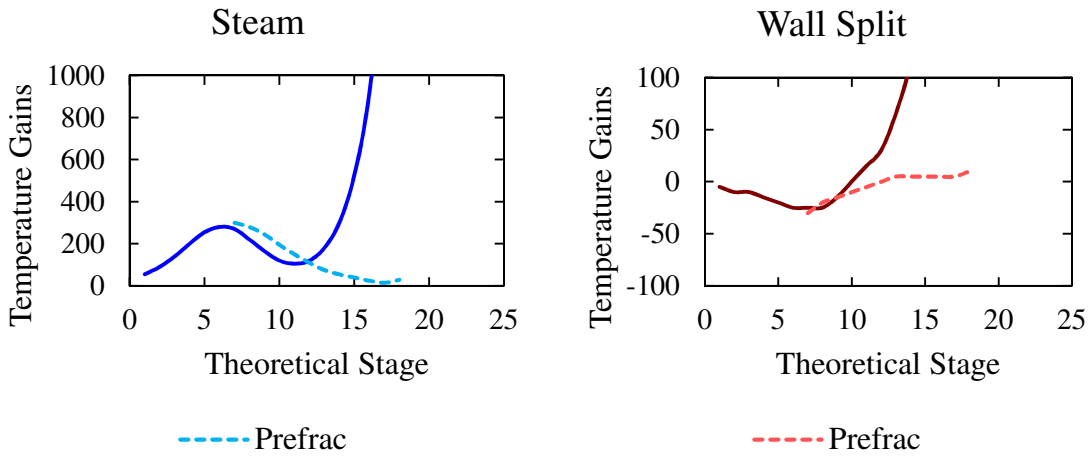

Figure 4-8 – Change in temperature over normalized change in manipulated variable for steam and wall split. Steam affects rectifying temperatures more than the wall split does which explains the RGA pairing of steam with rectifying temperature and wall split with stripping temperature.

Case study [2MP, C6, Tol/mX]

The original model for case [2MP/C6, Tol, mX] resulted in a temperature in the prefractionator section paired with the steam and a temperature in the stripping section paired with the side product flow (Figure 4-3). This control strategy does not seem promising from an intuitive point of view. The temperature controllers would be expected to interact with one another as changes in steam would presumably affect the stripping section temperature. However, this would have to be verified with dynamic testing.

The conditions of the original model did not match those seen on the pilot plant (Figure 4-9), and an alternative control structure was commissioned instead (Chapter 5). After experimental testing, the model was updated to more closely match the conditions seen on the pilot plant on July 19th (Chapter 6), and an SVD and RGA analysis was done on the updated model. Using the updated model, SVD determined that the steam and side product were still the most sensitive inputs to the column (Equation A-34). However, the two most sensitive temperatures changed to a temperature in the stripping section and a temperature in the upper half of the mainfrac (Equation A-35). As can be seen from Figure 4-11, there are a couple of candidate temperatures in the upper mainfrac that could be used for control.

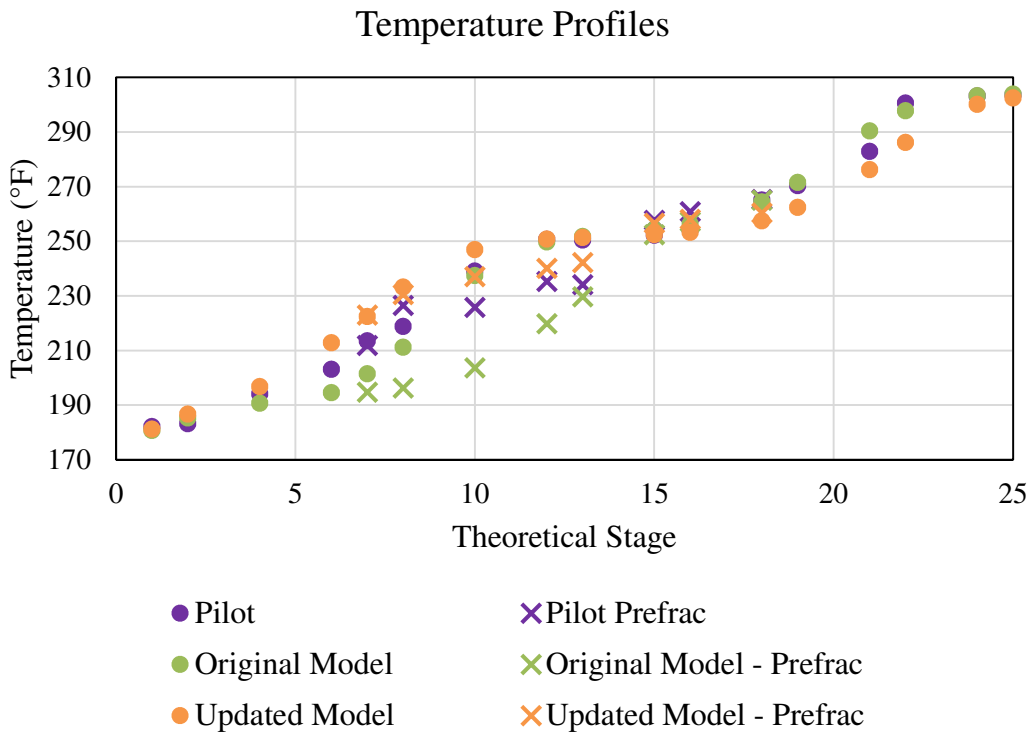

Figure 4-9 – The original model predicted a larger temperature difference than what was seen on the pilot plant

Table 4-4. Condition Numbers for Temperature SVD of case [2MP/C6, Tol, mX]

System Size	Condition Number
4 x 4	244.54
3 x 3	5.52
2 x 2	3.33

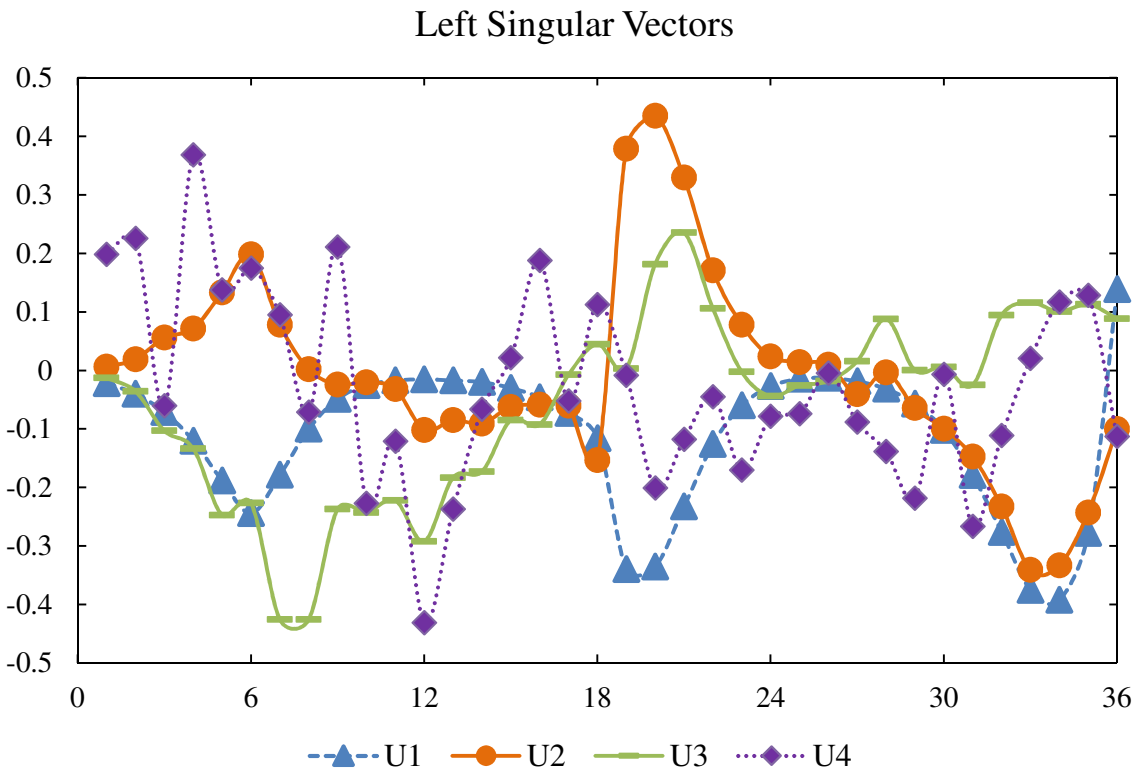

Figure 4-10 – Graphical representation of the four columns of the U matrix. Note that 1-6 are the rectifying temperatures, 7-18 are the prefrac temperatures, 19-30 are the mainfrac temperatures, and 31-36 are the stripping temperatures.

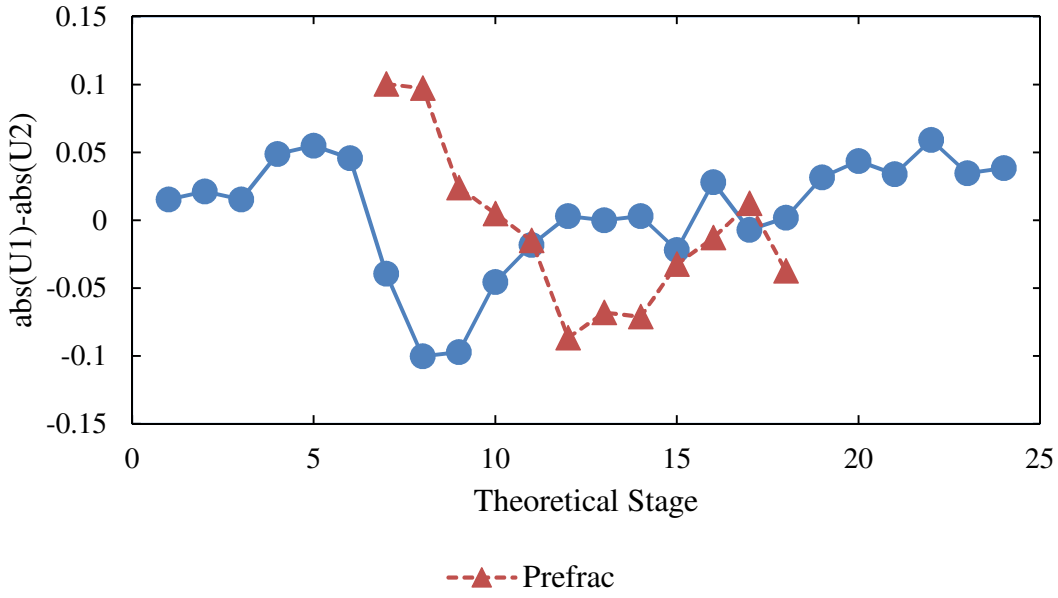

Figure 4-11 – abs(U1) – abs(U2) vs. Theoretical Stage

Steam, overhead reflux, a stripping section temperature (T34), and a mainfrac temperature (TB12) were used in RGA analysis (Equation 4-9). Pairing elements close to 1 resulted in the stripping section temperature paired with the side product and the mainfrac temperature paired with the steam. This is the reverse of the pairing that was used on the pilot column. This is a result of the steady state nature of RGA since the steady state gain between the side product flowrate and the upper mainfrac temperatures is very small (Figure 4-12).

$$\Lambda = \begin{matrix} \\ T_{Stripping} \\ T_{Mainfrac} \end{matrix} \begin{matrix} \begin{matrix} Steam & Side \end{matrix} \\ \begin{bmatrix} 0.000 & 1.000 \\ 1.000 & 0.000 \end{bmatrix} \end{matrix} \quad \textbf{(4-9)}$$

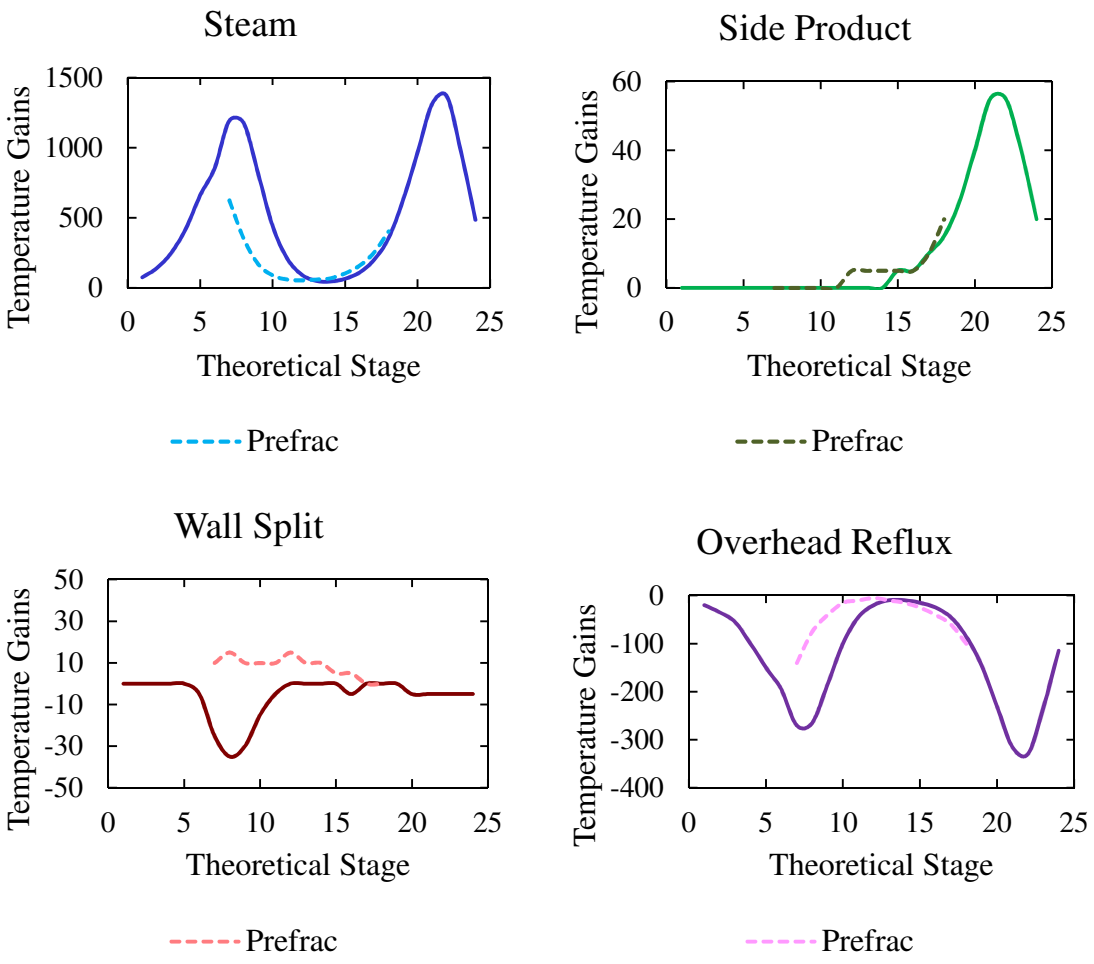

Figure 4-12 – Change in temperature over normalized change in manipulated variable for steam, wall split, sidedraw reflux, and reflux.

CONCLUSIONS

In conclusion, SVD and RGA provide promising results for multiple operating points. For the cases of no trace component, toluene and m-xylene as the bottoms product, and toluene and cyclohexane as the side product, SVD and RGA suggest a 2-point temperature control strategy. This strategy includes a stripping temperature controlled by the steam and a rectifying temperature controlled by the reflux. The specific location of the stripping section temperature changes between cases due to changes in the overall

temperature profile in the column. However, all three of these cases are characterized by relatively flat temperature profiles across the wall section leading to sensitive temperatures clustering at the top of the wall and at the base of the column. This similar distribution of temperatures could explain why RGA analysis did not favor three temperature controllers for any of these cases. Although the two-point temperature control strategy looks promising for all three of these cases, the performance of the controllers would have to be verified with dynamic disturbance testing. For this testing, the sidedraw reflux will be operated in ratio to the feed. The temperature setpoints for these controllers could be obtained from a simulation where the control was supplemented with a composition to temperature cascade strategy since RGA suggested two composition controllers were feasible for all cases.

For the case of pure toluene sidedraw, the combination of RGA and SVD led to multiple different control strategies. The controller pairings that resulted from the original model did not seem favorable from an intuitive point of view. The pairing of stripping temperature with sidedraw flow and prefrac temperature with steam, though supported by the composition control strategy, has the potential for controller interaction and large time constants. The control strategy from SVD and RGA changed after the model was updated to more closely match experimental data from the pilot column. The resulting control pairings resembled that used on the pilot column. However, due to the steady state nature of RGA and the low steady state gain between the side product and the mainfrac temperature, the pairing of controlled and manipulated variables was opposite that used on the pilot column.

The combination of SVD and RGA is one of many methods to determine temperature location and control pairings.[5,6,9] Expecting SVD and RGA to be successful for all distillation columns is not reasonable. Rather, the insight gained from these tools should be combined with engineering knowledge and additional tools as necessary. Therefore, the combination of SVD and RGA working for three out of four cases is promising.

Chapter 5: Experimental Equipment, Procedures, and non-disturbance Results

PILOT PLANT

As previously mentioned, very few experimental studies about dividing wall columns are available in the open literature. While simulation-based studies certainly have their benefits, pilot plant studies allow the physics of the process to be captured without oversimplifying assumptions. Furthermore, pilot studies provide scale-up data without the high capital investment of industrially-sized units.

A pilot dividing wall column originally built as part of the graduate studies of Bailee Roach[40] was used to verify the results from SVD and RGA (Figure 5-1). This chapter highlights the equipment and instrumentation on the pilot column, the run plan followed for the experimental testing of the control structures, and some of the results obtained. Additional information regarding instrumentation and case results can be found in Appendix B.

Figure 5-1 – Pilot DWC viewed from the south

Equipment Setup

The column was operated as a continuous process. The pilot plant dividing wall column setup is shown in Figure 5-2 and includes two 500 gallon tanks, V-600A and V-600B, that served as feed and product tanks, a stainless steel schedule 40 column shell, a total condenser, and a kettle reboiler.

The feed entered the column in the middle of the prefrac. At the top of the wall, there was a total trapout tray (Figure B-2) that redirected all liquid leaving the rectifying section to an external 20 gallon tank, V-630. This tank was operated with an inventory of approximately three gallons to minimize residence time. Using a magnetic drive gear pump, the liquid from this tank was sent back to the column below the trapout tray through two Fisher throttling control valves (one for either side of the wall). This allowed for precise control over the liquid split. The side product was withdrawn in a similar manner. There was a semicircular trapout tray halfway down the product side of the wall that withdrew all liquid to an external 20 gallon tank, V-640. A magnetic drive gear pump and two Fisher throttling control valves were used to drawoff the side product and to send the remaining liquid back to the column as a sidedraw reflux. To combat any heat loss, the prefrac, mainfrac, and sidedraw reflux streams were all heated to the temperature at which they came off the column using steam heaters and temperature controllers. The overhead vapor from the column was condensed using a horizontal shell and tube total condenser operated with cooling water. The resulting liquid stream was collected in an overhead accumulator before it was divided into reflux and distillate flow. The column had a horizontal shell and tube kettle reboiler heated with 130 psia steam (Figure B-1).

Column and Internals

The column was six inches in diameter and 35 feet tall and had 19 feet of mass transfer zone. The column consisted of six flanged sections: rectifying, upper dividing wall, lower dividing wall, stripping, and two connecting sections to the condenser and reboiler. Each section was constructed from 6 inch schedule 40 pipe and insulated with two inch

thick foam glass insulation. To combat heat loss, the tubing lines were also insulated with 7/16 inch thick Speed Wrap® ES insulation. In the horizontal and vertical middle of the column, there was a welded wall fabricated from a 1/4 inch thick 304 stainless steel plate. This plate was uninsulated.

The column contained Mellapak 500Y structured packing. There were seven packing elements both above and below the wall and fourteen elements on either side of the wall each with a packing element height of 8.125 inches. The packing in the dividing wall section was semi cylindrical in shape. A detailed discussion of the column internals and construction can be found in previous work.[40]

Feed and Product Tanks

Three tanks were available as the feed and product tanks, V-600A, V-600B, and V-601. V-600A and V-600B were located in the tank farm while V-601 was located next to the column. Because they are larger, V-600A and V-600B were used as the main product and feed tanks while V-601 was used as a tank dedicated to the trace component. V-600A and V-600B would alternate serving as the product and feed tanks. For example, V-600A would be charged with chemical and serve as the feed tank while an empty V-600B served as the product tank. After V-600A reached low level or before shift change, V-600B was used to feed the column and products were sent to V-600A. Before switching tanks, the product tank would be recirculated for approximately twenty minutes to ensure a homogenous composition. V-601 was filled with pure toluene and was used for feed composition disturbance testing and for inventorying the column with additional toluene when needed.

Two control valves, FC601 and FC600, were used to control the feed to the column (Figure 5-3 and Figure 5-4). FC601 was used to control the feed from V-601. FC600 was located downstream of the mixing point where the feeds from V-601 and the tank farm met and was used to control the overall feed flow to the column. After passing through FC600,

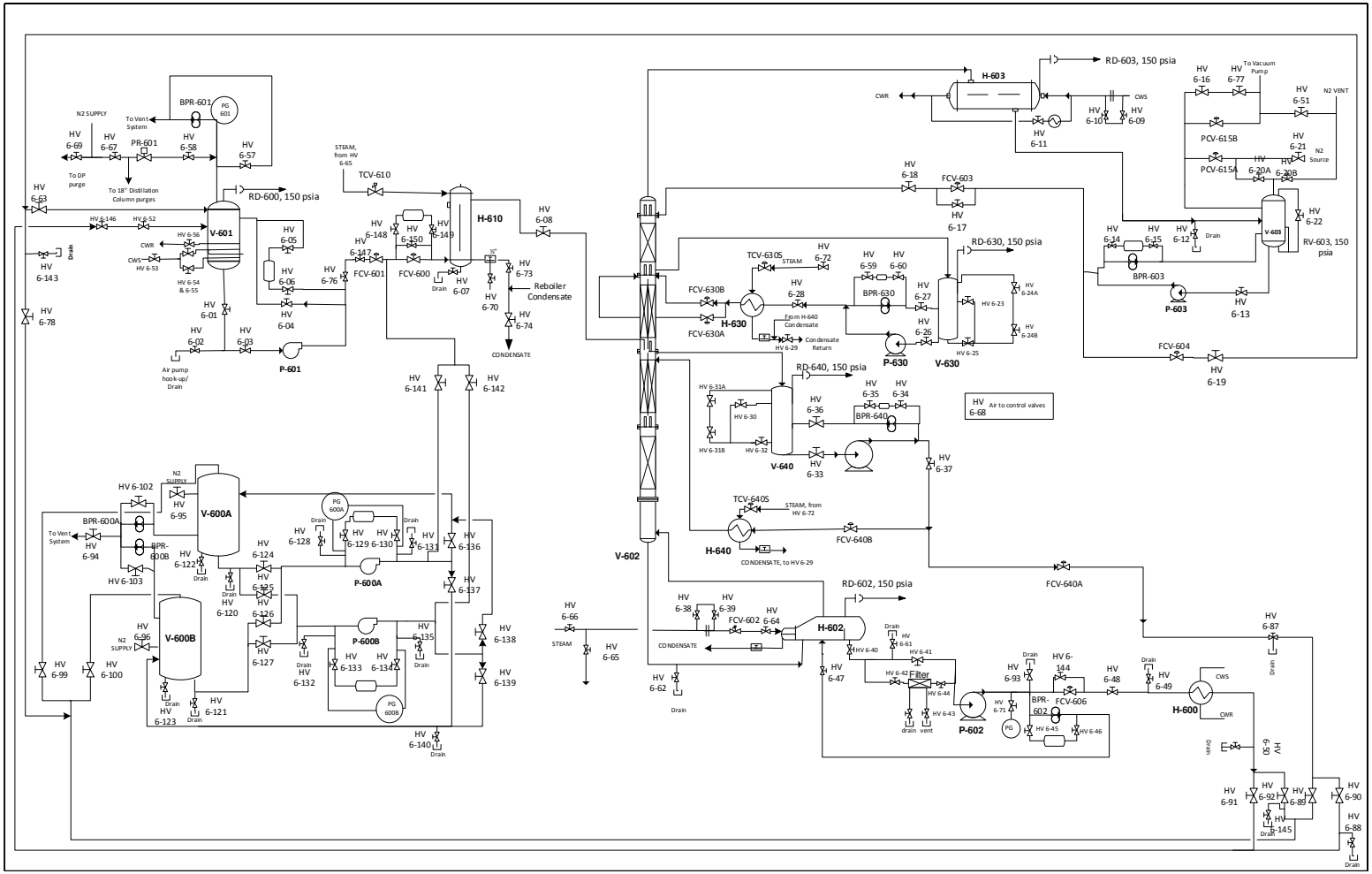

Figure 5-2 – Process flow diagram of dividing wall distillation column

the feed to the column was preheated to its bubbling point using a vertical shell and tube heat exchanger, H-610.

Measurement and Control Devices

The pilot DWC was extensively instrumented thanks to technology donated from Emerson. For ease of installation, numerous wirelessHART transmitters were used. To save on battery life, all wireless devices were configured with an eight second update rate. The column was operated using a DeltaV™ distributed control system (DCS). Operator screens and tuning parameters can be found in Appendix B.

All liquid inlet and oulet streams were measured using Micro Motion™ mass flow meters. In addition, there were three orifice flow meters measuring the water to the condenser and the steam to both the reboiler and the feed preheater. The transmitter for the reboiler steam flow was wireless. The levels of the overhead accumulator, the top of the wall tank, the side product tank, and the column were all measured using Rosemount™ Wireless Level Transmitters. The levels of the larger two feed/product tanks were recorded using wired transmitters. In addition to temperature transmitters on all streams entering and leaving the column, there were 24 Rosemount™ resistance temperature detectors (RTDs) along the column (4 per bed of packing). These were communicated wirelessly through the Rosemount™ Wireless Temperature Multiplexer (TMX).

The column pressure was controlled through the overhead accumulator and a split range controller. Two control valves, one connected to the nitrogen supply and the other connected to the relief system, were used to control the pressure of the column. When the column pressure was under setpoint, the nitrogen valve opened to add nitrogen to the system. Three wireless sensors were used to measure the differential pressure of the column: one to calculate the pressure drop across the entire column, another to measure the pressure drop in the stripping section, and a third to measure the pressure drop in the prefrac section below the feed.

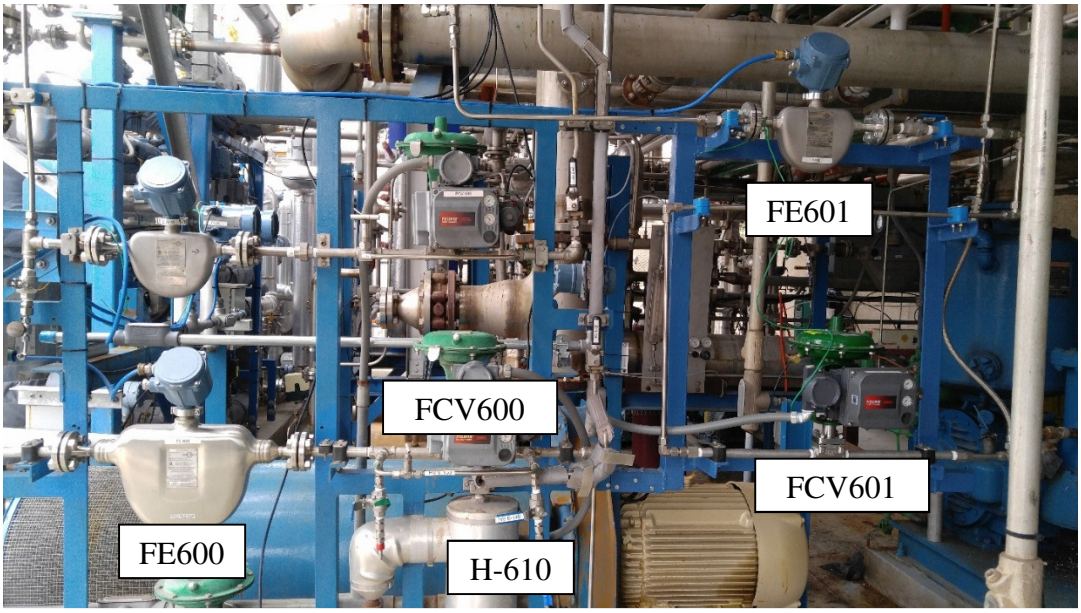

Figure 5-3 – Control valves and MicroMotions for feed tanks

GAS CHROMATOGRAPHY

During operation, liquid samples were collected from the feed, the three product streams, and the top of the wall tank. These samples were analyzed offline using an Agilent 6890 Gas Chromatogram (GC) using hydrogen carrier gas, a Rxi-624 Sil MS fused Silica column and a Flame Ionization Detector (FID). During steady state operation, samples were collected every two to three hours. During dynamic testing, samples were taken every hour. Additional samples were taken on an as needed basis. The following section outlines the operation of the GC. Information regarding method conditions, method development, and calibration can be found in Appendix B.

GC Operation

Samples were diluted in methanol before being injected into the GC. Using a 3 mL plastic pipette, two drops of sample were placed in 10 mL of methanol. After mixing the prepared sample, 0.3 µL was manually injected into the GC. Manually injecting samples requires consistent technique. Hesitating at the injector inlet caused loss of light materials

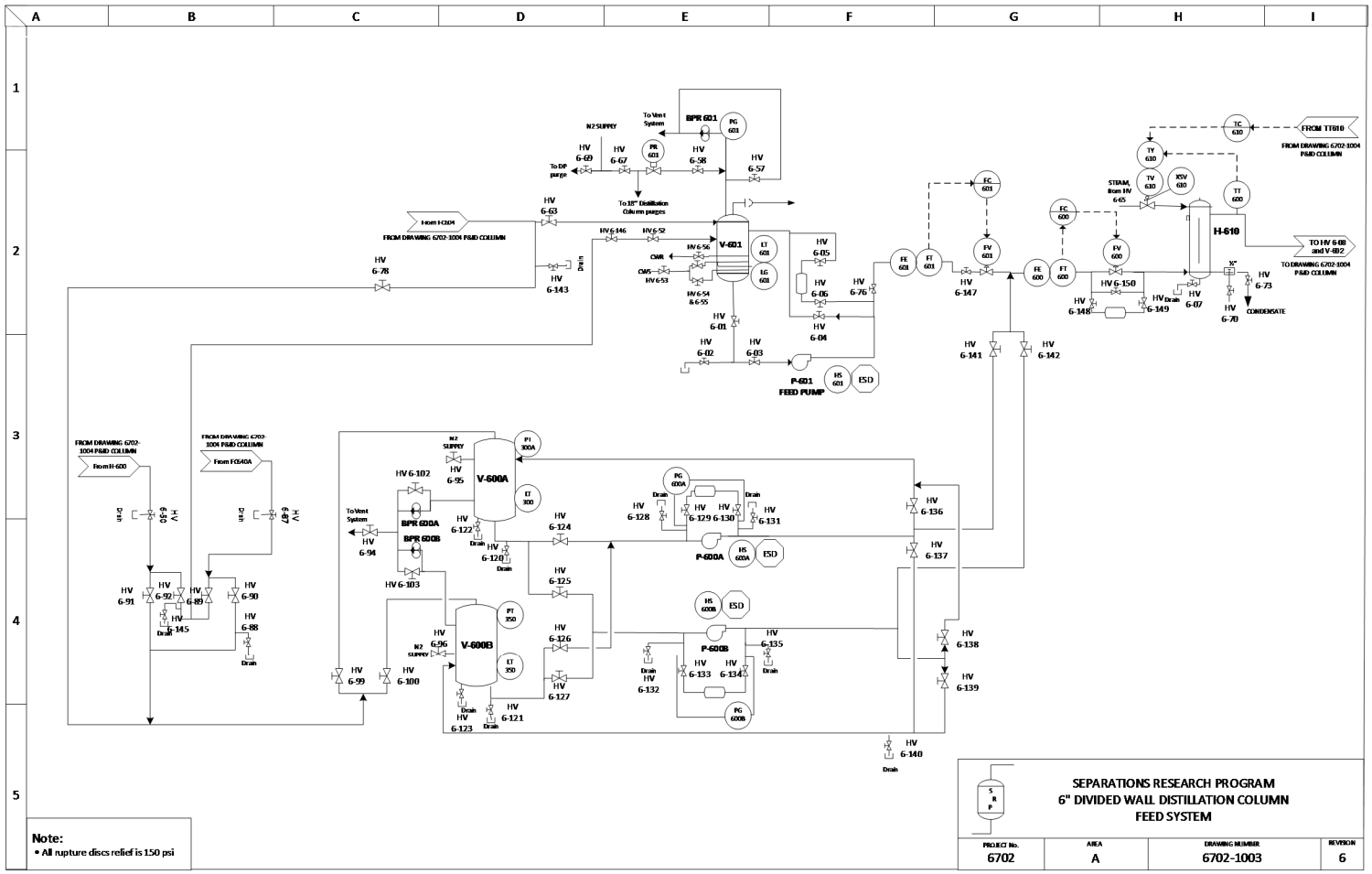

Figure 5-4 – Feed system piping and instrumentation diagram

while poor injection technique or improper removal of the syringe resulted in loss of heavier components. To verify that a complete injection entered the column, methanol area counts were tracked. For a 0.3 μL injection, a typical methanol area count was in the range of $3*10^7$. A bad injection could sometimes affect subsequent samples. Therefore, a methanol blank was run in between different samples. Samples were analyzed two to three times to ensure reproducibility.

RUN PLAN OVERVIEW

A successful campaign was run in July 2017 on the pilot scale dividing wall column to test the control configurations determined by SVD and RGA (Chapter 4). Table 5-1 summarizes the simplified run plan. The start and end times listed include start-up, shutdown, setpoint changes, and controller tuning in addition to steady state. Table 5-2 summarizes the control schemes used. To transition between steady states, setpoints of select controllers were ramped in DeltaV™. Further data and analysis for each particular case is included in the succeeding sections and Appendix B. The case [2MP/C6, Tol, mX] was ran twice to allow for disturbance testing. The data from July 19th is discussed below while the data from July 25th can be found in Appendix B.

Table 5-1. Outline of pilot campaign

Start Time	End Time	Objective
7/13/2017 7:30	7/14/2017 8:30	[2MP, C6, mX]
7/16/2017 16:00	7/17/2017 11:00	[2MP, C6, mX]
7/17/2017 12:00	7/17/2017 14:00	Addition of toluene
7/17/2017 14:00	7/18/2017 8:50	[2MP, C6, Tol/mX]
7/18/2017 8:50	7/18/2017 10:20	Transition toluene from bottoms to side
7/18/2017 10:20	7/19/2017 6:30	[2MP, C6/Tol, mX]
7/19/2017 6:30	7/19/2017 15:00	Transition cyclohexane from side to distillate
7/19/2017 15:00	7/20/2017 7:30	[2MP/C6, Tol, mX]
7/20/2017 7:30	7/20/2017 12:00	Step change in reflux
7/20/2017 12:00	7/20/2017 16:00	Step change in top of wall ratio
7/25/2017 6:00	7/26/2017 6:00	[2MP/C6, Tol, mX]
7/26/2017 6:00	7/26/2017 16:30	Feed composition disturbance testing

Table 5-2. Summary of temperature controllers

Case	Temperature Controller #1		Temperature Controller #2	
	Location	Setpoint	Location	Setpoint
[2MP, C6, mX]	TT60710	163°F	TT6071	202.5 °F
[2MP, C6, tol/mX]	TT60710	166°F	TT6071	210°F
[2MP, C6/tol, mX]	TT60710	167°F	TT6072	270°F
[2MP/C6, tol, mX]	TT6077B	220°F	TT6072	270°F

RESULTS

Case [2MP, C6, Tol/mX]

Using the control configuration shown in Figure 4-3, the column was operated with the toluene trace component as part of the bottoms product. The steady state conditions and temperature profile for this case study are shown in Figure 5-5 and Figure 5-6, respectively. The compositions shown are the average of multiple samples over the course of six hours. As expected from SVD and RGA, the temperature profile was mostly flat through the wall section. Because of this, two temperature controllers were sufficient to keep the column steady. The stripping section temperature controller maintained the separation between toluene and cyclohexane while the rectifying section temperature controller maintained the separation between 2-methylpentane and cyclohexane. The sidedraw reflux was set in local automatic flow control at the value used in the initial simulation for SVD and RGA testing. Though not confirmed with dynamic testing, the sidedraw reflux sets the liquid traffic in the column. Increasing the sidedraw reflux flow would temporarily lower the stripping section temperature causing the steam to increase to bring this temperature back to setpoint. Increased steam in the column would increase the liquid traffic and increase the rectifying temperature. However, the overhead reflux would increase to bring the rectifying temperature controller back to setpoint therefore steadying out the column. The steady state performance of the temperature controllers is shown in Figure 5-7 and Figure 5-8. PV designates the present value of the controlled variable or process variable, SP designates the controller setpoint, and MV designates the manipulated variable of the controller.

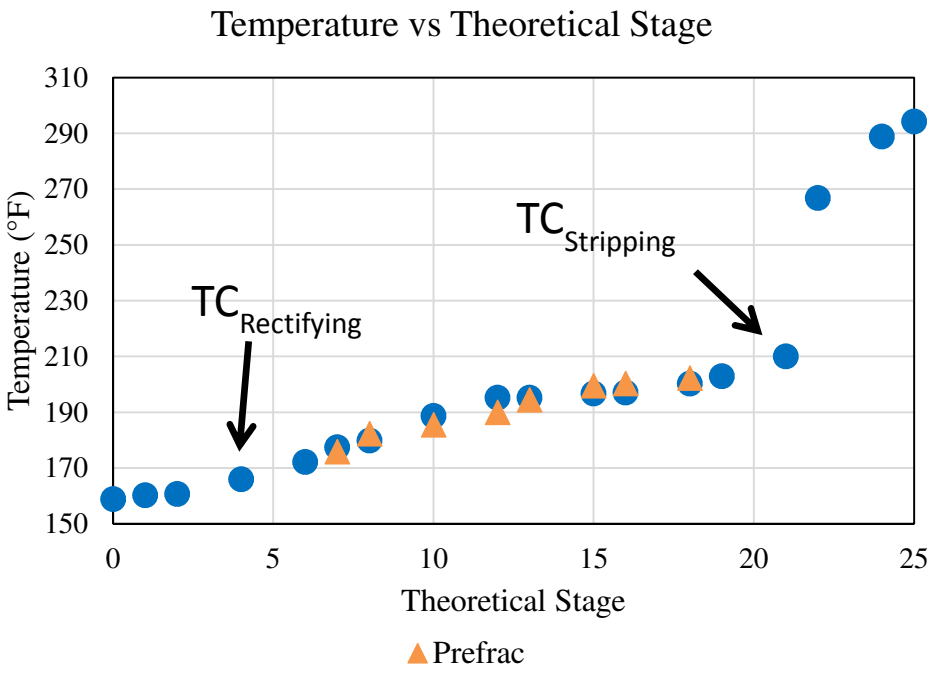

Figure 5-5 – Temperature profile for case [2MP, C6, Tol/mX]

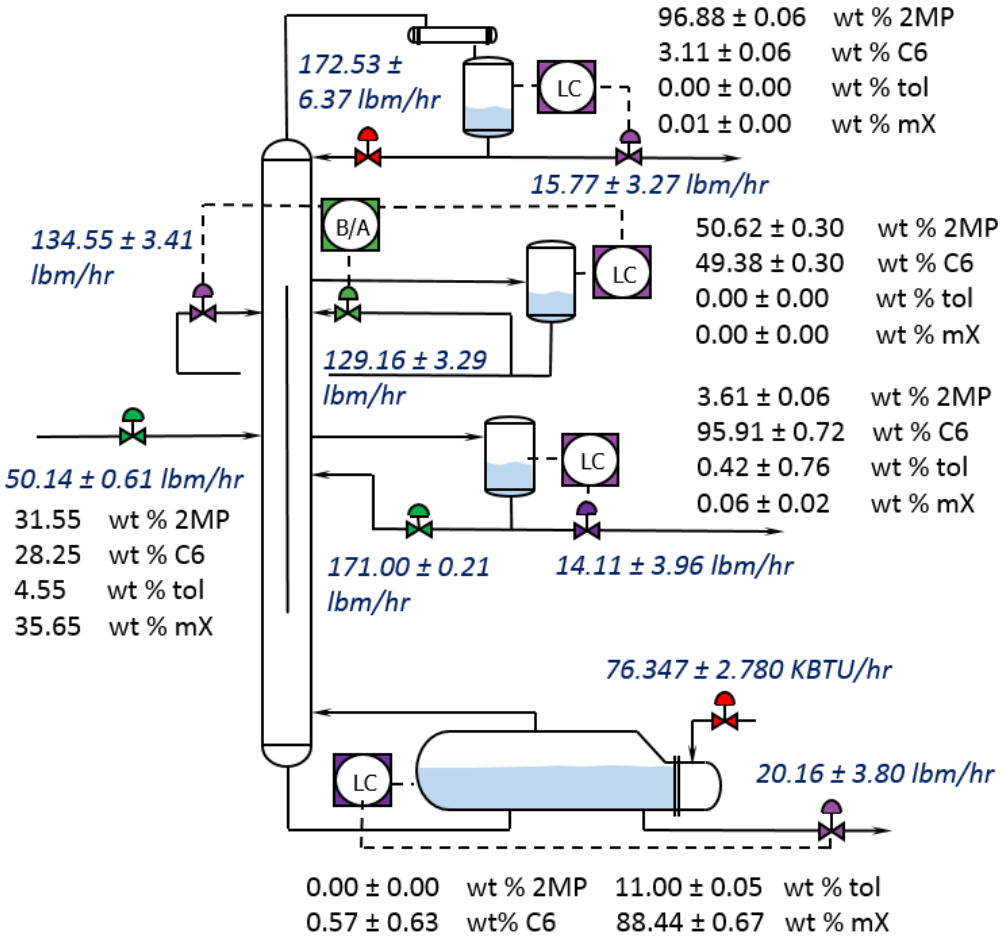

Figure 5-6 – Steady state conditions for [2MP, C6, Tol/mX]. Purple valves are used for level control, green valves are in local automatic flow control, and red valves are manipulated variables for temperature control.

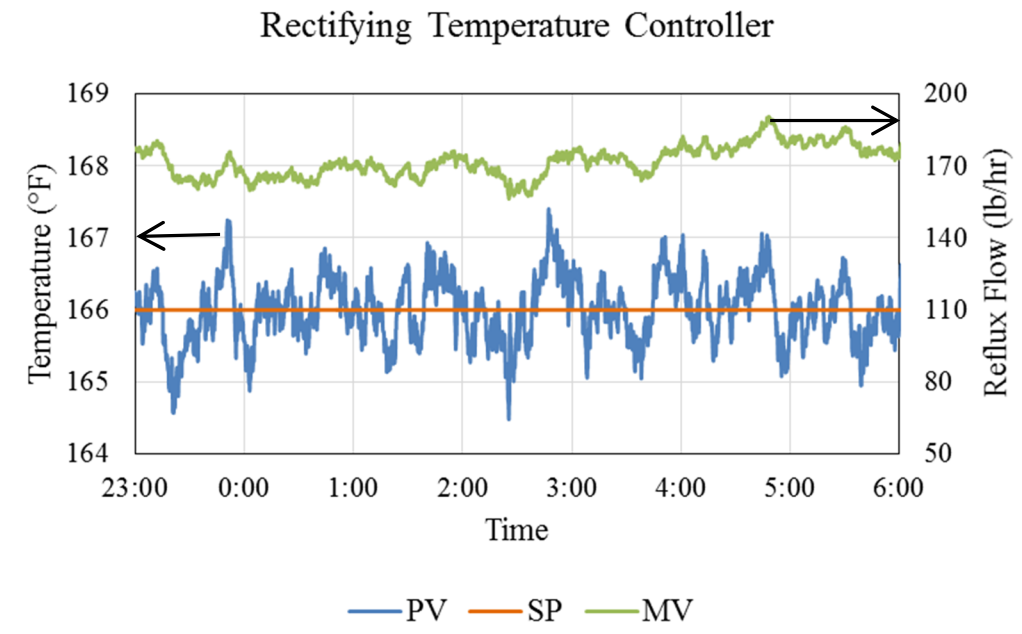

Figure 5-7 – Rectifying temperature controller for case [2MP, C6, Tol/mX]

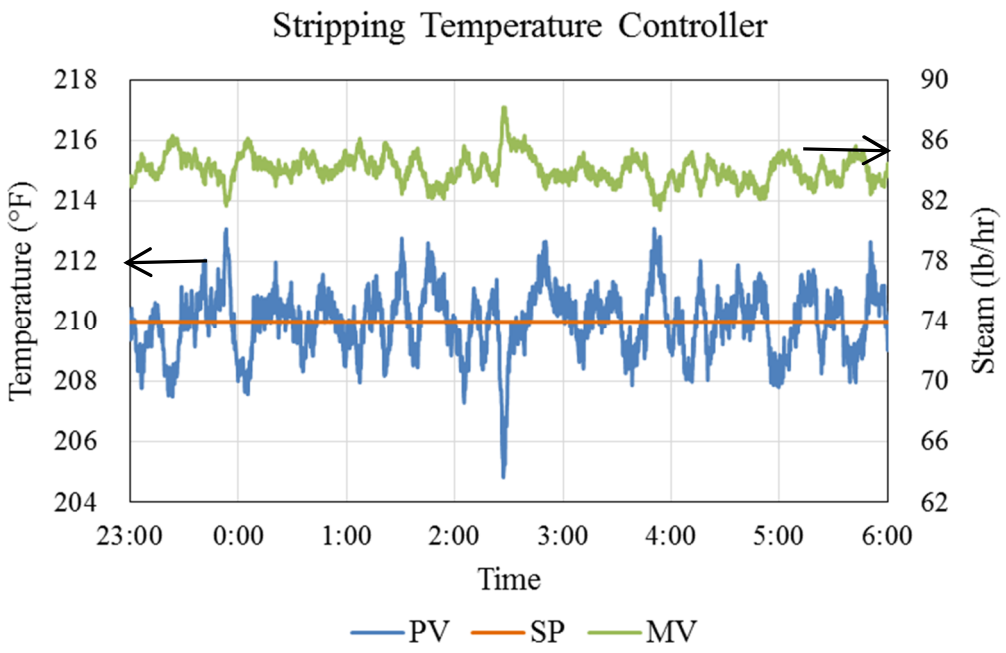

Figure 5-8 – Stripping temperature controller for case [2MP, C6, Tol/mX]

The material balance flows and column temperatures are shown in Figure 5-9 through Figure 5-13. The tuning of the level loops was changed from case [2MP, C6, mX]; however, some oscillations remained. This is believed to be part of the column's nature and does not interfere with operation. Because the feed had been previously used for the three component testing (Appendix B) and did not yet have the desired toluene composition, V-601 was used to supplement the feed. The overall feed to the column was still 50 lbm/hr. However, the feed came from two sources and had to be sampled across the feed valve. This sampling caused a minor process upset at approximately 2:30am when the feed flow spiked though this data was not used to calculate steady state averages. The spike in feed flow had the largest effect on the bottom half of the column decreasing column temperatures and increasing the bottoms flow rate. However, the controls were able to bring the column back to steady state relatively quickly.

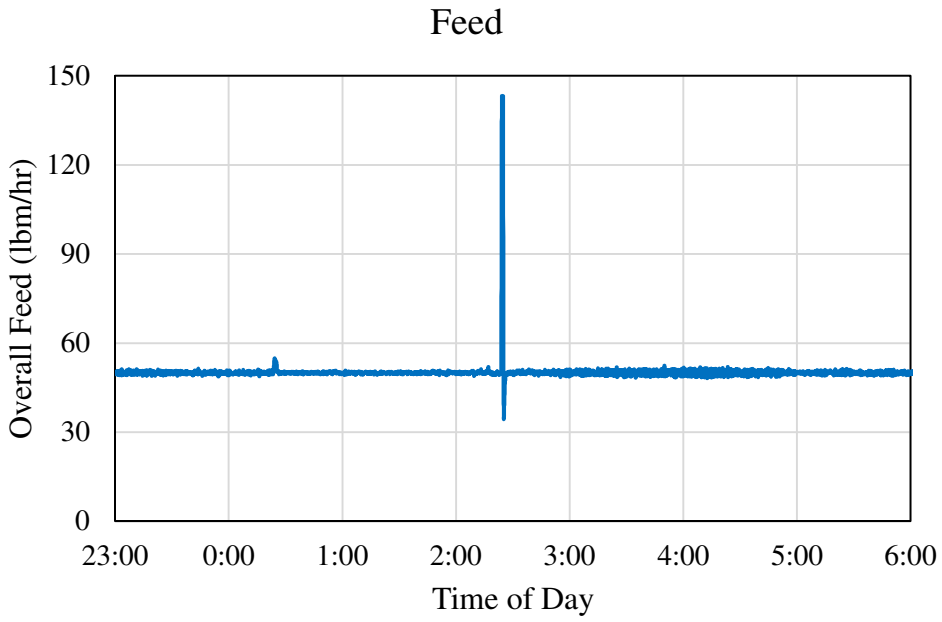

Figure 5-9 – Feed flow for case [2MP, C6, Tol/mX]. The spike close to 2:30 am was due to problems when taking a feed sample.

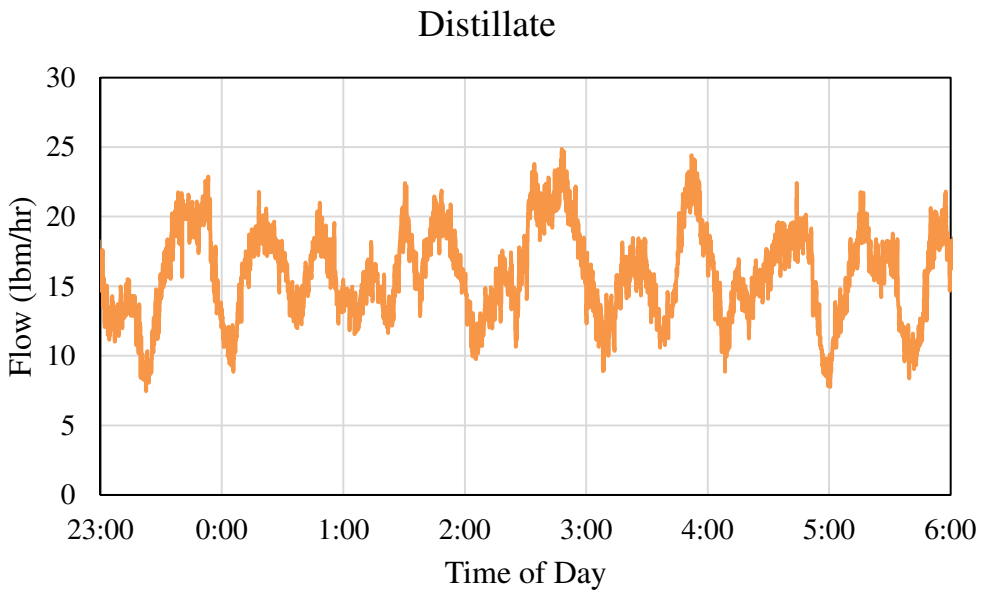

Figure 5-10 – Distillate flow used to control reflux drum level for case [2MP, C6, Tol/mX]

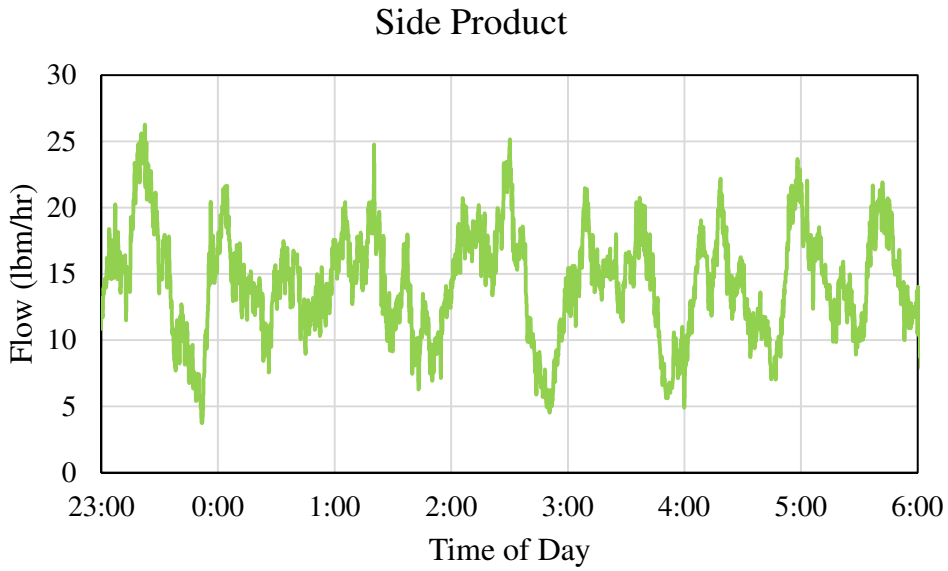

Figure 5-11 – Side product used to control side tank level for case [2MP, C6, Tol/mX]

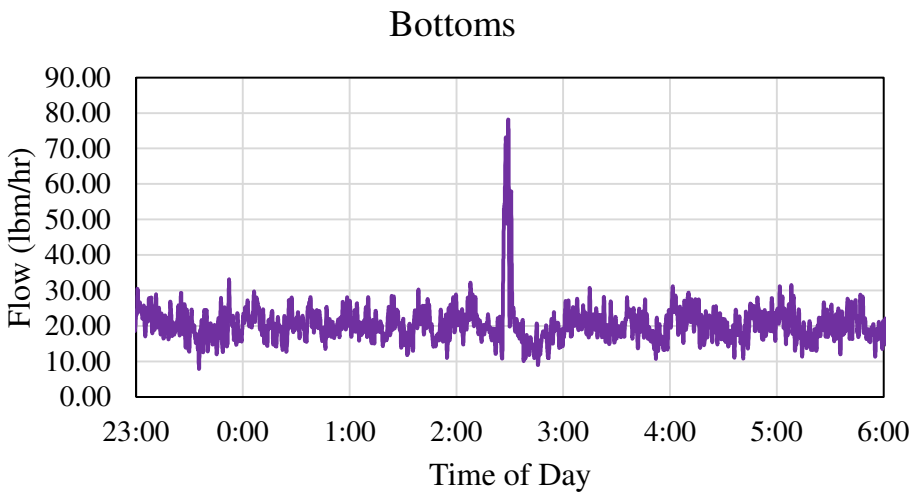

Figure 5-12 – Bottoms product used to control column level for case [2MP, C6, Tol/mX]. The spike close to 2:30 am was due to the increase in feed flow caused by sampling issues.

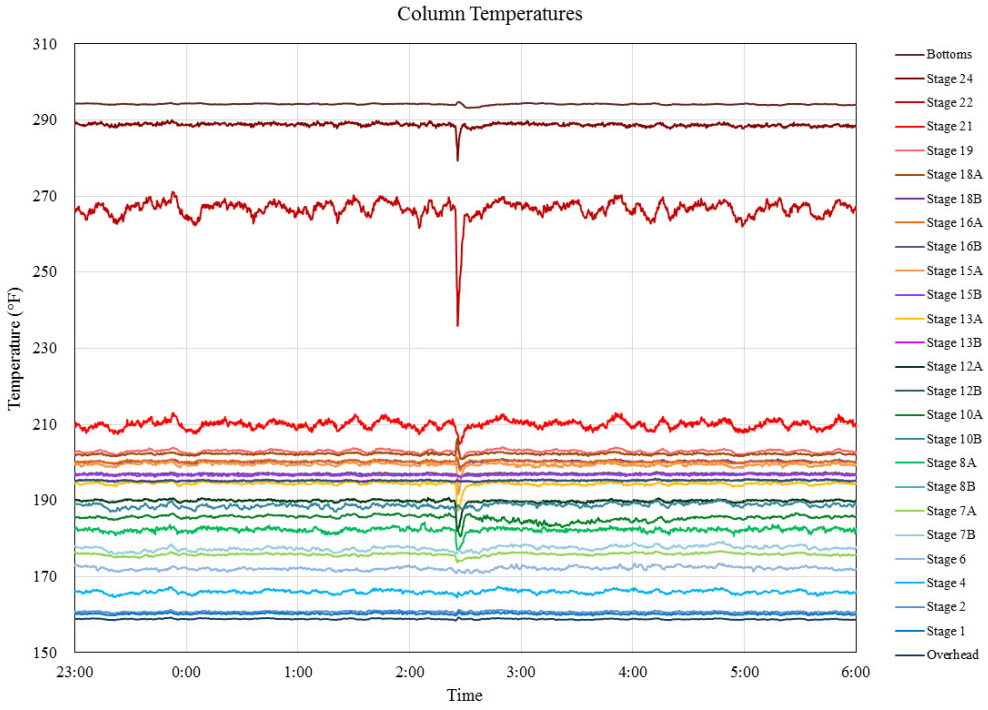

Figure 5-13 – All column temperatures for case [2MP, C6, Tol/mX]

Transition from Case [2MP, C6, Tol/mX] to Case [2MP, C6/Tol, mX]

To move the toluene from the bottoms product to the side, controller setpoints were ramped in DeltaV™ over an hour and a half (Table 5-3). The target setpoints for the controllers was determined from the initial steady state simulation used for SVD and RGA. The wall split was decreased to allow more reflux on the prefrac side (Figure 5-14), and the side reflux was decreased to allow more toluene to move up the side product side of the wall (Figure 5-15). The setpoint of the stripping section temperature controller was increased to purify the bottoms product (Figure 5-16). As the toluene moved from the base of the column to the side product, the temperature profile increased as well (Figure 5-17).

Table 5-3. Transition from [2MP, C6, Tol/mX] to [2MP, C6/Tol, mX]

Loop	Initial	Final	Ramp
Wall Split	0.96	0.62	-0.000063 /s
Side Reflux	171 lbm/hr	91.5 lbm/hr	-0.0147222 lbm/hr/s
Stripping Temperature	210°F	268°F	0.0107407 °F/s

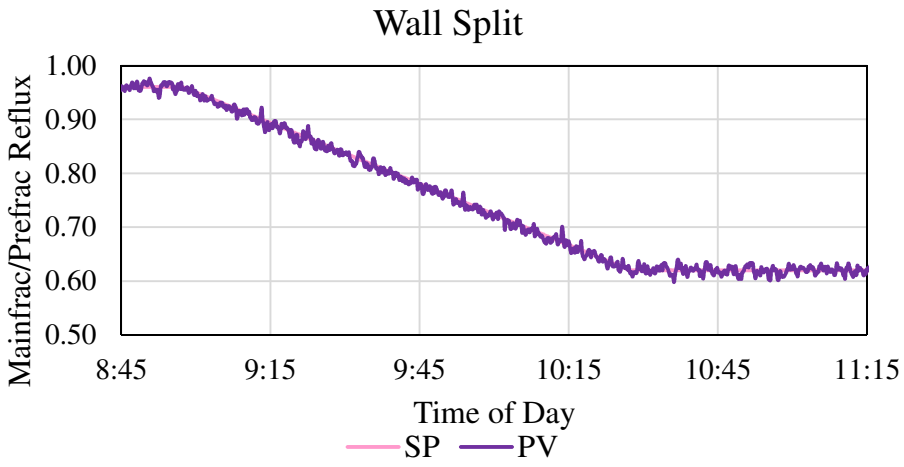

Figure 5-14 – Wall split ramp to transition from [2MP, C6, Tol/mX] to [2MP, C6/Tol, mX]

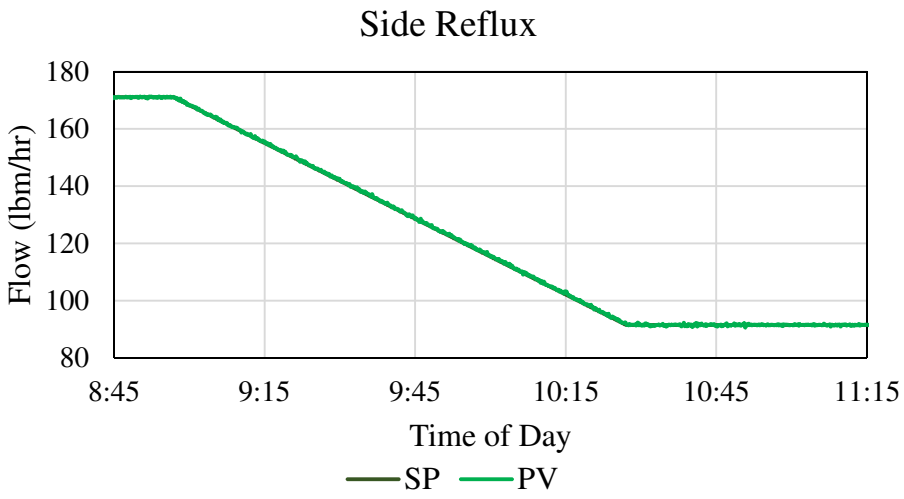

Figure 5-15 – Side reflux ramp to transition from case [2MP, C6, Tol/mX] to [2MP, C6/Tol, mX]

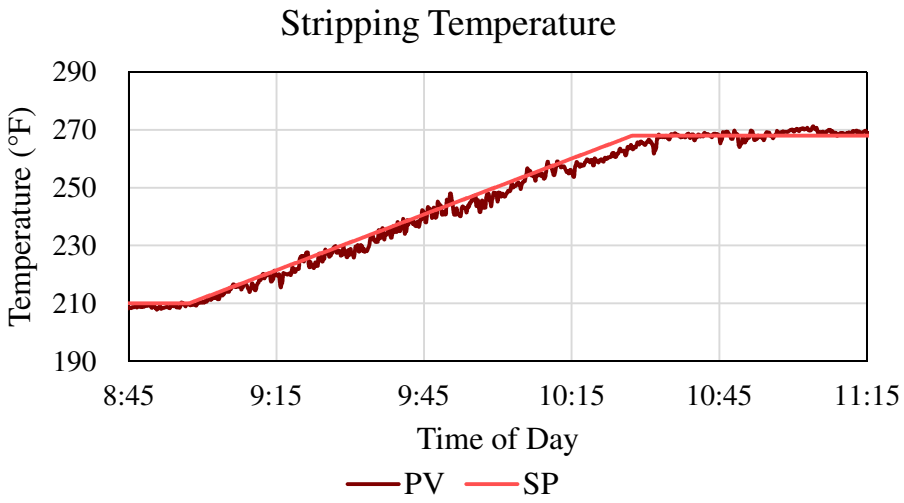

Figure 5-16 – Ramp in stripping temperature to transition toluene out of the bottoms to the side product

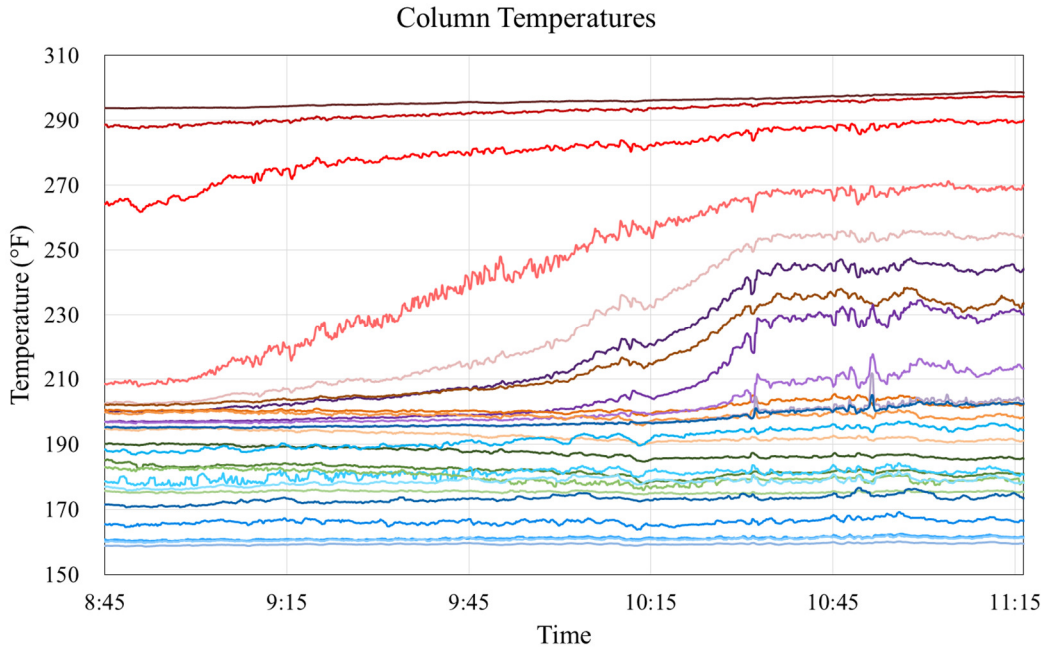

Figure 5-17 – Increase in stripping (shades of red) and mainfrac (shades of purple) temperatures as toluene moves from base of column to side product

During this transition, the two temperature controllers performed well. They were both able to reach their new setpoints without a high degree of interaction (Figure 5-18 and Figure 5-19). Even though the setpoint of the stripping section temperature was increased and the controller was reverse acting, the steam to the column actually decreased. This was a result of changing the wall split. The impact of the wall split on column operation and energy consumption is further discussed in later chapters (Chapter 8).

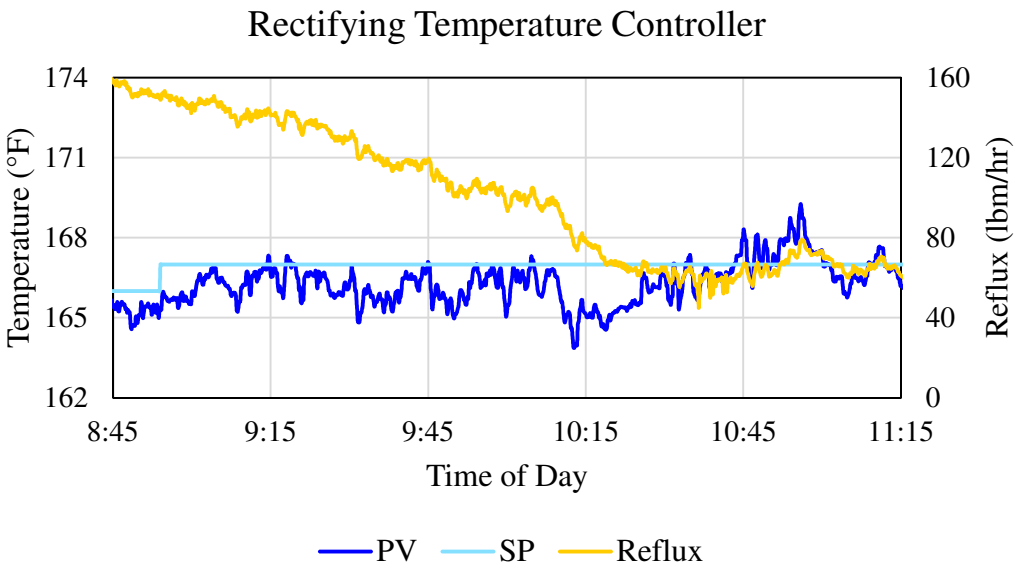

Figure 5-18 – Rectifying section temperature controller during transition from toluene in the bottoms product to side product

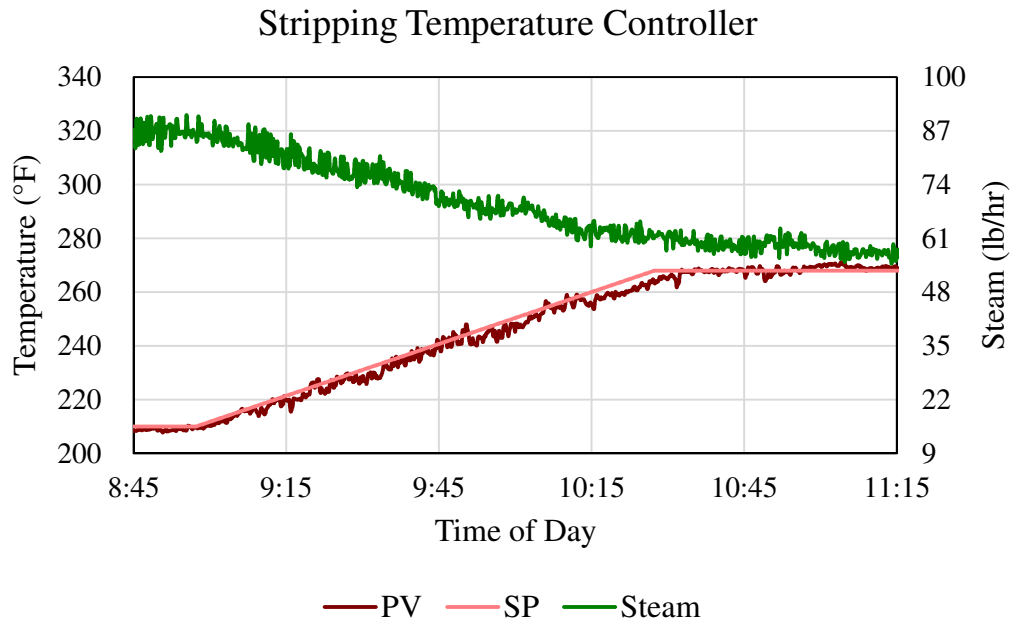

Figure 5-19 – Stripping section temperature controller during transition from toluene in the bottoms product to side product

Case [2MP, C6/Tol, mX]

Case [2MP, C6/Tol, mX] was operated with the same two-point temperature control strategy as was case [2MP, C6, Tol/mX]. Compared to the previous case, the location of the stripping temperature controller was shifted closer to the bottom of the wall. This was done because the change in bottoms composition created a flatter temperature profile at the bottom of the stripping section that was no longer good for control (Figure 5-21). The two temperature controllers were sufficient to keep the column steady, and their performance is shown in Figure 5-22 and Figure 5-23.

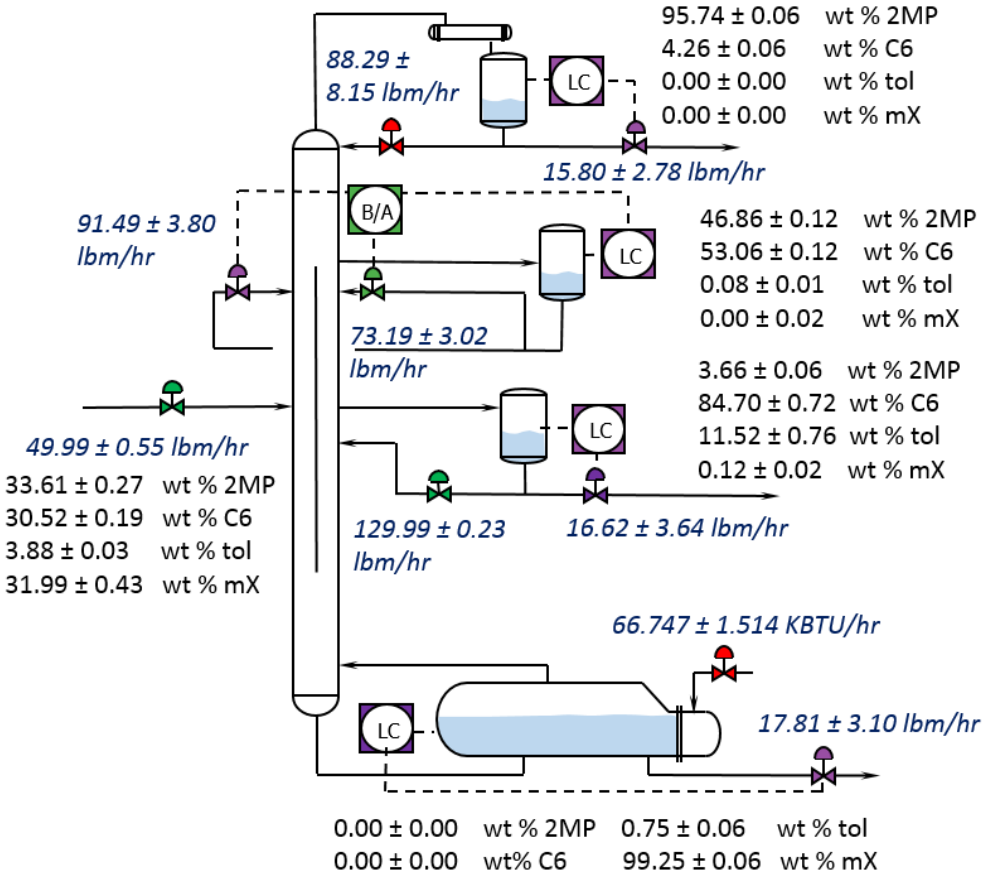

Figure 5-20 – Steady state conditions for [2MP, C6/Tol, mX]. Purple valves are used for level control, green valves are in local automatic flow control, and red valves are manipulated variables for temperature control.

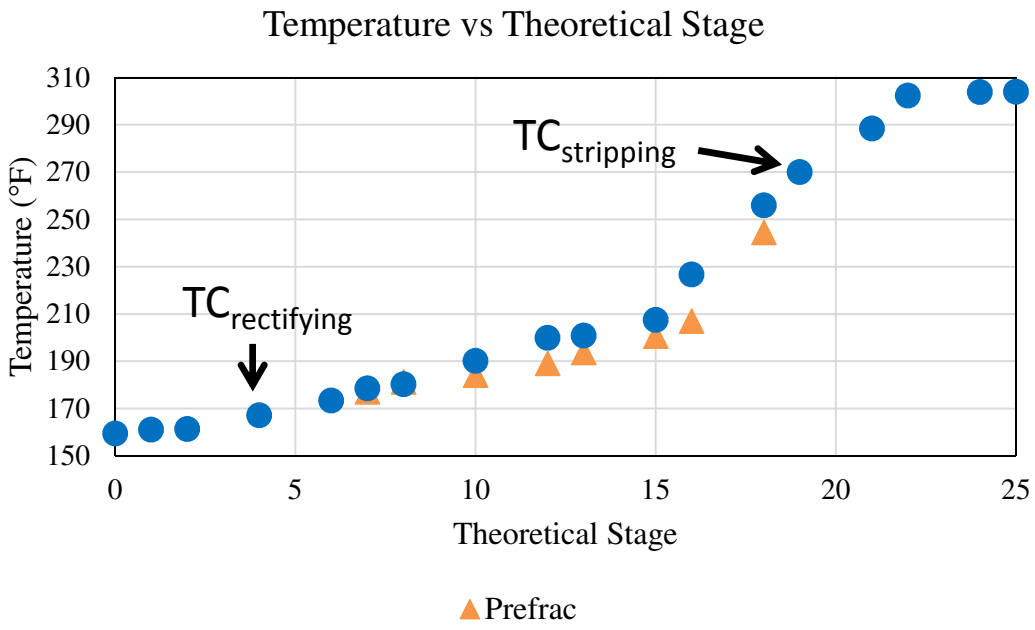

Figure 5-21 – Temperature profile for case [2MP, C6/Tol, mX]

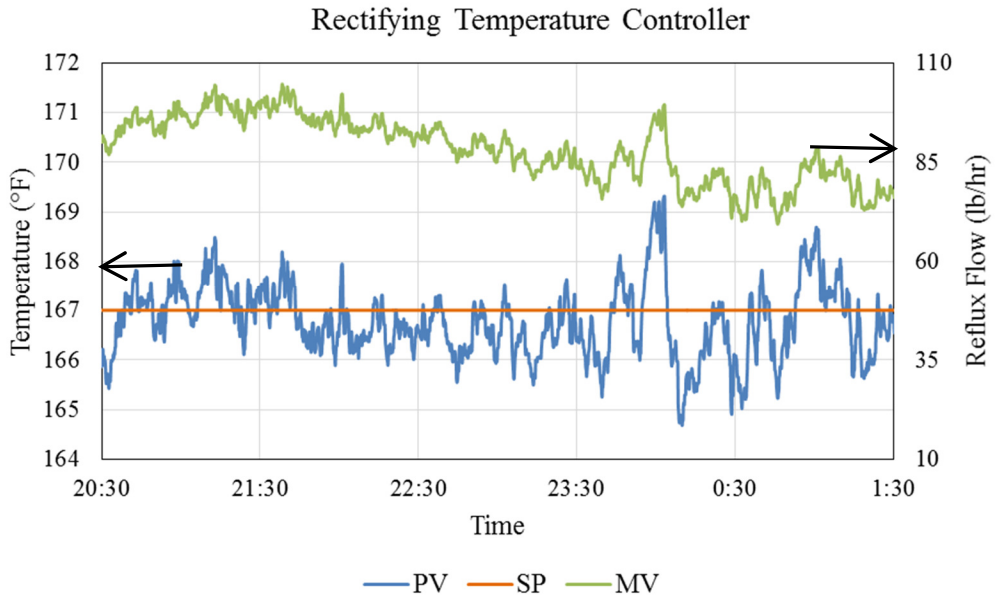

Figure 5-22 – Rectifying temperature controller for case [2MP, C6/Tol, mX]

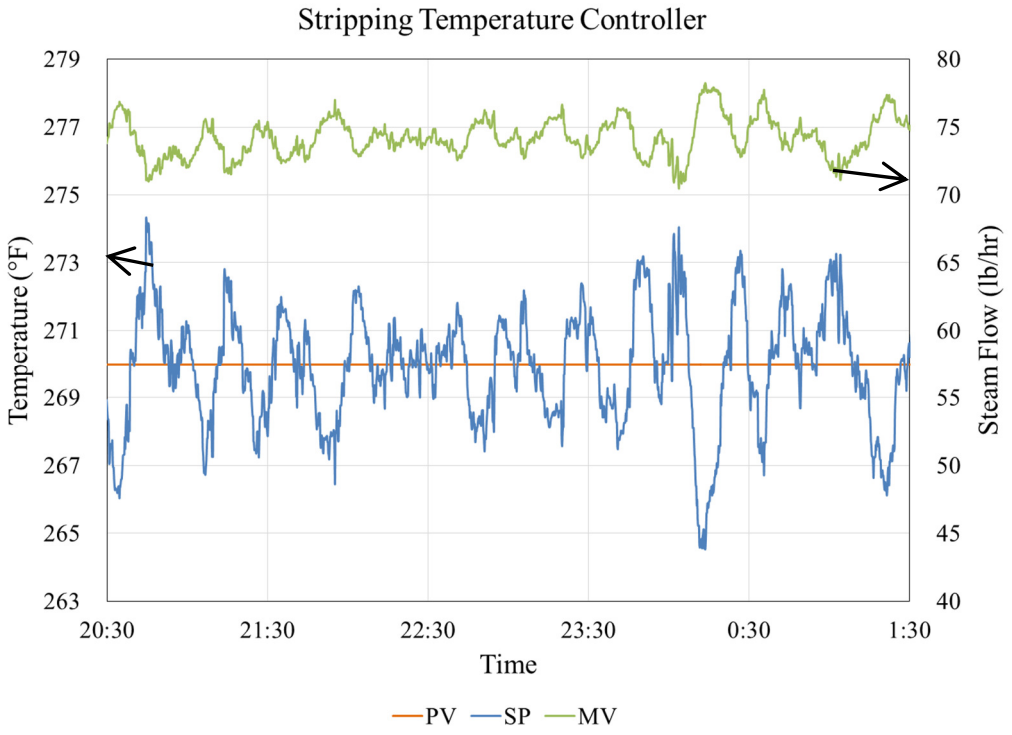

Figure 5-23 – Stripping temperature controller for case [2MP, C6/Tol, mX]

The material balance flows showed slight oscillation which can be seen in the column temperatures (Figure 5-24 through Figure 5-28). However, the steady compositions and temperature controllers indicate that these oscillations did not negatively impact the column.

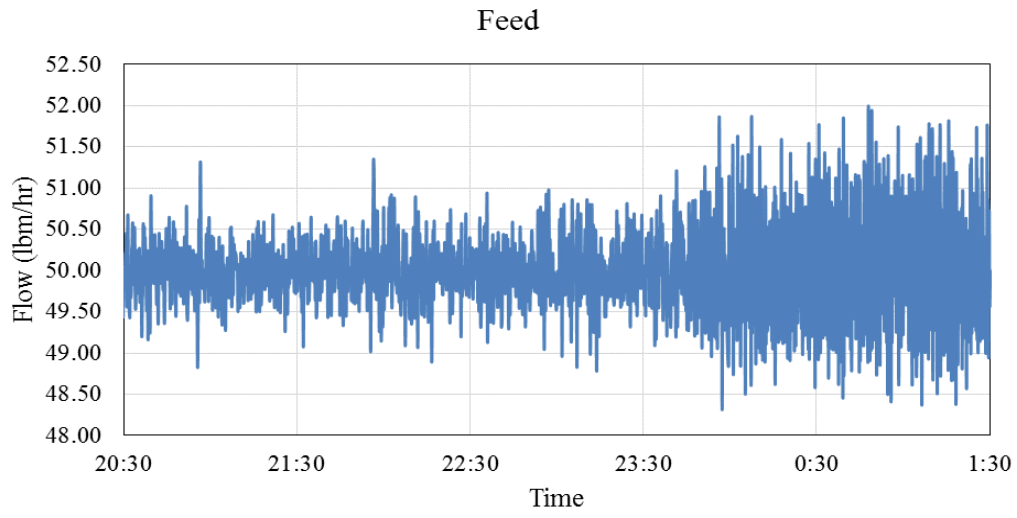

Figure 5-24 – Feedflow for case [2MP, C6/Tol, mX]

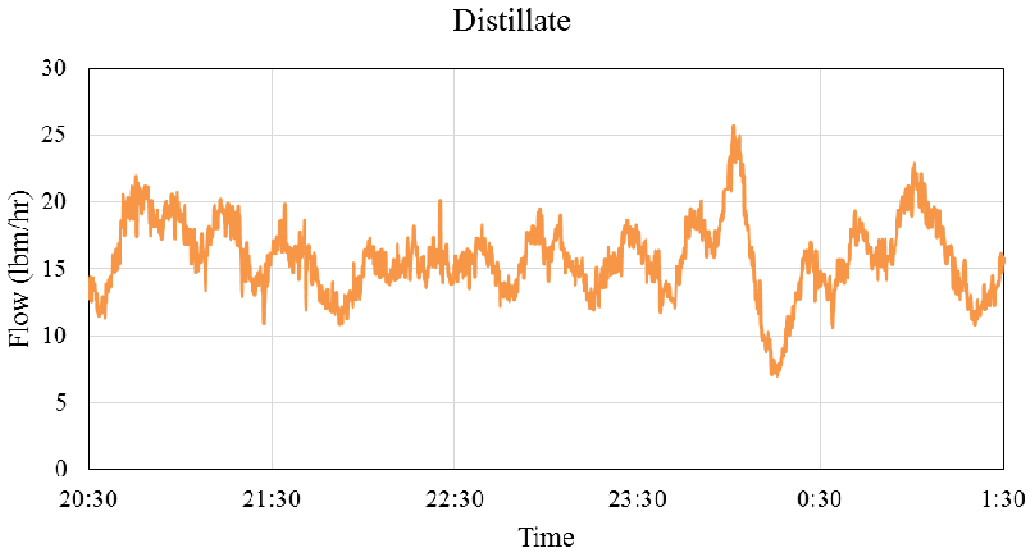

Figure 5-25 – Distillate flow used to control reflux drum level for case [2MP, C6/Tol, mX]

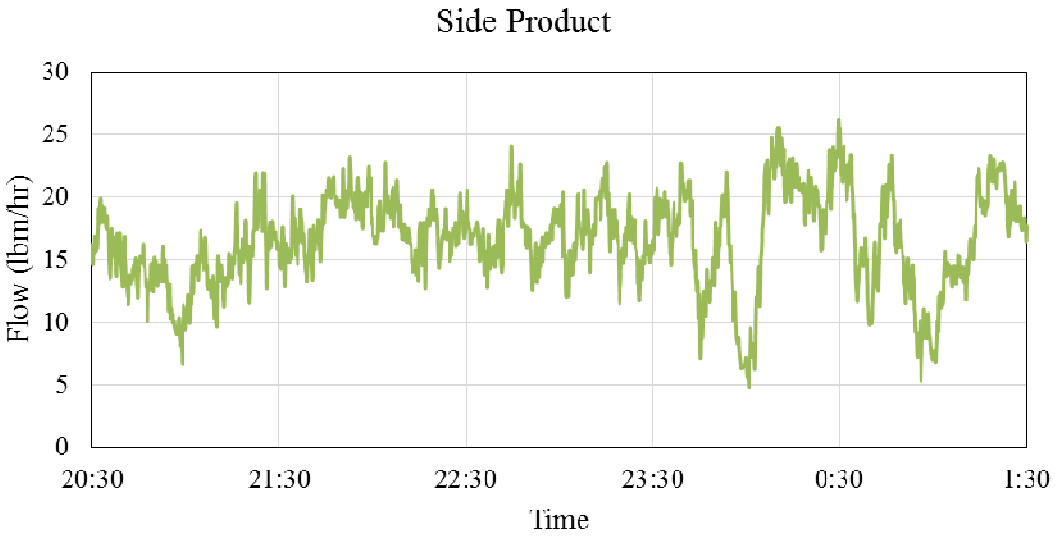

Figure 5-26 – Side product used to control side tank level for case [2MP, C6/Tol, mX]

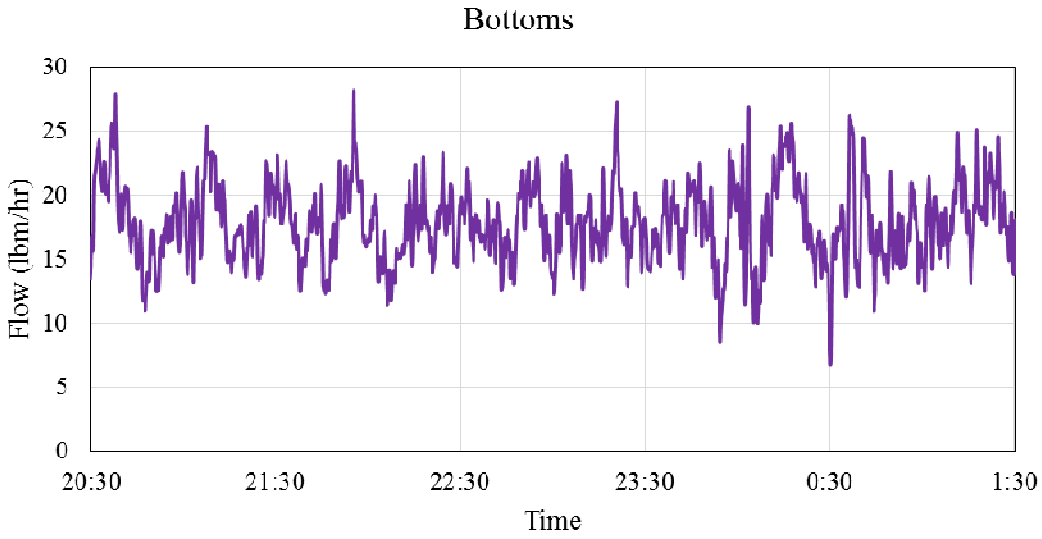

Figure 5-27 – Bottoms product used to control column level for case [2MP, C6/Tol, mX]

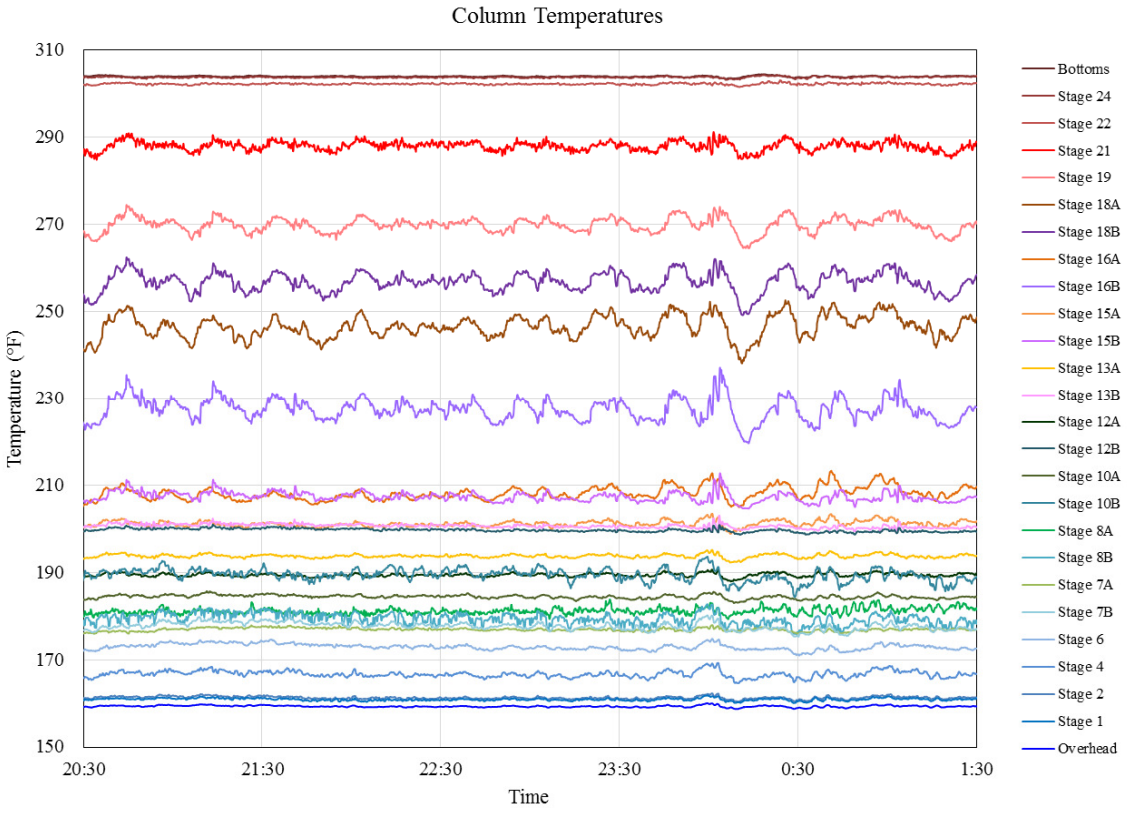

Figure 5-28 – All column temperatures for case [2MP, C6/Tol, mX]

Case [2MP/C6, Tol, mX]

The control configuration originally proposed by SVD and RGA for case [2MP/C6, Tol, mX] was not ran on the pilot column. Though not verified with disturbance testing, the controller pairings resulting from SVD and RGA (Figure 5-29) could have a large degree of interaction. Furthermore, a better control strategy became apparent while the column was transitioned to a pure toluene side product. This control strategy was easier to implement, simpler to tune, and more transparent in regards to column behavior and dynamics. Believing that a simpler and more straightforward approach is superior, the intuitive control pairings were commissioned on the column. The utility of SVD and RGA as controller design tools for DWCs should not be dismissed based on this case study. In fact, as shown in Chapter 4, after the model was updated to better reflect the process

conditions seen on the pilot plant, SVD and RGA resulted in a control structure similar to that used on the pilot column. SVD and RGA are simply mathematical tools that identify sensitivities and potential controller interaction. As with most tools, SVD and RGA cannot be expected to always be successful. Furthermore, the success of SVD and RGA is dependent upon the quality of the original gain matrix. Changing the heat transfer in the model changed the areas of sensitivity within the model and therefore the results of SVD and RGA. If anything, this case study emphasizes the importance of experimental studies and verified models.

From a process perspective, to maintain steady state for case [2MP/C6, Tol, mX] assuming that all column inventories are stable, the controllers must maintain the separation between toluene and m-xylene and the separation between cyclohexane and toluene. The stripping section controller in case [2MP, C6/Tol, mX] maintained the separation between toluene and m-xylene in the base of the column. Since this separation was still desired, the stripping section temperature controller was left unchanged. The movement of toluene and cyclohexane in the column can be seen through the mainfrac temperatures (Figure B-35). As the sidedraw became more concentrated in toluene, the mainfrac temperatures increased to reflect the increased amount of heavier boiling component. This process knowledge was used to determine a temperature controller pairing. A side product temperature controller was commissioned to control a temperature located above the side product draw by manipulating the side product flowrate. As this temperature became hotter reflecting a build-up of toluene, the side product flow would increase to take off more toluene.

Using the controls approach outlined in Figure 5-29, a relatively pure toluene side product was obtained (Figure 5-30). The performance of these temperature controllers is shown in Figure 5-32 and Figure 5-33. The mainfrac temperature controller was significantly de-tuned such that the product flow slowly followed the temperature trend. Since the flow of toluene side product was so small, it was acceptable for the valve to be

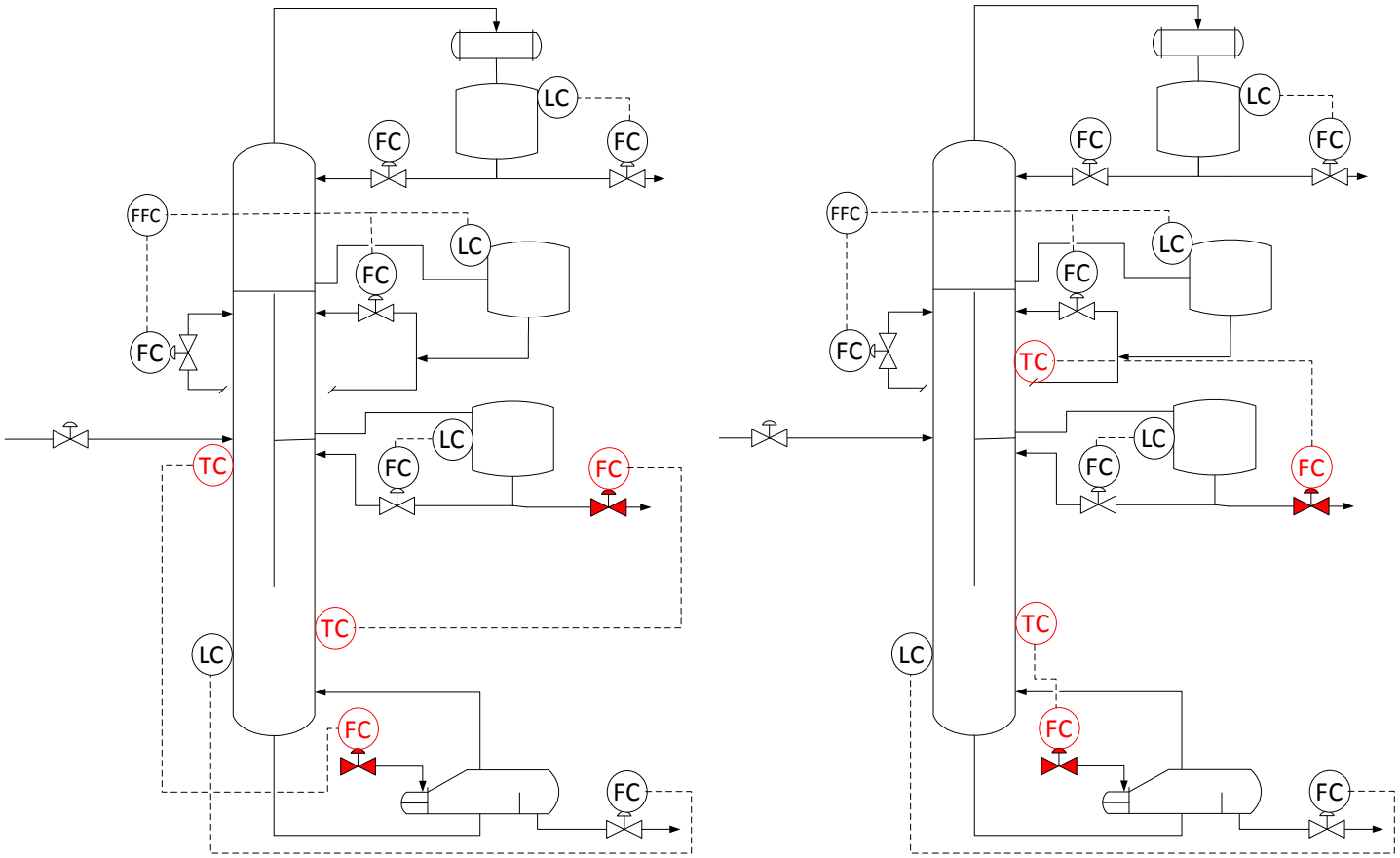

Figure 5-29 – Comparison of control configuration suggested by SVD and RGA (left) and that used on the pilot column (right) for case [2MP/C6, Tol, mX]

shut occasionally. The location of the stripping temperature controller was maintained from the previous case to maintain the desired separation between m-xylene and toluene.

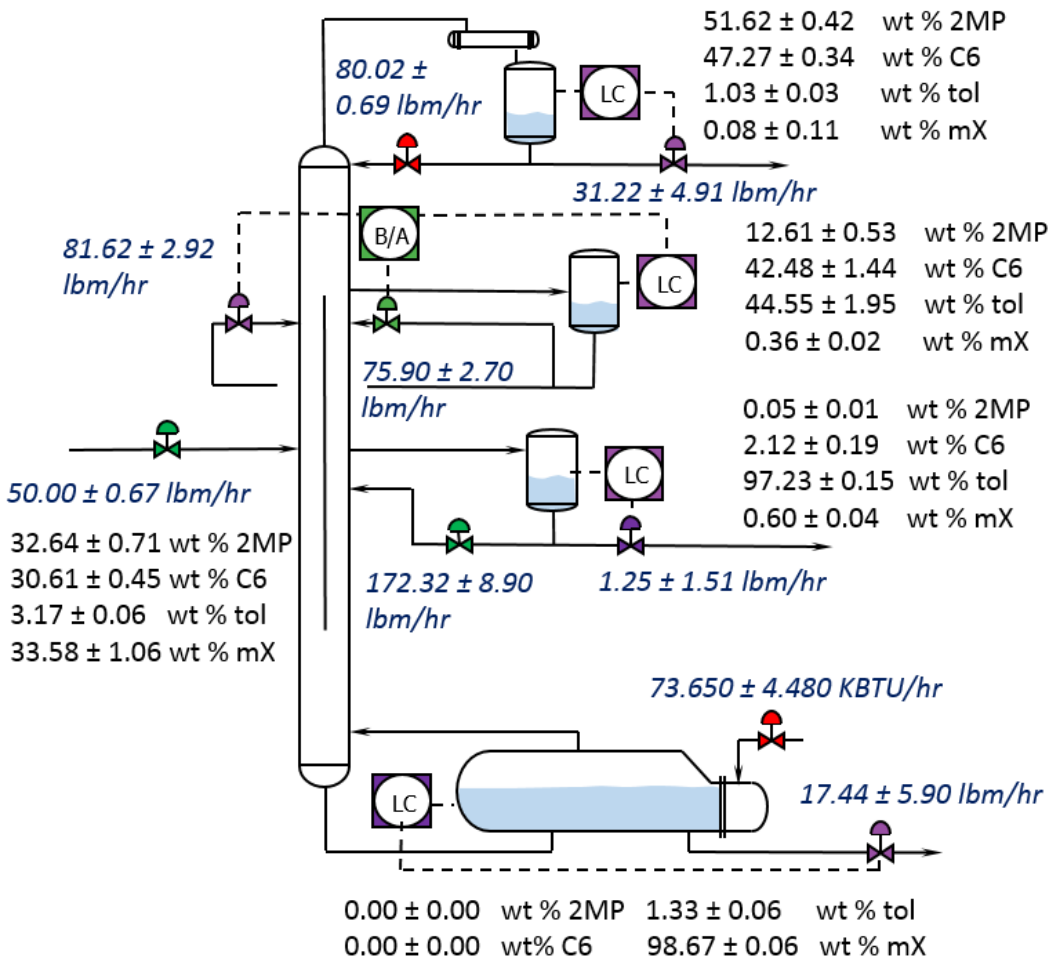

Figure 5-30 – Steady state conditions for [2MP/C6, Tol, mX]. Purple valves are used for level control, green valves are in local automatic flow control, and red valves are manipulated variables for temperature control.

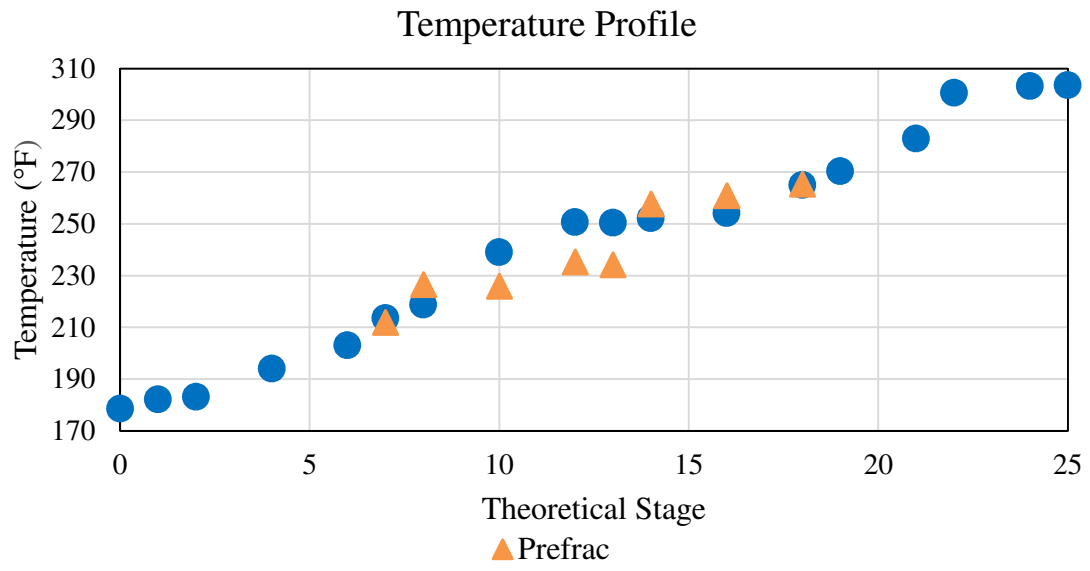

Figure 5-31 – Temperature profile for case [2MP/C6, Tol, mX]

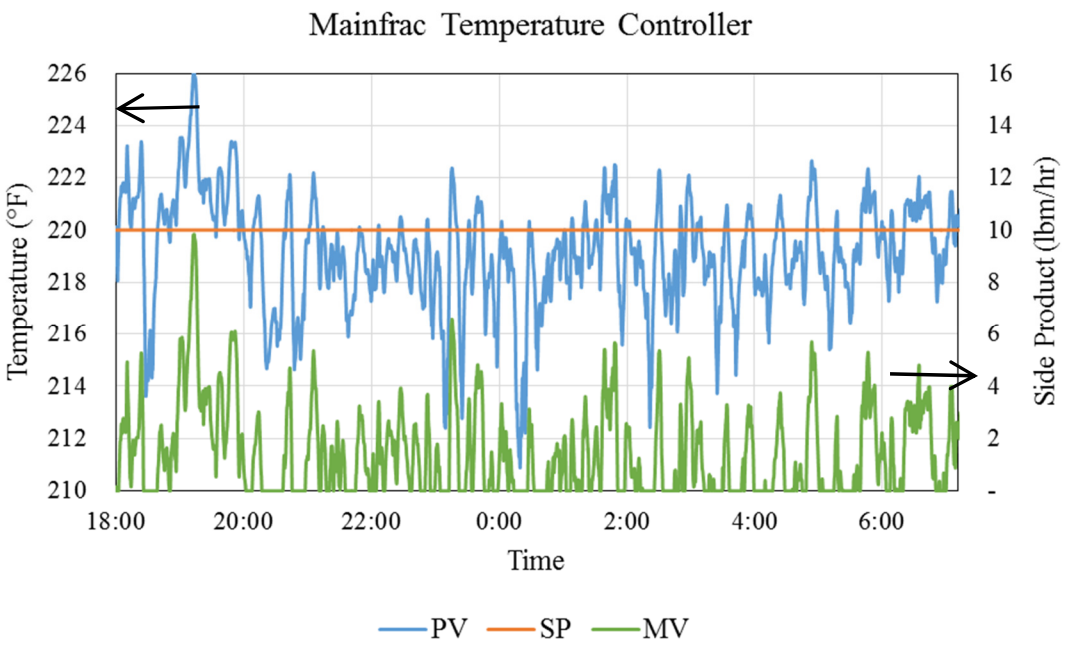

Figure 5-32 – Mainfrac temperature controller for case [2MP/C6, Tol, mX]

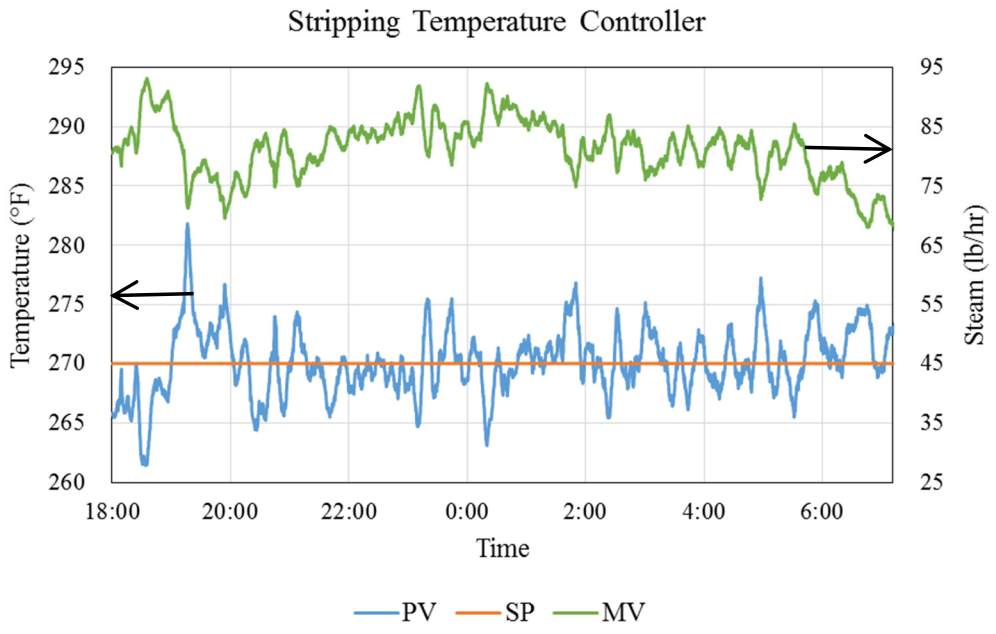

Figure 5-33 – Stripping temperature controller for case [2MP/C6, Tol, mX] Run 1

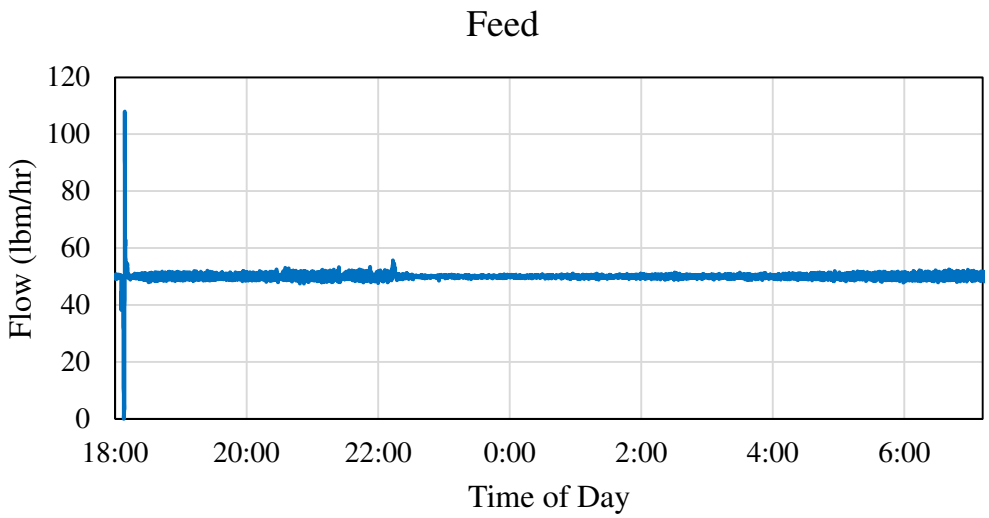

Figure 5-34 – Feed flow for case [2MP/C6, Tol, mX] Run 1

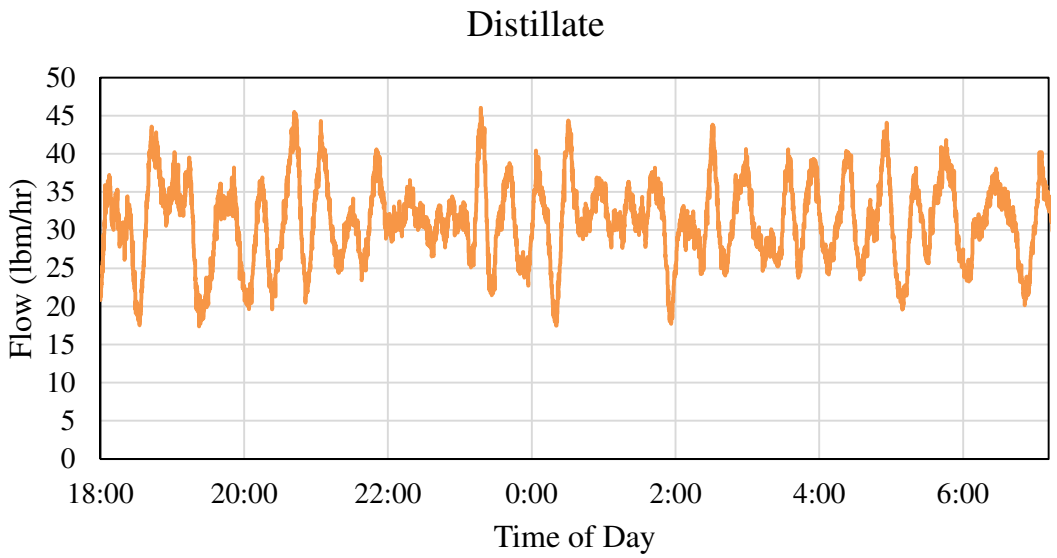

Figure 5-35 – Distillate flow controlling reflux drum level for case [2MP/C6, Tol, mX] Run 1

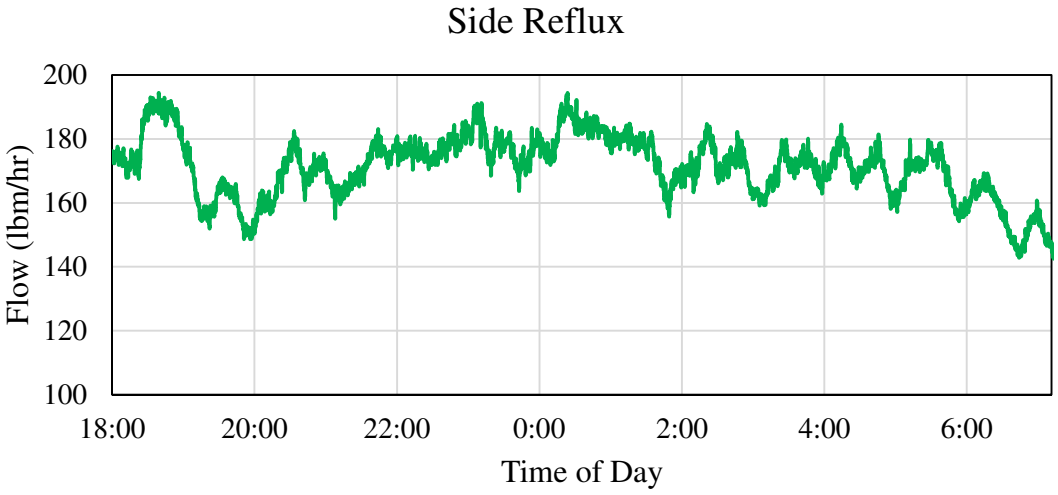

Figure 5-36 – Sidedraw reflux flow controlling side product tank level for case [2MP/C6, Tol, mX] Run 1

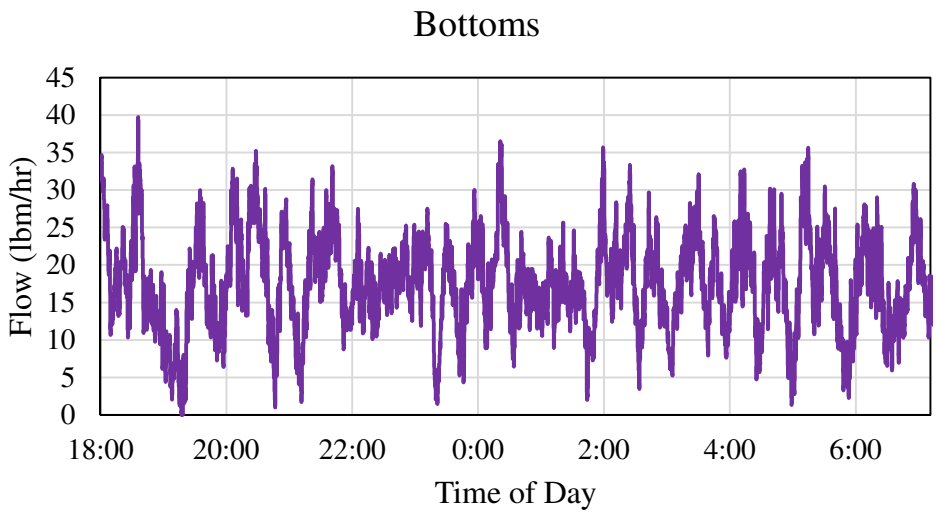

Figure 5-37 – Bottoms flow controlling column level for case [2MP/C6, Tol, mX] Run 1

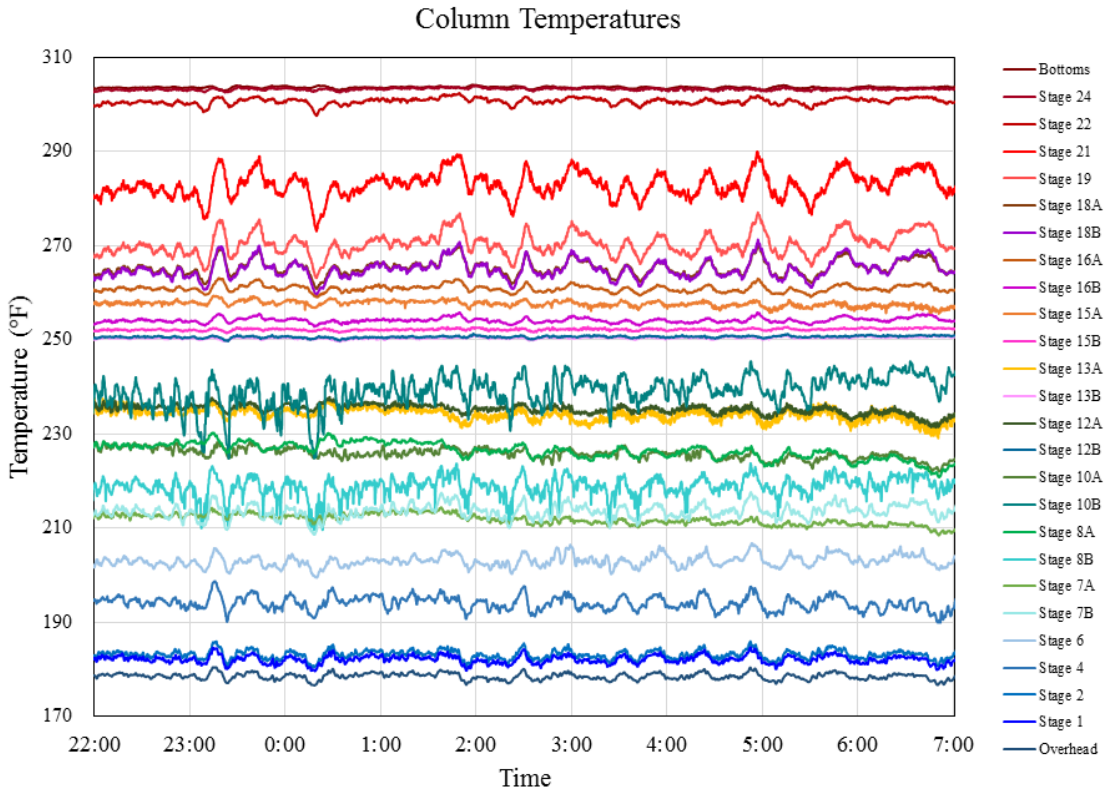

Figure 5-38 – Column temperatures for case [2MP/C6, Tol, mX]

As previously stated, case [2MP/C6, Tol, mX] was run twice on the pilot column with the same control structure and wall split. As can be seen from Table 5-4, the two runs had very similar product flow rates and compositions. However, the two cases differed in ambient temperature, reboiler duty, and reflux flows. It should be noted that the overhead reflux for both runs was in local automatic flow control with a setpoint of 80 lbm/hr. These different sets of data highlight the impact of ambient temperature on a six inch diameter column. How this was accounted for in the model is highlighted in Chapter 3 and Chapter 6. The similar product compositions but different energy usage and internal flow rates is reminiscent of the multiple steady state phenomena that has been discussed in previous work. However, unlike those works, these two data sets have the same wall split and vapor split. Therefore, energy and flow rate differences are assumed to be a result of heat loss. Sensitivity to ambient conditions is not typically seen on a commercial scale larger diameter tower. Therefore, this is a result of working on a pilot scale distillation column.

CONCLUSIONS

In conclusion, a four component mixture was successfully controlled at multiple operating points on the pilot plant DWC using a two-point temperature control approach. The column was started as a three component column before a trace amount of toluene was added to the feed. The toluene trace component was moved between different product tanks by gradually ramping select control variables to their new steady state values. The temperature control structures used for the three component case, the case of toluene and m-xylene bottoms product, and the case of toluene and cyclohexane as side product were determined using the steady state control design tools of singular value decomposition and relative gain array analysis. RGA and SVD did not produce a successful temperature control structure for the case of pure toluene side product. However, a temperature control structure was developed for this case using engineering insight.

Table 5-4. Comparison of two runs of case [2MP/C6, Tol, mX]

Variable	Run 1 – July 19th		Run 2 – July 25th	
	Average	Standard Deviation	Average	Standard Deviation
Product Compositions (mol %)				
Distillate				
2MP	51.08	± 0.41	49.87	± 0.41
C6	47.89	± 0.34	49.02	± 0.34
Tol	0.96	± 0.03	1.11	± 0.03
mX	0.07	± 0.09	0.00	± 0.09
Top of Wall				
2MP	12.86	± 0.52	11.57	± 0.52
C6	44.36	± 1.44	45.75	± 1.44
Tol	42.49	± 1.95	42.61	± 1.95
mX	0.30	± 0.02	0.08	± 0.02
Side				
2MP	0.05	± 0.02	0.03	± 0.02
C6	2.31	± 0.20	1.76	± 0.20
Tol	97.11	± 0.17	97.61	± 0.17
mX	0.53	± 0.04	0.60	± 0.04
Bottoms				
2MP	0.00	± 0.00	0.00	± 0.00
C6	0.00	± 0.00	0.00	± 0.00
Tol	1.60	± 0.07	1.84	± 0.07
mX	98.40	± 0.07	98.16	± 0.07
Material Balance Flows (lbmol/hr)				
Distillate	0.366	± 0.058	0.366	± 0.077
Side	0.014	± 0.016	0.009	± 0.018
Bottoms	0.165	± 0.056	0.174	± 0.061
Internal Flows				
Overhead Reflux (lbmol/hr)	0.938	± 0.008	0.938	± 0.010
Prefrac Reflux (lbmol/hr)	0.929	± 0.033	0.869	± 0.028
Mainfrac Reflux (lbmol/hr)	0.864	± 0.031	0.808	± 0.025
Side Reflux (lbmol/hr)	1.873	± 0.097	1.691	± 0.077
Reboiler Duty (BTU/hr)	73650	± 4480	68680	± 3330
Ambient Temperature (°F)	82.87	± 3.71	99.34	± 1.90

Chapter 6: Steady State Data Analysis and Modeling

The first step in matching the model to the pilot data was determining heat transfer coefficients. As stated previously, the pilot column was affected by changes in ambient temperature and weather conditions because of the column's scale. Environmental effects and heat transfer through the dividing wall have been shown to play a less significant role on larger scale columns.[40] Nevertheless, heat transfer coefficients are important for matching the model to the pilot data.

A systematic procedure for matching the model to experimental data that is subject to measurement noise and process variability was developed. Using this approach, reflux flow rates and reboiler duties were matched plus/minus one standard deviation of their steady state experimental values. An optimization procedure that matched particular flows to determine particular heat transfer coefficients was created. When further refinement was needed, temperatures and compositions were examined. This approach lead to matched simulations for five of the six data sets. Heat transfer coefficients varied slightly between data sets though this may be a result of unaccounted changes in column variables.

STATISTICAL DATA ANALYSIS PROCEDURE

All process data, such as flow rates, temperatures, and compositions, are subject to measurement error and process variability. Such is the nature of experimental work. However, this variability and error can lead to violations of material balances and other known constraints. This further complicates applications where the data are used such as simulation, optimization, and parameter estimation. Fortunately, techniques of data reconciliation, or the use of process model constraints to reduce the effect of random errors in process data, have been used by chemical engineers for years.[85,86] This section highlights the work done to reconcile steady state compositions and flows such that a model could be fit to the data.

Composition Analysis

The work below outlines the steps taken to determine the standard deviation of sample compositions. Standard deviation accounts for reproducibility of sample compositions and any inaccuracies or particular biases in the gas chromatogram itself. For help with this process, the UT Department of Statistics and Data Sciences and other sources[87] were consulted.

Feed Samples

Because the feed tank was not receiving any products while in operation and the approximately 200 gallon contents was continually mixed at a rate of approximately ten gpm, each batch of feed was assumed constant and homogeneous. In this case, batch refers to the contents of the feed tank before the product and feed tanks were switched. For example, if the tanks were switched at 5pm so that V-600A switched from the product tank to the feed tank. The contents in V-600B before 5pm and the contents within V-600A after 5pm would be two different feed batches. The assumption that each feed batch was constant greatly increased the sample size. All samples from a particular batch of feed were grouped together and averaged after outliers were detected. Outliers were determined either due to low or high methanol area counts in the GC analysis or from a univariate chart in which one component was plotted against another (Appendix C). The standard deviation of the resulting feed compositions was also calculated and is reported with case results.

Product Samples

Each product sample was injected into the GC two or three times. However, that is not a large enough sample size to determine a reasonable standard deviation. Therefore standard deviations were calculated from samples where the same physical sample had been injected approximately six times. Because not all samples had a high number of injections, standard deviations were assumed to be the same for sample locations (distillate, side, etc.) with similar compositions (Table 6-1).

Steady state was determined by consistent product compositions from samples measured three hours apart. Compositions for each sample point were averaged over the duration of steady state and reported as steady state compositions.

Analysis of Flows

Process data (flows, temperatures, levels, pressures, etc.) from the pilot plant were recorded at 10 second intervals. All process variables were averaged over the duration of steady state, and standard deviations were calculated. However, process variability in product and feed flows (Figure B-18) prevented complete material balance closure. Therefore, an effort to ensure a closed material balance such that a model could reasonably fit the data, the material balance flow rates together with the compositions discussed above were used in a nonlinear optimization in which the objective function in Equation 6-1 was minimized. Constraint functions for the optimization included the summation of all compositions of the same stream to 1, and all decision variables were constrained by their standard deviations. The resulting feed composition, feed flow, distillate flow, and side flow were used in Aspen Plus® as discussed below. Note that this procedure was not used for case [2MP, C6, tol/mX] due to process disruptions caused by feed sampling.

$$\text{Min } (F - D - S - B)^2 + \sum_{i=2MP}^{mX} (x_{F,i}F - x_{D,i}D - x_{S,i}S - x_{B,i}B)^2 \qquad \textbf{(6-1)}$$

DETERMINING HEAT TRANSFER COEFFICIENTS

Just as was previously discussed in Chapter 3, the dividing wall column experienced heat transfer both to the environment and through the wall. This heat transfer was accounted for in the model through heat transfer coefficients. The heat transfer coefficients used for the SVD and RGA testing in Chapter 4 were calculated for a similar chemical system.[40] However, the availability of pilot data for the four component system allowed the heat transfer coefficients to be recalculated in hopes of providing a better fitting model. The following sections describe the procedure for determining the heat transfer coefficients.

Table 6-1. Composition standard deviations for all cases

Case	Plant Area	Standard Deviation (wt %)			
		2MP	C6	Tol	mX
[2MP, C6, mX]	Feed	2.07	0.74	0.03	2.66
	Distillate	0.06	0.06	0.00	0.00
	Top of Wall	0.30	0.30	0.00	0.00
	Side	0.06	0.72	0.76	0.02
	Bottoms	0.00	0.63	0.05	0.67
[2MP, C6, tol/mX]	Distillate	0.06	0.06	0.00	0.00
	Top of Wall	0.30	0.30	0.00	0.00
	Side	0.06	0.72	0.76	0.02
	Bottoms	0.00	0.63	0.05	0.67
[2MP, C6/tol, mX]	Feed	0.27	0.19	0.03	0.43
	Distillate	0.06	0.06	0.00	0.00
	Top of Wall	0.12	0.12	0.01	0.02
	Side	0.06	0.72	0.76	0.02
	Bottoms	0.00	0.00	0.06	0.06
[2MP/C6, tol, mX] Run 1	Feed	0.71	0.45	0.06	1.06
	Distillate	0.42	0.34	0.03	0.11
	Top of Wall	0.53	1.44	1.95	0.02
	Side	0.01	0.19	0.15	0.04
	Bottoms	0.00	0.00	0.06	0.06
[2MP/C6, tol, mX] Run 2	Feed	1.33	1.23	0.22	2.34
	Distillate	0.42	0.34	0.03	0.11
	Top of Wall	0.53	1.44	1.95	0.02
	Side	0.01	0.19	0.15	0.04
	Bottoms	0.00	0.00	0.06	0.06

Model Details

An Aspen Plus® model previously developed[40] was used to determine the optimal heat transfer coefficients. The design optimization software HEEDS connected to the Aspen Plus® model as well as to a spreadsheet in Microsoft® Excel™. HEEDS modified inputs in Excel™ and Aspen Plus® to minimize the difference between the model reflux flows and those from the pilot data. Using an external optimization software allowed for efficient investigation of a large design space.

A steady state dividing wall column model was created in Aspen Plus® following the approach of Luyben[88] and others[89] in that the column was represented as multiple sections. The model contained a rectifying column complete with a total condenser, a prefractionator column, an upper and lower mainfractionator column, and a stripping column complete with a kettle reboiler. The packing in each section was specified as Mellapak 500Y with an HETP of 9.5 inches. The mainfractionator was split into two sections to reflect the total trapout tray used in the pilot column. The upper and lower mainfractionator sections each had six stages, and the prefractionator had twelve stages with the feed entering above the seventh stage. The rectifying and stripping sections each had seven stages to account for the total condenser and reboiler, respectively. The model also included three splitters to specify the liquid split at the top of the wall, the vapor split at the bottom of the wall, and the side product flowrate. Heaters were placed on the prefrac, mainfrac, and sidedraw reflux flows so that subcooling seen on the pilot column could be matched. The model used an equilibrium stage approach based on the NRTL-VLE model. Inputs to the model include feed composition, feed pressure, feed temperature, and feed flow, column pressure, distillate rate, overhead reflux temperature, prefrac reflux temperature, mainfrac reflux temperature, sidedraw reflux temperature, side product rate, reboiler duty, and total heat loss per stage.

The total heat loss per stage was specified using an external Excel™ spreadsheet. This spreadsheet calculated the heat loss to the environment and the heat transfer through the wall. Aspen Plus® permits the total heat loss per stage to be specified; therefore, the two heat loss values, atmosphere and wall, were added before being entered into Aspen Plus®. The heat loss to the atmosphere was calculated using the appropriate area based on region of the column as explained in Chapter 3, the temperature difference between the column temperature and ambient temperature both recorded from the pilot column, and a user-specified heat transfer coefficient ($U_{i,ATM}$, where the i denotes that the internal diameter of the column was used). The heat transfer through the wall was calculated using a user-specified wall heat transfer coefficient (U_{WALL}), the wall area (Chapter 3), and the

temperature difference across the wall. Although the pilot column had 24 RTD's along the length of the column, each theoretical stage did not have a temperature reading. For theoretical stages that did not have a corresponding RTD reading, the temperature was inferred from surrounding experimental temperatures using MATLAB®'s pchip function (Piecewise Cubic Hermite Interpolating Polynomial). This proved to be a good fit (Figure 6-2).

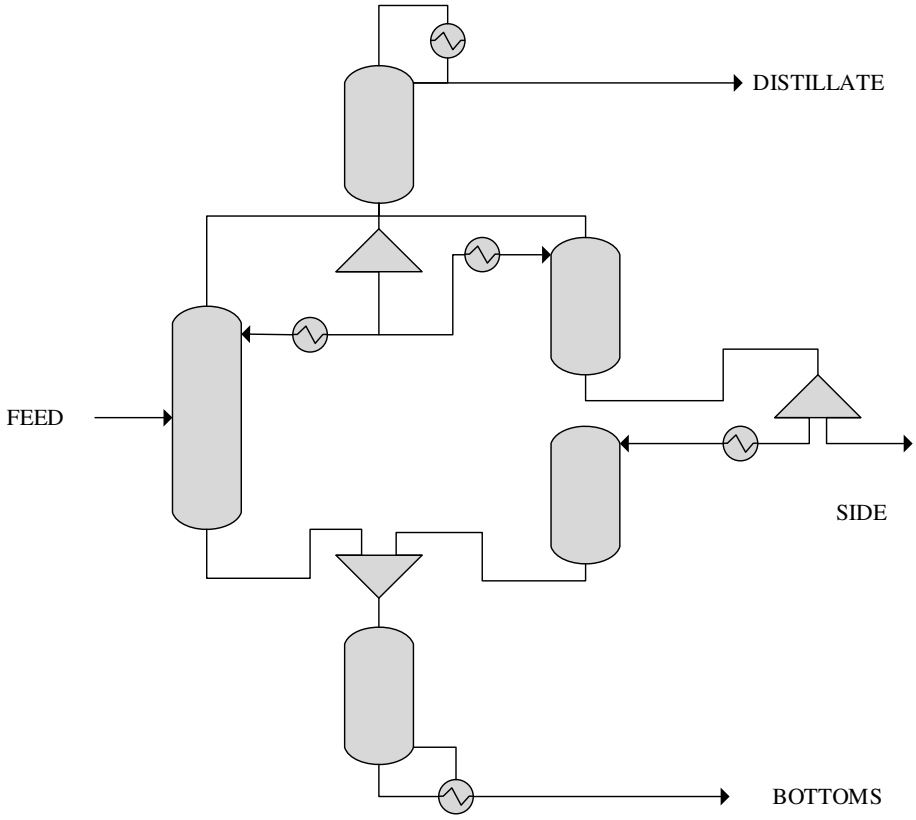

Figure 6-1 – Diagram of AspenPlus® model

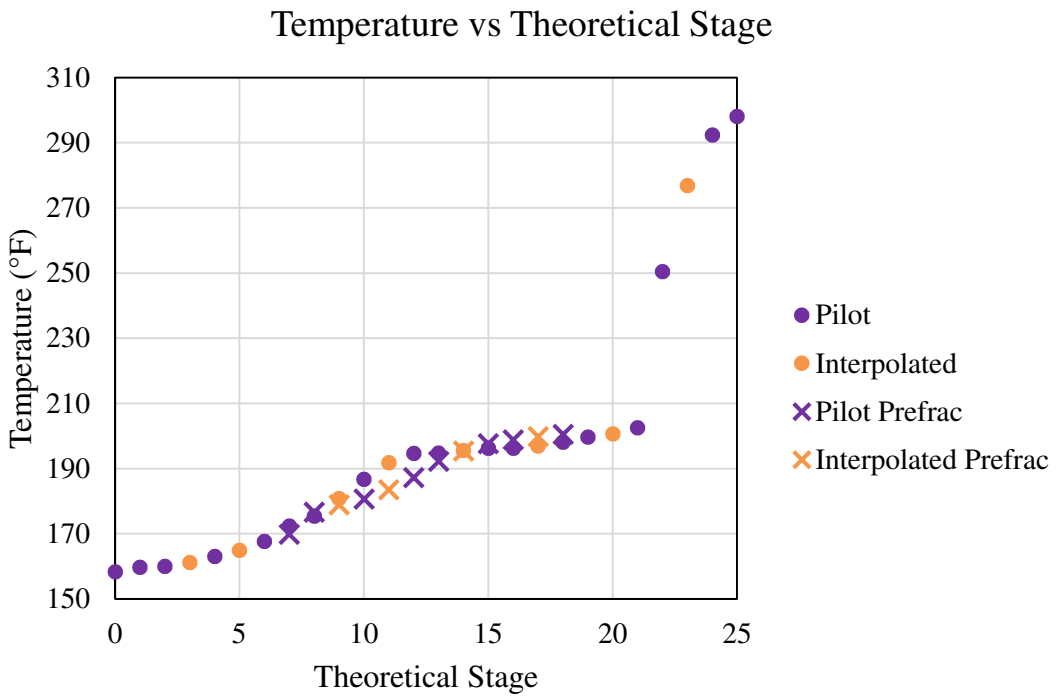

Figure 6-2 – Temperature profile for [2MP, C6, mX] finite reflux showing temperatures from experimental data and those interpolated with pchip.

HEEDS allowed the heat loss values calculated in Excel™ to be fed to Aspen Plus®. Through HEEDS, the user specified the heat transfer coefficients in Excel™ and the reboiler duty, distillate flow, and side product flow in Aspen Plus®. The optimization method used in this research was the HEEDS proprietary method SHERPA (Simultaneous Hybrid Exploration Robust Progressive Adaptive). HEEDS was operated on a PC running Windows 7© 64-bit, having a 2.8 GHz Intel® Xeon® Core processor with 8 GB of RAM and 8 threads.

Procedure

The objective function used in HEEDS depended upon the pilot data being matched and the type of heat transfer coefficient being determined. Total reflux data was used to determine the atmospheric heat transfer coefficient while finite reflux data was used to

determine the wall heat transfer coefficient. In some cases, finite reflux data was used to determine both U_{WALL} and $U_{i,ATM}$.

Total Reflux

During total reflux, there are no feeds entering or product streams leaving the column. Therefore, the composition and temperature profiles on either side of the dividing wall are the same. With no driving force, it can be assumed that there is little to no heat transfer through the wall. The only heat loss occurring during total reflux is heat loss to the environment. Therefore, total reflux data was used to determine the atmospheric heat transfer coefficient, $U_{i,ATM}$.

During start-up, the pilot column was operated in total reflux. However, because the column was transitioned between steady states while in continuous operation, the only start-up total reflux data available was from the initial start-up as a 3 component system (2-methylpentane, cyclohexane, and m-xylene). This data was used to determine $U_{i,ATM}$ for the 3-component case. This atmospheric heat transfer coefficient was also tested on the other cases, and the results of this are discussed below.

Aspen Plus® does not have the ability to run a total reflux simulation. Therefore, total reflux was mimicked by using a small feed of 1 lbm/hr. The distillate and side product streams were scaled from their finite reflux steady state values to suit a 1lbm/hr feed. The feed composition and temperature were also taken from the 3-component finite reflux steady state data. The overhead reflux subcooling, the column operating pressure, the prefrac reflux temperature, the mainfrac reflux temperature, the sidedraw reflux temperature, the wall split, and the reboiler duty were from the pilot total reflux data.

To determine the atmospheric heat transfer coefficient, the heat transfer coefficient and reboiler duty were varied so that the overhead, prefrac, mainfrac, and sidedraw reflux flows matched the values from the pilot plant within the appropriate standard deviations. To aid convergence since the feed and product flows were relatively small, the distillate and side product were also varied within ± 2 % of their previously specified values.

Finite Reflux

Matching finite reflux data was slightly more difficult because both heat transfer to the atmosphere and heat transfer through the wall play a role. HEEDS optimized the finite reflux simulations by varying the reboiler duty within one standard deviation of the pilot plant average and the specified heat transfer coefficients. Efforts were made to avoid simulations that changed $U_{i,ATM}$ and U_{WALL} at the same time. The atmospheric heat transfer coefficient from the total reflux case was first used in determining U_{WALL}. Keeping $U_{i,ATM}$ constant, U_{WALL} and Q_R were varied to match the overhead and side reflux. A feasible solution was one which matched all reflux flows within their standard deviations as determined by the experimental data. If a feasible solution could not be found, the objective function was changed to match the overhead, prefrac, and mainfrac reflux flows by keeping U_{WALL} constant and changing $U_{i,ATM}$. If possible, U_{WALL} was set to a value determined from the optimization of a previous case study.

Case Study [2MP, C6, mX]

The three component case is presented below as an example of determining heat transfer coefficients. The three component case was chosen because this is the only case for which there is total and finite reflux data.

Total Reflux

As stated previously, in addition to the heat transfer coefficient, variations in the reboiler duty, distillate, and side product flow were made during this optimization. To allow the effects of the heat transfer coefficient to be seen and to limit the number of variables changed, constant reboiler duty data is shown below (Q_R = 72.15 KBTU/hr). The distillate flow and side product flow were still varied to ease with convergence.

As can be seen from Figure 6-3, the optimal value of the atmospheric heat transfer coefficient could not be determined from internal flows alone. In general, increasing the atmospheric heat transfer coefficient decreased the mainfrac and other reflux flows. As heat loss to the atmosphere increased, less of the vapor reached the upper portions of the

column before condensing. However, when considering the simulations in which all of the reflux flows are matched within their standard deviations, no clear trend is present and a range of optimum heat transfer coefficients exist. As seen in Figure 6-3, the range of feasible values of the atmospheric heat transfer coefficient was 9.51 to 9.85 BTU/(hrft^2°F) with no clear optimum.

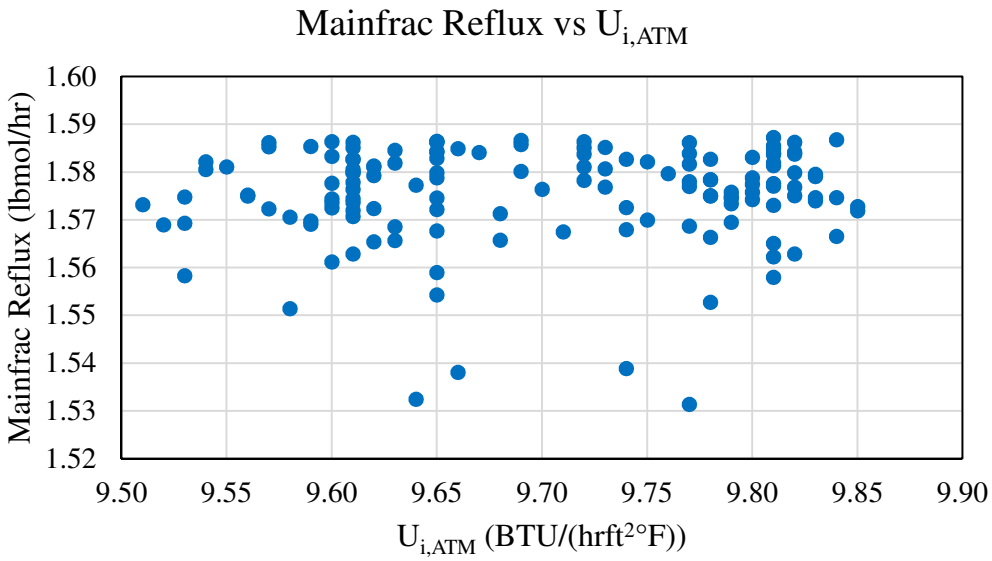

Figure 6-3 – Mainfrac reflux versus $U_{i,ATM}$ for [2MP, C6, mX] total reflux. Increasing the atmospheric heat transfer coefficient decreased the prefrac reflux flow. Feasible values are those between the upper and lower limits.

No composition samples were collected during total reflux. However, because distillation temperatures reflect composition profiles within the column, temperatures were used to further determine the optimum heat transfer coefficient. Due to the relatively flat temperature profile in the rest of the column, temperatures in the stripping section had the highest variability for feasible simulations. Figure 6-4 shows the top stage temperature of the stripping section versus atmospheric heat transfer coefficient for simulations which meet the feasibility requirements based on flows. Though the change in temperature is more due to changes in material balance flows than changes in values of $U_{i,ATM}$, temperature considerations were still helpful in narrowing the range of acceptable heat

transfer coefficient values. Ultimately, $U_{i,ATM}$ of 9.82 BTU/(hrft^2°F) was chosen because the corresponding simulation provided the best match for the entirety of the stripping section. Figure 6-5 and Table 6-2 show how well this value of $U_{i,ATM}$ fits the data.

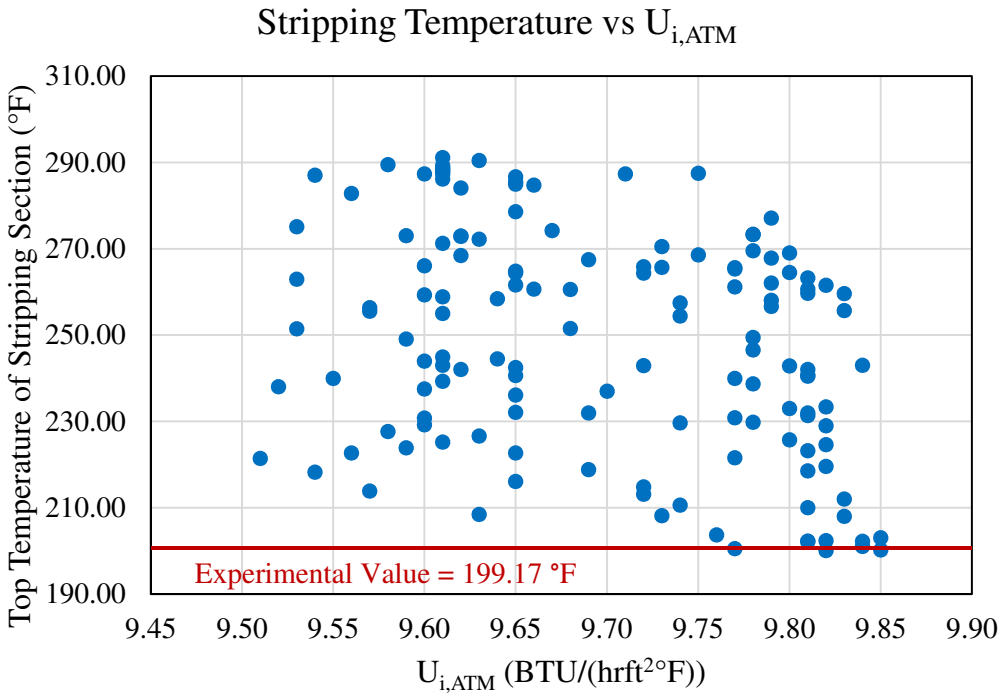

Figure 6-4 – Top stripping section stage temperature versus atmospheric heat transfer coefficient for simulations which meet the reflux feasibility requirements. The corresponding temperature from the experimental data was 199.17 ± 0.65 °F.

Table 6-2. Pilot and Model Comparison for [2MP, C6, mX] Total Reflux

Stream	Pilot Data		Model, $U_{i,ATM}$ = 9.82 BTU/(hrft^2°F)
	Average (lbmol/hr)	Standard Deviation (lbmol/hr)	Flow (lbmol/hr)
Overhead Reflux	2.418	0.097	2.392
Prefrac Reflux	1.870	0.069	1.925
Mainfrac Reflux	1.553	0.057	1.575
Sidedraw Reflux	2.003	0.103	1.901

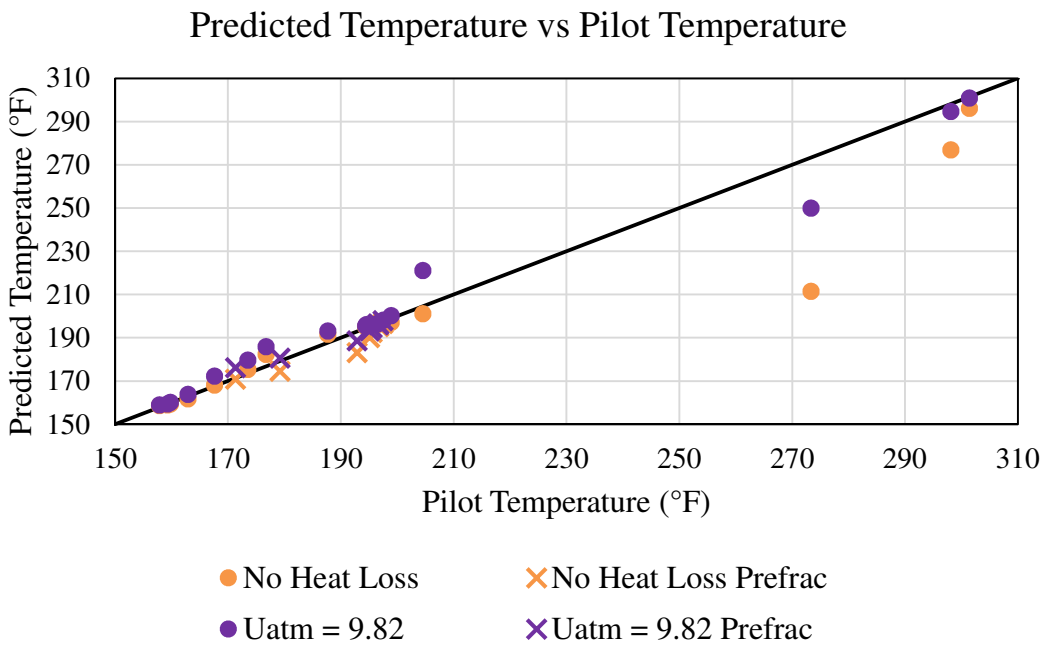

Figure 6-5 – Comparison of model and pilot temperatures for [2MP, C6, mX] total reflux with and without heat loss

This analysis was done with a constant reboiler duty equal to the average pilot plant reboiler duty for this case. When varying Q_R within one standard deviation, a range of 8.96 – 10.27 BTU/(hrft^2°F) was found.

Finite Reflux

The 3-component finite reflux data could not be matched without including wall heat transfer in the model. Table C-3 shows the flows and compositions from an Aspen Plus® simulation with a $U_{i,ATM}$ of 9.82 BTU/(hrft^2°F), no U_{WALL} , and a reboiler duty matching the average reboiler duty (Q_R) from the finite reflux pilot data. Compared to the pilot data, the simulation overestimated the overhead, prefrac, and mainfrac reflux flows while underestimating the sidedraw reflux. Lowering the reboiler duty to match that of the lower limit of the pilot data decreased the overhead, prefrac, and mainfrac reflux flows to

values within the standard deviations but also further decreased the sidedraw reflux. To create a better fitting model, heat transfer through the wall was included.

Figure 6-6 shows the range of wall heat transfer coefficients for which when $U_{i,ATM}$ is 9.82 BTU/(hrft^2°F), the side reflux and all other reflux flows are within their feasible regions as defined by the standard deviation of the pilot data. The range of feasible wall heat transfer coefficients was 373 - 406 BTU/(hrft^2°F). Multiple sidedraw reflux flows for constant U_{WALL} are a result of varying reboiler duty.

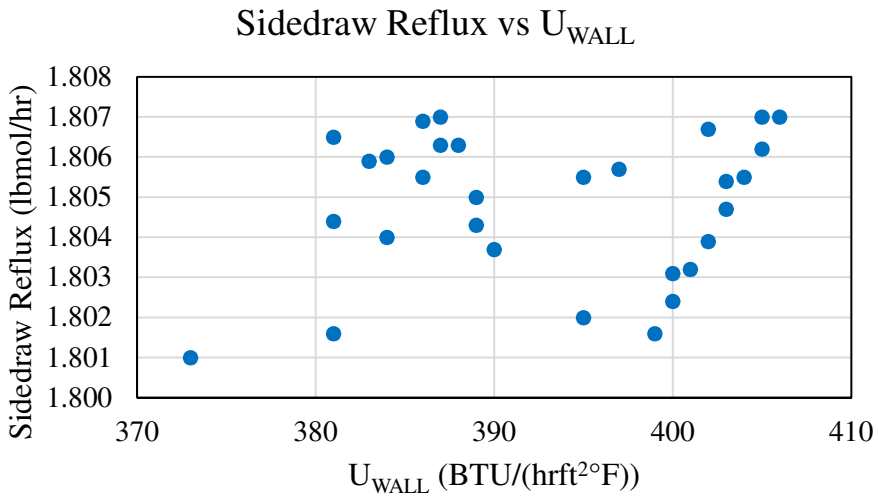

Figure 6-6 – Sidedraw reflux versus wall heat transfer coefficient for [2MP, C6, mX] finite reflux. Sidedraw reflux and all other reflux values were within their feasible ranges as defined by the standard deviation of the pilot data. Without considering compositions, it is unclear which heat transfer coefficient value is optimal.

Compositions were used to further determine the optimum heat transfer coefficient. Figure 6-7 to Figure 6-10 show how varying the wall heat transfer coefficient affected the product compositions. In Figure 6-7, increasing the wall heat transfer coefficient increased the amount of cyclohexane in the distillate. Increasing the wall heat transfer decreased the overhead reflux flow which in turn negatively impacted the separation performance. Marked in red on the figure, U_{WALL} of 388 BTU/(hrft^2°F) corresponded to the cyclohexane distillate composition that most closely matched the pilot value of 2.11 mole percent.

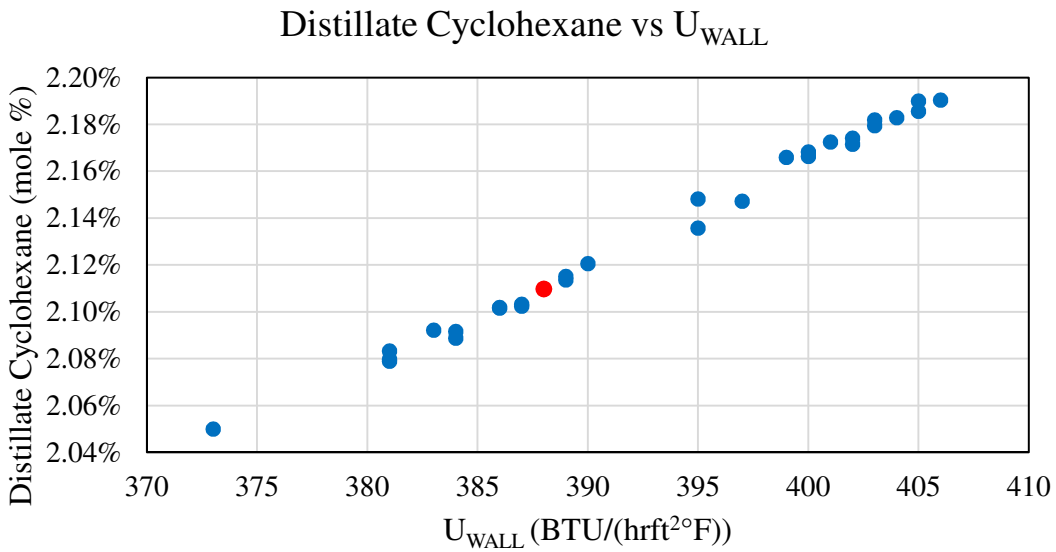

Figure 6-7 – Distillate cyclohexane composition vs U_{WALL} for [2MP, C6, mX] finite reflux. U_{WALL} of 388 BTU/(hrft^2°F) (red) best matches the pilot composition of 2.11 mole percent cyclohexane.

In Figure 6-8, increasing the wall heat transfer coefficient decreased the amount of 2-methylpentane at the top of the wall. Increasing the wall heat transfer decreased the reflux flows at the top of the wall which in turn negatively impacted the separation performance allowing heavier components to rise over the wall. Marked in red, U_{WALL} of 373 BTU/(hrft^2°F) corresponded to the 2-methylpentane top of wall composition that most closely matched the pilot value of 65.04 ± 0.30 mole percent. Simulations that provide a closer match to the 2-methylpentane composition do not match the reflux flow rates.

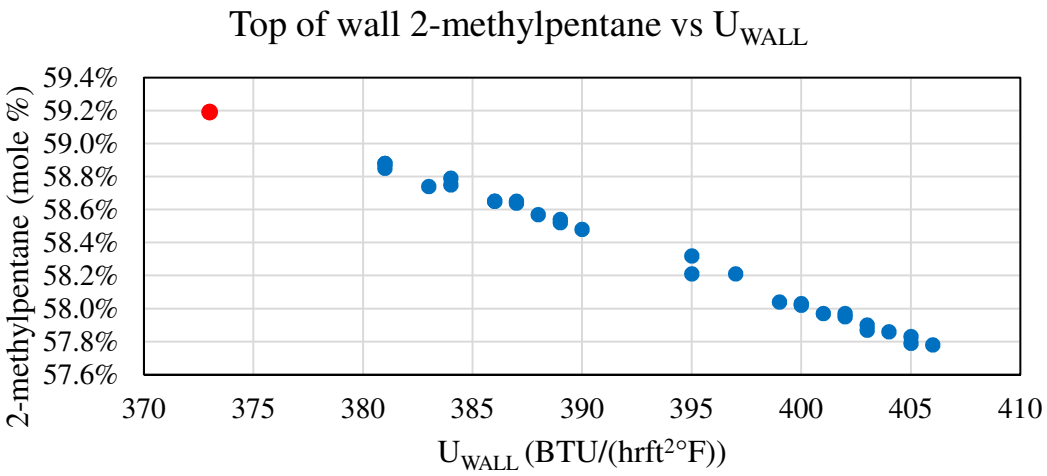

Figure 6-8 – Top of wall 2-methylpentane composition vs U_{WALL} for [2MP, C6, mX] finite reflux. Within the models which match the reflux flows, U_{WALL} of 373 BTU/(hrft^2°F) (red) best matches the pilot composition of 65.04 ± 0.30 mole percent 2-methylpentane.

In Figure 6-9, increasing the wall heat transfer coefficient increased the amount of 2-methylpentane in the side product. Increasing the wall heat transfer decreased the reflux flows in the column which in turn negatively impacted the separation performance. Marked in red, U_{WALL} of 406 BTU/(hrft^2°F) corresponded to the 2-methylpentane side composition that most closely matched the pilot value of 4.20 mole percent. Higher values for the wall heat transfer coefficient would more closely match the 2-methylpentane composition but would violate the reflux flow constraints.

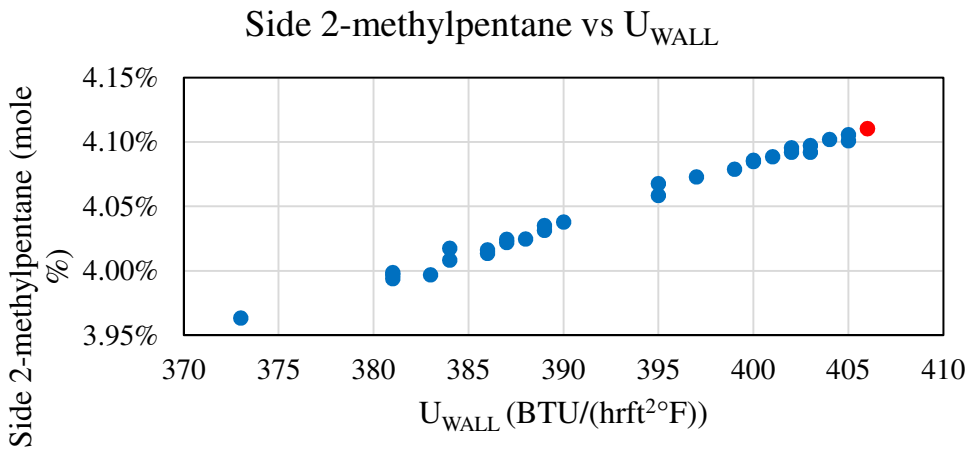

Figure 6-9 – Side 2-methylpentane composition vs U_{WALL} for [2MP, C6, mX] finite reflux. Within the values of U_{WALL} which match the sidedraw reflux flow, U_{WALL} of 406 BTU/(hrft^2°F) (red) best matches the pilot composition of 4.20 mole percent 2-methylpentane.

Figure 6-10 shows that the wall heat transfer coefficient had little effect on the bottoms cyclohexane composition. This was because the bottoms cyclohexane composition was also impacted by the reboiler duty, which was changing.

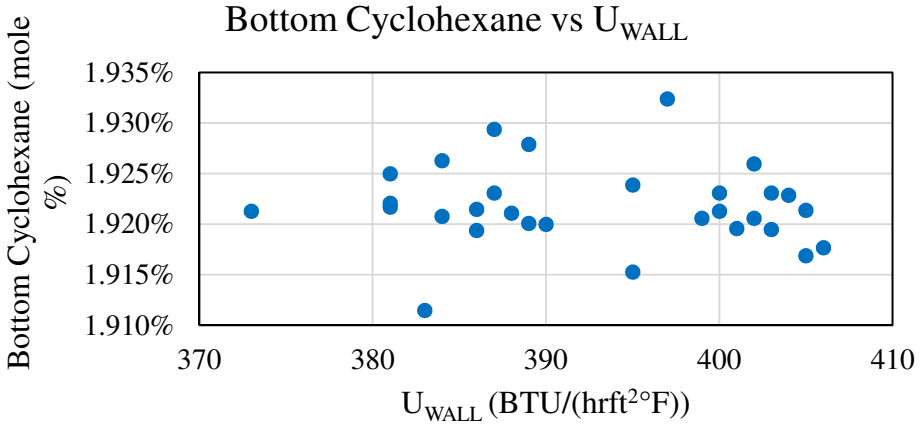

Figure 6-10 – Bottoms cyclohexane composition vs U_{WALL} for [2MP, C6, mX] finite reflux. U_{WALL} does not have a large effect on bottoms composition. Pilot cyclohexane composition was 1.67 mole percent.

Considering all of this, a U_{WALL} of 388 BTU/(hrft^2°F) was chosen as the optimum value because it matched all of the reflux flows and matched the distillate cyclohexane composition. While this U_{WALL} does not provide the closest match to either the top of wall or side composition, it is between those that do. A comparison of temperature profiles is shown in

Figure 6-11. When compared to a simulation without heat loss and one without heat transfer across the wall, incorporating the optimal values $U_{i,ATM}$ and U_{WALL} led to the best match of the upper portion of the mainfrac. The pilot temperature of 250 °F, corresponding to theoretical stage 22, was not matched in any of the models. One possible explanation is that the RTD could be located slightly off of stage 22 or that the HETP in the stripping section is different than predicted. There was close to a 100 °F difference between the top and bottom of the stripping section. With such a sharp temperature profile, slight differences in temperature locations have a larger impact. Table 6-2 compares the pilot compositions and flows with those from the model where $U_{i,ATM}$ is 9.82 BTU/(hrft^2°F) and U_{WALL} is 388 BTU/(hrft^2°F).

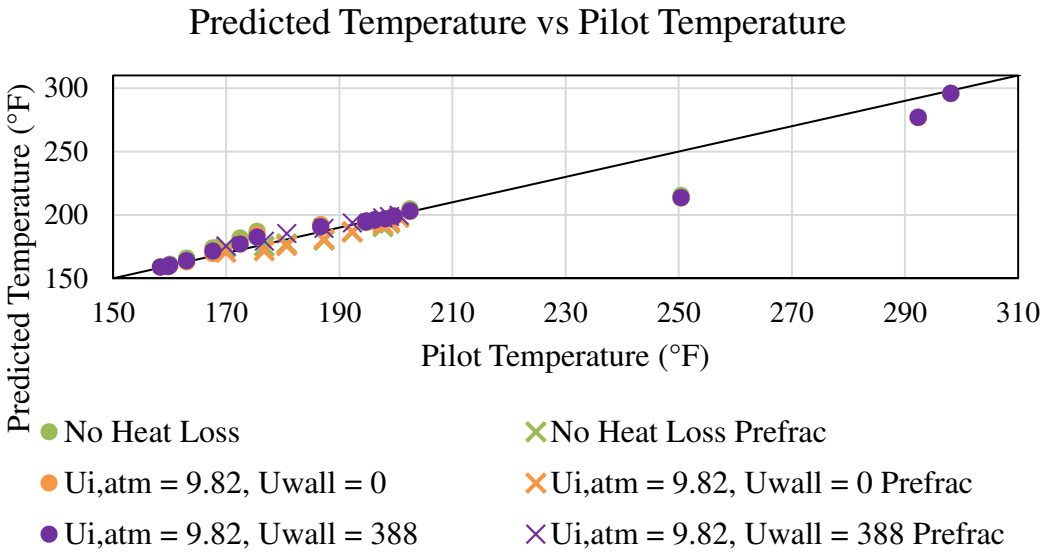

Figure 6-11 – Comparison of model and pilot temperatures for [2MP, C6, mX] finite reflux with and without heat loss

Summary of Results

Table 6-3 provides a summary of the heat transfer coefficients that best fit the pilot plant data. Because of the nonlinear nature of the process and the fact that HEEDS was matching a range of reflux flow values, a range of heat transfer coefficients were shown to be feasible. However, a singular heat transfer coefficient must be chosen for each case for modeling purposes. Sensitivity analysis testing for determining the optimal heat transfer coefficient as well as performance of the optimal heat transfer coefficients in matching the pilot data is provided in Appendix D.3. Reasons for differences in heat transfer coefficients are unknown. Though differences in liquid loadings were considered, a clear trend was not evident. The wall heat transfer coefficient seems to most closely correlate to the ambient temperature and the reboiler duty. However, this is not supported by L/V ratios in the column. More data and run conditions are needed to determine a better causality for changes in heat transfer coefficients.

Table 6-3. Heat Transfer Coefficients for All Cases

Case	$U_{i,ATM}$ BTU/(hrft^2°F)	U_{WALL} BTU/(hrft^2°F)
Total Reflux		
[2MP, C6, mX]	9.82	0
Finite Reflux		
[2MP, C6, mX]	9.82	388
[2MP, C6, tol/mX]	9.82	715.26
[2MP, C6/tol, mX]	11.23	106
[2MP/C6, tol, mX] Run 1	10.78	388
[2MP/C6, tol, mX] Run 2	10.78	222.5

PRESSURE DROP CALCULATIONS

Because the measured pressure drop is often different than the actual pressure drop of a column and the Stichlmair correlation was previously shown to match the dividing wall column well,[40] the pressure drop for the dynamic model was calculated using the Stichlmair correlation.[90] The column was separated into six sections (rectifying, upper prefrac, lower prefrac, upper mainfrac, lower mainfrac, and stripping). The average liquid

and gas rates, liquid and gas densities, and liquid and gas viscosities were calculated per section using the results from the AspenPlus® simulation. The constants used for the Stichlmair correlation are shown in Table 6-4. There are no Stichlmair constants available for Mellapak 500Y. Therefore, the constants from BX were used because BX has the most similar packing area to Mellapak 500Y. Furthermore, these constants have been previously shown to provide the best fit.[40]) The void fraction and effective packing area are from Mellapak 500Y. The resulting pressure drops per section are shown in Table 6-5.

Table 6-4. Constants used for Stichlmair calculations

C1	C2	C3	Void fraction	Effective area (m^2/m^3)
15	2	0.35	0.975	507

Table 6-5. Results from Stichlmair Calculations

Case	Pressure Drop (kPa/m)					
	Rectifying	Upper Prefrac	Upper Mainfrac	Lower Prefrac	Lower Mainfrac	Stripping
[2MP, C6, mX]	0.090	0.148	0.118	0.202	0.212	0.268
[2MP, C6, Tol/mX]	0.101	0.139	0.158	0.216	0.251	0.306
[2MP, C6/Tol, mX]	0.041	0.105	0.049	0.156	0.108	0.242
[2MP/C6, Tol, mX] Run 1	0.042	0.128	0.059	0.173	0.225	0.346
[2MP/C6, Tol, mX] Run 2	0.038	0.107	0.052	0.154	0.183	0.285

COMPARISON TO DYNAMIC MODEL

Table 6-6 compares the compositions and flows from the pilot data, the AspenPlus® model and the dynamic model. The AspenPlus® model and the dynamic model use the same heat transfer coefficients and areas. The dynamic model also includes pressure drop. Though there are some slight differences between the experimental data and the models, both models do a good job of matching the data.

Table 6-6. Comparison of pilot data, AspenPlus® model, and dynamic model for case [2MP, C6, mX]. AspenPlus® and the dynamic model use U_{WALL} = 388 BTU/(hrft^2°F) and $U_{i,ATM}$ = 9.82 BTU/(hrft^2°F). The dynamic model also accounts for pressure drop.

Variable	Pilot Data		Aspen	Dynamic Model
	Average	Standard Deviation		
Product Compositions (mol %)				
Distillate				
2MP	97.89		97.89	97.97
C6	2.11		2.11	2.03
Tol	0.00		0.00	0.00
mX	0.00		0.00	0.00
Top of Wall				
2MP	65.04	± 0.30	58.57	59.28
C6	34.96	± 0.30	41.43	40.72
Tol	0.00	± 0.00	0.00	0.00
mX	0.00	± 0.00	0.00	0.00
Side				
2MP	4.20		4.02	3.98
C6	95.76		95.95	96.00
Tol	0.04		0.03	0.02
mX	0.00		0.00	0.00
Bottoms				
2MP	0.00		0.00	0.00
C6	1.73		1.92	1.97
Tol	1.46		1.71	1.70
mX	96.81		96.37	96.33
Material Balance Flows (lbmol/hr)				
Distillate	0.185		0.185	0.185
Side	0.176		0.177	0.176
Bottoms	0.183		0.182	0.182
Internal Flows				
Overhead Reflux (lbmol/hr)	1.769	± 0.141	1.874	1.940
Prefrac Reflux (lbmol/hr)	1.543	± 0.089	1.606	1.638
Mainfrac Reflux (lbmol/hr)	1.281	± 0.069	1.314	1.360
Side Reflux (lbmol/hr)	1.804	± 0.003	1.806	1.870
Reboiler Duty (BTU/hr)	71767	± 1980	70163.2	70163

SUMMARY AND CONCLUSIONS

Evidence for heat transfer in the DWC pilot column was presented, and a systematic procedure for determining heat transfer coefficients to model the heat transfer was developed. In the dividing wall pilot column, heat was transferred to the atmosphere and through the non-insulated stainless steel dividing wall. Heat transfer resulted in condensation of vapor traffic and therefore increased reflux flows. By matching the column's reflux flows within a standard deviation of their steady state values, a range of feasible heat transfer coefficients were determined while accounting for process variability. To further refine the ranges of these heat transfer coefficients, temperatures and compositions were considered. To remove any modeling issues caused by material balance violations of noisy data, an optimization procedure was developed to determine optimal material balance flows to be placed in the model. This work resulted in steady state models that matched five of the six data sets. Heat transfer coefficients were still determined for the sixth data set, [2MP, C6/tol, mX]. Although these resulted in product compositions that were close to their experimental values, the sidedraw reflux was still too low for this case. Values of optimal heat transfer coefficients varied between cases though effort was made to find a universal set of heat transfer coefficients. Reasons for differences in heat transfer coefficients are unknown. Since the material of the column is not changing, changes in heat transfer coefficients are representative of changes in film thickness or wall wettability. Heat transfer coefficients are used in this work as a modeling parameter to better match the data. There may still be changes in the physical phenomena occurring within the column which are not understood.

Chapter 7: Dynamics

In addition to testing if the control configurations could be used to transition the column between steady states, the control configurations were tested against disturbances. Because changes in feed conditions are most common in process plants, feed disturbances were tested. Using two temperature controllers, the column successfully rejected a series of disturbances, which is impressive given that the column was not designed for this chemical system. However, matching the model dynamics to the process data was not successful. While the model successfully rejected the feed disturbances, the response direction of many temperatures in the model did not match that of the pilot data.

EXPERIMENTAL FEED DISTURBANCE

A series of disturbances were tested on case [2MP/C6, Tol, mX] to test the ability of the control structure to reject feed disturbances. Pulse disturbances were conducted for the feed flow, feed temperature, and feed composition (Figure 7-1). The feed composition was changed such that the toluene feed composition was increased (Table 7-1). After the feed flow and feed temperature changes, 10 lbm/hr of additional pure toluene was fed to the column for thirty minutes while the overall feed flow remained constant.

Table 7-1. Feed composition before and during feed composition disturbance

	Component Weight Percent			
	2MP	**C6**	**Tol**	**mX**
Before	32.51	30.75	3.60	33.14
After	26.42	24.76	22.86	25.96

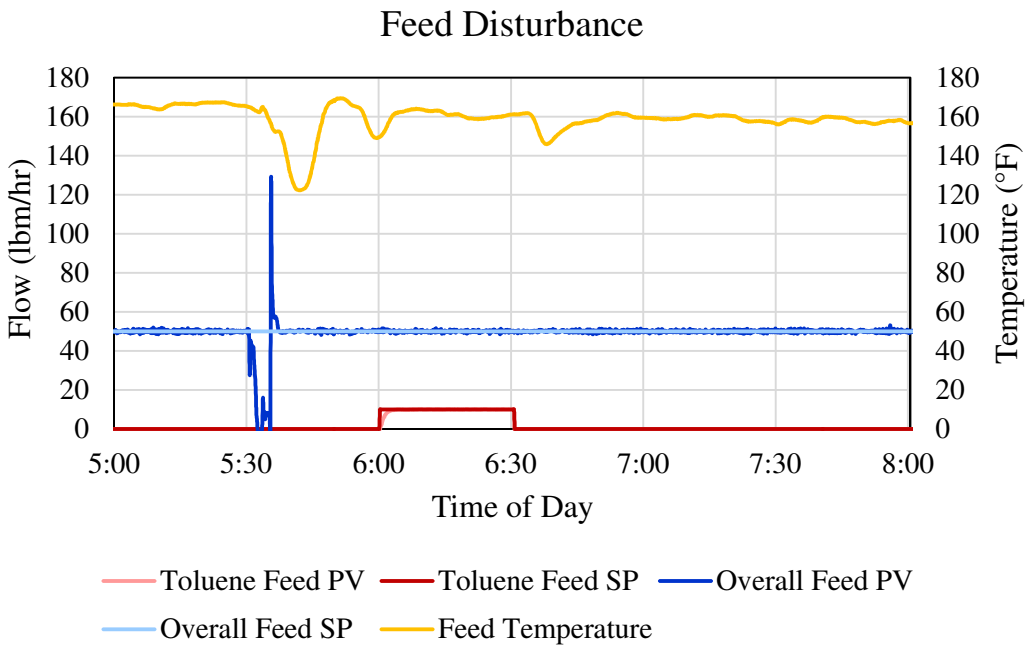

Figure 7-1 – Series of feed disturbances starting with feed flow followed by feed temperature and finally composition

The column successfully rejected all disturbances. The decrease in feed flow had the largest impact on the column. Cutting off the feed to the column significantly decreased the liquid traffic in the prefractionator. Without the same liquid to vapor ratio, the prefractionator could not perform the necessary separation. The deteriorated separation is evidenced by the change in prefractionator temperatures. The lower and upper portions of the prefractionator move closer to the same temperature indicating a consistent composition throughout the prefractionator (Figure 7-2). The distillate flow also decreased since the flow was manipulating the reflux drum level and the feed to the column was essentially cut off. The decreased distillate flow pushed the lighter components down the column as evidenced by the decreasing temperatures throughout the column (except for the upper prefrac as explained earlier) (Figure 7-2). Because the change in feed flow was drastic, the effects of the disturbance masked the effects of the feed temperature change. The feed flow disturbance was still working its way through the column when the feed

composition disturbance was started. As shown in Table 7-1, the composition of m-xylene fell as more toluene was added to the feed. This lowered the stripping temperature which was already falling due to the feed flow disturbance. The controller responded to this change by increasing the steam flow therefore increasing the vapor traffic in the column. As the vapor rose up the column, so did the temperatures. As toluene rose out of the stripping section and up the mainfrac side of the wall, the mainfrac temperatures increased, and the side product flow was increased to its steady state level. When the increased vapor reached overhead, the distillate responded to the increase in reflux drum level, and the material balance was restored. After the increased toluene was worked out of the system, the reboiler duty moved back to its original value though somewhat different due to changes in ambient conditions.

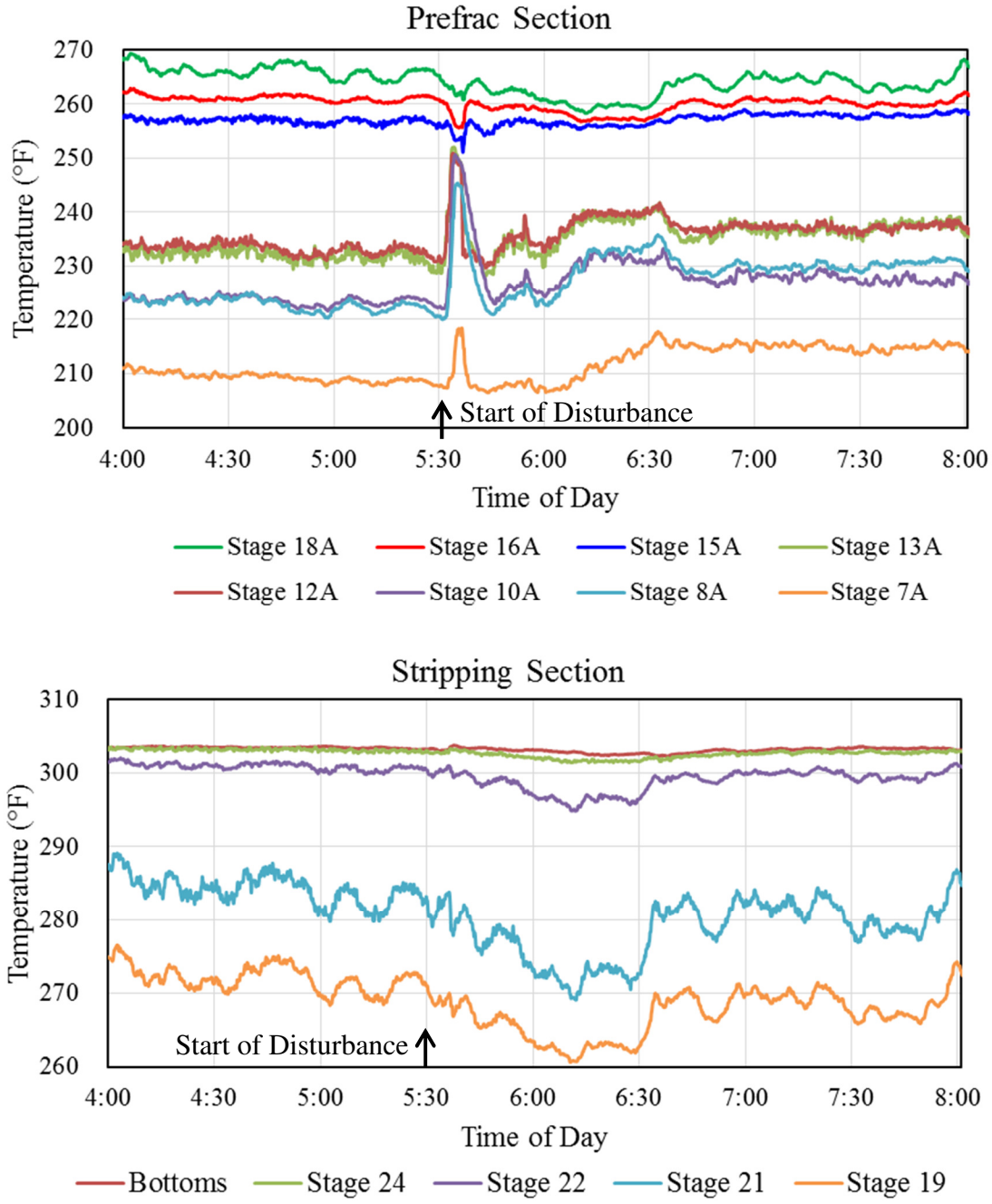

Figure 7-2 – While temperatures in the stripping section decreased, the temperatures in the prefractionator section moved towards one another signifying a deteriorated separation following the feed disturbance

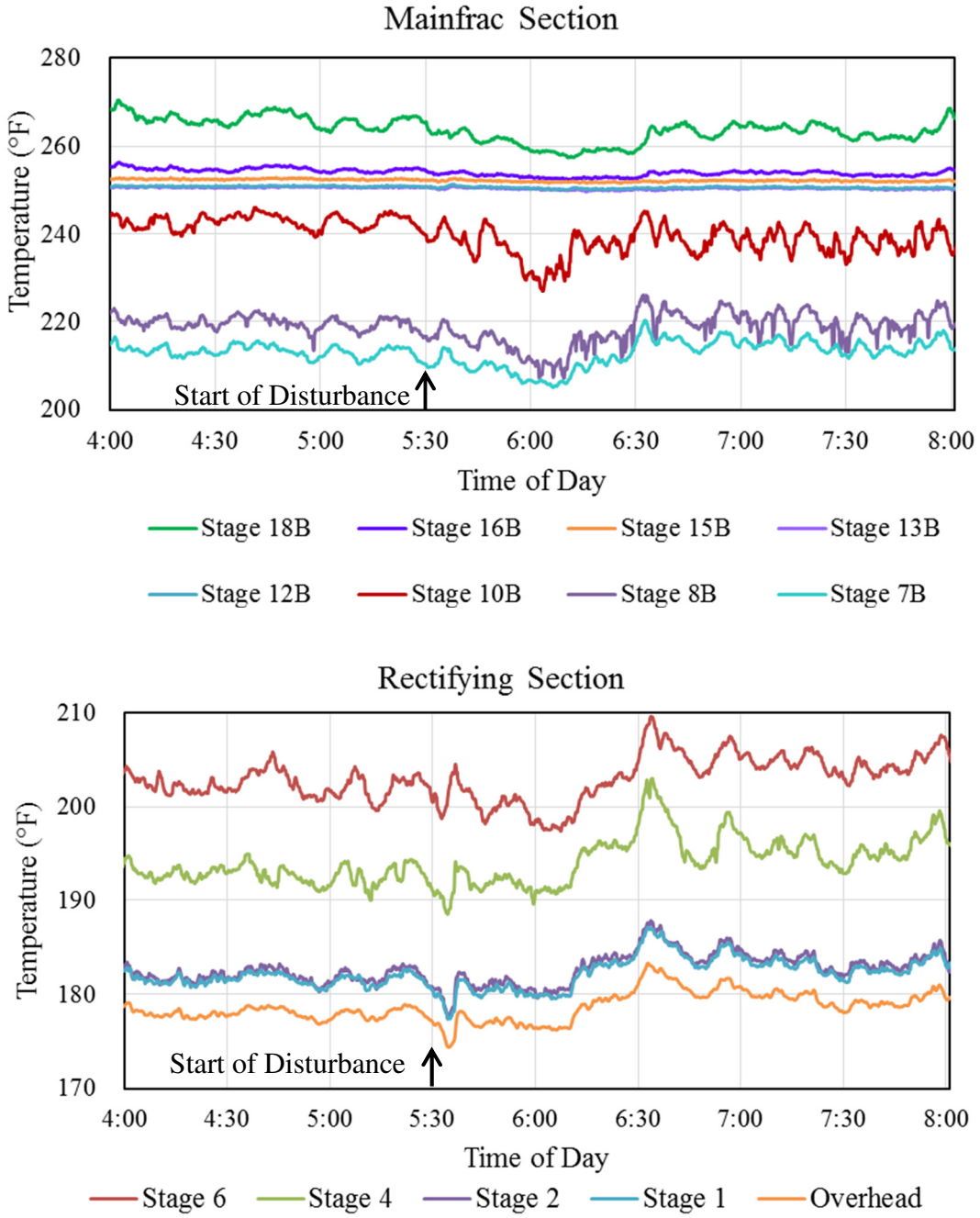

Figure 7-3 – Following the disturbance at 5:30, the temperatures in the prefractionator section moved towards one another signifying a deteriorated separation following the feed disturbance

Product samples confirmed the performance of the two temperature controllers (Figure 7-4 - Figure 7-7). Though both the bottoms and the side product compositions varied slightly, both compositions returned to their original steady state values. The bottoms composition returned slightly faster due to the tighter tuning of the stripping temperature controller while the side product was slightly slower due to the more relaxed tuning of the mainfrac temperature controller.

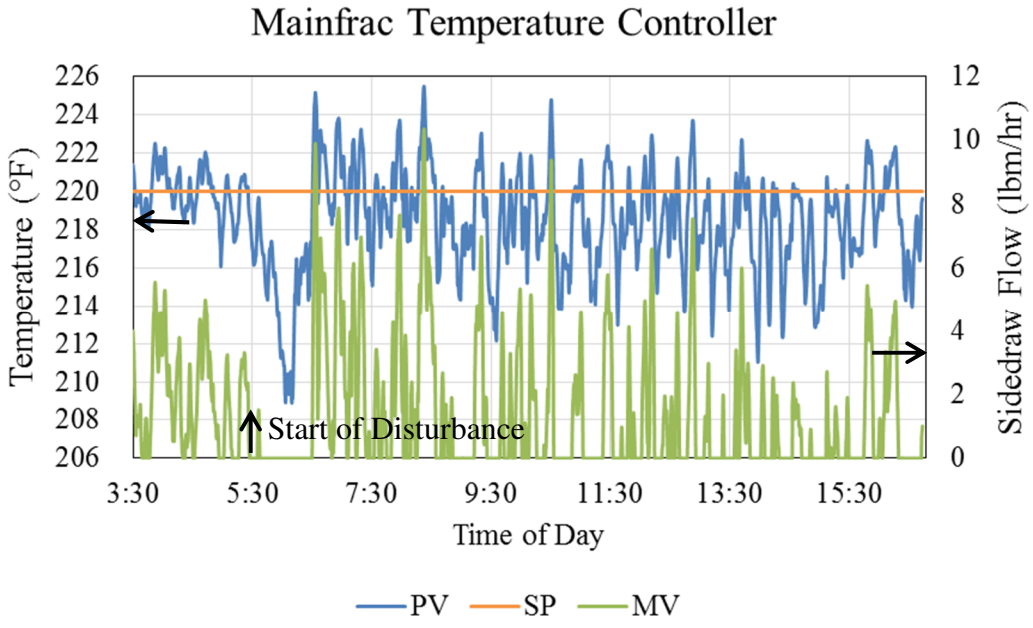

Figure 7-4 – Mainfrac temperature controller during feed disturbance

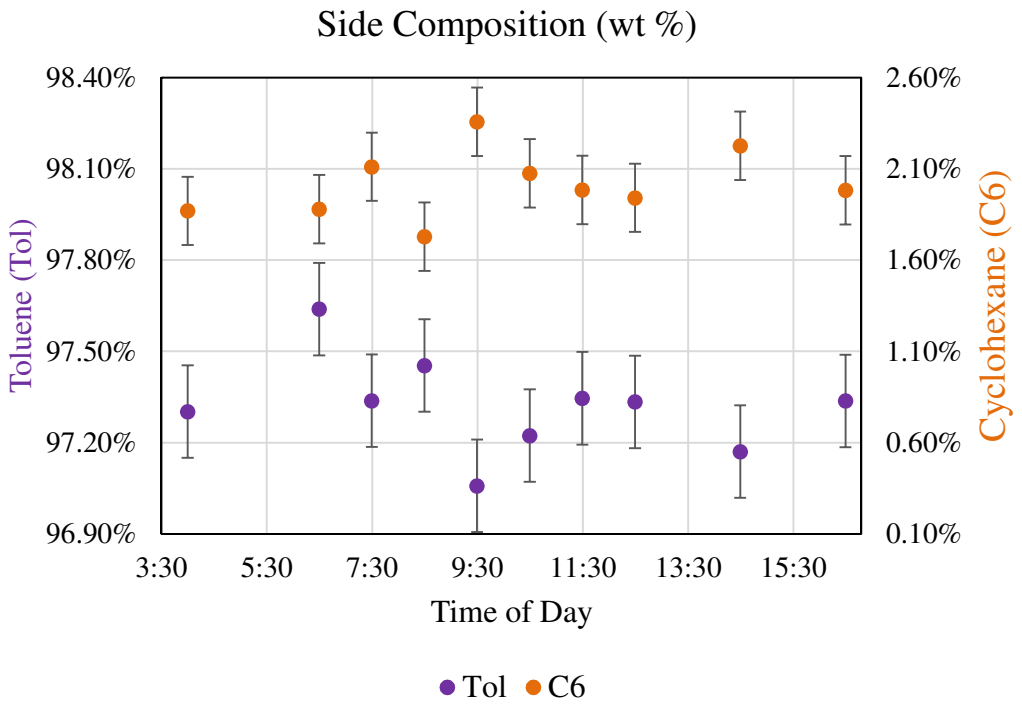

Figure 7-5 – Sidedraw composition during feed disturbance

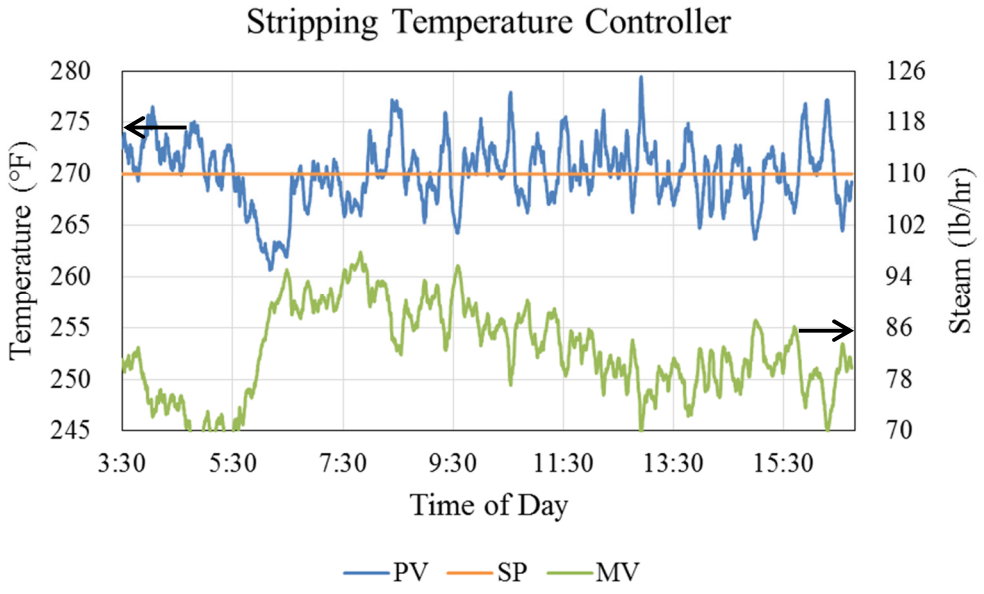

Figure 7-6 – Stripping temperature controller during feed disturbance

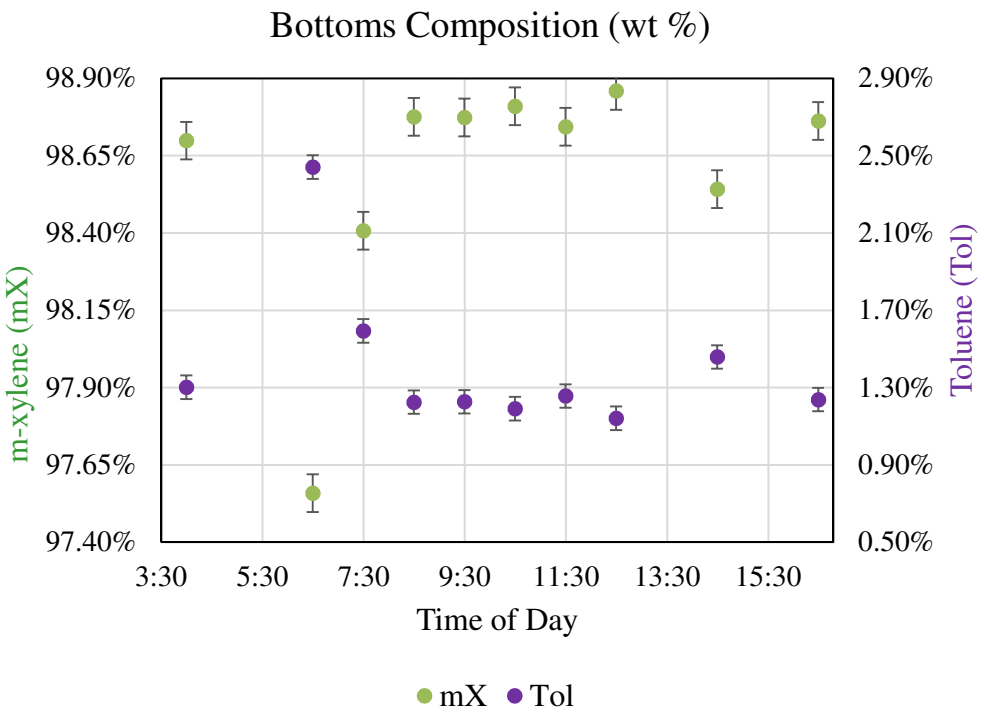

Figure 7-7 – Bottoms composition during feed disturbance

SIMULATION FEED DISTURBANCE

The same feed disturbance was replicated on the model to compare the model's dynamic response. Though the model successfully rejected the series of disturbances, some of the compositions and temperatures in the model exhibited different responses than seen on the pilot column.

Model Tuning

Because the identification of control structures was steady-state based and the pilot tuning had to be updated for each set of run conditions (Table B-3), the tuning of the dynamic model was updated. The dynamic model and the DeltaV™ DCS use different

units for tuning parameters. Therefore, the DeltaV™ tuning parameters were converted before being placed in the dynamic model. The conversion process and tuning parameters are discussed in Appendix D.

Procedure

Case [2MP/C6, Tol, mX] run 2 was the base model used for the feed disturbance. Flow temperatures were updated with the experimental temperatures averaged over a three hour period before the disturbance testing. The feed composition was also updated to match that used during the disturbance testing and minor adjustments were made so that the control temperatures were at setpoint. Though there were some differences in the sidedraw reflux and the top of the wall and bottoms compositions, the model matched the data well (Table D-2 and Figure D-1).

The dynamic model has the ability to read in data and to write this data as inputs to the column. Therefore, experimental data recorded at 10 second intervals was imported into the model. Experimental data from the overall feed flow (FC600) and feed temperature (TT610) was used as the model's feed flow and feed temperature. For plotting reasons, ninety minutes of data before the disturbance was included. The start of this data is referenced as 0:00 simulation time. The composition data was not continuous and the model did not have a separate toluene feed flow like the pilot column. Therefore, the feed composition disturbance was conducted manually. Thirty minutes after the start of the feed flow disturbance (2 hours overall simulation time), the model was stopped, and the composition was changed to match the experimental data (Table D-1). The composition was returned to its initial value after 30 minutes of simulation time (2:30 overall simulation time).

Results

Although the model successfully rejected the feed disturbance, the model response did not match that of the experimental column. Decreasing the feed flow on the experimental column caused all of the temperatures in the prefractionator to move towards one another as the separation deteriorated. This phenomena was not seen on the model. Instead, all of the temperatures in the prefrac section increased following the change in feed flow (Figure 7-8).

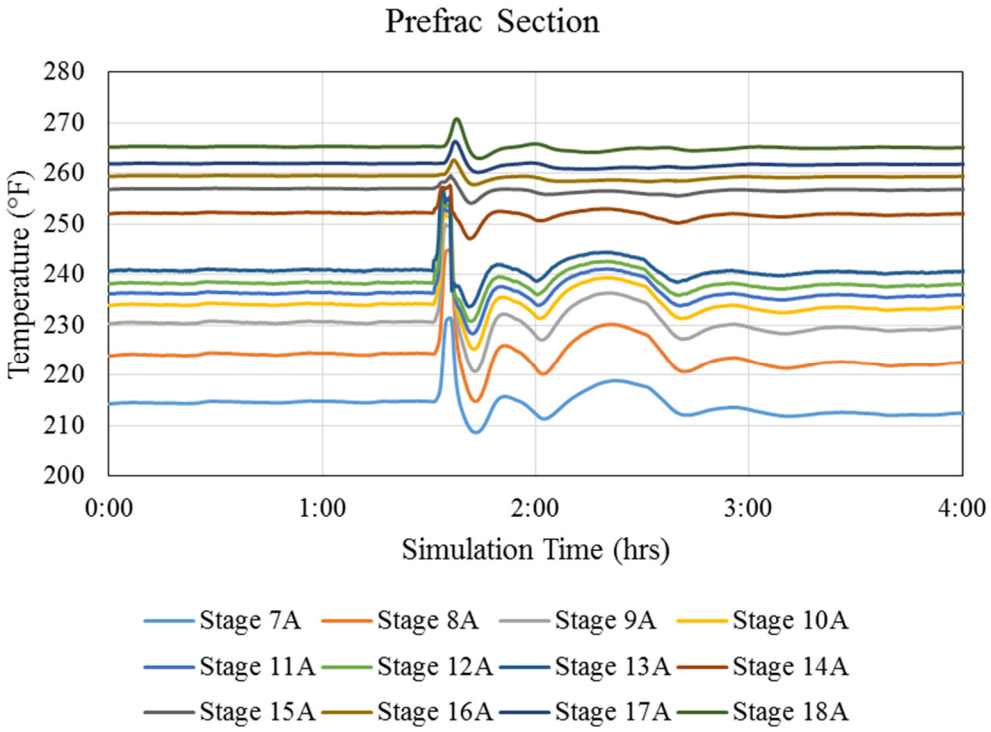

Figure 7-8 – All prefractionator temperatures in the model increased following the change in feed flow and feed temperature starting at 1:30 signifying heavy components moving up the column

Following the disturbance in feed flow on the pilot column, the distillate flow decreased. The same response was seen in the model (Figure 7-9). However, while the

change in experimental distillate flow was almost instantaneous, there was a slight delay in the model. This caused the decrease in rectifying section temperatures to also be delayed (Figure 7-10). Following the disturbance, there was an initial increase in the model's distillate flow which caused many of the column temperatures to increase. The same increase in many column temperatures was not seen on the pilot column though a small increase in distillate flow would not be discernable due to the low signal to noise ratio.

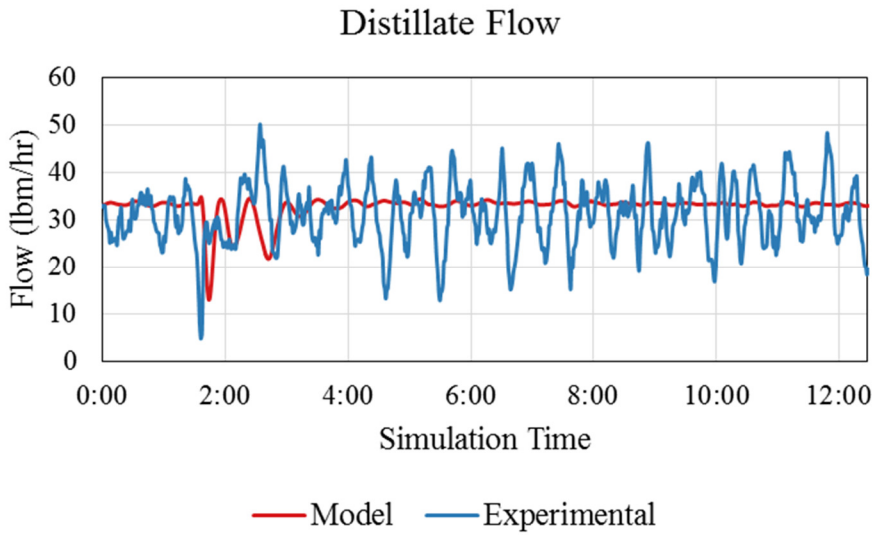

Figure 7-9 – Similar to the pilot column, the distillate flow decreased after the feed flow and temperature disturbance at 1:30 simulation time. However, the decrease in distillate flow occurred later in the model therefore delaying the decrease in the rectifying section temperatures.

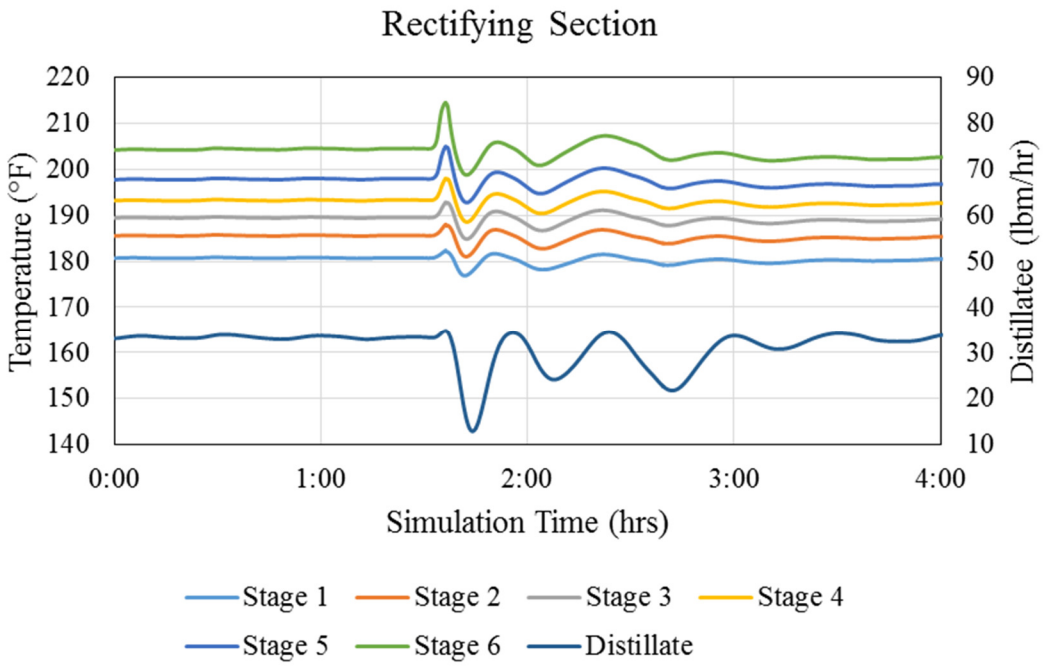

Figure 7-10 – Temperatures in the rectifying section initially increased after the feed flow disturbance. However, they decreased after the change in distillate flow.

Temperatures in the mainfractionator also decreased due to the decrease in distillate flow (Figure 7-11). This follows the trend seen in the pilot column. The similar trends of the model and experimental mainfractionator temperatures extends to the mainfrac temperature controller (Figure 7-12). Both temperatures decreased following the disturbance, with the experimental temperature decreasing more than that on the model. In response, both controllers decreased the sidedraw flow. After enough toluene was accumulated to increase the mainfractionator temperature, the sidedraw flow was increased. The accumulation of toluene occurred faster in the model than on the pilot column as seen by the faster increase in side product flowrate (Figure 7-13). In addition, the temperature controller in the model takes almost ten hours to return to setpoint.

However, comparing this to the pilot column is difficult because of the large amount of noise.

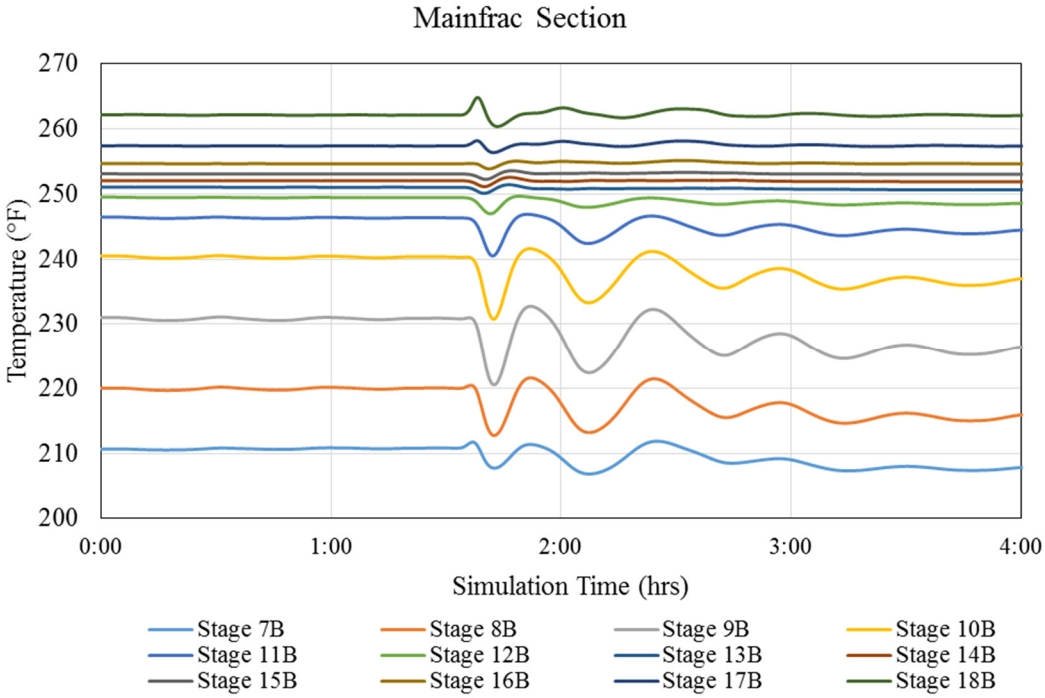

Figure 7-11 – Temperatures in the mainfractionator section decreased in the model, matching those of the pilot column

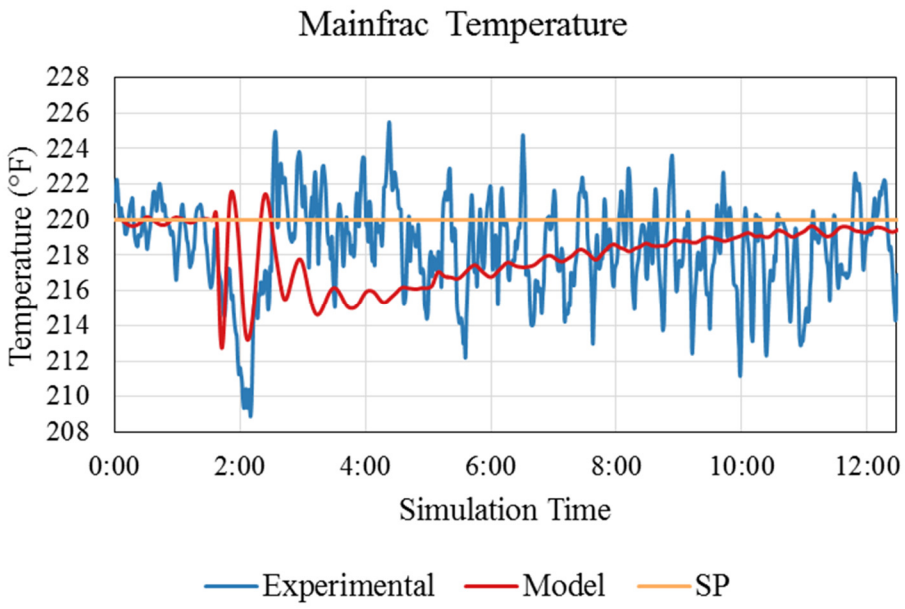

Figure 7-12 – The mainfractionator temperature controller of both the model and the pilot column responded similarly to the disturbance

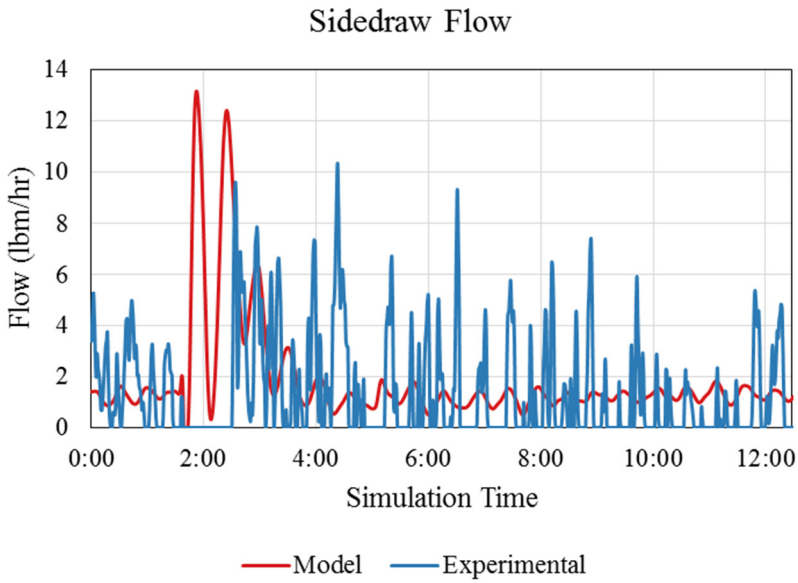

Figure 7-13 – Sidedraw flow was the manipulated variable of the mainfrac temperature controller. The model increased the sidedraw flowrate faster in response to the disturbance than the experimental controller

While the temperature controller behaved similarly, the compositions did not. The model and experimental sidedraw compositions are compared in Figures 7-14 and 7-15. The time of the experimental data has been changed to time relative to the start of the data that was imported into the dynamic model. Zero hours refers to the same feed temperature and flow in both the model and experimental plots. Overall, the disturbance caused in increase in sidedraw cycolohexane for both the model and the pilot column though the cyclohexane composition changed more in the model and the pilot data composition had more fluctuation.

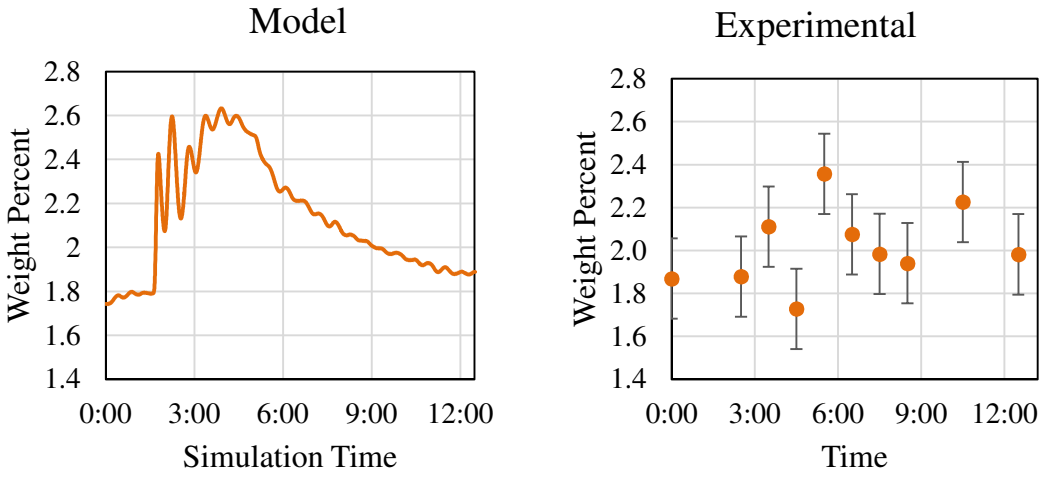

Figure 7-14 – Sidedraw Cyclohexane composition during feed disturbance

The sidedraw toluene composition behaved differently in the model than seen on the pilot column. The toluene composition in the model decreased after the disturbance while the experimental toluene initially increased (Figure 7-15).

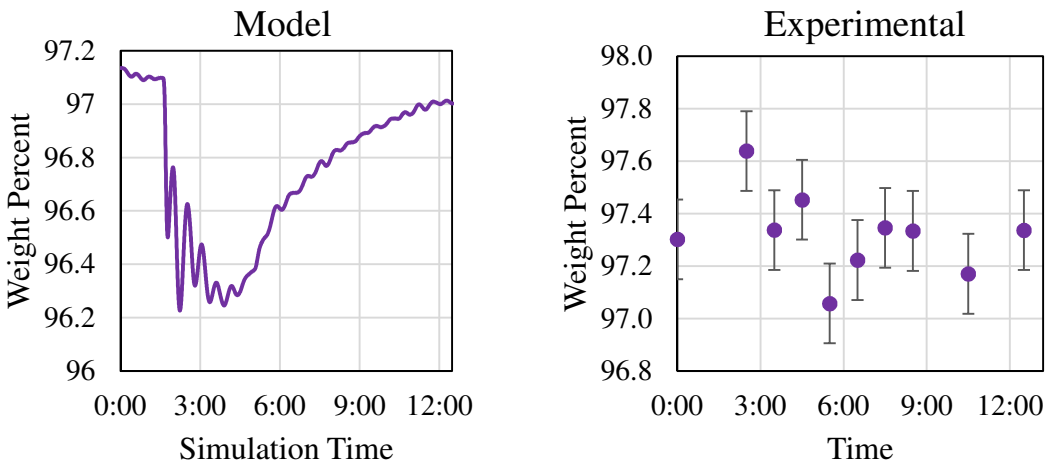

Figure 7-15 – Sidedraw Toluene composition during feed disturbance

Unlike the pilot column, the model stripping section temperatures increased following the feed disturbances. The reason for this difference is unclear though the difference in response in prefractionator temperatures could be related.

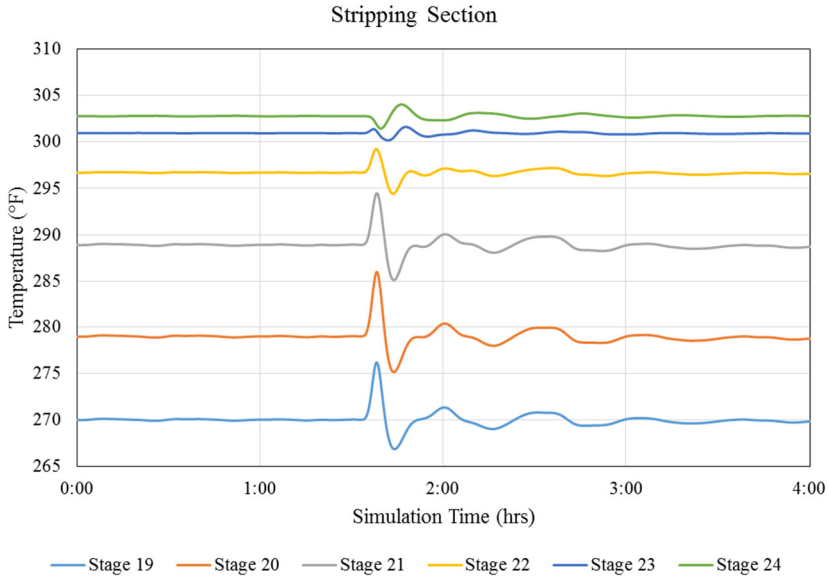

Figure 7-16 – Unlike the pilot column, the model stripping section temperatures increased following the disturbance in feed flow and temperature (1:30)

Because the stripping temperatures responded differently to the disturbance, the stripping temperature controller of the model had the opposite response of that on the pilot column (Figure 7-17). The bottoms composition also behaved in a manner opposite to that seen on the pilot column. Experimental composition was analyzed every 60 minutes. Therefore, if the composition was oscillating as frequently as the model suggests then some of those fluctuations could have been missed due to sampling. To negate the increase in temperature, the controller decreased the steam flow rather than increasing the steam like on the pilot column (Figure 7-18). The difference in steam flow of the model and experimental data also impacted the internal flows of the column (mainfrac, prefrac, and sidedraw reflux) (Figure 7-21). The high noise to signal ratio of the experimental data should once again be noted.

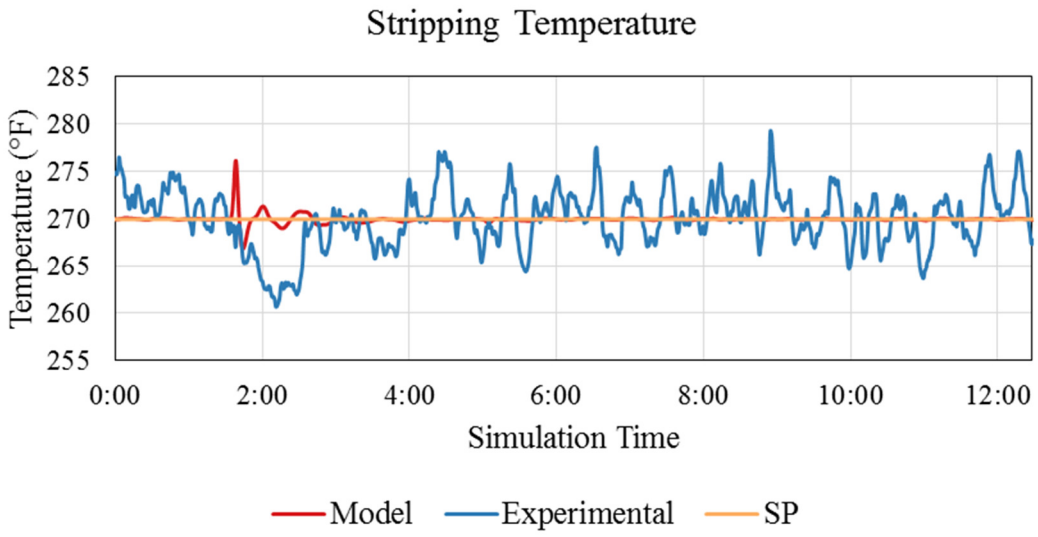

Figure 7-17 – The stripping control temperature of the model responded in the opposite direction of the experimental temperature

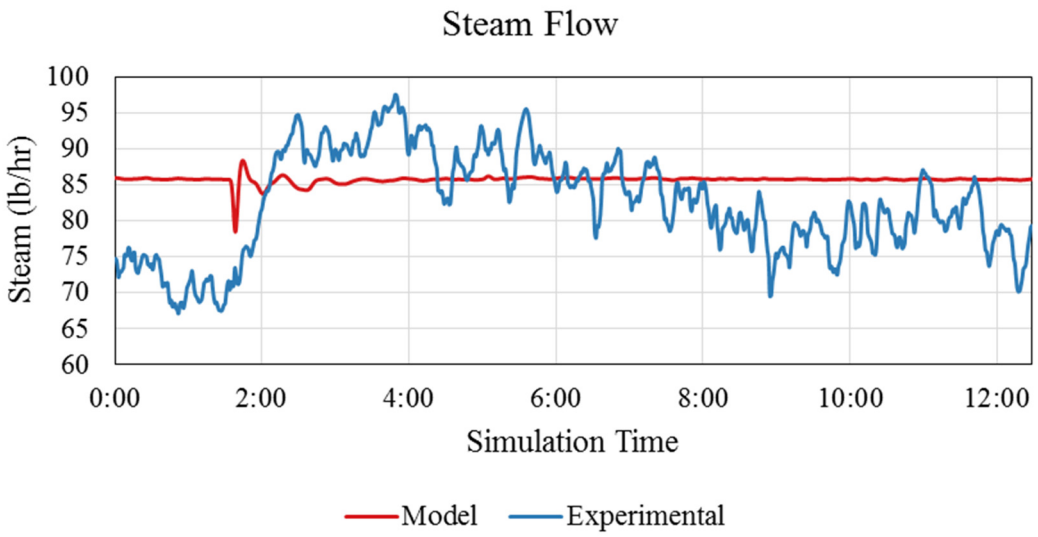

Figure 7-18 – Steam flow was the manipulated variable of the stripping section temperature controller. The magnitude and direction of the change in steam flow was different between the model and the experimental data.

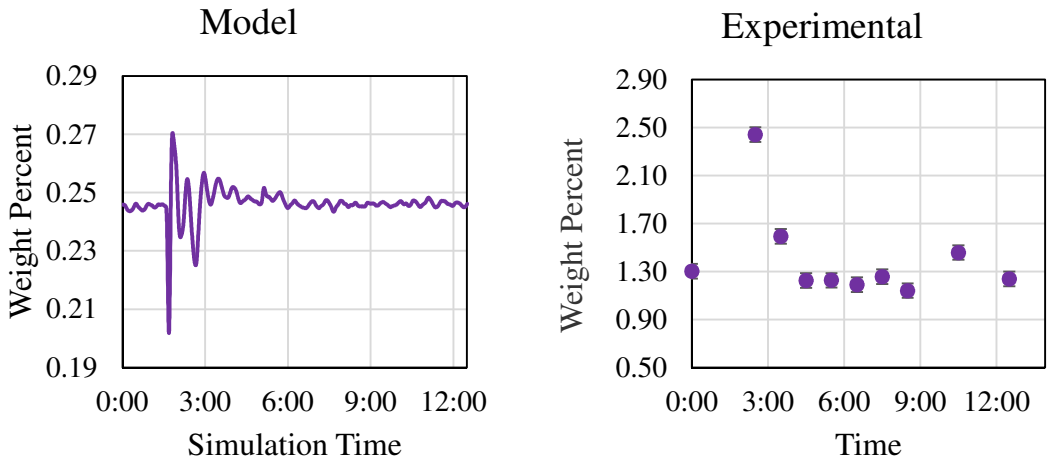

Figure 7-19 – Bottoms toluene composition during feed disturbance; the experimental data had a much larger change in bottoms toluene composition following the disturbance

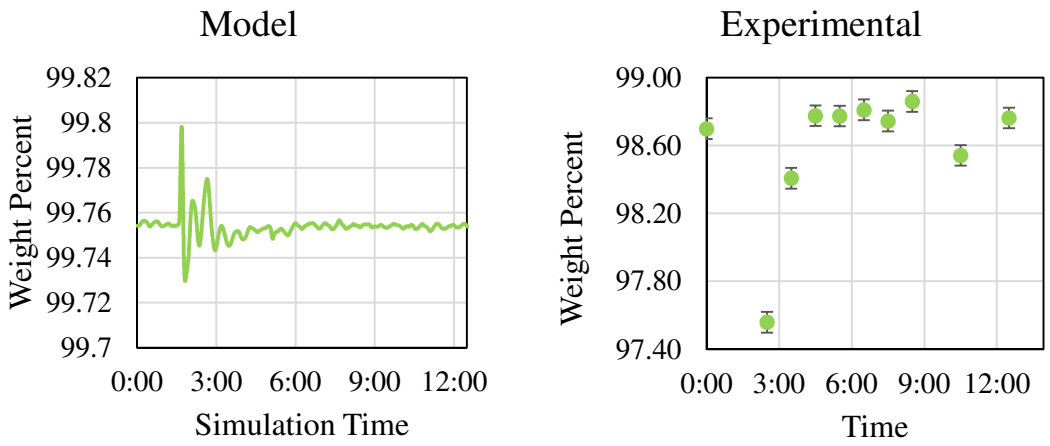

Figure 7-20 – Bottoms m-xylene composition during feed disturbance

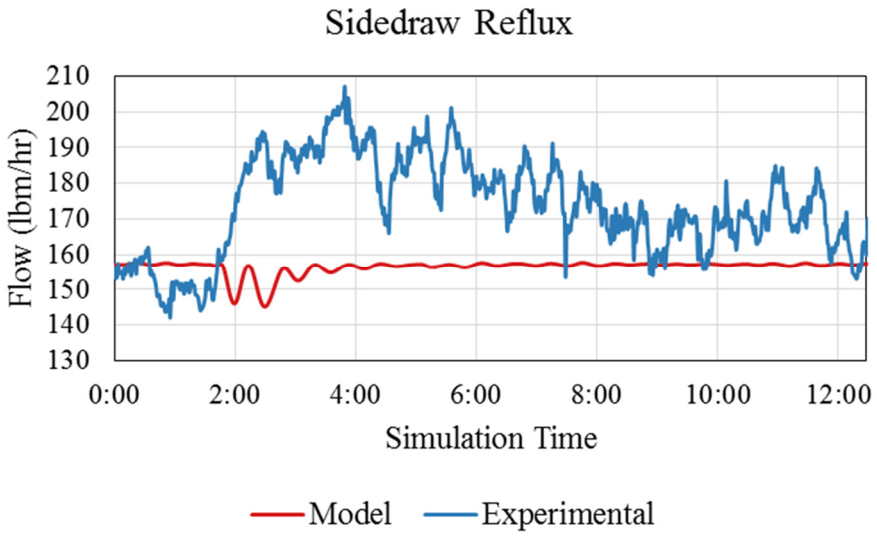

Figure 7-21 – Sidedraw reflux was used for level control of the side product tank; the experimental value fluctuated more due to the higher fluctuation in steam flow

In summary, the response of the pilot column to changes in feed flow, temperature, and composition could not be replicated on the dynamic model. Though some elements such as the mainfractionator temperature controller and the distillate flow behaved in a

similar manner to those on the pilot column, other items such as the sidedraw toluene composition, lower prefractionator temperatures, and the stripping section temperature controller had the opposite response to that seen on the pilot column. While there are many potential reasons for these differing responses, there is no obvious explanation.

One potential reason the model did not match the data is that the model used a series of flash tanks to approximate a packed column. A series of flash tanks could potentially have a slower response. Methods exist for modeling packed columns, and changing the model in this manner could improve the column's response time. This would improve the model's ability to match the response of the distillate flow and the rectifying section temperatures. However, the model was not always slower than the experimental data. For example, the accumulation of sidedraw toluene was faster on the model than on the pilot column.

Another potential reason the model did not match the data is misunderstood effects of the pilot plant such as heat loss and effects from the metal packing. The heat loss was incorporated into the model as a constant value. However, unaccounted changes in heat transfer either through the wall or to the atmosphere would impact column operation.

Finally, the pilot column could have not been steady at the start of the disturbance. Due to its high surface area to volume ratio, the column was susceptible to changes in ambient conditions. A change in atmospheric temperature or wind speed or direction could disrupt column operation. Additionally, changes in steam pressure caused large fluctuations in steady-state steam flow. When averaged over hours of column operation, these effects do not impact column operation. However, changes prior to the feed disturbance could impact the column's response.

Chapter 8: Minimum Energy

This work examines an experimentally-validated rigorous model scaled to the size of an industrial column. The model includes heat transfer both through the dividing wall and to the atmosphere. A response surface which plots the minimum reboiler duty necessary to meet product specifications for various liquid and vapor split values is presented, and potential control variables are investigated. Though conclusions are specific to the particular chemical system and column design investigated, this work highlights a general method with which DWC design and control can be rigorously explored.

MODEL DETAILS AND PROCEDURE

The Aspen Plus® steady state dividing wall column model previously connected to HEEDS to model heat transfer was used for this study. The model for case [2MP, C6, Tol/mX] was scaled to a 6 foot diameter tower to study a more industrially-relevant column size where the effects of heat transfer would be minimized. The feed composition and number of stages remained the same, and the feed and product flows were scaled with the cross sectional area. The reboiler duty was determined by matching overhead reflux flow with the scaled experimental reflux flow therefore insuring that the hydraulics in the column remained the same. Previous work on the pilot column[40] has shown that the liquid loading on the pilot DWC was not enough to impact the vapor split at the bottom of the wall, though it should be noted that both sides of the wall had similar internals and the same packing. Because of this, the vapor split can be assumed to follow the wall placement. The same heat transfer coefficients (9.82 BTU/(hrft^2°F) $U_{i,ATM}$ and 715.26 BTU/(hrft^2°F) U_{WALL}) were used, but the areas were updated to reflect the change in column size. The pilot column temperatures were used to calculate the heat transfer values. Stichlmair model was used to calculate the pressure drop, and the feed was saturated liquid.

The AspenPlus® model was connected to HEEDS so that various simulations could be run simultaneously and automatically. The user specified the reboiler duty, distillate flow, side product flow, liquid split, and vapor split through HEEDS, and these were then

fed to the Aspen simulation. Component recoveries were specified as 97 percent 2-methylpentane recovery in the distillate, 96 percent cyclohexane recovery in the side, and 97 percent toluene recovery in the bottoms product. These recoveries were determined from experimental data. A range of liquid and vapor splits were investigated, and for each liquid and vapor split, the solution which had the minimum reboiler duty and satisfied the product recoveries was determined. The optimization method used in this research was the HEEDS proprietary method SHERPA (Simultaneous Hybrid Exploration Robust Progressive Adaptive). HEEDS was operated on a PC running Windows 7© 64-bit, having a 2.8 GHz Intel© Xeon© Core processor with 8 GB of RAM and 8 threads.

RESULTS

Response Surface

The optimal solutions of the model were plotted as a solution surface to show the minimum energy demand necessary to meet the constraints of product recovery for given vapor and liquid splits. The resulting response surface is shown in Figure 8-1. The surface is characterized by a region of fairly consistent energy requirement and a steep wall at which the energy requirement increases drastically. Because the column had a finite number of stages, the desired component recoveries could not be met for all combinations of liquid and vapor split. Halvorsen and Skogestad[17] found that for a hypothetical chemical system with relative volatilities [4,2,1] in a column with 100 total stages, in an equilibrium stage model with constant relative volatility, pressure and molar flows and no heat transfer the solution surface looked like a hull of a ship for a partially vaporized feed (q = 0.477). The solution surface in Figure 8-1 does not look like a hull of a ship because the column design does not have enough stages to make all combinations of liquid and vapor split feasible. As pointed out by Halvorsen and Skogestad,[17] changes in some directions along the minimum energy surface lead to gradual increases in reboiler duty while changes along other directions lead to significant increases in energy demand. Feasible solutions with a lower energy requirement favor a vapor split at which more vapor goes to the prefrac side

rather than the mainfrac side as seen in Figure 8-2. This suggests that while adding stages to the column will help prevent regions of product spec infeasibility, changing the wall placement will do the same.

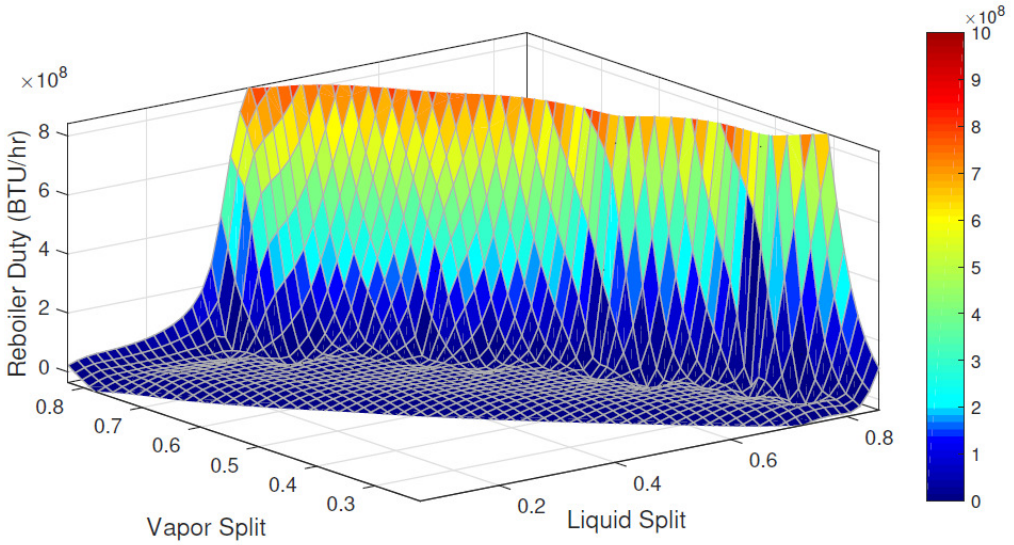

Figure 8-1 – Response surface showing minimum energy satisfying product specifications for a given vapor and liquid split

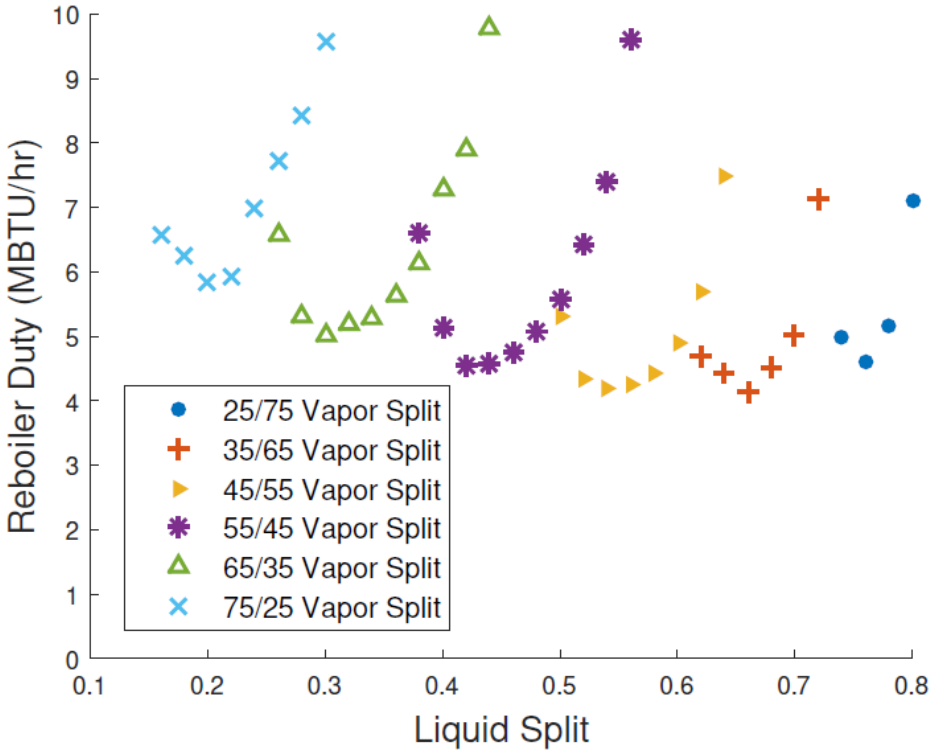

Figure 8-2 – The absolute minimum reboiler duty coincides with a vapor split of 35 percent of the flow to the prefractionator and 65 percent of the flow to the mainfractionator and a liquid split of 0.66. However, the region of minimum reboiler duty is fairly flat, and similar reboiler duties can be found for other vapor and liquid splits.

The absolute minimum of Figure 8-1 corresponds to a vapor split of 0.35 and a liquid split of 0.66 though Figure 8-2 shows that other vapor and liquid splits can lead to similar reboiler values. The composition profiles for this case are shown in Figure 8-3 and Figure 8-4.

Figure 8-3 shows the composition profiles of the rectifying, mainfrac, and stripping sections. The mainfrac section or wall portion extends from theoretical stage 7 to 18. Similar to previous results,[17,39] the maximum compositions of 2-methylpentane, cyclohexane, and m-xylene align with the stages of the product streams. Figure 8-4 shows the composition profiles of the prefrac section where the feed enters at theoretical stage 13. Because they were part of the bottoms product, most of the toluene and m-xylene traveled

to the bottom of the wall with only a very small portion going over the wall. Conversely, most of the lightest component, 2-methylpentane, traveled to the top of the wall. The side product, cyclohexane, split both above and below the wall. This agrees with previous studies that showed the prefractionator to perform the separation between the lightest and heaviest components.[17] However, because of the additional toluene in the bottoms product, the separation in the prefractionator is between the 2-methylpentane and the toluene. Similar to previous work, the rectifying section and portion of the mainfractionator above the sidedraw serve as a binary column in which 2-methylpentane and cyclohexane are separated. The lower portion of the mainfractionator and the stripping section separate the remaining cyclohexane from the heavier components. Including heat transfer and a trace component has not significantly changed the composition profiles of the column.

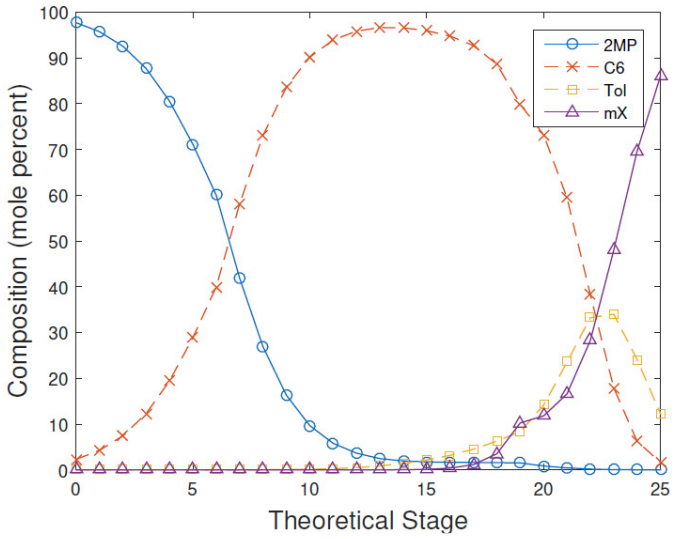

Figure 8-3 – Composition profile of absolute minimum energy solution for the rectifying (stages 0-6), mainfrac (stages 7-18), and stripping (stages 19-15) sections

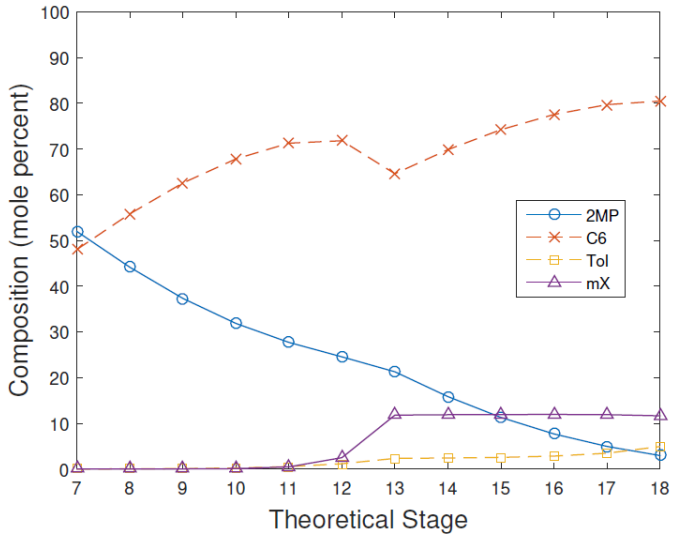

Figure 8-4 – Composition profile of absolute minimum energy solution for the prefrac section where the saturated liquid feed enters at theoretical stage 13

Of course, composition profiles of an operating column are difficult and impractical to monitor. To avoid costly composition analyzers, temperatures are often used for control instead. The temperature profile associated with the composition profiles shown in Figure 8-3 and Figure 8-4 is shown in Figure 8-5. As with temperature profiles of traditional distillation columns, all products are removed close to their boiling points. Because heat transfer through the wall is included in the model and the feed and side product compositions are close in boiling temperature (200.66 °F and 184.28 °F, respectively), there is little temperature difference across the wall. In addition, Figure 8-5 shows a relatively small change in temperature from the top of the wall (stage 7) to the bottom of the wall (Stage 18). The composition profiles show that the wall regions of the column are dominated by cyclohexane. The wall regions below the feed and sidedraw (stages 13-18) are particularly flat because most of the separation between cyclohexane and toluene occurs in the stripping section. Because of this, a temperature in the lower region of the wall would not be a good candidate for control.

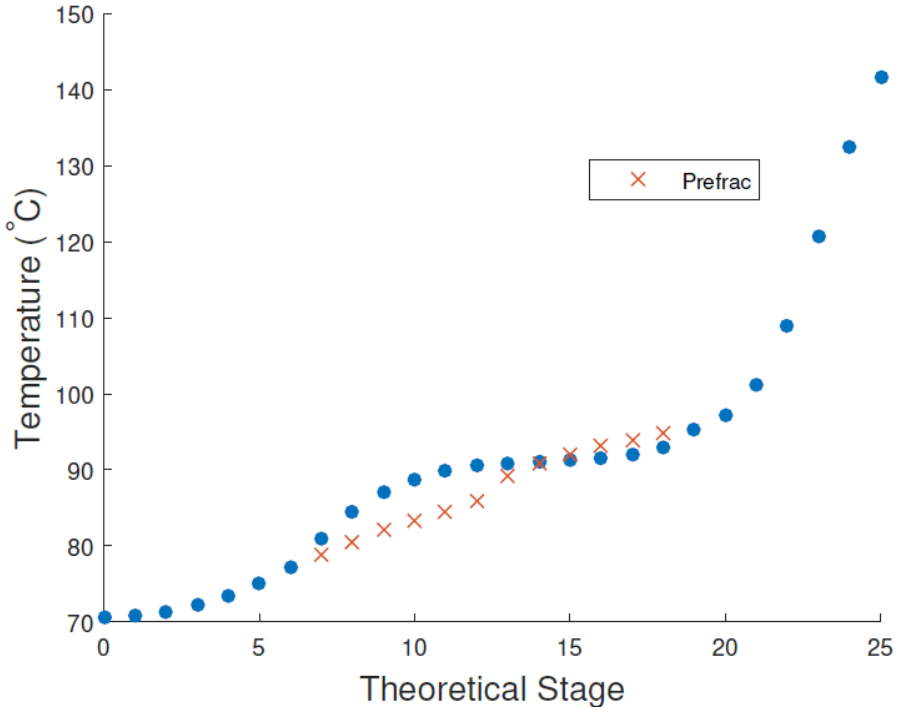

Figure 8-5 – Minimum energy temperature profile

Previous studies have found that a partially or fully vaporized feed flattens the minimum energy response surface therefore improving operational flexibility.[17,74] Similar results were found for this chemical system. Figure 8-6 compares the relationship of reboiler duty and liquid split for a constant 0.35 vapor split for a saturated liquid feed (q = 1) and a partially vaporized feed (q = 0.5). For a partially vaporized feed, the minimum reboiler duty is lower and the shape of the curve is flatter. This suggests that operating with a partially vaporized feed is more favorable for maintaining minimum energy operation. However, Figure 8-6 shows that a constant liquid split should not be used if large disturbances in feed temperature are expected. Using a constant liquid split of 0.66 would minimize the column's energy usage for a saturated liquid feed. However, the column's reboiler duty would increase if the feed quality changed to include more vapor. Conversely, using a constant liquid split of 0.7 would minimize the energy usage if the feed was

partially vaporized. However, the column's reboiler duty would increase if the feed changed to a saturated liquid.

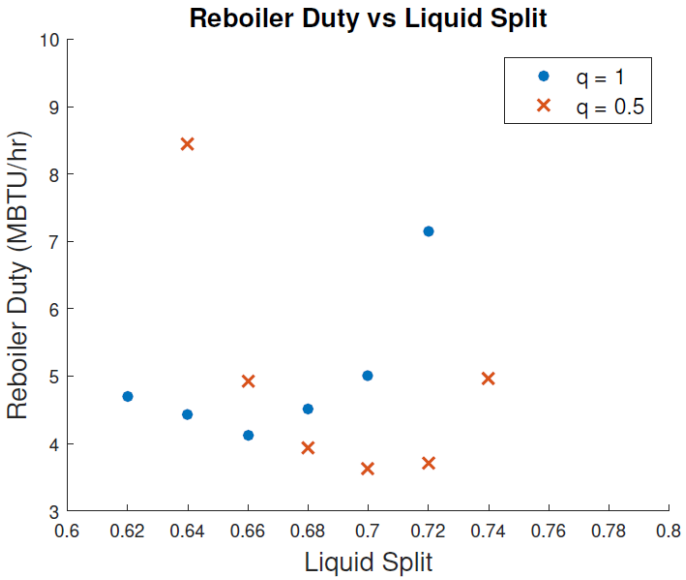

Figure 8-6 – Operating a DWC with a partially vaporized feed flattens the response surface for favorable operation. However, changes in feed quality require changes in liquid split if vapor split is assumed constant and minimum reboiler duty is desired.

Component Split

Numerous studies have examined how the flow of components in the column impact the column operation in regards to energy usage.[17,39,52] Specifically, authors have looked at component recoveries defined as the net flow of a component traveling over the wall in relation to the amount of that component fed to the column. These studies have found that optimal operation requires scarcely any heavy component traveling over the wall and all of the light component traveling over the wall. This agrees with the composition profiles previously shown in this work in which there was no 2-methylpentane at the base of the wall and very little m-xylene at the top of the wall (Figure 8-3 and Figure 8-4). Studies have particularly focused on the middle boiling component which travels both above and below the wall to reach the side product stage. How this component splits above

and below the wall is dependent upon the vapor and liquid splits in the column and has been linked to minimum energy operation.

The recovery of middle boiling component, termed component split ($CS_{\hat{B}}$, where $\hat{B}$ denotes the middle boiling component of an $\hat{A}$,$\hat{B}$, $\hat{C}$ mixture) by Ehlers et al.,[39] can be calculated by Equation 8-1 where $V_{out,top}$ is the vapor flow leaving the top of the prefractionator, $L_{in,top}$ is the liquid reflux at the top of the prefractionator, and $F_{\hat{B}}$ is the flow of middle-boiling component in the column feed (Figure 8-7). In essence, the component split is the portion of the middle-boiling component that is fed to the column that travels over the wall. Similarly, there is the flow of middle boiling component underneath the wall, termed $CS^*_{\hat{B}}$ (Equation 8-2).[39] $CS^*_{\hat{B}}$ describes the portion of middle-boiling component that travels to the bottom of the wall in relation to the amount of middle-boiling component fed to the column. Because the middle-boiling component material balance in the prefractionator must be closed, $CS_{\hat{B}}$ and $CS^*_{\hat{B}}$ must add up to one (Equation 8-3).

$$CS_{\hat{B}} = \frac{V_{out,top} * y_{out,top,\hat{B}} - L_{in,top} * x_{in,top,\hat{B}}}{F_{\hat{B}}} \quad \textbf{(8-1)}$$

$$CS^*_{\hat{B}} = \frac{L_{out,bot} * x_{out,bot,\hat{B}} - V_{in,bot} * y_{in,bot,\hat{B}}}{F_{\hat{B}}} \quad \textbf{(8-2)}$$

$$CS^*_{\hat{B}} + CS_{\hat{B}} = 1 \quad \textbf{(8-3)}$$

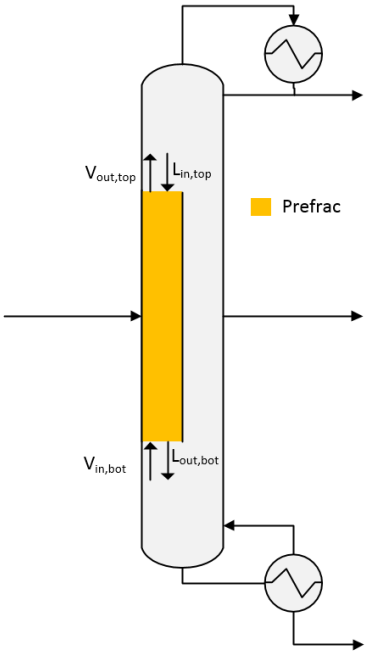

Figure 8-7 – A component split can be calculated for both the flow over the wall and the flow underneath the wall. However, both of these values have to add to 1 to preserve the middle boiling component material balance in the prefractionator.

However, as remarked by Ehlers et al.,[39] $CS_{\hat{B}}$ and $CS^*_{\hat{B}}$ are not confined between 0 and 1. Figure 8-8 documents the internal flow of middle-boiling component for different values of $CS_{\hat{B}}$ assuming a 100 mole/hr feed of middle-boiling component. The first image is an example of a component split value between 0 and 1 where part of the middle-boiling component travels above the wall and the remainder travels below the wall. A component split of 1 or 0 denotes that all of the middle-boiling component travels in one direction. For example, a component split of 1 signifies that all of the middle-boiling component travels above the wall. A negative component split signifies that the middle-boiling component is traveling from the mainfrac to the prefrac at the top of the wall. This is a result of middle-boiling component circling the wall after traveling under the wall to the mainfractionator. Finally, a component split greater than one or less than negative one represents a case where

a flow of middle-boiling component higher than that fed to the column is circling the wall. Component split values where the middle-boiling component accumulates and travels around the wall are often viewed as energetically inefficient.[17,39]

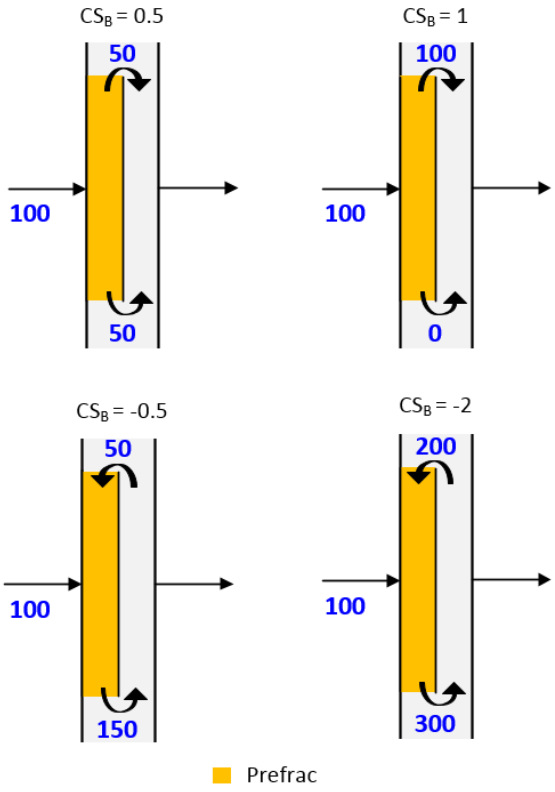

Figure 8-8 – Examples of middle component flows for multiple $CS_{\hat{B}}$ values assuming a 100 mole/hr feed of middle-boiling component

The component split for the absolute minimum case discussed earlier was -0.18. This means that the lowest energy solution had 18 percent of the middle boiling component, cyclohexane, circling around the wall and did not coincide with the even split of middle boiling component above and below the wall that was seen in previous work.[39] In addition, the optimum component split value changed with changing vapor split in the column (Figure 8-9). The optimum component split for the 50/50 vapor split (50 percent of the vapor flow to the prefractionator, 50 percent of the vapor flow to the mainfractionator) is -

0.05. The internal flows for this optimum would be similar to that of the -0.5 $CS_{\hat{B}}$ shown in Figure 8-8; however, a smaller percentage of the middle-boiling component would be circling the wall. The optimum component split for the 70/30 vapor split (70 percent of the vapor flow to the prefractionator, 30 percent of the vapor flow to the mainfractionator) is 0.24. This internal flows of the middle-boiling component around the dividing wall would be similar to those of the 0.5 $CS_{\hat{B}}$ shown in Figure 8-8 although for this case, more of the middle-boiling component would be traveling underneath the wall. The optimum component split for the 80/20 vapor split (80 percent of the vapor flow to the prefractionator, 20 percent of the vapor flow to the mainfractionator) is 0.47. The internal middle-boiling component flows for this case are similar to that of a 0.5 component split shown in Figure 8-8. The studies that included heat transfer through the wall found that doing so would change component split values because wall heat transfer changes the vapor flow in the column. However, a changed component split resulting from wall heat transfer was usually correlated to an increased energy consumption.[10,39] To aid this and to maintain a proper component split value, Ehlers et al. suggested controlling a temperature in the prefractionator with the liquid split. This is discussed in the following section. This work uses a different chemical system, a more rigorous model, less stages, and heat transfer to the atmosphere. More work would have to be done to make a direction comparison between these findings.

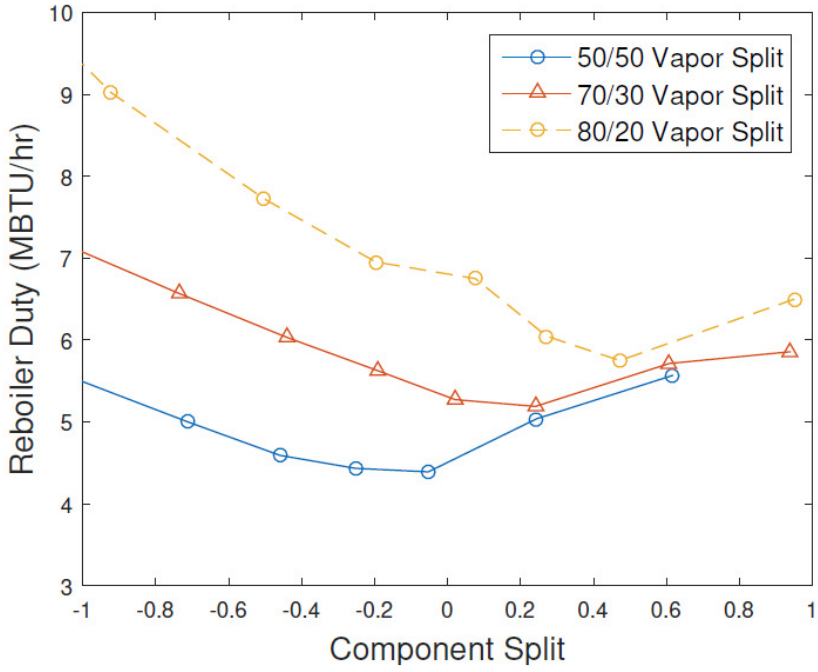

Figure 8-9 – The optimum component split changes with column vapor split

Control

However, the component split is impractical to monitor in column operation because the measurement of vapor compositions and flows is difficult. Therefore, many studies have examined self-optimizing control variables to maintain minimum energy operation. Numerous variables and combinations of variables have been examined as potential self-optimizing control variables for dividing wall columns.[17,61,63,64] Most promising amongst these are the control of a composition at the top of the wall[17,61] and the control of a temperature in the prefractionator.[39,62] Because of the difficulty in manipulating the vapor split, the liquid split is the manipulated variable most often used.

Multiple variables were examined from a steady state perspective as potential control variables for maintaining minimum reboiler duty. Numerous authors have investigated the composition of the heavy component at the top of the wall as a potential control variable. Authors have suggested minimizing this composition to avoid additional energy usage. However, as Figure 8-10 shows, the m-xylene composition at the top of the

wall can be minimized only to a particular limit before the reboiler duty drastically increases. Additional energy is needed to generate the necessary reflux to sufficiently separate all of the m-xylene from the other components at the top of the dividing wall. Controlling the m-xylene composition at a setpoint above this value could be a viable control strategy. However, due to the very small composition of m-xylene, highly accurate composition analyzers would be necessary.

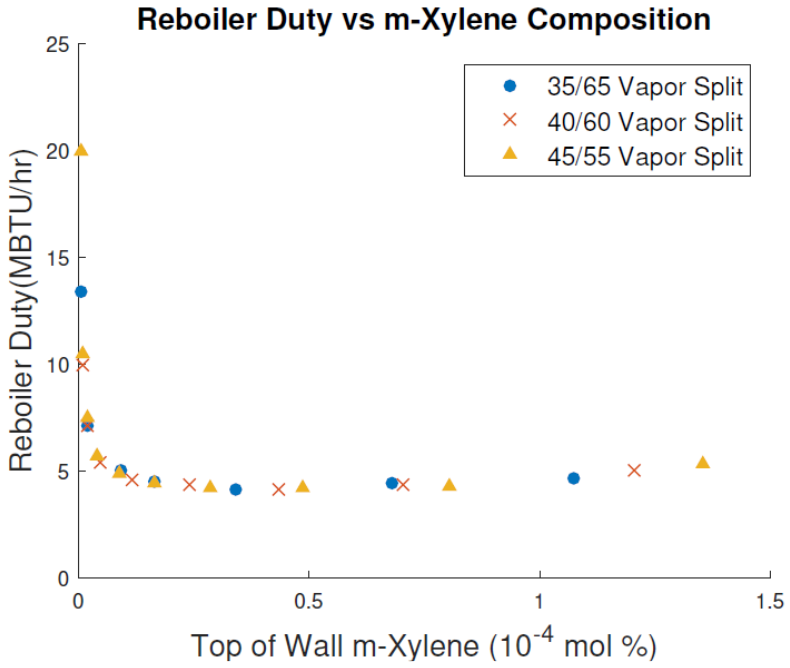

Figure 8-10 – The m-xylene composition at the top of the wall could be controlled above a lower bound to maintain a near constant reboiler duty even with uncertainty in the vapor split. However, the very small composition may require expensive analytical instruments.

Controlling an alternative composition at the top of the wall would avoid the necessity for highly sensitive composition analyzers. Toluene is the next heaviest component, is also found in the bottoms product, and is only slightly present at the top of the wall. Therefore, toluene would be the next logical choice in control variable. However, the toluene composition at the top of the wall does not correlate well with reboiler duty, as seen in Figure 8-11. A single toluene composition does not ensure a single reboiler duty.

Note that the range of reboiler duties is the same as that of Figure 8-10. Furthermore, if the vapor split should change due to any natural noise in the system, maintaining toluene composition would not maintain minimum energy operation. A similar trend can be seen in the cyclohexane composition at the top of the wall (Figure 8-12).

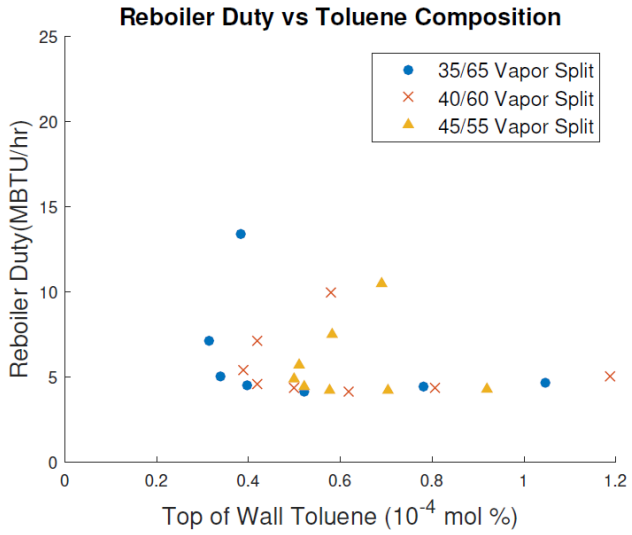

Figure 8-11 – Toluene composition at the top of the wall does not correlate well with the reboiler duty

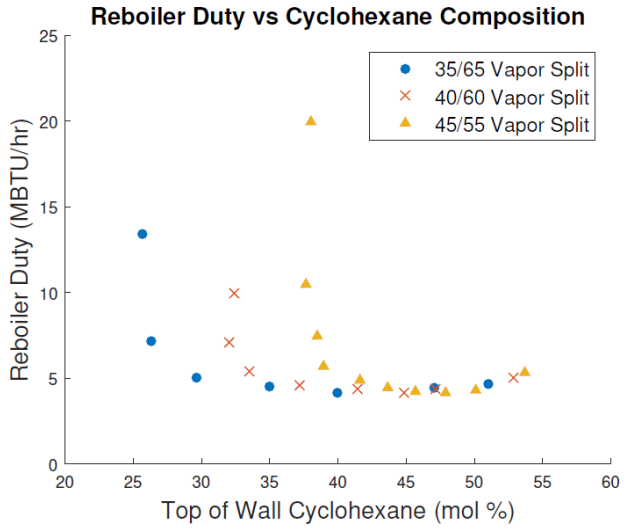

Figure 8-12 – Cyclohexane composition at the top of the dividing wall does not correlate well with reboiler duty. Therefore, cyclohexane composition would not be a good self-optimizing control variable.

Temperature control is often preferable to composition control because temperature measurements do not require the high cost and long lag time of composition analyzers. Because temperatures of a distillation column are reflective of composition, temperature control can be used to infer compositions. Multiple studies have controlled a temperature in the prefractionator with the liquid split to infer minimum energy operation. The temperature in the lower portion of the prefractionator section is fairly flat therefore making temperatures in the lower section of the prefractionator bad control candidates. Because of this, temperatures of prefractionator stages 9 through 11 (T9A-T11A) were examined for control. The location of these temperatures are shown in Figure 8-13. These temperatures were chosen because their distance from the prefractionator reflux and the feed make them less susceptible to small fluctuations in flow or temperature.

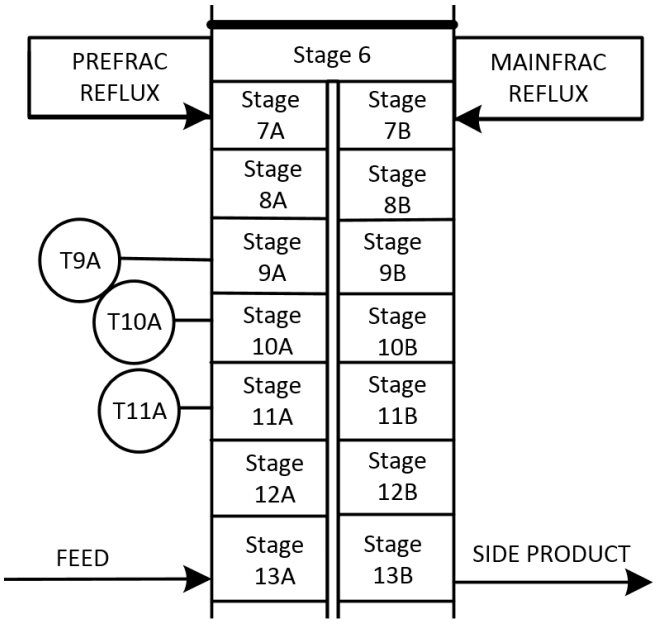

Figure 8-13 – Locations of prefractionator temperatures examined for temperature control

Figure 8-14 shows the minimum reboiler duty as a function of temperature for changing liquid splits and a constant vapor split of 0.35. All temperatures appear to be good candidate control temperatures because they all correlate with reboiler duty. The rise in

reboiler duty for lower temperature values is reflective of the rise in reboiler duty seen for lower compositions of m-xylene.

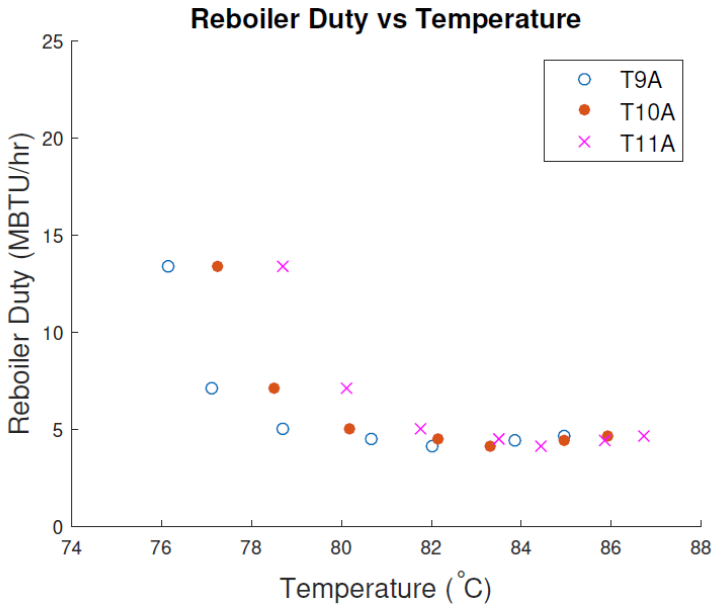

Figure 8-14 – All three temperatues in the prefractionator appear good for control

Figure 8-15 shows the relationship of minimum reboiler duty and the value of T10A for a saturated liquid feed (q = 1) and a partially vaporized feed (q = 0.5). T10A is a good candidate control temperature for both feed qualities. Should disturbances in feed quality be expected, maintaining T10A at setpoint would maintain minimum energy operation. Furthermore, operating the DWC with a partially vaporized feed would benefit operation. T10A would not have to be as tightly controlled for a partially vaporized feed because the minimum is flatter.

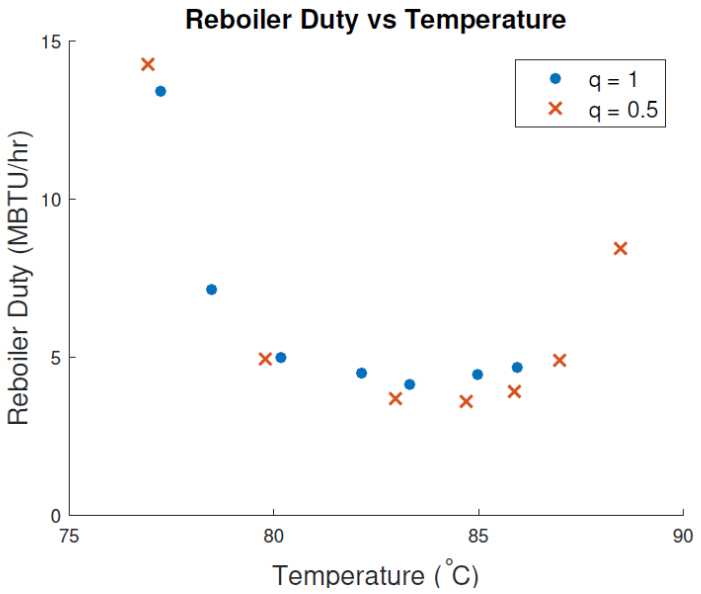

Figure 8-15 – Reboiler duty vs T10A for different feed qualities

Chapter 9: Conclusions and Recommendations

Concluding Remarks

Control configurations were successfully designed to manage trace components in an experimental dividing wall distillation column. The column was continuously operated and transitioned smoothly between steady states. Disturbances in feed flow, temperature, and composition were successfully rejected using two temperature controllers. A novel data analytics approach was developed to determine heat transfer coefficients to match the steady state model to the pilot data. These heat transfer coefficients were used in a rigorous steady state model to create a minimum energy operating surface for various liquid and vapor splits.

Multiple operating points were examined to provide insight into how the control structure had to change based on the operational objectives of the column. Due to their similar temperature profiles, there was little difference in control structure for the three component case, the case of trace in the bottoms, and the case of trace and cyclohexane side product other than a slight change in temperature location as the composition profiles slightly shifted in the column. However, the case of isolated toluene trace component required a different control configuration. The smaller side product flow required a different level configuration resulting in different control handles available for temperature control. In addition, the locations of sensitive temperatures changed due to significantly different composition profiles. Because there was a larger temperature difference between the feed and the side product, the model's ability to accurately predict the wall heat transfer impacted the effectiveness of singular value decomposition and relative gain array analysis for this case.

This work proves that, for this chemical system, a dividing wall distillation column is controllable using traditional approaches to distillation control. Temperature control remained robust in the presence of multiple components, and more advanced control was not necessary to handle controller interaction. Conventional controller design tools did not break down due to the intensified nature of the process. These are important results because

while there is no overarching DWC control scheme feasible for all chemical systems, design tools can streamline the process in determining the best control configuration for a given system. If dividing wall columns are to become industry standard, then tools must be available for their design and control that do not rely on simplifying assumptions and specialized models. The operation and design of dividing wall columns is different for different feed systems. Though some chemical systems are closer to ideal, such as the chemical system in this work, others are very complex. Furthermore, this study highlights the importance of heat transfer. Being able to model systems where heat transfer and chemical non-ideality play a significant role is important in the march to widespread DWC acceptance.

FUTURE WORK

There are numerous ways in which this research can be continued beyond the scope of this dissertation. One of these avenues is further dynamic testing and model validation. As shown in Chapter 7, despite the pilot column's ability to reject a series of disturbances in feed flow, temperature, and composition, the column response was not accurately predicted by the model. Though the model also rejected these disturbances, the speed, direction, and magnitude of some of the model responses differed from those on the pilot column. One possible solution is to model the DWC as a packed column rather than a series of flash tanks. This would quicken the response time of the model. Alternatively, more dynamic data may be needed to validate the model. The model may not match the dynamic data because the pilot DWC was not steady before the disturbance testing. If additional disturbance testing is to be conducted, the disturbances should be large, such as those seen in this work. The pilot DWC has a lot of noise, and the column response much be of a larger magnitude such that it can be distinguished from the noise. In addition, modifications, if feasible, should be made such that the steam flow is stabilized. After the model is successfully validated, it can be used to run additional disturbance testing. This

disturbance testing could include work that is not easily feasible on the pilot column such as feed composition spikes of multiple components or minimum energy testing.

Future work could also include the examination of different trace components and different feed systems. This work examined a trace component that was the second heaviest component in the system and was moved between the bottoms and side products. Additional studies could examine a trace component that is the second lightest component and would be moved between the distillate and side products. The trace component could also be isolated as the side product while the bottoms product became a mixture stream. Column sensitivities and control structures would be expected to change as the selection of trace component and therefore column objectives change. Just as with traditional distillation columns, the operation and control of dividing wall columns changes with different feed systems. The selection of feed system in this study was based on the separation capability of the already built pilot column. However, different feed systems can be separated using a dividing wall column. The relative volatilities of the system used in this study resulted in an easier separation at the base of the column and a progressively more difficult separation along the length of the column. The most difficult separation was at the top of the column where there are more control handles due to liquid split at the top of the wall. Changing the feed system such that the more difficult separation occurred in the lower portion of the column would provide important information regarding the design and applicability of dividing wall columns.

Additional work also includes investigating the relationship between the required reboiler duty and the location of the trace component product. This work examined a pure distillate product with the trace component in the side product and the trace component in the bottoms product. However, there may be a distribution of trace component between the side and bottoms products that the column naturally favors. Perhaps distributing the trace component between the two products leads to a lower reboiler duty or a more stable operating point. This would be a question worth investigating if a pure distillate product

was desired and there were no impurity constraints on the trace component in the side and bottoms product.

In addition, more work is needed regarding heat transfer through the dividing wall. Because of the scale of the pilot column, this work included heat transfer through the dividing wall and heat transfer to the environment. The values of heat transfer coefficients used to model this heat transfer impacted the control structure resulting for SVD and RGA for the case of isolated trace side product. Using heat transfer coefficients to fit the steady state data resulted in a range of feasible values for the different cases. No explanations are obvious for why the heat transfer coefficient and assumed area drastically change; however, the number of cases analyzed with resulting heat transfer coefficients is small. The lack of clear causality suggests that there is an unknown or misunderstood phenomena occurring on the fundamental level. Heat transfer through the wall and to the atmosphere is assumed to have little impact on larger diameter columns.

Finally, the work regarding minimum energy operation can be expanded. This work used a rigorous model to examine the impact of liquid and vapor splits on reboiler duty. Though previous works employing more simplified models were referenced, the two modeling approaches were never directly compared because other researchers have not looked at the chemical system used in this work. A modeling comparison would elucidate whether differences, particularly in the optimum component split, were a result of the chemical system or heat transfer. In addition, the minimum energy response surface was generated for only one of the four cases discussed in this work. Examining different cases could provide interesting insights, in particular the case of toluene and cyclohexane side product because two major components are traveling around the wall. Finally, the work presented in this dissertation only examined changes in feed temperature. The effect of feed composition disturbances on minimum energy operation should also be examined.

Appendices

Appendix A: SVD MATRICES

CASE [2MP, C6, MX]

To distinguish if the control methodologies of SVD and RGA analysis break down due to the intensified nature of dividing wall columns or due to the addition of a forth trace component, a three component mixture without a trace component was examined. In addition to serving as a test for SVD and RGA, this case provided steady state targets and a target control structure for column operation. When the trace component studies were run on the pilot plant column, the column was started up as a three component column with no trace component.

Steady State Considerations

Steady state flows and compositions for the three component case are shown in Table A-1, and the temperature profile is shown in Figure A-1. The profile is steepest in the stripping section where the cyclohexane and m-xylene are separated and flatter in the lower dividing wall section where there is pure cyclohexane. There is very little temperature difference across the dividing wall, and there is a slight temperature change from the upper portions of the dividing wall to the rectifying section. Similar to case [2MP, C6, Tol/mX], the distillate and side product impurity compositions were set based on the more difficult 2-methylpentane and cyclohexane separation. The wall split and steam flow values were chosen such that these desired product compositions were possible.

Table A-1. [2MP, C6, mX] Base Case Conditions

Stream Name	Total Mass Flow (lbm/hr)	Temperature (°F)	Composition (wt %)			
			2MP	C6	Tol	mX
Feed	50.00	195.00	33.33	33.33	0.00	33.34
Distillate	16.657	90.00	97.50	2.50	0.00	0.00
Reflux	185.74	70.00	97.50	2.50	0.00	0.00
Prefrac Reflux	151.410	160.00	54.18	45.82	0.00	0.00
Mainfrac Reflux	128.690	160.00	54.18	45.82	0.00	0.00
Side Product	16.357	195.60	2.50	97.50	0.00	0.001
Side Reflux	146.570	195.00	2.50	97.50	0.00	0.001
Bottoms	16.986	298.08	0.00	1.68	0.00	98.32
Steam (KBTU/hr)	69.72					

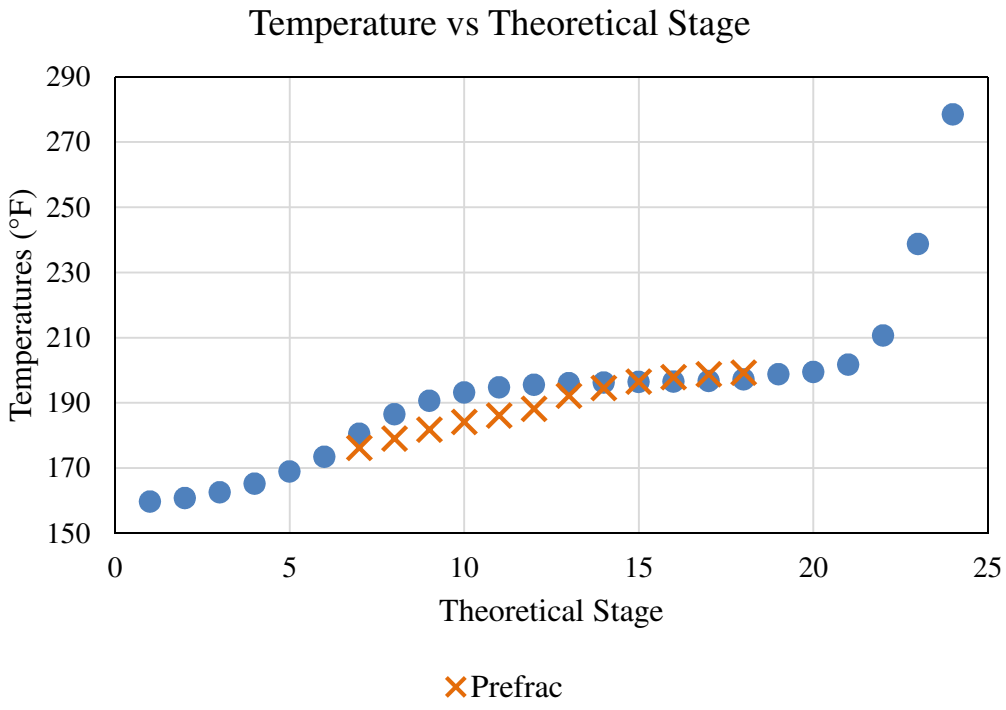

Figure A-1 – Temperature profile for [2MP, C6, mX]. Heat transfer to the environment and through the wall is included in the model.

Temperature Control

The level control structure used for this case is shown in Figure 4-2. Given this level control structure, the remaining variables available for temperature control are reflux, steam, wall split, and sidedraw reflux (Figure A-2). The condition numbers indicate that two or three controllers could work, but four controllers would most likely result in too much interaction (Table A-2). (A-4) shows that the two most sensitive temperatures correspond to the 7^{th} and 35^{th} rows of the U matrix of left singular values (T35 and TA11 in the model). However, finding other sensitive temperatures from the third and fourth left singular vectors proves to be difficult since larger values cluster near the top of the wall and at the base of the column (Figure A-3). From a plot of the difference of the absolute values of the first and second left singular vectors, temperatures corresponding to theoretical stage 6 or stage 7 on the prefrac and stage 23 (T6 or TA11 and T35 in the model) appear to be the best for control (Figure A-4). This idea was extended to the difference of the absolute values of the first three left singular vectors (Figure A-5). In addition to the temperatures that appeared in Figure A-4, Stage 22 (T34) appears as a candidate control temperature in Figure A-5. However, the close proximity of T34 and T35 would make them difficult to control simultaneously. In order of most to least sensitive, sensitive inputs are steam, reflux, wall split, and sidedraw reflux (A-4).

The RGA analysis for the inputs of steam and reflux and temperatures of T35 and T6 is shown in Equation (A-1). T6 was used rather than TA11 to avoid a temperature right below the total trapout tray and one that would be sensitive to heat loss in the prefrac reflux stream. The resulting pairing is stripping temperature with steam and rectifying temperature with reflux. An RGA analysis for three temperatures and three valves was not done because the choice of temperature location for the third controller was unclear.

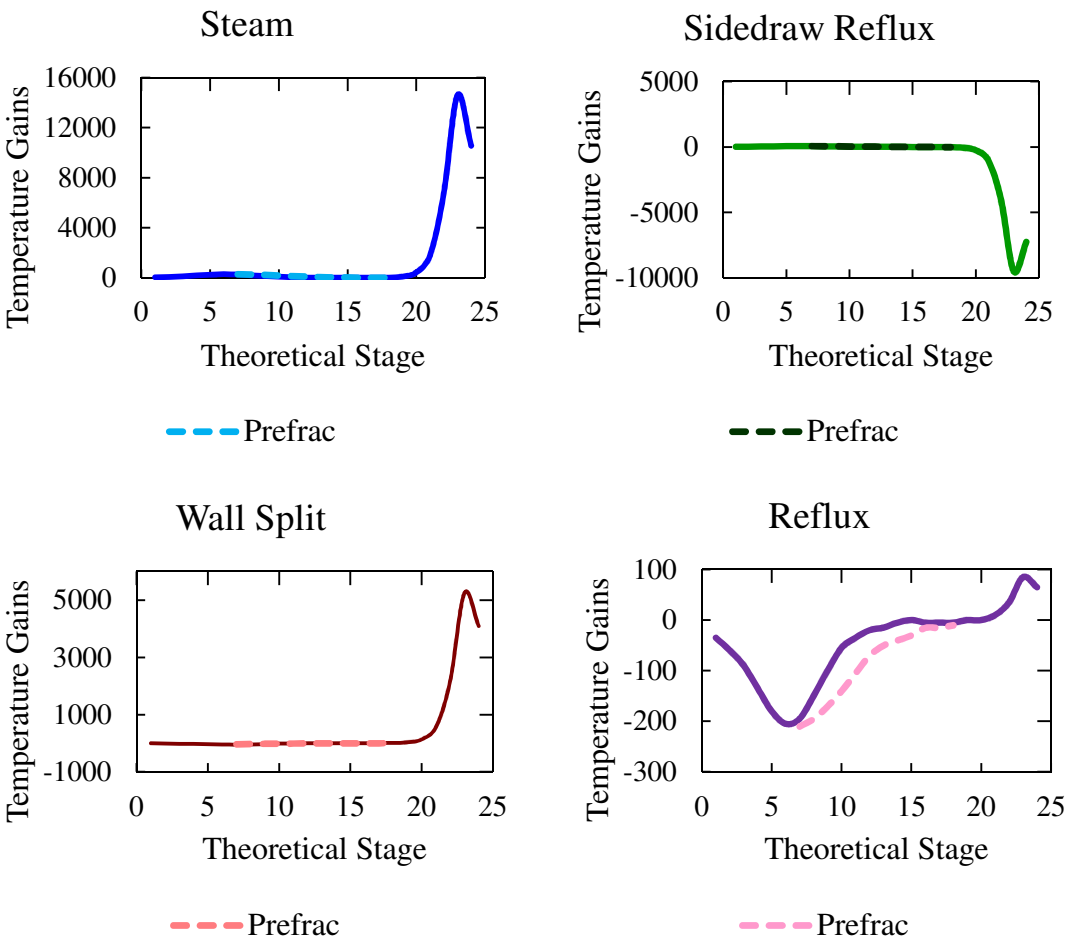

Figure A-2 – Graphical representation of gain matrix

Table A-2. Condition Numbers for Temperature SVD of case [2MP, C6, mX]

System Size	Condition Number
4 x 4	575.97
3 x 3	76.75
2 x 2	24.80

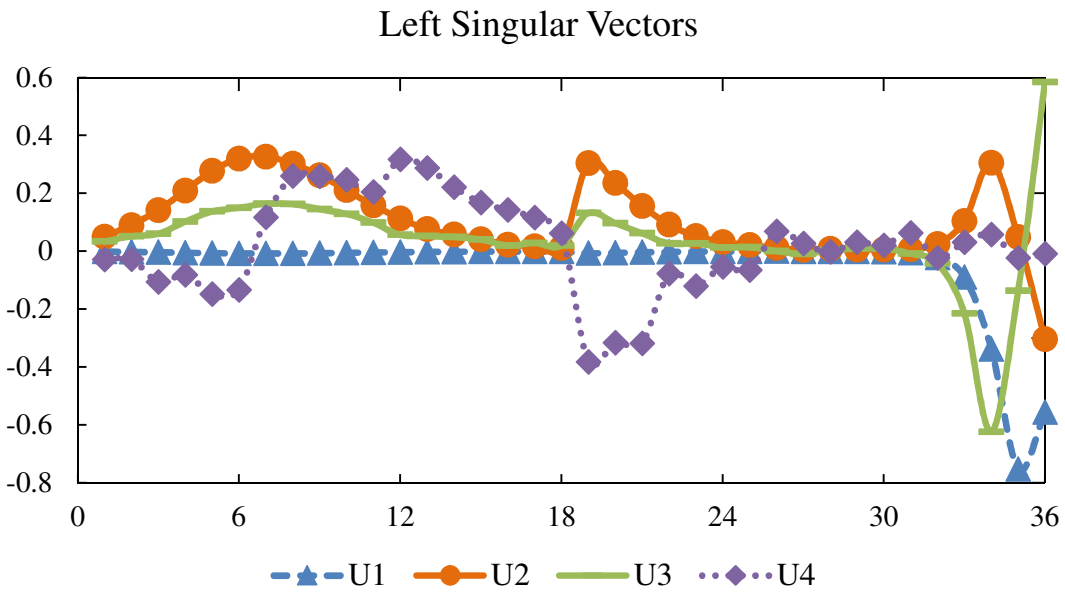

Figure A-3 – Graphical representation of the four columns of the U matrix. Note that 1-6 are the rectifying temperatures, 7-18 are the prefrac temperatures, 19-30 are the mainfrac temperatures, and 31-36 are the stripping temperatures.

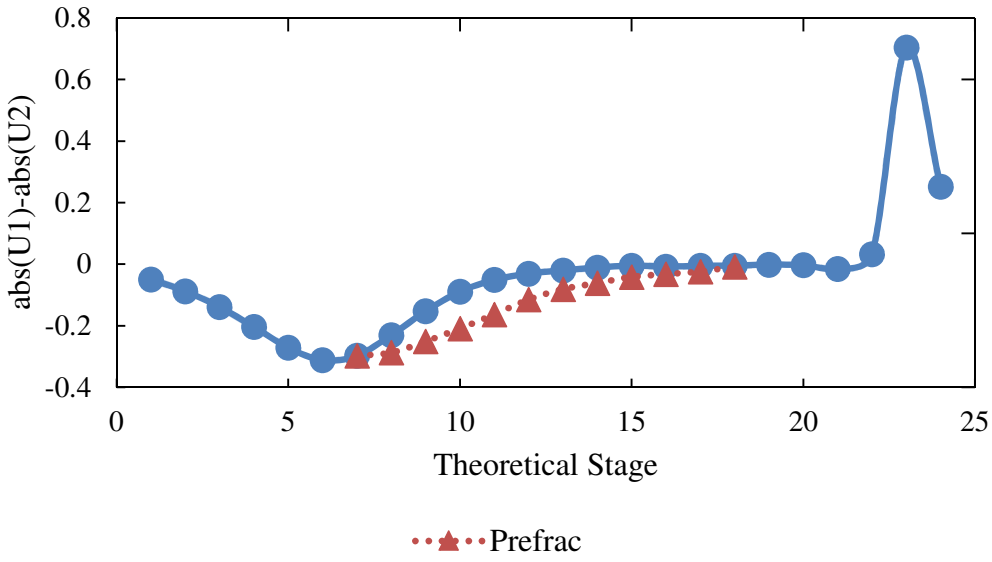

Figure A-4 – abs(U1) – abs(U2) vs. Theoretical Stage

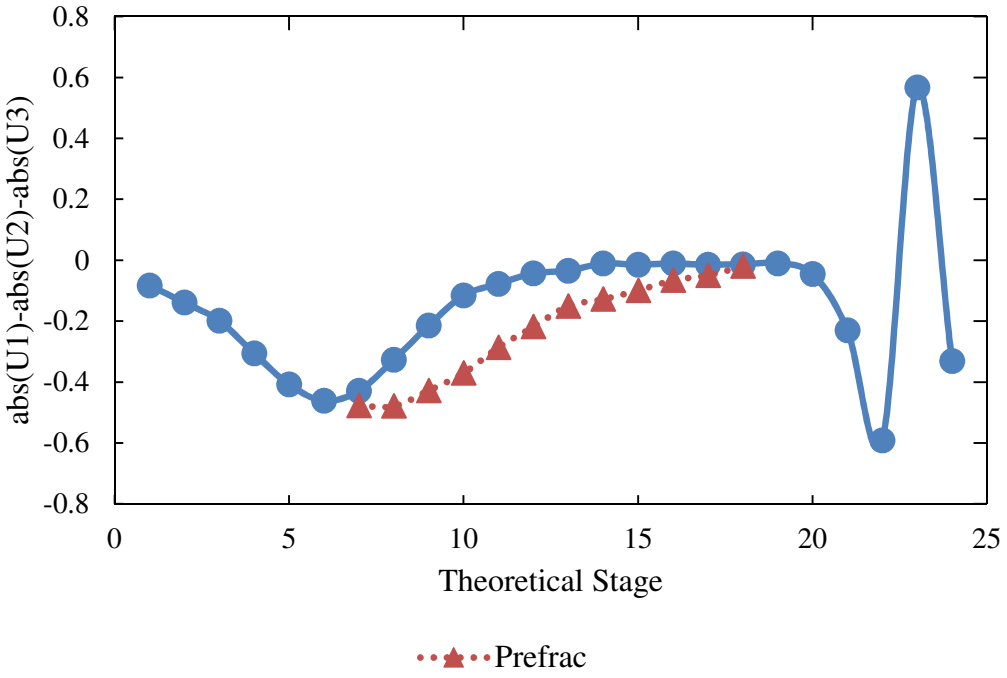

Figure A-5 – abs(U1) – abs(U2) – abs(U3) vs. Theoretical Stage

$$\Lambda = \begin{matrix} \textit{Steam} & \textit{Reflux} \\ \begin{bmatrix} 0.992 & 0.008 \\ 0.008 & 0.992 \end{bmatrix} & \begin{matrix} T_{Stripping} \\ T_{Rectifying} \end{matrix} \end{matrix} \qquad \textbf{(A-1)}$$

Matrices for Temperature Control

$$K = \begin{array}{c} \left.\frac{\delta T_i}{\delta L}\right|_{\beta_L,SL,V} \\ \\ \left[\begin{array}{c} 45.000 \\ 80.000 \\ 130.000 \\ 190.000 \\ 250.000 \\ 290.000 \\ 300.000 \\ 280.000 \\ 245.000 \\ 195.000 \\ 150.000 \\ 110.000 \\ 75.000 \\ 55.000 \\ 40.000 \\ 25.000 \\ 15.000 \\ 30.000 \\ 270.000 \\ 210.000 \\ 140.000 \\ 85.000 \\ 45.000 \\ 30.000 \\ 15.000 \\ 10.000 \\ 10.000 \\ 10.000 \\ 15.000 \\ 30.000 \\ 105.000 \\ 430.000 \\ 1795.000 \\ 6745.000 \\ 14595.000 \\ 10550.000 \end{array}\right. \end{array} \begin{array}{c} \left.\frac{\delta T_i}{\delta \beta_L}\right|_{L,SL,V} \\ \\ \begin{array}{c} 10.000 \\ 20.000 \\ 30.000 \\ 45.000 \\ 60.000 \\ 70.000 \\ 75.000 \\ 70.000 \\ 60.000 \\ 50.000 \\ 35.000 \\ 30.000 \\ 20.000 \\ 15.000 \\ 10.000 \\ 5.000 \\ 5.000 \\ -10.000 \\ 65.000 \\ 50.000 \\ 30.000 \\ 20.000 \\ 10.000 \\ 5.000 \\ 5.000 \\ 5.000 \\ 0.000 \\ 0.000 \\ -5.000 \\ -15.000 \\ -60.000 \\ -255.000 \\ -1055.000 \\ -4065.000 \\ -9495.000 \\ -7250.000 \end{array} \end{array} \begin{array}{c} \left.\frac{\delta T_i}{\delta SL}\right|_{L,\beta_L,V} \\ \\ \begin{array}{c} -5.000 \\ -10.000 \\ -20.000 \\ -25.000 \\ -35.000 \\ -40.000 \\ -30.000 \\ -40.000 \\ -15.000 \\ -10.000 \\ -5.000 \\ 0.000 \\ 5.000 \\ 5.000 \\ 5.000 \\ 5.000 \\ 5.000 \\ 10.000 \\ -50.000 \\ -40.000 \\ -30.000 \\ -15.000 \\ -10.000 \\ -5.000 \\ -5.000 \\ 0.000 \\ 0.000 \\ 0.000 \\ 5.000 \\ 10.000 \\ 35.000 \\ 135.000 \\ 560.000 \\ 2180.000 \\ 5250.000 \\ 4095.000 \end{array} \end{array} \begin{array}{c} \left.\frac{\delta T_i}{\delta V}\right|_{L,\beta_L,SL} \\ \\ \left[\begin{array}{c} -35.000 \\ -60.000 \\ -90.000 \\ -135.000 \\ -180.000 \\ -205.000 \\ -210.000 \\ -205.000 \\ -170.000 \\ -140.000 \\ -105.000 \\ -70.000 \\ -50.000 \\ -40.000 \\ -30.000 \\ -15.000 \\ -15.000 \\ -10.000 \\ -195.000 \\ -150.000 \\ -100.000 \\ -55.000 \\ -35.000 \\ -20.000 \\ -15.000 \\ -5.000 \\ 0.000 \\ 0.000 \\ -5.000 \\ -5.000 \\ -5.000 \\ 0.000 \\ 10.000 \\ 35.000 \\ 85.000 \\ 65.000 \end{array}\right. \end{array} \begin{array}{c} \textit{Theoretical Stage} \\ \\ \left[\begin{array}{c} \textit{1} \\ \textit{2} \\ \textit{3} \\ \textit{4} \\ \textit{5} \\ \textit{6} \\ \textit{A11} \\ \textit{A12} \\ \textit{A13} \\ \textit{A14} \\ \textit{A15} \\ \textit{A16} \\ \textit{A21} \\ \textit{A22} \\ \textit{A23} \\ \textit{A24} \\ \textit{A25} \\ \textit{A26} \\ \textit{B11} \\ \textit{B12} \\ \textit{B13} \\ \textit{B14} \\ \textit{B15} \\ \textit{B16} \\ \textit{B21} \\ \textit{B22} \\ \textit{B23} \\ \textit{B24} \\ \textit{B25} \\ \textit{B26} \\ \textit{31} \\ \textit{32} \\ \textit{33} \\ \textit{34} \\ \textit{35} \\ \textit{36} \end{array}\right. \end{array} \quad \textbf{(A-2)}$$

$$\Sigma = \begin{bmatrix} 24{,}147 & 0 & 0 & 0 \\ 0 & 974 & 0 & 0 \\ 0 & 0 & 315 & 0 \\ 0 & 0 & 0 & 42 \end{bmatrix} \quad \textbf{(A-3)}$$

$$V = \begin{array}{c} \begin{matrix} \textit{Steam} & \textit{Side Reflux} & \textit{Wall Split} & \textit{Reflux} \end{matrix} \\ \begin{bmatrix} -0.8005 & 0.5081 & -0.2982 & 0.1101 \\ 0.5241 & 0.5750 & -0.2082 & 0.5927 \\ -0.2907 & -0.3548 & 0.4573 & 0.7619 \\ -0.0042 & -0.5341 & -0.8116 & 0.2368 \end{bmatrix} \end{array} \quad \textbf{(A-4)}$$

$$
U = \begin{bmatrix}
-0.0012 & 0.0504 & 0.0388 & -0.0290 & T1 \\
-0.0021 & 0.0901 & 0.0512 & -0.0277 & T2 \\
-0.0034 & 0.1422 & 0.0600 & -0.1062 & T3 \\
-0.0050 & 0.2088 & 0.1021 & -0.0815 & T4 \\
-0.0065 & 0.2773 & 0.1368 & -0.1477 & T5 \\
-0.0076 & 0.3196 & 0.1495 & -0.1333 & T6 \\
-0.0079 & 0.3269 & 0.1642 & 0.1171 & TA11 \\
-0.0075 & 0.3017 & 0.1623 & 0.2603 & TA12 \\
-0.0066 & 0.2620 & 0.1448 & 0.2591 & TA13 \\
-0.0052 & 0.2117 & 0.1287 & 0.2467 & TA14 \\
-0.0041 & 0.1583 & 0.0983 & 0.2049 & TA15 \\
-0.0030 & 0.1135 & 0.0565 & 0.3177 & TA16 \\
-0.0021 & 0.0765 & 0.0519 & 0.2882 & TA21 \\
-0.0016 & 0.0577 & 0.0484 & 0.2215 & TA22 \\
-0.0012 & 0.0414 & 0.0401 & 0.1679 & TA23 \\
-0.0008 & 0.0224 & 0.0190 & 0.1425 & TA24 \\
-0.0004 & 0.0172 & 0.0284 & 0.1162 & TA25 \\
-0.0013 & 0.0116 & 0.0185 & 0.0627 & TA26 \\
-0.0069 & 0.3044 & 0.1314 & -0.3818 & TB11 \\
-0.0054 & 0.2359 & 0.0967 & -0.3156 & TB12 \\
-0.0036 & 0.1565 & 0.0618 & -0.3181 & TB13 \\
-0.0022 & 0.0918 & 0.0263 & -0.0772 & TB14 \\
-0.0011 & 0.0522 & 0.0265 & -0.1198 & TB15 \\
-0.0008 & 0.0314 & 0.0126 & -0.0543 & TB16 \\
-0.0003 & 0.0208 & 0.0139 & -0.0655 & TB21 \\
-0.0002 & 0.0109 & 0.0001 & 0.0687 & TB22 \\
-0.0003 & 0.0052 & -0.0095 & 0.0263 & TB23 \\
-0.0003 & 0.0080 & 0.0034 & -0.0020 & TB24 \\
-0.0007 & 0.0058 & 0.0093 & 0.0313 & TB25 \\
-0.0014 & 0.0059 & 0.0089 & 0.0202 & TB26 \\
-0.0052 & 0.0066 & -0.0089 & 0.0635 & T31 \\
-0.0214 & 0.0246 & -0.0426 & -0.0226 & T32 \\
-0.0891 & 0.1041 & -0.2149 & 0.0317 & T33 \\
-0.3381 & 0.3054 & -0.6241 & 0.0573 & T34 \\
-0.7531 & 0.0489 & -0.1371 & -0.0232 & T35 \\
-0.5564 & -0.3041 & 0.5836 & -0.0090 & T36
\end{bmatrix} \qquad \textbf{(A-5)}
$$

Composition Control

Although not tested on the pilot plant, column compositions were also tested, and SVD and RGA resulted in a two controller and three controller approach that looked promising. Product impurities rather than purities were controlled based on standard practice. Using the most sensitive inputs of steam and reflux (Equation A-9) and most sensitive compositions of bottoms cyclohexane and distillate cyclohexane (Equation A-10) resulted in the RGA matrix shown in Equation A-6. The pairing of bottoms composition with steam and distillate composition with reflux makes sense from an intuitive point of view and nicely follows the results from the temperature RGA. One could simulate bottoms composition to T35 to steam and distillate composition to T6 to reflux to determine temperature set points. Adding the third composition and the liquid split to the RGA analysis results in the control strategy of bottoms composition to steam, distillate composition to reflux, and sidedraw composition to wall split. This is favorable because the control and manipulate variables are located in close proximity to one another leading to favorable time constants and dynamics. However, the high condition number for the three controller system suggests a high degree of interaction (Table A-3).

$$\Lambda = \begin{matrix} \\ X_{B,C6} \\ X_{D,C6} \end{matrix} \begin{matrix} \begin{matrix} \textit{Steam} & \textit{Reflux} \end{matrix} \\ \begin{bmatrix} 0.985 & 0.015 \\ 0.015 & 0.985 \end{bmatrix} \end{matrix} \tag{A-6}$$

$$\Lambda = \begin{matrix} \\ X_{B,\,C6} \\ X_{D,\,C6} \\ X_{S,\,2MP} \end{matrix} \begin{matrix} \begin{matrix} \textit{Steam} & \textit{Reflux} & \textit{Wall Split} \end{matrix} \\ \begin{bmatrix} 0.6142 & 0.0044 & 0.3813 \\ -4.6789 & 7.331 & -1.6542 \\ 5.0647 & -6.3375 & 2.2729 \end{bmatrix} \end{matrix} \tag{A-7}$$

Table A-3. Condition Numbers for Composition SVD of case [2MP, C6, mX]

System Size	Condition Number
3 x 3	569.72
2 x 2	14.87

Matrices for Composition Control

$$\Sigma = \begin{bmatrix} 671.5 & 0 & 0 & 0 \\ 0 & 45.2 & 0 & 0 \\ 0 & 0 & 1.2 & 0 \end{bmatrix} \quad \textbf{(A-8)}$$

$$V = \begin{array}{c} \begin{matrix} \textit{Steam} & \textit{Side Reflux} & \textit{Wall Split} & \textit{Reflux} \end{matrix} \\ \begin{bmatrix} -0.7838 & 0.4771 & 0.2081 & 0.3389 \\ 0.5410 & 0.5154 & -0.1840 & 0.6387 \\ -0.3050 & -0.3043 & -0.8658 & 0.2546 \\ -0.0036 & -0.6436 & 0.4163 & 0.6423 \end{bmatrix} \end{array} \quad \textbf{(A-9)}$$

$$U = \begin{bmatrix} -0.0309 & 0.8398 & -0.5421 \\ 0.0211 & -0.5416 & -0.8403 \\ 0.9993 & 0.0374 & 0.0010 \end{bmatrix} \begin{matrix} X_{D,\,C6} \\ X_{S,\,2MP} \\ X_{B,\,C6} \end{matrix} \quad \textbf{(A-10)}$$

CASE [2MP, C6, TOL/MX]

Matrices for Temperature Control

$$\Sigma = \begin{bmatrix} 33{,}818 & 0 & 0 & 0 \\ 0 & 931 & 0 & 0 \\ 0 & 0 & 645 & 0 \\ 0 & 0 & 0 & 241 \end{bmatrix} \quad \textbf{(A-11)}$$

$$V = \begin{bmatrix} -0.7613 & 0.5210 & -0.1418 & 0.3589 \\ 0.5754 & 0.3399 & -0.5366 & -0.5152 \\ -0.2988 & -0.6694 & 0.6765 & -0.0707 \\ -0.0027 & -0.4061 & -0.4840 & -0.7751 \end{bmatrix} \quad \textbf{(A-12)}$$

$$K = \begin{bmatrix} \left.\frac{\delta T_i}{\delta L}\right|_{\beta_L,SL,V} & \left.\frac{\delta T_i}{\delta \beta_L}\right|_{L,SL,V} & \left.\frac{\delta T_i}{\delta SL}\right|_{L,\beta_L,V} & \left.\frac{\delta T_i}{\delta V}\right|_{L,\beta_L,SL} & \textit{Theoretical Stage} \\ 55.000 & 10.000 & -5.000 & -40.000 & \textit{1} \\ 90.000 & 15.000 & -5.000 & -65.000 & \textit{2} \\ 145.000 & 25.000 & -10.000 & -100.000 & \textit{3} \\ 205.000 & 35.000 & -15.000 & -150.000 & \textit{4} \\ 265.000 & 45.000 & -25.000 & -185.000 & \textit{5} \\ 285.000 & 50.000 & -20.000 & -200.000 & \textit{6} \\ 250.000 & 45.000 & -15.000 & -180.000 & \textit{A11} \\ 205.000 & 40.000 & -5.000 & -145.000 & \textit{A12} \\ 150.000 & 35.000 & -5.000 & -105.000 & \textit{A13} \\ 100.00 & 20.000 & 0.000 & -70.000 & \textit{A14} \\ 75.000 & 15.000 & 5.000 & -45.000 & \textit{A15} \\ 65.000 & 0.000 & 10.000 & -30.000 & \textit{A16} \\ 70.000 & -25.000 & 20.000 & -20.000 & \textit{A21} \\ 125.000 & -70.000 & 45.000 & -15.000 & \textit{A22} \\ 255.000 & -175.000 & 105.000 & -10.000 & \textit{A23} \\ 555.000 & -390.000 & 215.000 & -5.000 & \textit{A24} \\ 1205.000 & -865.000 & 475.000 & -5.000 & \textit{A25} \\ 2635.000 & -1895.000 & 1030.000 & 5.000 & \textit{A26} \\ 280.000 & 40.000 & -25.000 & -190.000 & \textit{B11} \\ 230.000 & 20.000 & -25.000 & -150.000 & \textit{B12} \\ 175.000 & 10.000 & -15.000 & -105.000 & \textit{B13} \\ 130.000 & -10.000 & 0.000 & -65.000 & \textit{B14} \\ 115.000 & -30.000 & 10.000 & -40.000 & \textit{B15} \\ 125.000 & -65.000 & 30.000 & -20.000 & \textit{B16} \\ 190.000 & -120.000 & 60.000 & -15.000 & \textit{B21} \\ 310.000 & -220.000 & 115.000 & -5.000 & \textit{B22} \\ 540.000 & -385.000 & 205.000 & -5.000 & \textit{B23} \\ 950.000 & -685.000 & 365.000 & 0.000 & \textit{B24} \\ 1715.000 & -1225.000 & 660.000 & 0.000 & \textit{B25} \\ 3145.000 & -2260.000 & 1220.000 & 5.000 & \textit{B26} \\ 5715.000 & -4155.000 & 2255.000 & 10.000 & \textit{31} \\ 10385.000 & -7795.000 & 4250.000 & 15.000 & \textit{32} \\ 14790.000 & -11465.000 & 6100.000 & 30.000 & \textit{33} \\ 14515.000 & -11100.000 & 5405.000 & 30.000 & \textit{34} \\ 9345.000 & -6805.000 & 3015.000 & 15.000 & \textit{35} \\ 4260.000 & -3000.000 & 1275.000 & 10.000 & \textit{36} \end{bmatrix} \quad \textbf{(A-13)}$$

$$
U = \begin{bmatrix}
-0.0011 & 0.0515 & -0.0373 & 0.0215 & T1 \\
-0.0017 & 0.0892 & -0.0668 & 0.0229 & T2 \\
-0.0026 & 0.1383 & -0.1162 & 0.0627 & T3 \\
-0.0038 & 0.2009 & -0.1700 & 0.1144 & T4 \\
-0.0049 & 0.2523 & -0.2072 & 0.1358 & T5 \\
-0.0053 & 0.2805 & -0.2267 & 0.1538 & T6 \\
-0.0048 & 0.2542 & -0.2114 & 0.1251 & TA11 \\
-0.0038 & 0.2041 & -0.1842 & 0.1108 & TA12 \\
-0.0028 & 0.1532 & -0.1443 & 0.0658 & TA13 \\
-0.0020 & 0.1056 & -0.1050 & 0.0401 & TA14 \\
-0.0014 & 0.0714 & -0.0703 & 0.0332 & TA15 \\
-0.0015 & 0.0444 & -0.0511 & 0.0129 & TA16 \\
-0.0021 & 0.0262 & -0.0347 & -0.0030 & TA21 \\
-0.0041 & 0.0148 & -0.0297 & 0.0027 & TA22 \\
-0.0088 & 0.0110 & -0.0299 & -0.0144 & TA23 \\
-0.0194 & 0.0088 & -0.0314 & -0.0314 & TA24 \\
-0.0426 & 0.0102 & -0.0557 & -0.0934 & TA25 \\
-0.0939 & 0.0274 & -0.1143 & -0.2284 & TA26 \\
-0.0052 & 0.2665 & -0.2090 & 0.1310 & TB11 \\
-0.0043 & 0.2178 & -0.1593 & 0.1250 & TB12 \\
-0.0035 & 0.1507 & -0.1035 & 0.0858 & TB13 \\
-0.0029 & 0.0918 & -0.0669 & 0.0518 & TB14 \\
-0.0030 & 0.0523 & -0.0401 & 0.0159 & TB15 \\
-0.0041 & 0.0306 & -0.0188 & 0.0158 & TB16 \\
-0.0067 & 0.0146 & -0.0154 & 0.0015 & TB21 \\
-0.0113 & 0.0107 & -0.0156 & -0.0156 & TB22 \\
-0.0199 & 0.0113 & -0.0226 & -0.0512 & TB23 \\
-0.0349 & 0.0141 & -0.0338 & -0.0684 & TB24 \\
-0.0624 & 0.0270 & -0.0772 & -0.1539 & TB25 \\
-0.1138 & 0.0388 & -0.1369 & -0.2797 & TB26 \\
-0.2067 & 0.0203 & -0.2337 & -0.4398 & T31 \\
-0.3852 & -0.1354 & -0.3736 & -0.3526 & T32 \\
-0.5653 & -0.3781 & -0.2352 & 0.3246 & T33 \\
-0.5570 & -0.0483 & 0.3111 & 0.3969 & T34 \\
-0.3522 & 0.4645 & 0.4539 & -0.2000 & T35 \\
-0.1584 & 0.3190 & 0.2324 & -0.2620 & T36
\end{bmatrix}
\qquad \textbf{(A-14)}
$$

Composition Control

Although not implemented on the pilot plant, composition control was also screened, and SVD and RGA resulted in a favorable two controller approach. Using the most sensitive inputs of steam and reflux (Equation A-18) and most sensitive compositions of bottoms cyclohexane and distillate cyclohexane (Equation A-19 resulted in the RGA matrix shown in Equation A-15). The pairing of bottoms composition with steam and distillate composition with reflux makes sense from an intuitive point of view and nicely follows the results from the temperature RGA. One could simulate bottoms composition to T34 to steam and distillate composition to T6 to reflux to determine temperature set points. Adding the third composition and the wall split to the RGA analysis results in the matrix shown in Equation A-16. The strategy from the three component case (pairing steam with bottoms composition, reflux with distillate composition, and wall split with sidedraw composition) results in two elements that are negative. This should be avoided as negative RGA values suggest that controller gains will change sign when any other loop in the system switches from closed-loop to open. Choosing non-negative elements to avoid potential changes in gain sign results in the pairing of bottoms composition to wall split, distillate composition to reflux, and sidedraw composition to steam. The bottoms composition and the wall split are at almost opposite ends of the column. Therefore, the lag time of this loop would make the strategy unfavorable. The notion that three compositions cannot be controlled simultaneously is further supported by the high condition number for the 3x3 system (Table A-4).

$$\Lambda = \begin{array}{c} \begin{matrix} \textit{Steam} & \textit{Reflux} \end{matrix} \\ \begin{bmatrix} 0.996 & 0.004 \\ 0.004 & 0.996 \end{bmatrix} \end{array} \begin{matrix} X_{B,C6} \\ X_{D,C6} \end{matrix} \qquad \textbf{(A-15)}$$

$$\Lambda = \begin{array}{c} \begin{matrix} \textit{Steam} & \textit{Reflux} & \textit{Wall Split} \end{matrix} \\ \begin{bmatrix} -0.3404 & -0.0033 & 1.3438 \\ -3.8148 & 5.9690 & -1.1542 \\ 5.1552 & -4.9656 & 0.8104 \end{bmatrix} \end{array} \begin{matrix} X_{B,C6} \\ X_{D,C6} \\ X_{SD,2MP} \end{matrix} \quad \textbf{(A-16)}$$

Table A-4. Condition Numbers for Composition SVD of case [2MP, C6, Tol/mX]

System Size	Condition Number
3 x 3	1147.7
2 x 2	35.43

Matrices for Composition Control

$$\Sigma = \begin{bmatrix} 1489.3 & 0 & 0 & 0 \\ 0 & 42.0 & 0 & 0 \\ 0 & 0 & 1.3 & 0 \end{bmatrix} \quad \textbf{(A-17)}$$

$$V = \begin{array}{c} \begin{matrix} \textit{Steam} & \textit{Side Reflux} & \textit{Wall Split} & \textit{Reflux} \end{matrix} \\ \begin{bmatrix} -0.7958 & 0.4372 & 0.1022 & 0.4064 \\ 0.5602 & 0.5147 & -0.2391 & 0.6034 \\ -0.2300 & -0.2525 & -0.9381 & 0.0572 \\ -0.0022 & -0.6930 & 0.2287 & 0.6837 \end{bmatrix} \end{array} \quad \textbf{(A-18)}$$

$$U = \begin{bmatrix} -0.0146 & 0.8029 & -0.5960 \\ 0.0172 & -0.5958 & -0.8030 \\ 0.9997 & 0.0220 & 0.0051 \end{bmatrix} \begin{matrix} X_{D,\,C6} \\ X_{S,\,2MP} \\ X_{B,\,C6} \end{matrix} \quad \textbf{(A-19)}$$

CASE [2MP, C6/TOL, MX]

Steady State Considerations

Steady state flows and compositions for the case of cyclohexane and toluene side product are shown in Table A-5, and the temperature profile is shown in Figure A-6. The profile is steepest in the stripping and lower dividing wall sections where the toluene and m-xylene are separated. There is very little temperature difference across the dividing wall, and there is a slight temperature change from the upper portions of the dividing wall to the rectifying section. In an effort to ensure most of the toluene was removed as side product rather than bottoms, the recovery of toluene out the side was set to 97 percent and controlled with the steam flow. The wall split was determined through sensitivity analysis. The liquid wall split was varied, and the value that minimized the reboiler duty while meeting the desired toluene recovery and distillate product compositions was chosen. Figure A-7 shows the reboiler duty plotted against the wall split.

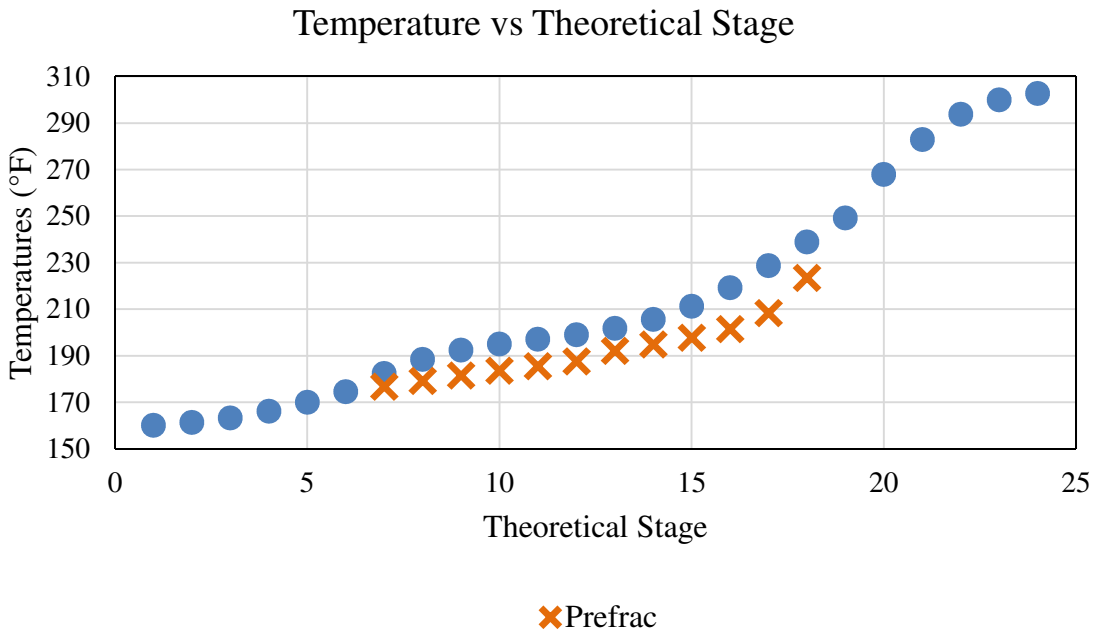

Figure A-6 – Temperature profile for [2MP, C6/Tol, mX]. Heat transfer to the environment and through the wall is included in the model.

Table A-5. Base Case Conditions

Stream Name	Total Mass Flow (lbm/hr)	Temperature (°F)	Composition (wt %)			
			2MP	C6	Tol	mX
Feed	50.00	195.00	32.00	32.00	4.00	32.00
Distillate	16.13	90.00	97.00	3.00	0.00	0.00
Reflux	139.26	70.00	97.00	3.00	0.00	0.00
Prefrac Reflux	132.27	160.00	51.61	48.30	0.09	0.00
Mainfrac Reflux	82.01	160.00	51.61	48.30	0.09	0.00
Side Product	17.82	198.98	1.97	87.07	10.89	0.07
Side Reflux	91.70	175.00	1.97	87.07	10.89	0.07
Bottoms	16.05	303.69	0.00	0.00	0.37	99.63
Steam (KBTU/hr)	62.90					

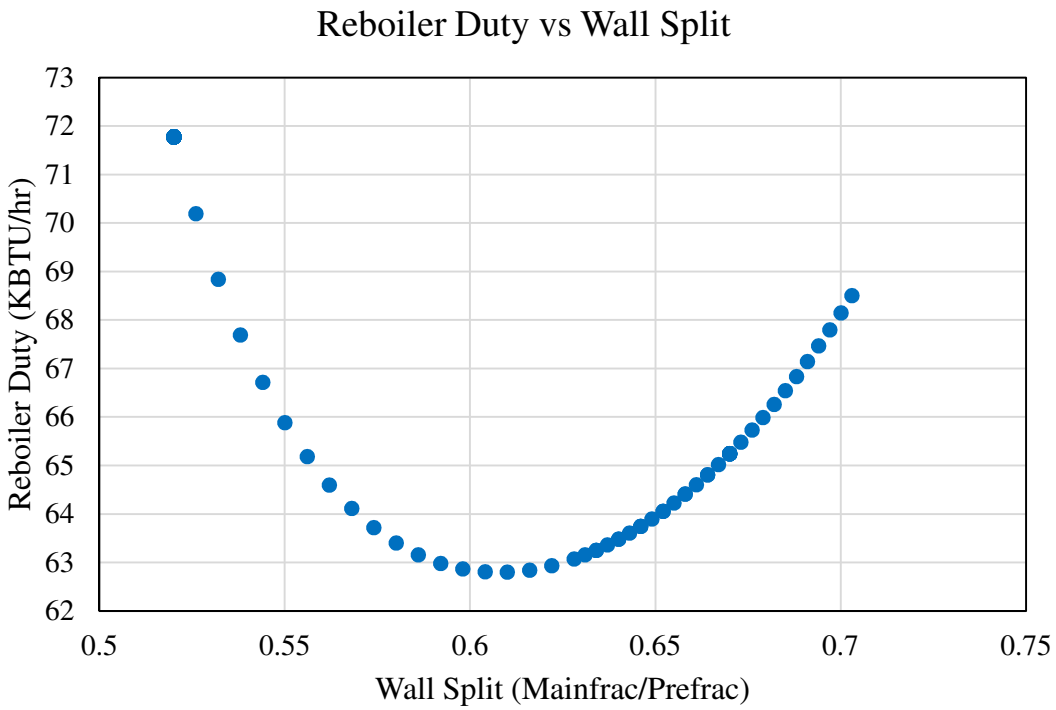

Figure A-7 – Sensitivity analysis for [2MP, C6/Tol, mX]

Temperature Control

RGA and SVD predicted the same control structure for this case as the others already discussed. Figure A-8 shows the changes in stage temperatures divided by the normalized change in manipulated variable. These are the columns of the gain matrix that was used for SVD (Equation A-21). Temperatures at the base of the column changed in response to changes in all manipulated variables. For the steam, sidedraw reflux, and wall split, the temperatures in the base and the lower portion of the wall changed orders of magnitude more than the other temperatures in the column.

SVD analysis of this case suggests using two or three temperature controllers (Table A-6). In order of most to least sensitive, sensitive inputs are steam, reflux, sidedraw reflux, and wall split (Equation A-23). The two most sensitive temperatures are T32 and TA11 (Equation A-24). However, finding other sensitive temperatures from the third and

fourth left singular vectors proves to be difficult since larger values cluster near T32 and TA11. A plot of the left singular values (Figure A-9) confirms that temperatures seem to cluster at the top of the wall on either side and at the base of the column close to the base of the wall. A plot of the difference of the absolute values of the first and second left singular vectors shows sensitivity and interaction on the same plot (Figure A-10). From this plot, stage 6 and stage 20 (T6 and T32 in the model) appear to be the best for control. Extending this idea to the difference of the absolute values of the first three left singular vectors identifies additional candidate temperatures for control (Figure A-11). In addition to the temperatures that appeared in Figure A-10, Stage 22 (T34) or Stage 18 (TB26) appear as candidate control temperatures in Figure A-11. However, the close proximity of T32 and T34 and TB26 may make them difficult to control simultaneously.

The RGA analysis for the inputs of steam and reflux and temperatures of T32 and T6 is shown in Equation A-20. T6 rather than TA11 was used to avoid a temperature right below the total trapout tray and one that would be sensitive to heatloss in the prefrac reflux stream. The resulting pairing is stripping temperature with steam and rectifying temperature with reflux. Although disturbance testing would be the ultimate test of controller performance, the diagonal values close to one and the close proximity of controlled and manipulated variables looks promising. An RGA analysis for three temperatures and three valves was not done because it was unclear what control temperature to choose for the third temperature.

Table A-6. Condition Numbers for Temperature SVD of case [2MP, C6/Tol, mX]

System Size	Condition Number
4 x 4	361.66
3 x 3	61.74
2 x 2	18.13

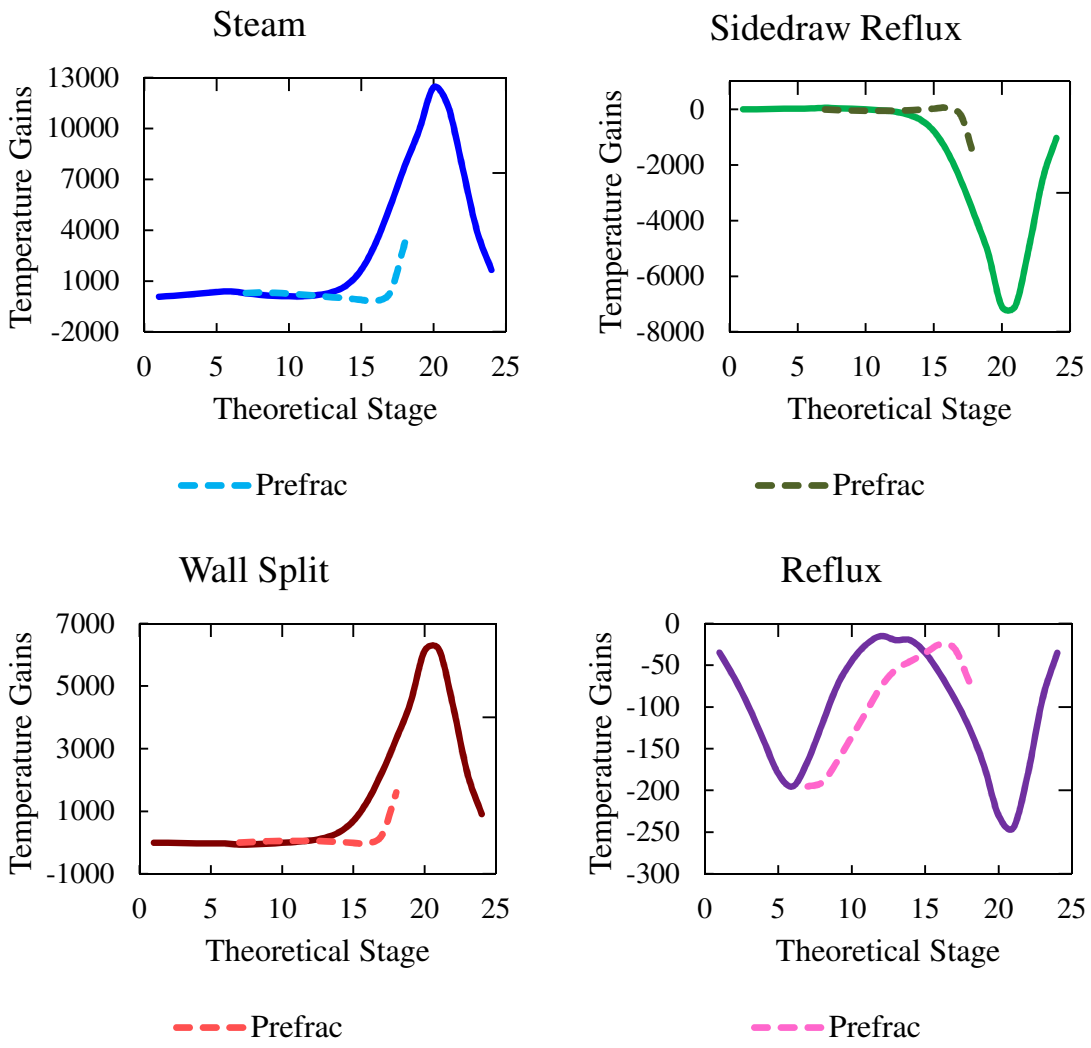

Figure A-8 – Change in temperature over normalized change in manipulated variable for steam, wall split, sidedraw reflux, and reflux.

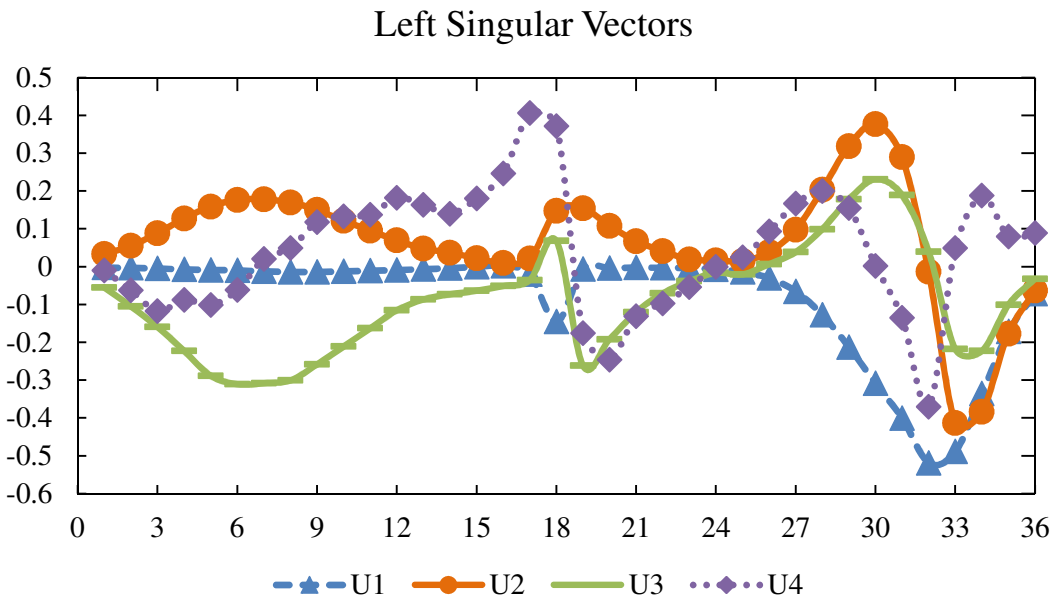

Figure A-9 – Graphical representation of the four columns of the U matrix. Note that 1-6 are the rectifying temperatures, 7-18 are the prefrac temperatures, 19-30 are the mainfrac temperatures, and 31-36 are the stripping temperatures.

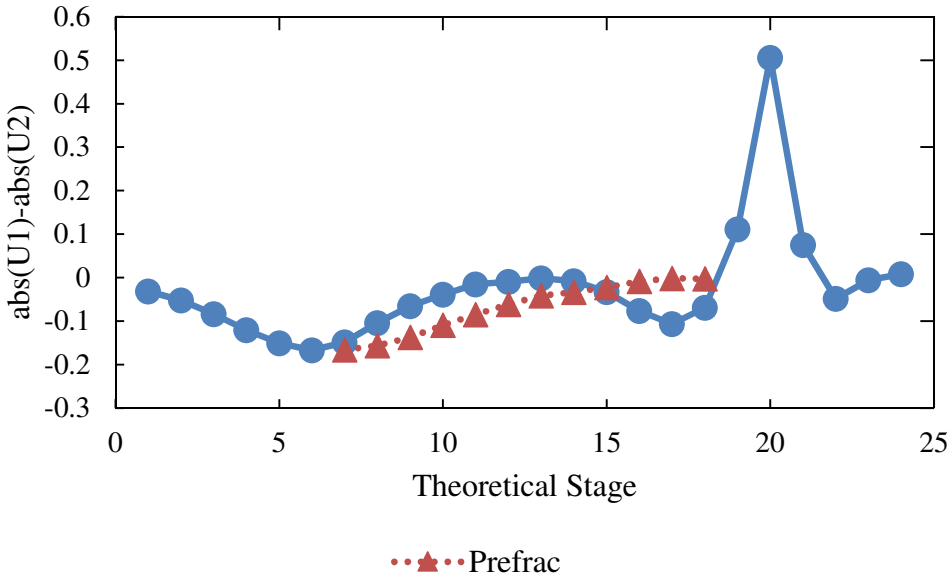

Figure A-10 – abs(U1) – abs(U2) vs. Theoretical Stage

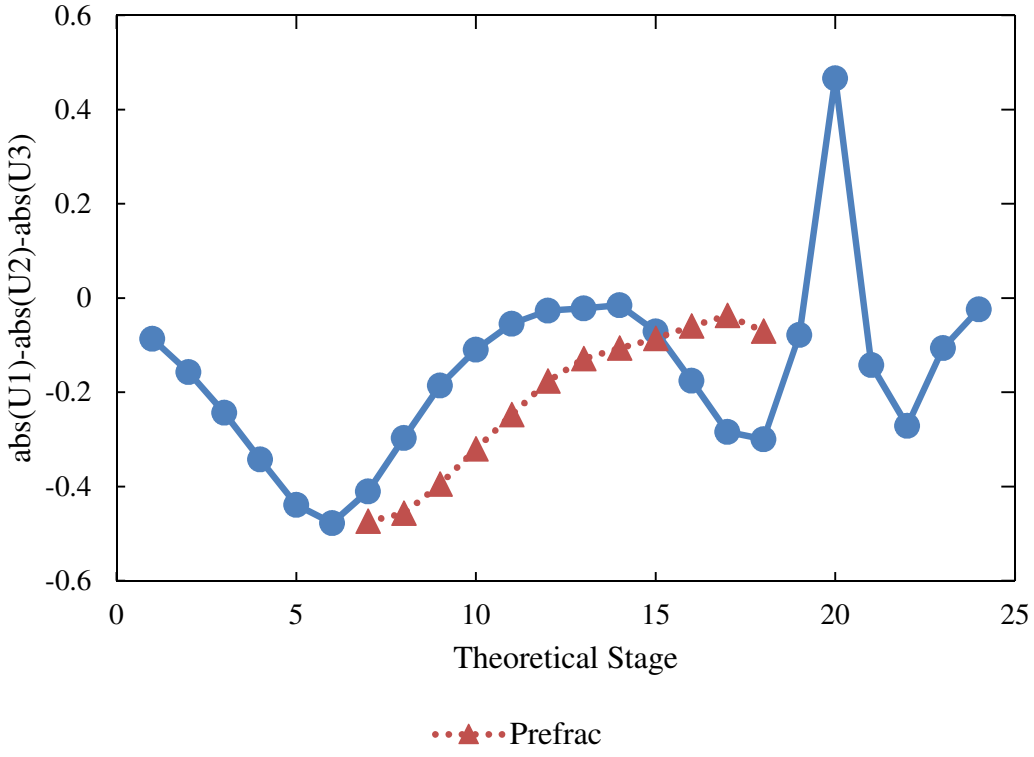

Figure A-11 – abs(U1) – abs(U2) – abs(U3) vs. Theoretical Stage

$$\Lambda = \begin{matrix} \\ T_{Stripping} \\ T_{Rectifying} \end{matrix} \begin{matrix} \textit{Steam} & \textit{Reflux} \\ \begin{bmatrix} 1.038 & -0.038 \\ -0.038 & 1.038 \end{bmatrix} \end{matrix} \qquad \textbf{(A-20)}$$

Matrices for Temperature Control

$$K = \begin{bmatrix} \left.\frac{\delta T_i}{\delta L}\right|_{\beta_L,SL,V} & \left.\frac{\delta T_i}{\delta \beta_L}\right|_{L,SL,V} & \left.\frac{\delta T_i}{\delta SL}\right|_{L,\beta_L,V} & \left.\frac{\delta T_i}{\delta V}\right|_{L,\beta_L,SL} & \textit{Theoretical Stage} \\ 75.000 & 5.000 & -5.000 & -35.000 & \textit{1} \\ 125.000 & 5.000 & -10.000 & -65.000 & \textit{2} \\ 195.000 & 10.000 & -20.000 & -100.000 & \textit{3} \\ 280.000 & 20.000 & -25.000 & -140.000 & \textit{4} \\ 350.000 & 25.000 & -30.000 & -180.000 & \textit{5} \\ 390.000 & 30.000 & -30.000 & -195.000 & \textit{6} \\ 455.000 & 0.000 & 5.000 & -195.000 & \textit{A11} \\ 480.000 & -25.000 & 30.000 & -190.000 & \textit{A12} \\ 465.000 & -40.000 & 50.000 & -165.000 & \textit{A13} \\ 410.000 & -50.000 & 60.000 & -135.000 & \textit{A14} \\ 345.000 & -50.000 & 60.000 & -105.000 & \textit{A15} \\ 275.000 & -45.000 & 60.000 & -75.000 & \textit{A16} \\ 190.000 & -30.000 & 45.000 & -55.000 & \textit{A21} \\ 125.000 & -10.000 & 25.000 & -45.000 & \textit{A22} \\ 20.000 & 30.000 & -5.000 & -35.000 & \textit{A23} \\ -40.000 & 50.000 & -15.000 & -25.000 & \textit{A24} \\ 500.000 & -230.000 & 245.000 & -30.000 & \textit{A25} \\ 3635.000 & -1815.000 & 1610.000 & -70.000 & \textit{A26} \\ 280.000 & 55.000 & -65.000 & -165.000 & \textit{B11} \\ 180.000 & 40.000 & -60.000 & -120.000 & \textit{B12} \\ 115.000 & 25.000 & -35.000 & -75.000 & \textit{B13} \\ 95.000 & 0.000 & -10.000 & -45.000 & \textit{B14} \\ 105.000 & -35.000 & 25.000 & -25.000 & \textit{B15} \\ 175.000 & -75.000 & 65.000 & -15.000 & \textit{B16} \\ 350.000 & -175.000 & 155.000 & -20.000 & \textit{B21} \\ 765.000 & -370.000 & 330.000 & -20.000 & \textit{B22} \\ 1665.000 & -785.000 & 695.000 & -35.000 & \textit{B23} \\ 3260.000 & -1525.000 & 1335.000 & -60.000 & \textit{B24} \\ 5420.000 & -2575.000 & 2235.000 & -90.000 & \textit{B25} \\ 7775.000 & -3830.000 & 3305.000 & -125.000 & \textit{B26} \\ 9900.000 & -5180.000 & 4470.000 & -170.000 & \textit{31} \\ 12425.000 & -7095.000 & 6130.000 & -230.000 & \textit{32} \\ 11300.000 & -7055.000 & 6130.000 & -230.000 & \textit{33} \\ 7660.000 & -4935.000 & 4340.000 & -180.000 & \textit{34} \\ 3935.000 & -2505.000 & 2200.000 & -90.000 & \textit{35} \\ 1650.000 & -1030.000 & 910.000 & -35.000 & \textit{36} \end{bmatrix} \quad \textbf{(A-21)}$$

$$\Sigma = \begin{bmatrix} 30{,}018 & 0 & 0 & 0 \\ 0 & 1656 & 0 & 0 \\ 0 & 0 & 486 & 0 \\ 0 & 0 & 0 & 83 \end{bmatrix} \quad \textbf{(A-22)}$$

$$V = \begin{array}{c} \begin{matrix} \textit{Steam} & \textit{Side Reflux} & \textit{Wall Split} & \textit{Reflux} \end{matrix} \\ \begin{bmatrix} -0.7989 & 0.5936 & 0.0956 & 0.0185 \\ 0.4537 & 0.5834 & 0.0386 & 0.6726 \\ -0.3946 & -0.5366 & -0.1088 & 0.7379 \\ 0.0161 & -0.1392 & 0.9887 & 0.0532 \end{bmatrix} \end{array} \quad \textbf{(A-23)}$$

$$
U = \begin{bmatrix}
-0.0019 & 0.0332 & -0.0549 & -0.0096 \\
-0.0032 & 0.0553 & -0.1050 & -0.0621 \\
-0.0048 & 0.0883 & -0.1598 & -0.1173 \\
-0.0069 & 0.1273 & -0.2225 & -0.0874 \\
-0.0086 & 0.1591 & -0.2885 & -0.1013 \\
-0.0096 & 0.1765 & -0.3108 & -0.0615 \\
-0.0123 & 0.1778 & -0.3082 & 0.0211 \\
-0.0136 & 0.1695 & -0.3007 & 0.0496 \\
-0.0137 & 0.1502 & -0.2585 & 0.1185 \\
-0.0125 & 0.1212 & -0.2113 & 0.1333 \\
-0.0108 & 0.0954 & -0.1631 & 0.1380 \\
-0.0088 & 0.0696 & -0.1155 & 0.1821 \\
-0.0061 & 0.0476 & -0.0869 & 0.1641 \\
-0.0038 & 0.0370 & -0.0733 & 0.1403 \\
0.0000 & 0.0223 & -0.0637 & 0.1807 \\
0.0020 & 0.0102 & -0.0514 & 0.2469 \\
-0.0200 & 0.0102 & -0.0514 & 0.2469 \\
-0.1454 & 0.1478 & 0.0679 & 0.3723 \\
-0.0059 & 0.1547 & -0.2616 & -0.1754 \\
-0.0035 & 0.1081 & -0.1920 & -0.2460 \\
-0.0023 & 0.0677 & -0.1201 & -0.1309 \\
-0.0024 & 0.0411 & -0.0706 & -0.0965 \\
-0.0037 & 0.0193 & -0.0386 & -0.0539 \\
-0.0067 & 0.0165 & -0.0166 & -0.0004 \\
-0.0140 & 0.0153 & -0.0204 & 0.0252 \\
-0.0303 & 0.0386 & 0.0065 & 0.0935 \\
-0.0653 & 0.0980 & 0.0383 & 0.1668 \\
-0.1274 & 0.2038 & 0.0991 & 0.2001 \\
-0.2126 & 0.3190 & 0.1779 & 0.1558 \\
-0.3083 & 0.3773 & 0.2306 & 0.0019 \\
-0.4006 & 0.2897 & 0.1890 & -0.1350 \\
-0.5186 & -0.0126 & 0.0398 & -0.3698 \\
-0.4886 & -0.4135 & -0.2176 & 0.0492 \\
-0.3356 & -0.3839 & -0.2232 & 0.1882 \\
-0.1715 & -0.1772 & -0.1006 & 0.0804 \\
-0.0715 & -0.0633 & -0.0322 & 0.0896
\end{bmatrix}
\begin{matrix}
T1 \\ T2 \\ T3 \\ T4 \\ T5 \\ T6 \\ TA11 \\ TA12 \\ TA13 \\ TA14 \\ TA15 \\ TA16 \\ TA21 \\ TA22 \\ TA23 \\ TA24 \\ TA25 \\ TA26 \\ TB11 \\ TB12 \\ TB13 \\ TB14 \\ TB15 \\ TB16 \\ TB21 \\ TB22 \\ TB23 \\ TB24 \\ TB25 \\ TB26 \\ T31 \\ T32 \\ T33 \\ T34 \\ T35 \\ T36
\end{matrix}
\qquad \textbf{(A-24)}
$$

Composition Control

SVD and RGA were executed with select compositions and resulted in a favorable two controller approach. Using the most sensitive inputs of steam and reflux (Equation A-28) and most sensitive compositions of bottoms toluene and distillate cyclohexane (Equation A-29) resulted in the RGA matrix shown in Equation A-25. The pairing of bottoms composition with steam and distillate composition with reflux makes sense from an intuitive point of view and nicely follows the results from the temperature RGA. In a simulation environment, the bottoms composition could be cascaded to the stripping temperature controller, and the distillate composition could be cascaded to the rectifying section temperature controller to determine temperature set points. Adding the third composition and the wall split to the RGA analysis results in the matrix shown in Equation A-26. Avoiding negative elements results in the pairing of bottoms composition to wall split, distillate composition to reflux, and sidedraw composition to steam. Once again, the bottoms composition and the wall split are at almost opposite ends of the column. Therefore, the lag time of this loop would make the strategy unfavorable. Furthermore, the high condition number for three controller approach suggests that controlling three compositions is not feasible (Table A-7).

$$\Lambda = \begin{array}{c} \begin{matrix} \textit{Steam} & \textit{Reflux} \end{matrix} \\ \begin{bmatrix} 1.045 & -0.045 \\ -0.045 & 1.045 \end{bmatrix} \end{array} \begin{matrix} X_{B,\ Tol} \\ X_{D,\ C6} \end{matrix} \qquad \textbf{(A-25)}$$

$$\Lambda = \begin{array}{c} \begin{matrix} \textit{Steam} & \textit{Reflux} & \textit{Wall Ratio} \end{matrix} \\ \begin{bmatrix} -2.4631 & 0.1281 & 3.3349 \\ -6.2270 & 8.1134 & -0.8864 \\ 9.6901 & -7.2415 & -1.4486 \end{bmatrix} \end{array} \begin{matrix} X_{B,\ Tol} \\ X_{D,\ C6} \\ X_{SD,\ 2MP} \end{matrix} \qquad \textbf{(A-26)}$$

Table A-7. Condition Numbers for Composition SVD of case [2MP, C6/Tol, mX]

System Size	Condition Number
3 x 3	1164.9
2 x 2	29.94

Matrices for Composition Control

$$\Sigma = \begin{bmatrix} 1397.9 & 0 & 0 & 0 \\ 0 & 46.7 & 0 & 0 \\ 0 & 0 & 1.2 & 0 \end{bmatrix} \quad \textbf{(A-27)}$$

$$V = \begin{array}{c} \begin{matrix} \textit{Steam} & \textit{Side Reflux} & \textit{Wall Split} & \textit{Reflux} \end{matrix} \\ \begin{bmatrix} -0.7738 & 0.5190 & 0.3438 & 0.1172 \\ 0.4765 & 0.4768 & 0.1033 & 0.7314 \\ -0.4170 & -0.4415 & -0.4864 & 0.6282 \\ 0.0175 & -0.5553 & 0.7966 & 0.2381 \end{bmatrix} \end{array} \quad \textbf{(A-28)}$$

$$U = \begin{bmatrix} -0.0236 & 0.8637 & -0.5034 \\ 0.0243 & -0.5029 & -0.8640 \\ 0.9994 & 0.0326 & 0.0091 \end{bmatrix} \begin{matrix} X_{D,\,C6} \\ X_{S,\,2MP} \\ X_{B,\,Tol} \end{matrix} \quad \textbf{(A-29)}$$

CASE [2MP/C6, TOL, MX] – ORIGINAL MODEL

Steady State Considerations

Steady state flows and compositions for the trace side product case are shown in Table A-8, and the temperature profile is shown in Figure A-12. There is still a large

temperature gradient in the stripping section where the toluene and m-xylene are separated. However, due to the larger composition difference between the feed and the pure toluene side product, there is a larger temperature difference across the wall. Furthermore, there is a large temperature difference between the middle and top of the dividing wall section than in the other cases because the cyclohexane and toluene separation has moved further up the column. Due to the small side product flow, the level configuration was changed to control the side tank level with the sidedraw reflux (Figure A-13). This configuration more closely mimics an industrial column where there would not be a side tank. To determine steady state conditions, the toluene recovery was set to 96 percent, and the wall split was varied.

Figure A-14 shows the optimization of reboiler duty regarding the wall split. Because two side product impurities were specified during this process, simulations did not converge with wall splits less than 0.7.

Table A-8. [2MP/C6, Tol, mX] Base Case Conditions

Stream Name	Total Mass Flow (lbm/hr)	Temperature (°F)	Composition (wt %)			
			2MP	C6	Tol	mX
Feed	50.00	195.00	32.00	32.00	4.00	32.00
Distillate	32.00	90.00	49.99	49.87	0.14	0.00
Reflux	112.73	70.00	49.99	49.87	0.14	0.00
Prefrac Reflux	110.86	175.00	10.07	79.93	9.99	0.01
Mainfrac Reflux	80.93	175.00	10.07	79.93	9.99	0.01
Side Product	2.00	249.80	0.02	2.00	96.00	1.98
Side Reflux	128.79	220.00	0.02	2.00	96.00	1.98
Bottoms	16.00	303.93	0.00	0.00	0.22	99.78
Steam (KBTU/hr)	68.51					

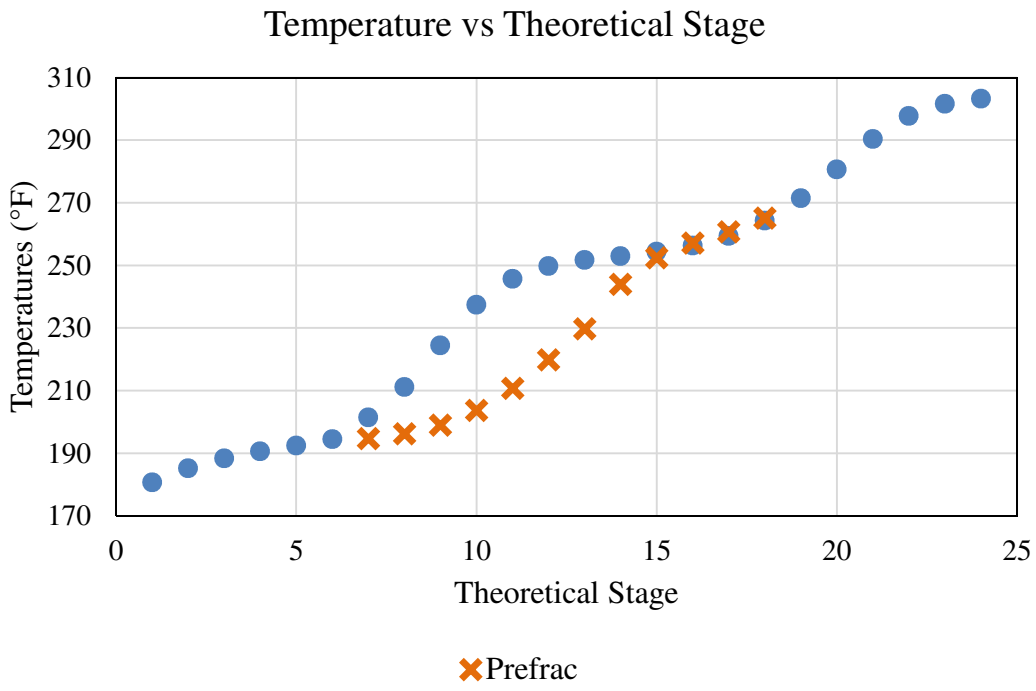

Figure A-12 – Temperature profile for case [2MP/C6, Tol, mX]. Heat transfer to the environment and through the wall is included in the model.

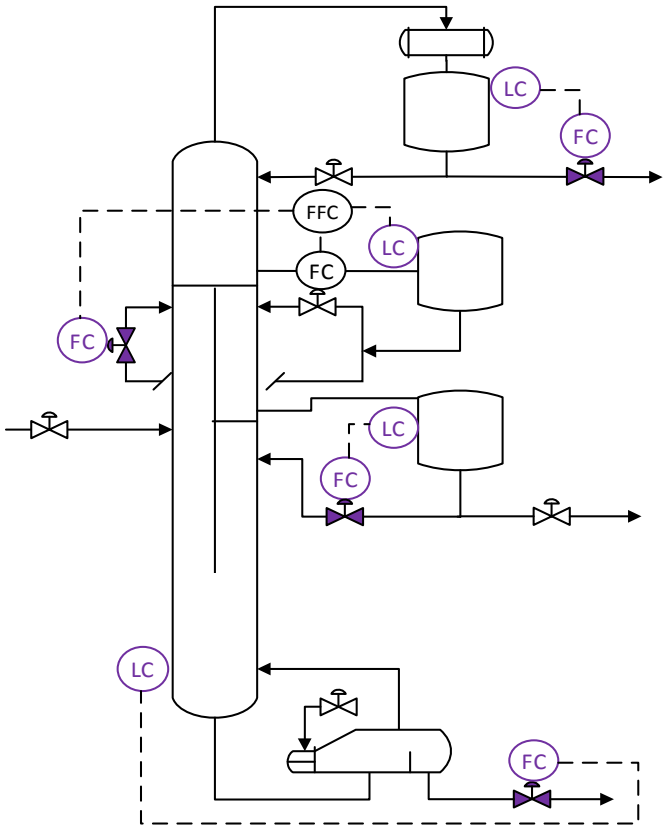

Figure A-13 – Level control structure for case [2MP/C6, Tol, mX]

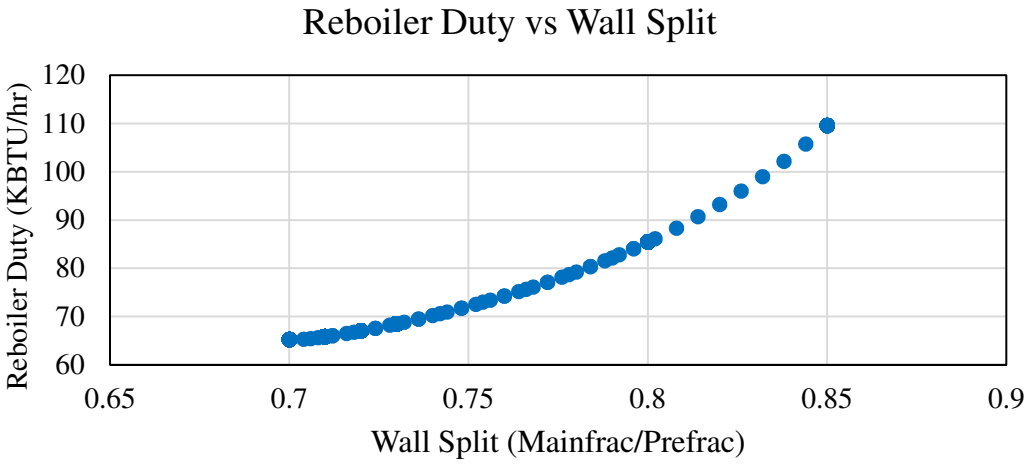

Figure A-14 – Sensitivity analysis for case [2MP/C6, Tol, mX]

Temperature Control

Due to different separation locations within the column and a different level control structure, a different temperature control structure was predicted for this case. Just as with the other cases, the condition numbers from SVD indicated that two or three temperature controllers may be used to control the column without a large degree of interaction (Table A-9). Multiple potential control temperatures appeared from the U matrix of left singular values (Equation A-35, Figure A-16). In order of left singular vectors and therefore sensitivity, the temperatures are TA16, T32, TB13, and TA22 in the model. This observation is confirmed from plotting the difference of absolute values, which accounts for sensitivity and interaction on the same plot (Figure A-17 and Figure A-18). Because the condition numbers discouraged four temperature controllers, only TA16, T32, and TB13 were used in RGA analysis. From the right matrix of singular values, the best manipulated variables for control are, in order, steam, sidedraw flow, wall split, and reflux (Equation A-34).

The RGA analysis for the inputs of steam and sidedraw and temperatures of T32 and TA16 is shown in Equation A-30. The resulting pairing is stripping temperature with sidedraw flow and prefrac temperature with steam. As desired, the diagonal values are close to one though the pairing does not appear to be intuitive. When expanding this analysis to include a third temperature controller, the manipulated variable for the prefrac temperature controller changes. The resulting control structure is prefrac temperature to wall split, stripping temperature to sidedraw flow, and mainfrac temperature to steam (Equation A-31). Figure A-15 elucidates why RGA analysis paired the stripping temperature with the side flow rather than with the steam. The sidedraw flow impacted the stripping temperatures much more than the other column temperatures while the steam influenced all temperatures, the prefrac temperature slightly more.

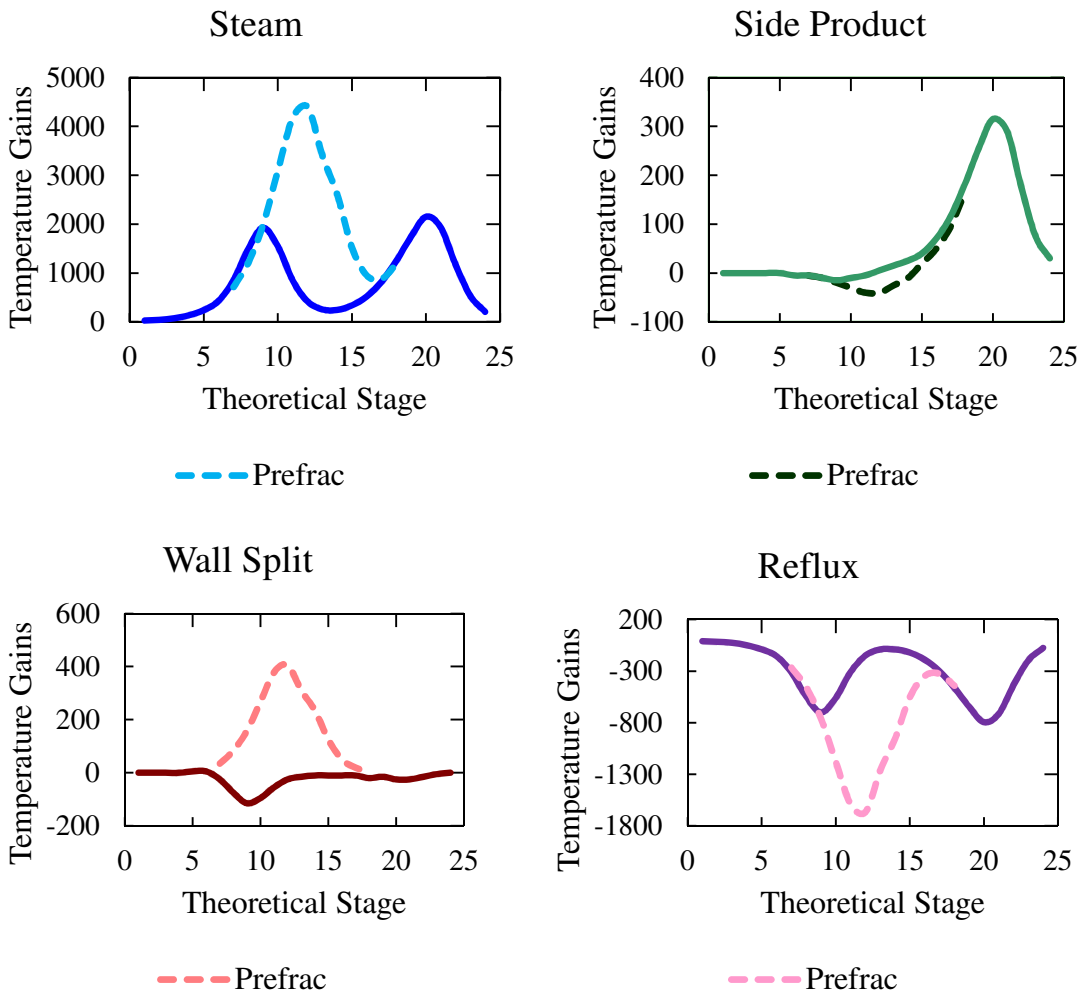

Figure A-15 – Change in temperature over normalized change in manipulated variable for steam, wall split, sidedraw reflux, and reflux.

Table A-9. Condition Numbers for Temperature SVD of case [2MP/C6, Tol, mX]

System Size	Condition Number
4 x 4	228.83
3 x 3	30.16
2 x 2	15.22

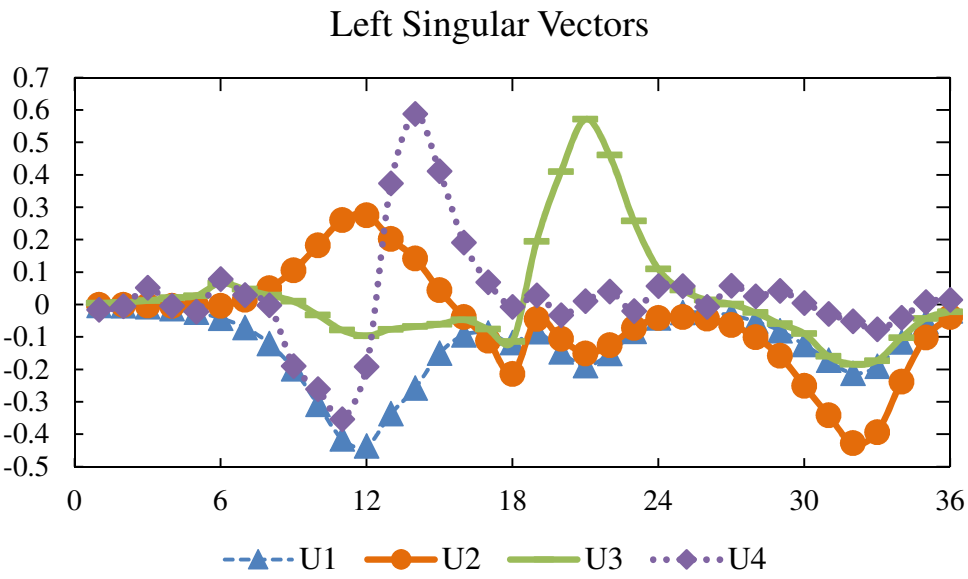

Figure A-16 – Graphical representation of the four columns of the U matrix. Note that 1-6 are the rectifying temperatures, 7-18 are the prefrac temperatures, 19-30 are the mainfrac temperatures, and 31-36 are the stripping temperatures.

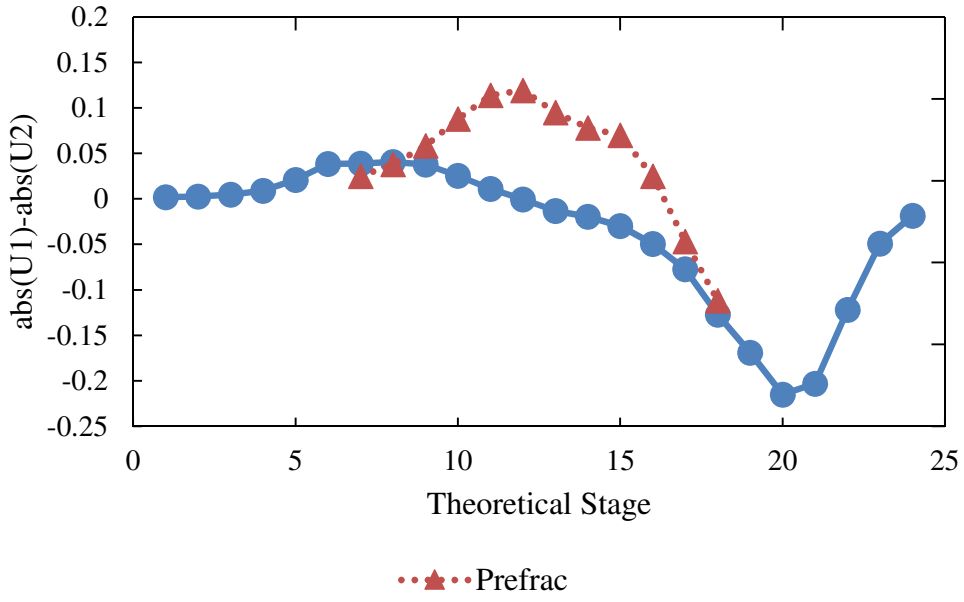

Figure A-17 – abs(U1) – abs(U2) vs. Theoretical Stage

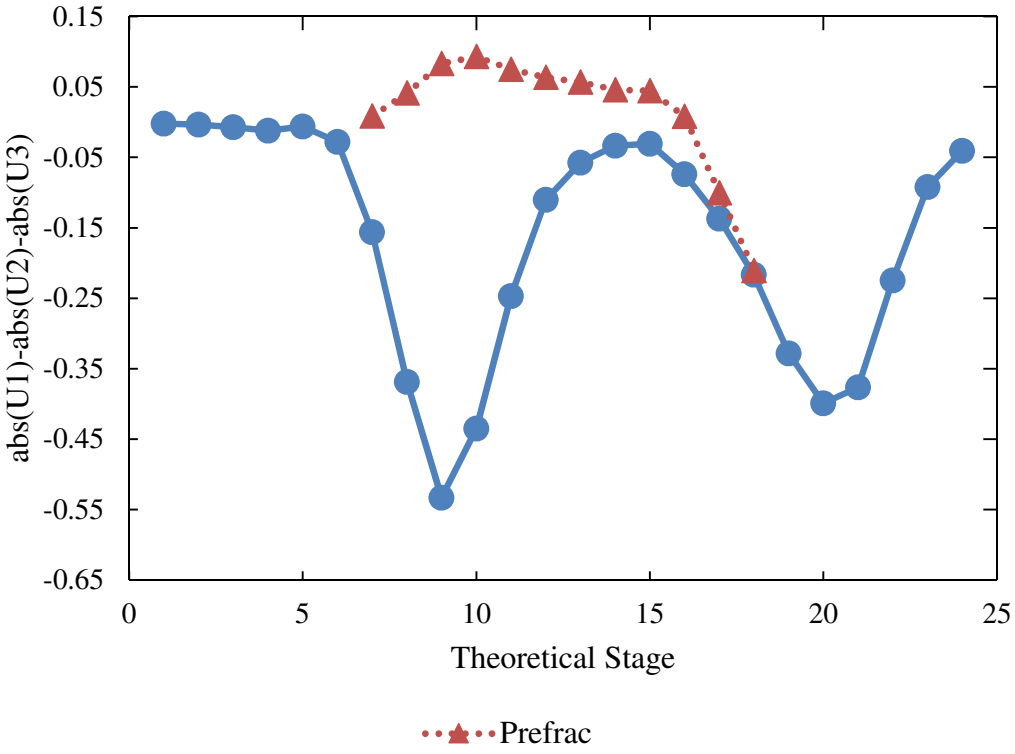

Figure A-18 – abs(U1) – abs(U2) – abs(U3) vs. Theoretical Stage

$$\Lambda = \begin{matrix} \\ T_{Prefrac} \\ T_{Stripping} \end{matrix} \begin{matrix} \begin{matrix} Steam & Side \end{matrix} \\ \begin{bmatrix} 0.942 & 0.058 \\ 0.058 & 0.942 \end{bmatrix} \end{matrix} \tag{A-30}$$

$$\Lambda = \begin{matrix} \\ T_{Prefrac} \\ T_{Stripping} \\ T_{Mainfrac} \end{matrix} \begin{matrix} \begin{matrix} Steam & Side & Wall\ Split \end{matrix} \\ \begin{bmatrix} 0.3766 & 0.0186 & 0.6048 \\ 0.0537 & 0.9470 & -0.0006 \\ 0.5698 & 0.0344 & 0.3958 \end{bmatrix} \end{matrix} \tag{A-31}$$

Matrices for Temperature Control

$$K = \begin{array}{c} \left.\frac{\delta T_i}{\delta L}\right|_{\beta_L,SL,V} \quad \left.\frac{\delta T_i}{\delta \beta_L}\right|_{L,SL,V} \quad \left.\frac{\delta T_i}{\delta SL}\right|_{L,\beta_L,V} \quad \left.\frac{\delta T_i}{\delta V}\right|_{L,\beta_L,SL} \\ \begin{bmatrix} 25.000 & 0.000 & 0.000 & -10.000 \\ 40.000 & 0.000 & 0.000 & -15.000 \\ 75.000 & 0.000 & 0.000 & -25.000 \\ 135.000 & 0.000 & 0.000 & -50.000 \\ 240.000 & 0.000 & 5.000 & -90.000 \\ 430.000 & -5.000 & 5.000 & -155.000 \\ 715.000 & -5.000 & 35.000 & -265.000 \\ 1215.000 & -10.000 & 85.000 & -455.000 \\ 2000.000 & -20.000 & 160.000 & -760.000 \\ 3105.000 & -30.000 & 270.000 & -1180.000 \\ 4180.000 & -40.000 & 380.000 & -1590.000 \\ 4400.000 & -40.000 & 405.000 & -1665.000 \\ 3400.000 & -25.000 & 310.000 & -1260.000 \\ 2605.000 & -10.000 & 235.000 & -950.000 \\ 1520.000 & 20.000 & 125.000 & -550.000 \\ 950.000 & 50.000 & 50.000 & -345.000 \\ 885.000 & 95.000 & 20.000 & -325.000 \\ 1190.000 & 165.000 & 0.000 & -440.000 \\ 850.000 & -5.000 & -25.000 & -310.000 \\ 1490.000 & -10.000 & -75.000 & -545.000 \\ 1925.000 & -15.000 & -115.000 & -700.000 \\ 1545.000 & -10.000 & -95.000 & -560.000 \\ 850.000 & -5.000 & -55.000 & -310.000 \\ 420.000 & 5.000 & -25.000 & -150.000 \\ 255.000 & 15.000 & -15.000 & -90.000 \\ 245.000 & 25.000 & -10.000 & -90.000 \\ 335.000 & 40.000 & -10.000 & -120.000 \\ 520.000 & 70.000 & -10.000 & -190.000 \\ 820.000 & 115.000 & -10.000 & -300.000 \\ 1250.000 & 180.000 & -20.000 & -460.000 \\ 1745.000 & 255.000 & -15.000 & -645.000 \\ 2150.000 & 315.000 & -25.000 & -795.000 \\ 1930.000 & 290.000 & -25.000 & -715.000 \\ 1175.000 & 175.000 & -15.000 & -435.000 \\ 530.000 & 75.000 & -5.000 & -195.000 \\ 205.000 & 30.000 & 0.000 & -75.000 \end{bmatrix} \begin{array}{l} T1 \\ T2 \\ T3 \\ T4 \\ T5 \\ T6 \\ TA11 \\ TA12 \\ TA13 \\ TA14 \\ TA15 \\ TA16 \\ TA21 \\ TA22 \\ TA23 \\ TA24 \\ TA25 \\ TA26 \\ TB11 \\ TB12 \\ TB13 \\ TB14 \\ TB15 \\ TB16 \\ TB21 \\ TB22 \\ TB23 \\ TB24 \\ TB25 \\ TB26 \\ T31 \\ T32 \\ T33 \\ T34 \\ T35 \\ T36 \end{array} \end{array} \quad \textbf{(A-32)}$$

$$\Sigma = \begin{bmatrix} 10{,}812 & 0 & 0 & 0 \\ 0 & 710 & 0 & 0 \\ 0 & 0 & 358 & 0 \\ 0 & 0 & 0 & 47 \end{bmatrix} \quad \textbf{(A-33)}$$

$$V = \begin{array}{c} \begin{matrix} \textit{Steam} & \textit{Side} & \textit{Wall Split} & \textit{Reflux} \end{matrix} \\ \begin{bmatrix} -0.9353 & -0.0357 & 0.0702 & 0.3450 \\ -0.0182 & -0.7585 & -0.6514 & 0.0046 \\ -0.0535 & 0.6497 & -0.7545 & 0.0758 \\ 0.3494 & -0.0358 & 0.0384 & 0.9355 \end{bmatrix} \end{array} \quad \textbf{(A-34)}$$

$$
U = \begin{bmatrix}
-0.0025 & -0.0008 & 0.0038 & -0.0154 & 1 \\
-0.0039 & -0.0013 & 0.0062 & -0.0049 & 2 \\
-0.0073 & -0.0025 & 0.0120 & 0.0527 & 3 \\
-0.0133 & -0.0043 & 0.0211 & -0.0042 & 4 \\
-0.0237 & -0.0030 & 0.0268 & -0.0215 & 5 \\
-0.0422 & -0.0039 & 0.0661 & 0.0785 & 6 \\
-0.0706 & 0.0147 & 0.0470 & 0.0297 & A11 \\
-0.1202 & 0.0502 & 0.0283 & -0.0015 & A12 \\
-0.1983 & 0.1054 & 0.0096 & -0.1890 & A13 \\
-0.3080 & 0.1823 & -0.0325 & -0.2606 & A14 \\
-0.4148 & 0.2602 & -0.0793 & -0.3533 & A15 \\
-0.4364 & 0.2758 & -0.0969 & -0.1917 & A16 \\
-0.3363 & 0.2027 & -0.0766 & 0.3742 & A21 \\
-0.2572 & 0.1425 & -0.0684 & 0.5881 & A22 \\
-0.1499 & 0.0442 & -0.0609 & 0.4117 & A23 \\
-0.0937 & -0.0381 & -0.0471 & 0.1911 & A24 \\
-0.0873 & -0.1113 & -0.0763 & 0.0686 & A25 \\
-0.1174 & -0.2139 & -0.1141 & -0.0065 & A26 \\
-0.0834 & -0.0447 & 0.1949 & 0.0282 & B11 \\
-0.1461 & -0.1054 & 0.4093 & -0.0321 & B12 \\
-0.1885 & -0.1508 & 0.5712 & 0.0107 & B13 \\
-0.1513 & -0.1257 & 0.4606 & 0.0405 & B14 \\
-0.0833 & -0.0721 & 0.2580 & -0.0199 & B15 \\
-0.0411 & -0.0418 & 0.1097 & 0.0573 & B16 \\
-0.0249 & -0.0380 & 0.0446 & 0.0574 & B21 \\
-0.0241 & -0.0436 & 0.0139 & -0.0066 & B22 \\
-0.0329 & -0.0627 & 0.0011 & 0.0580 & B23 \\
-0.0512 & -0.1005 & -0.0247 & 0.0258 & B24 \\
-0.0808 & -0.1581 & -0.0596 & 0.0428 & B25 \\
-0.1232 & -0.2503 & -0.0896 & 0.0050 & B26 \\
-0.1721 & -0.3414 & -0.1594 & -0.0282 & 31 \\
-0.2121 & -0.4274 & -0.1841 & -0.0511 & 32 \\
-0.1904 & -0.3937 & -0.1732 & -0.0760 & 33 \\
-0.1159 & -0.2378 & -0.1030 & -0.0402 & 34 \\
-0.0522 & -0.1015 & -0.0429 & 0.0084 & 35 \\
-0.0202 & -0.0386 & -0.0224 & 0.0148 & 36
\end{bmatrix} \qquad \textbf{(A-35)}
$$

Composition Control

SVD and RGA were executed with select compositions. In order of most to least sensitive, the sensitive inputs are steam, sidedraw, wall split, and reflux (Equation A-39). The most sensitive compositions are bottoms toluene, sidedraw cyclohexane, and sidedraw m-xylene (Equation A-40). Using the most sensitive inputs of steam and sidedraw and most sensitive compositions of bottoms toluene and sidedraw cyclohexane results in the RGA matrix shown in Equation A-36. The pairing of side composition with steam and bottoms composition with sidedraw has the potential for a large degree of interaction. However, this strategy follows the results from the temperature RGA. Equation A-37 shows the addition of the third composition and the wall split to the RGA analysis. Avoiding negative elements results in the pairing of bottoms composition to steam, heavy sidedraw composition to wall split, and light sidedraw composition to sidedraw. However, the high condition number for three controller system suggests that controlling three compositions is not feasible (Table A-10).

$$\Lambda = \begin{matrix} \\ X_{B,\,Tol} \\ X_{SD,\,C6} \end{matrix} \begin{matrix} \begin{matrix} \textit{Steam} & \textit{Side} \end{matrix} \\ \begin{bmatrix} 0.043 & 0.957 \\ 0.957 & 0.043 \end{bmatrix} \end{matrix} \qquad \textbf{(A-36)}$$

$$\Lambda = \begin{matrix} X_{B,\,Tol} \\ X_{SD,\,C6} \\ X_{SD,\,mX} \end{matrix} \begin{matrix} \begin{matrix} \textit{Steam} & \textit{Side} & \textit{Wall Split} \end{matrix} \\ \begin{bmatrix} 2.4269 & -0.9664 & -0.4605 \\ 1.0372 & 0.0455 & -0.0827 \\ -2.4641 & 1.9209 & 1.5432 \end{bmatrix} \end{matrix} \qquad \textbf{(A-37)}$$

Table A-10. Condition Numbers for Composition SVD of case [2MP/C6, Tol, mX]

System Size	Condition Number
3 x 3	130.7
2 x 2	15.4

Matrices for Composition Control

$$\Sigma = \begin{bmatrix} 312.6 & 0 & 0 & 0 \\ 0 & 20.3 & 0 & 0 \\ 0 & 0 & 2.4 & 0 \end{bmatrix} \quad \textbf{(A-38)}$$

$$V = \begin{array}{c} \begin{matrix} \textit{Steam} & \textit{Side Reflux} & \textit{Wall Split} & \textit{Reflux} \end{matrix} \\ \begin{bmatrix} -0.9338 & 0.0990 & 0.0139 & 0.3436 \\ -0.0998 & 0.9536 & 0.2840 & -0.0080 \\ 0.0259 & -0.2841 & -0.9394 & 0.1902 \\ 0.3427 & 0.0135 & 0.1915 & 0.9196 \end{bmatrix} \end{array} \quad \textbf{(A-39)}$$

$$U = \begin{bmatrix} 0.5041 & -0.8621 & 0.0523 \\ -0.4003 & -0.1796 & 0.8986 \\ 0.7653 & 0.4739 & 0.4357 \end{bmatrix} \begin{matrix} X_{S,\,C6} \\ X_{S,\,mX} \\ X_{B,\,Tol} \end{matrix} \quad \textbf{(A-40)}$$

CASE [2MP/C6, TOL, MX] – UPDATED MODEL

Steady State Considerations

Table A-11. Comparison of two models for [2MP/C6, Tol, mX]

Variable	Original Model	Model matched to Experimental Data
Product Compositions (wt %)		
Feed		
2MP	32.00	32.38
C6	32.00	30.15
Tol	4.00	3.12
mX	32.00	34.35
Distillate		
2MP	49.99	51.13
C6	49.87	47.59
Tol	0.14	1.28
mX	0.00	0.00
Top of Wall		
2MP	10.07	8.13
C6	79.93	34.56
Tol	9.99	56.96
mX	0.01	0.36
Side		
2MP	0.00	0.02
C6	2.00	0.65
Tol	96.00	98.63
mX	1.98	0.70
Bottoms		
2MP	0.00	0.00
C6	0.00	0.00
Tol	0.22	0.94
mX	99.78	99.06
Material Balance Flows (lbm/hr)		
Feed	50.00	49.69
Distillate	32.00	31.47
Side	2.00	1.00
Bottoms	16.00	17.22

Table A-11. continued

Internal Flows			
Overhead Reflux	Flow (lbm/hr)	112.73	81.34
	Temperature (°F)	70	77.70
Prefrac Reflux	Flow (lbm/hr)	110.86	82.22
	Temperature (°F)	175	178.58
Mainfrac Reflux	Flow (lbm/hr)	80.93	76.46
	Temperature (°F)	175	175.25
Side Reflux	Flow (lbm/hr)	128.79	170.23
	Temperature (°F)	220	233.24
Reboiler Duty (BTU/hr)		68510	78130
Ambient Temperature (°F)		80	82.87
Feed Temperature (°F)		195	156.45

Matrices for Temperature Control

$$K = \begin{array}{c} \left.\frac{\delta T_i}{\delta L}\right|_{\beta_L,S,V} \quad \left.\frac{\delta T_i}{\delta \beta_L}\right|_{L,S,V} \quad \left.\frac{\delta T_i}{\delta S}\right|_{L,\beta_L,V} \quad \left.\frac{\delta T_i}{\delta V}\right|_{L,\beta_L,S} \\ \begin{bmatrix} 75.000 & 0.000 & 0.000 & -20.000 \\ 140.000 & 0.000 & 0.000 & -35.000 \\ 250.000 & 0.000 & 0.000 & -55.000 \\ 420.000 & 0.000 & 0.000 & -100.000 \\ 660.000 & 0.000 & 0.000 & -150.000 \\ 855.000 & 0.000 & -5.000 & -195.000 \\ 625.000 & 0.000 & 10.000 & -140.000 \\ 350.000 & 0.000 & 15.000 & -75.000 \\ 170.000 & 0.000 & 10.000 & -40.000 \\ 90.000 & 0.000 & 10.000 & -15.000 \\ 60.000 & 0.000 & 10.000 & -10.000 \\ 55.000 & 5.000 & 15.000 & -5.000 \\ 60.000 & 5.000 & 10.000 & -10.000 \\ 70.000 & 5.000 & 10.000 & -15.000 \\ 105.000 & 5.000 & 5.000 & -25.000 \\ 160.000 & 5.000 & 5.000 & -40.000 \\ 255.000 & 10.000 & 0.000 & -60.000 \\ 405.000 & 20.000 & 0.000 & -100.000 \\ 1190.000 & 0.000 & -25.000 & -270.000 \\ 1175.000 & 0.02 & -35.000 & -265.000 \\ 815.000 & 0.000 & -30.000 & -185.000 \\ 440.000 & 0.000 & -15.000 & -100.000 \\ 210.000 & 0.000 & -5.000 & -45.000 \\ 95.000 & 0.000 & 0.000 & -20.000 \\ 50.000 & 0.000 & 0.000 & -10.000 \\ 45.000 & 0.000 & 0.000 & -10.000 \\ 65.000 & 5.000 & 0.000 & -15.000 \\ 110.000 & 5.000 & -5.000 & -25.000 \\ 200.000 & 10.000 & 0.000 & -45.000 \\ 355.000 & 15.000 & 0.000 & -85.000 \\ 625.000 & 25.000 & 0.000 & -145.000 \\ 965.000 & 40.000 & -5.000 & -230.000 \\ 1310.000 & 55.000 & -5.000 & -315.000 \\ 1370.000 & 55.000 & -5.000 & -330.000 \\ 970.000 & 40.000 & -5.000 & -235.000 \\ 485.000 & 20.000 & -5.000 & -115.000 \end{bmatrix} \end{array} \begin{array}{l} T1 \\ T2 \\ T3 \\ T4 \\ T5 \\ T6 \\ TA11 \\ TA12 \\ TA13 \\ TA14 \\ TA15 \\ TA16 \\ TA21 \\ TA22 \\ TA23 \\ TA24 \\ TA25 \\ TA26 \\ TB11 \\ TB12 \\ TB13 \\ TB14 \\ TB15 \\ TB16 \\ TB21 \\ TB22 \\ TB23 \\ TB24 \\ TB25 \\ TB26 \\ T31 \\ T32 \\ T33 \\ T34 \\ T35 \\ T36 \end{array} \quad \textbf{(A-41)}$$

$$\Sigma = \begin{bmatrix} 3594.8 & 0 & 0 & 0 \\ 0 & 81.2 & 0 & 0 \\ 0 & 0 & 49 & 0 \\ 0 & 0 & 0 & 14.7 \end{bmatrix} \quad \textbf{(A-42)}$$

$$V = \begin{array}{c} \begin{matrix} \textit{Steam} & \textit{Side} & \textit{Wall Split} & \textit{Reflux} \end{matrix} \\ \begin{bmatrix} -0.9735 & 0.0711 & -0.0765 & -0.2033 \\ -0.0216 & -0.8598 & 0.3800 & -0.3405 \\ 0.0091 & -0.4447 & -0.8856 & 0.1339 \\ 0.2274 & 0.2408 & -0.2559 & -0.9082 \end{bmatrix} \end{array} \quad \textbf{(A-43)}$$

$$
U = \begin{bmatrix}
-0.0216 & 0.0064 & -0.0127 & 0.1982 & 1 \\
-0.0401 & 0.0189 & -0.0359 & 0.2258 & 2 \\
-0.0712 & 0.0559 & -0.1032 & -0.0603 & 3 \\
-0.1201 & 0.0714 & -0.1337 & 0.3684 & 4 \\
-0.1882 & 0.1334 & -0.2474 & 0.1374 & 5 \\
-0.2439 & 0.1982 & -0.2266 & 0.1745 & 6 \\
-0.1781 & 0.0777 & -0.4255 & 0.0948 & A11 \\
-0.0995 & 0.0021 & -0.4258 & -0.0713 & A12 \\
-0.0485 & -0.0244 & -0.2372 & 0.2108 & A13 \\
-0.0253 & -0.0204 & -0.2428 & -0.2272 & A14 \\
-0.0169 & -0.0318 & -0.2221 & -0.1211 & A15 \\
-0.0152 & -0.1017 & -0.2920 & -0.4312 & A16 \\
-0.0169 & -0.0848 & -0.1833 & -0.2370 & A21 \\
-0.0199 & -0.0908 & -0.1729 & -0.0663 & A22 \\
-0.0300 & -0.0624 & -0.0850 & 0.0218 & A23 \\
-0.0459 & -0.0587 & -0.0925 & 0.1878 & A24 \\
-0.0729 & -0.0604 & -0.0074 & -0.0522 & A25 \\
-0.1161 & -0.1534 & 0.0448 & 0.1125 & A26 \\
-0.3394 & 0.3788 & 0.0032 & -0.0083 & B11 \\
-0.3351 & 0.4352 & 0.1812 & -0.2009 & B12 \\
-0.2325 & 0.3297 & 0.2353 & -0.1179 & B13 \\
-0.1255 & 0.1711 & 0.1060 & -0.0452 & B14 \\
-0.0597 & 0.0779 & -0.0026 & -0.1704 & B15 \\
-0.0270 & 0.0239 & -0.0439 & -0.0786 & B16 \\
-0.0142 & 0.0142 & -0.0259 & -0.0739 & B21 \\
-0.0128 & 0.0098 & -0.0181 & -0.0047 & B22 \\
-0.0186 & -0.0405 & 0.0156 & -0.0883 & B23 \\
-0.0314 & -0.0033 & 0.0878 & -0.1385 & B24 \\
-0.0571 & -0.0641 & 0.0002 & -0.2182 & B25 \\
-0.1016 & -0.0998 & 0.0058 & -0.0068 & B26 \\
-0.1786 & -0.1471 & -0.0250 & -0.2666 & 31 \\
-0.2761 & -0.2326 & 0.0945 & -0.1114 & 32 \\
-0.3750 & -0.3412 & 0.1159 & 0.0203 & 33 \\
-0.3922 & -0.3331 & 0.1005 & 0.1170 & 34 \\
-0.2778 & -0.2431 & 0.1128 & 0.1285 & 35 \\
-0.1388 & -0.1004 & 0.0885 & -0.1131 & 36
\end{bmatrix}
\qquad \textbf{(A-44)}
$$

Appendix B: EXPERIMENTAL EQUIPMENT, PROCEDURES, AND RESULTS

EQUIPMENT

Equipment Dimensions

Table B-1. Tank dimensions

Vessel	Description	Diameter (in)	Height (in)	Total Volume (gal)
V-601	Toluene Feed Tank	30	36	110
V-603	Reflux Drum	8	42	9
V-630	Top of Wall Tank	14	34	23
V-640	Side Product Tank	14	34	23

Table B-2. Reboiler dimensions

Weir Height	6.25 inches
Product Side Length	13.25 inches
Diameter	10 inches
Tube Length	83 inches
Number of Tubes	6 or 8
Tube Outer Diameter	0.75 inches
U-Tube Diameter	6 inches

Equipment Drawings

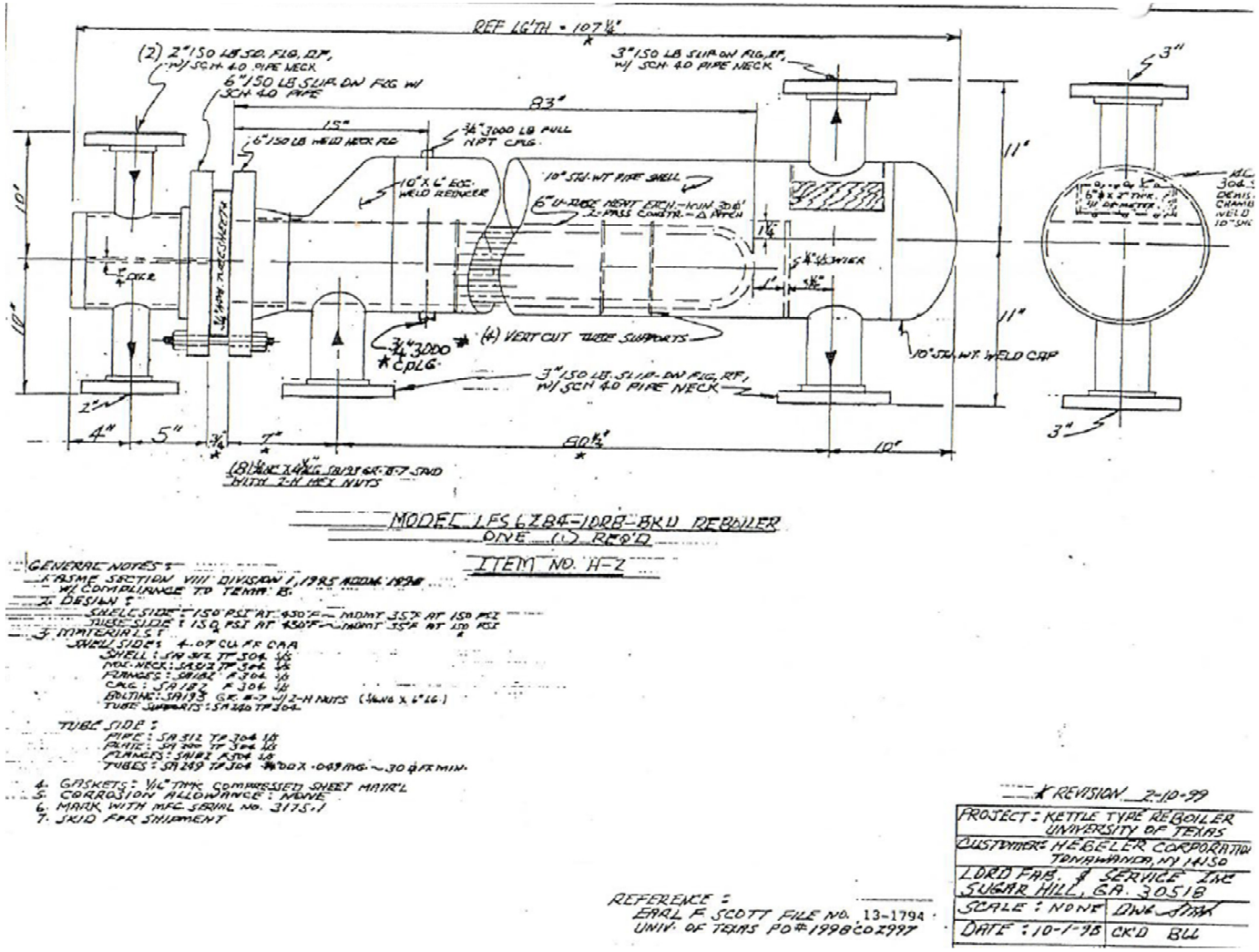

Figure B-1 – Reboiler drawing

Equipment Pictures

Figure B-2 – Total trapout tray placed at the top of the wall

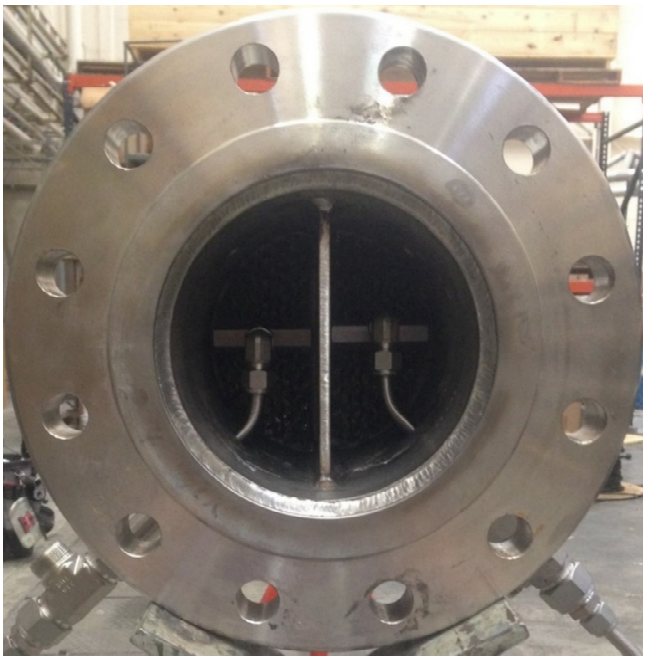

Figure B-3 – Top of the wall section showing the welded wall and the distributors for prefrac and mainfrac reflux flows

Piping and Instrumentation Diagram

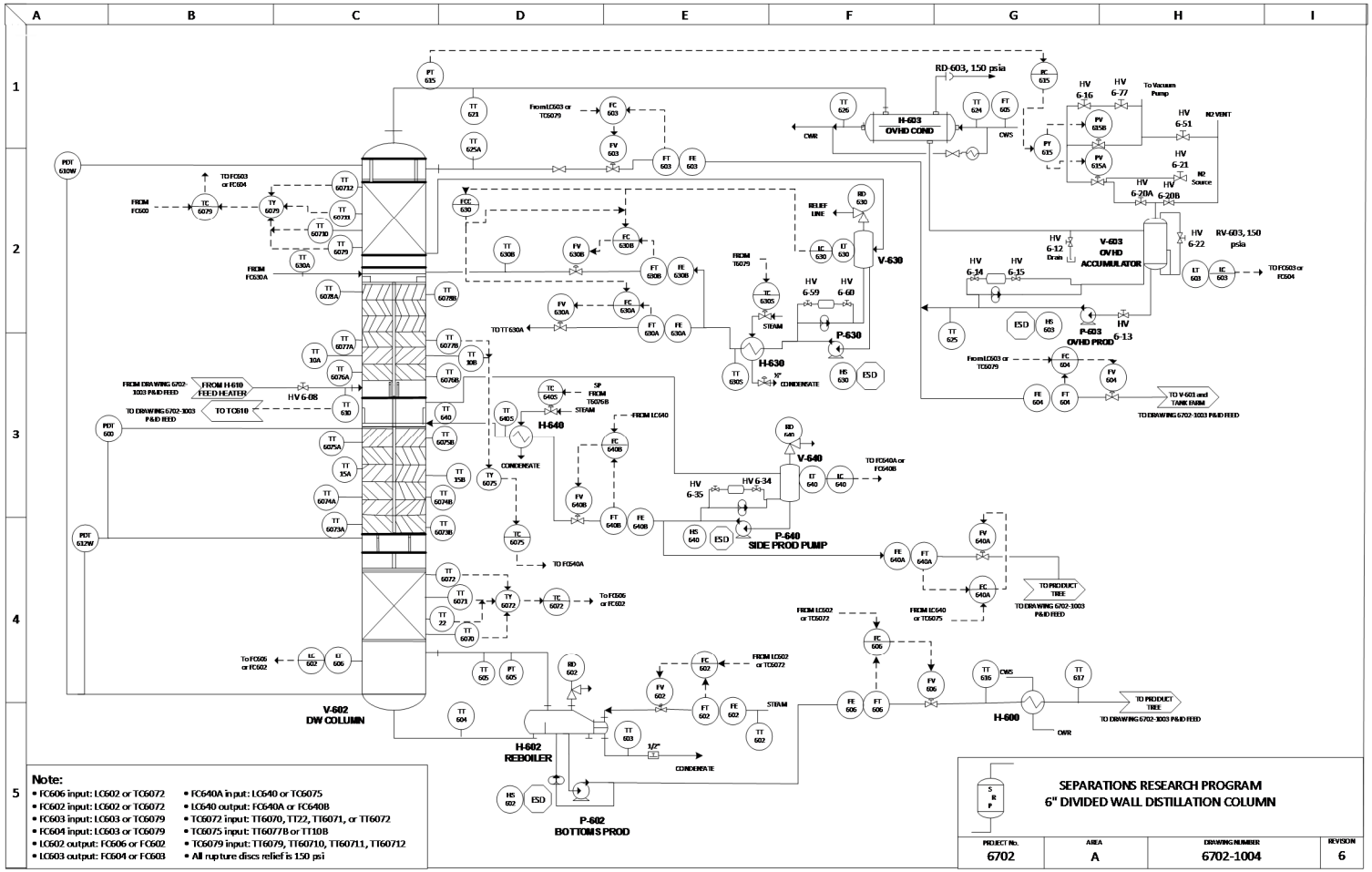

Figure B-4 – Overall column piping and instrumentation diagram

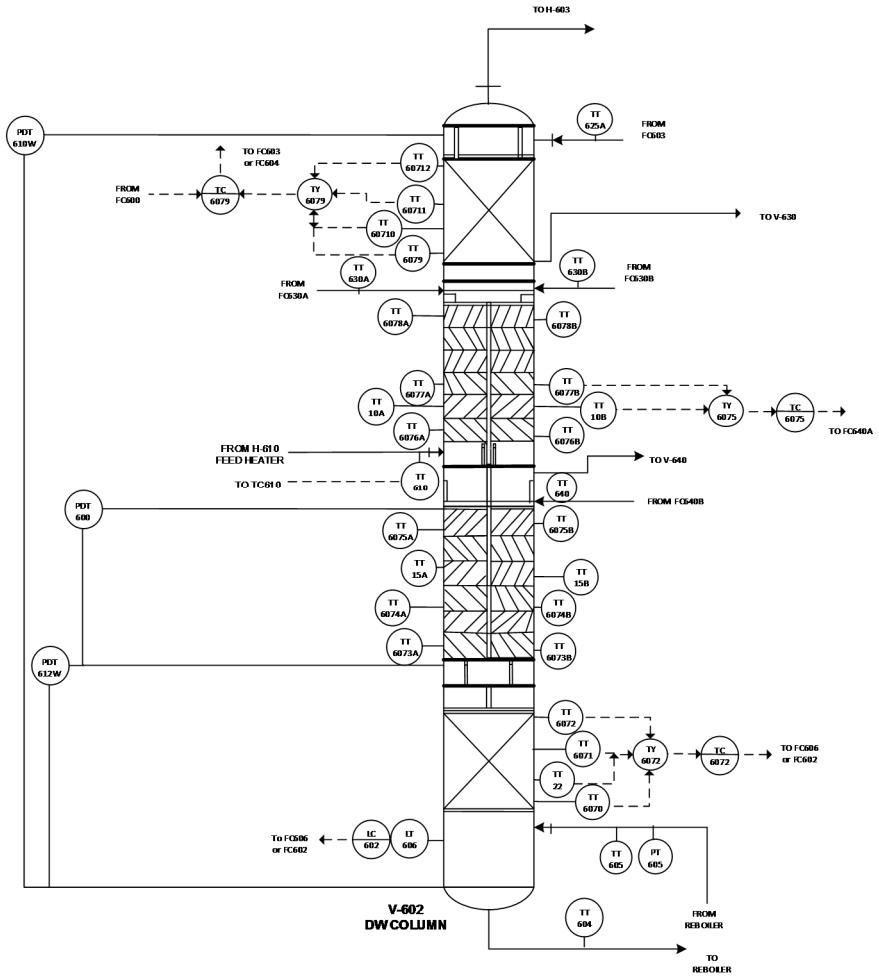

Figure B-5 – Column piping and instrumentation diagram

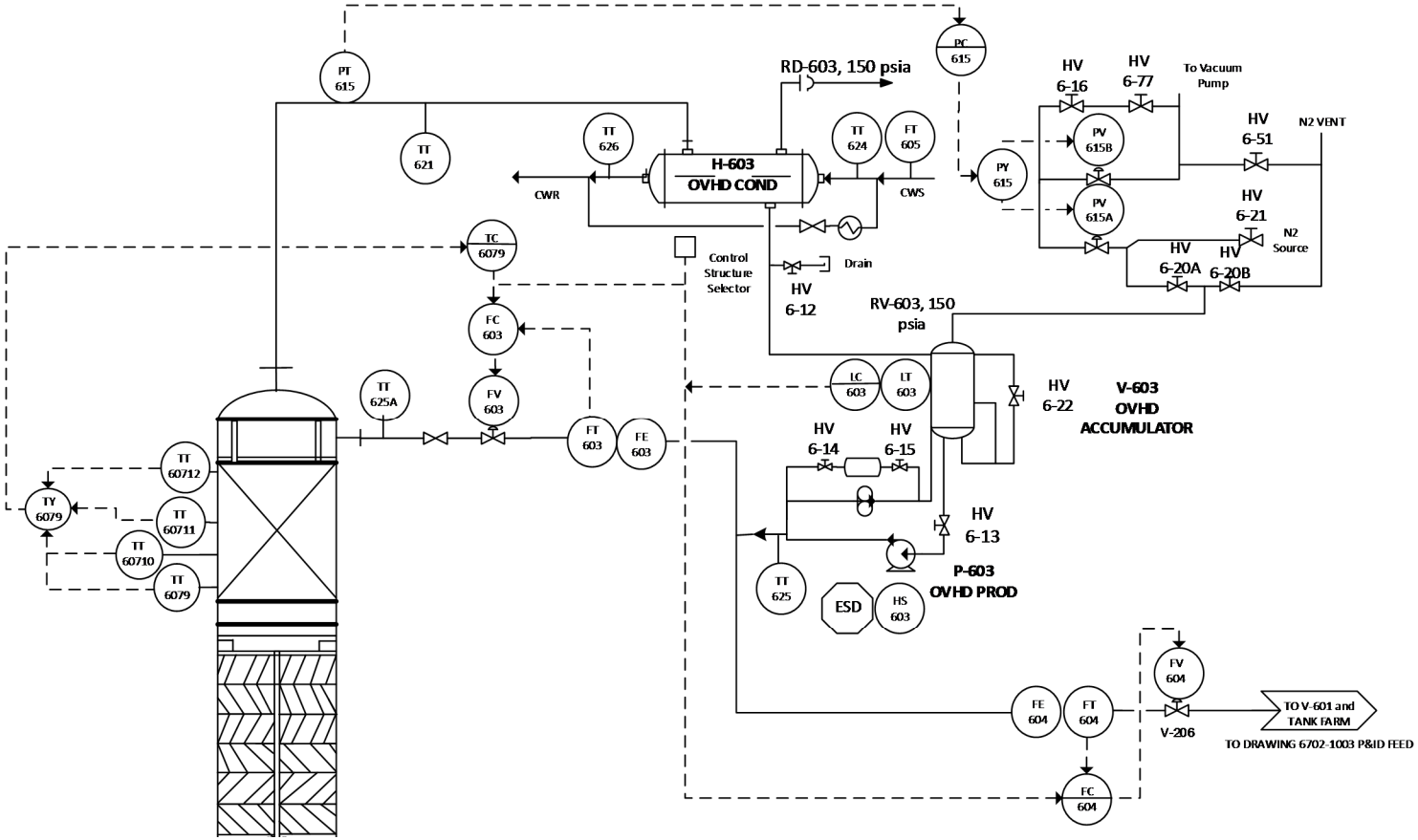

Figure B-6 – Overhead piping and instrumentation diagram

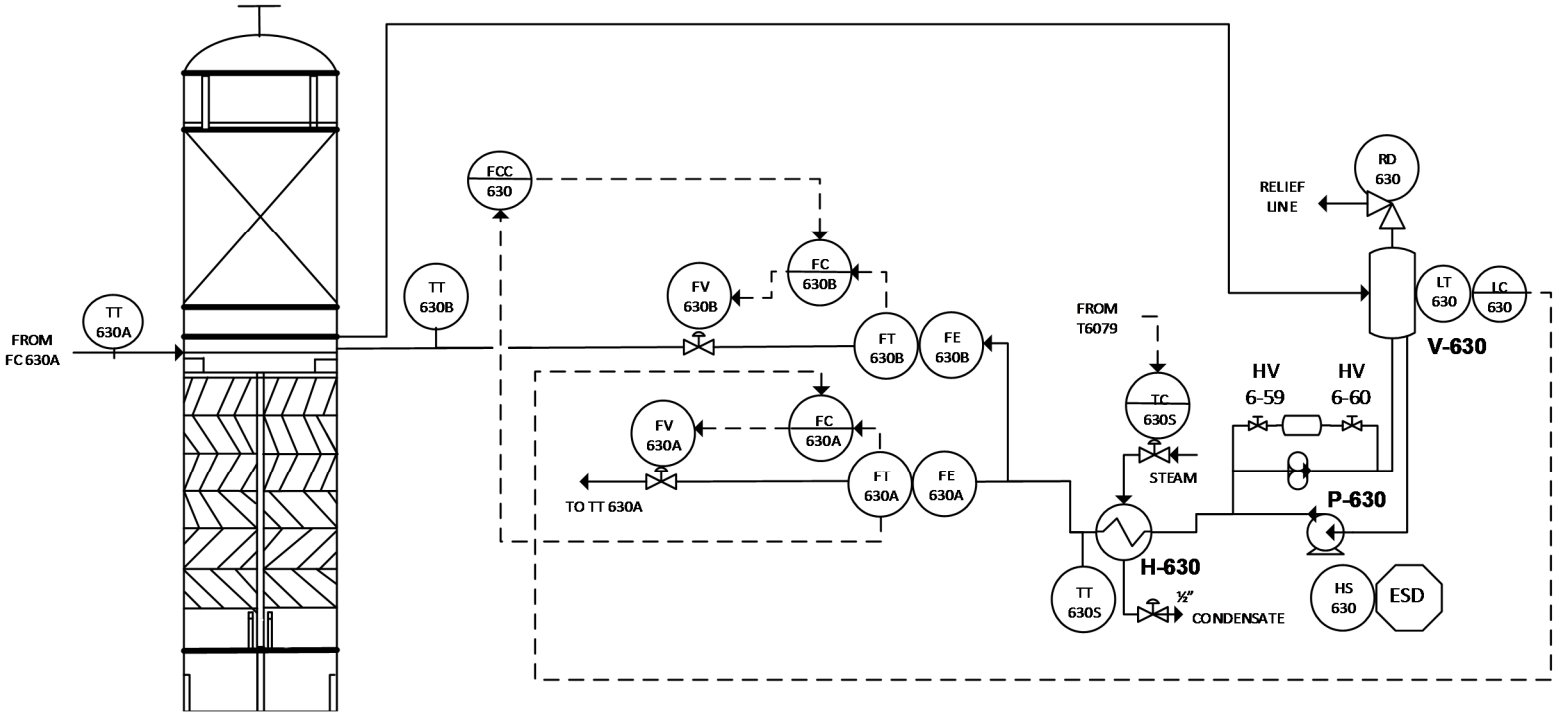

Figure B-7 – Top of wall piping and instrumentation diagram

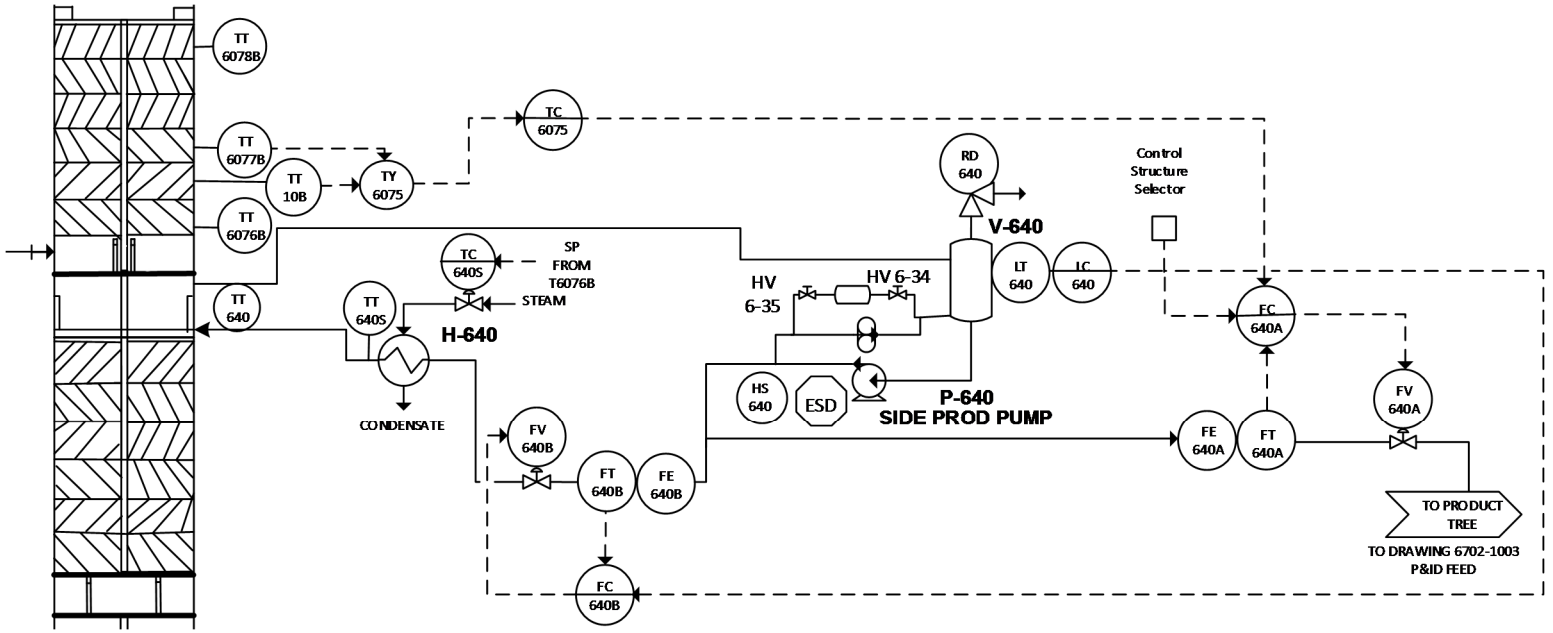

Figure B-8 –Side product piping and instrumentation diagram

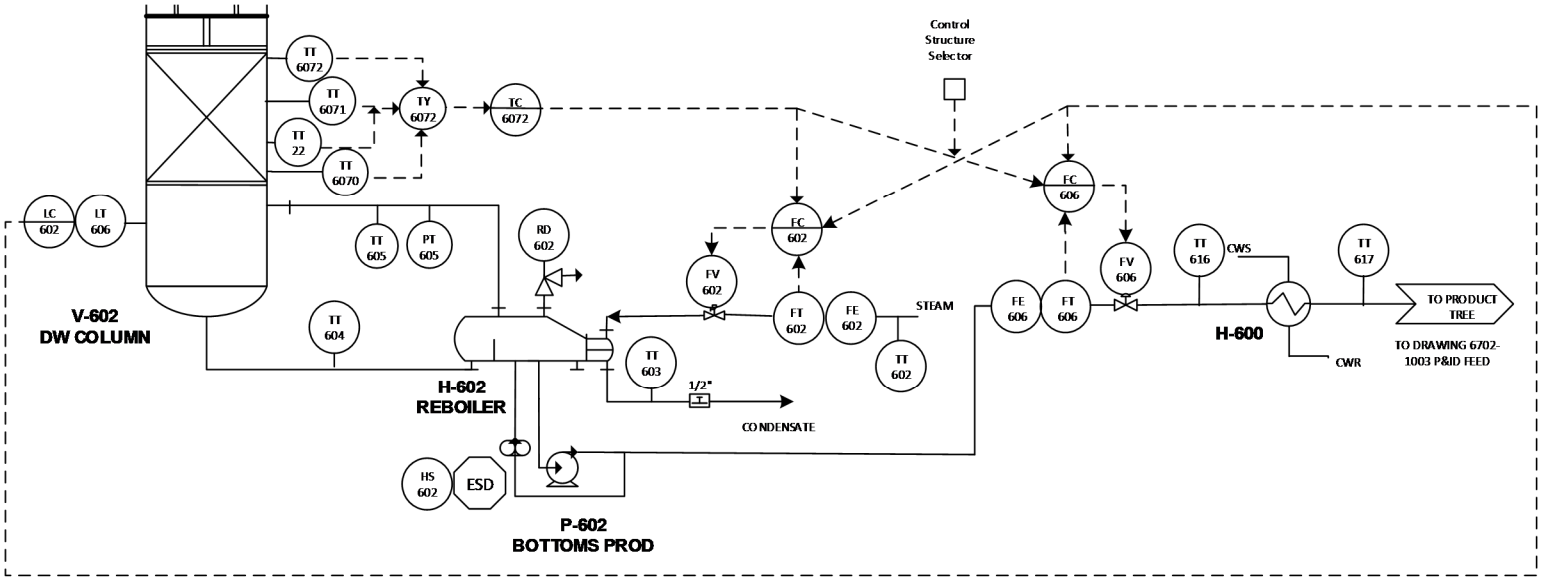

Figure B-9 –Column base piping and instrumentation diagram

Operator Screens

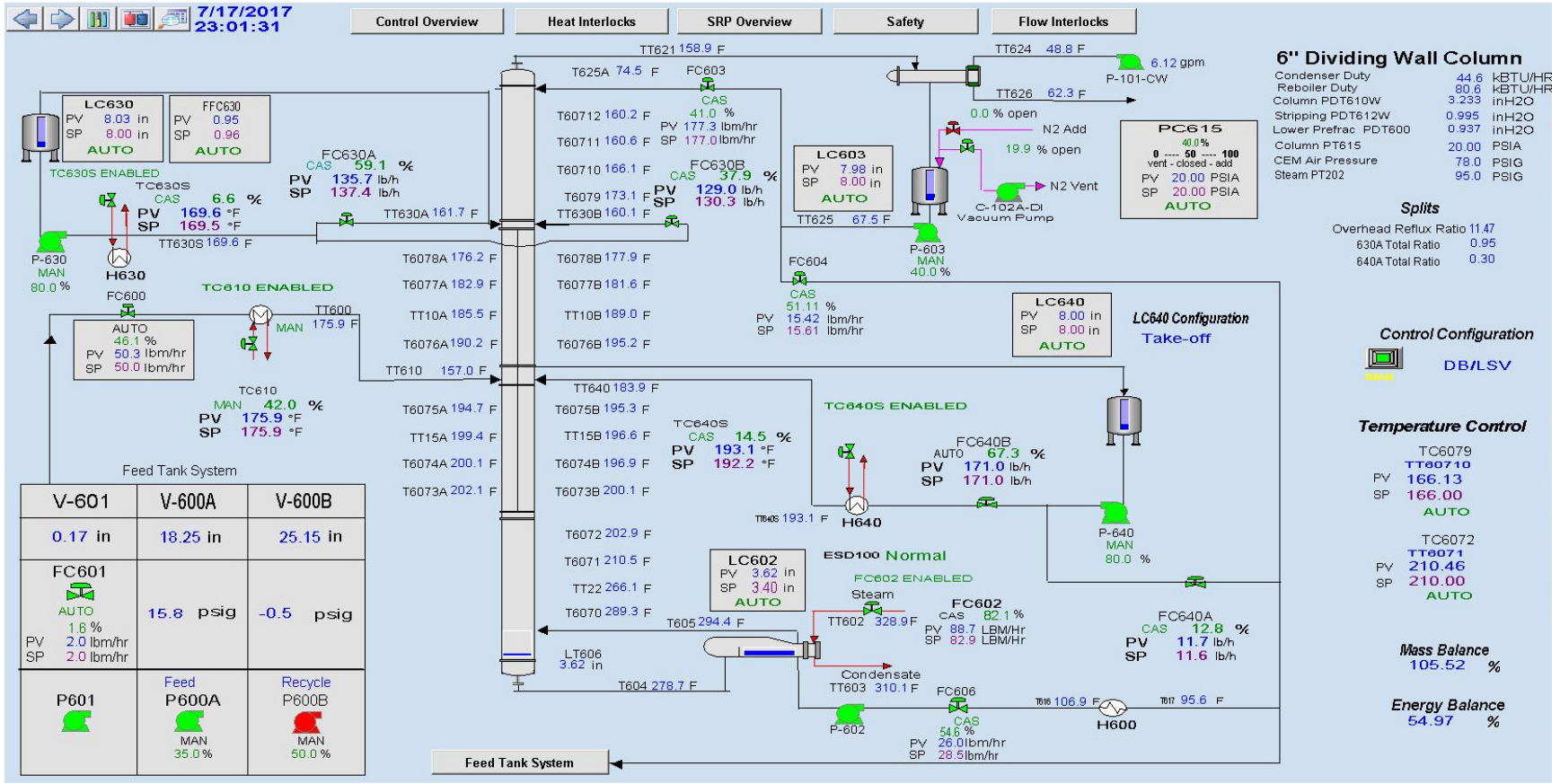

Figure B-10 – Operator screen - Column

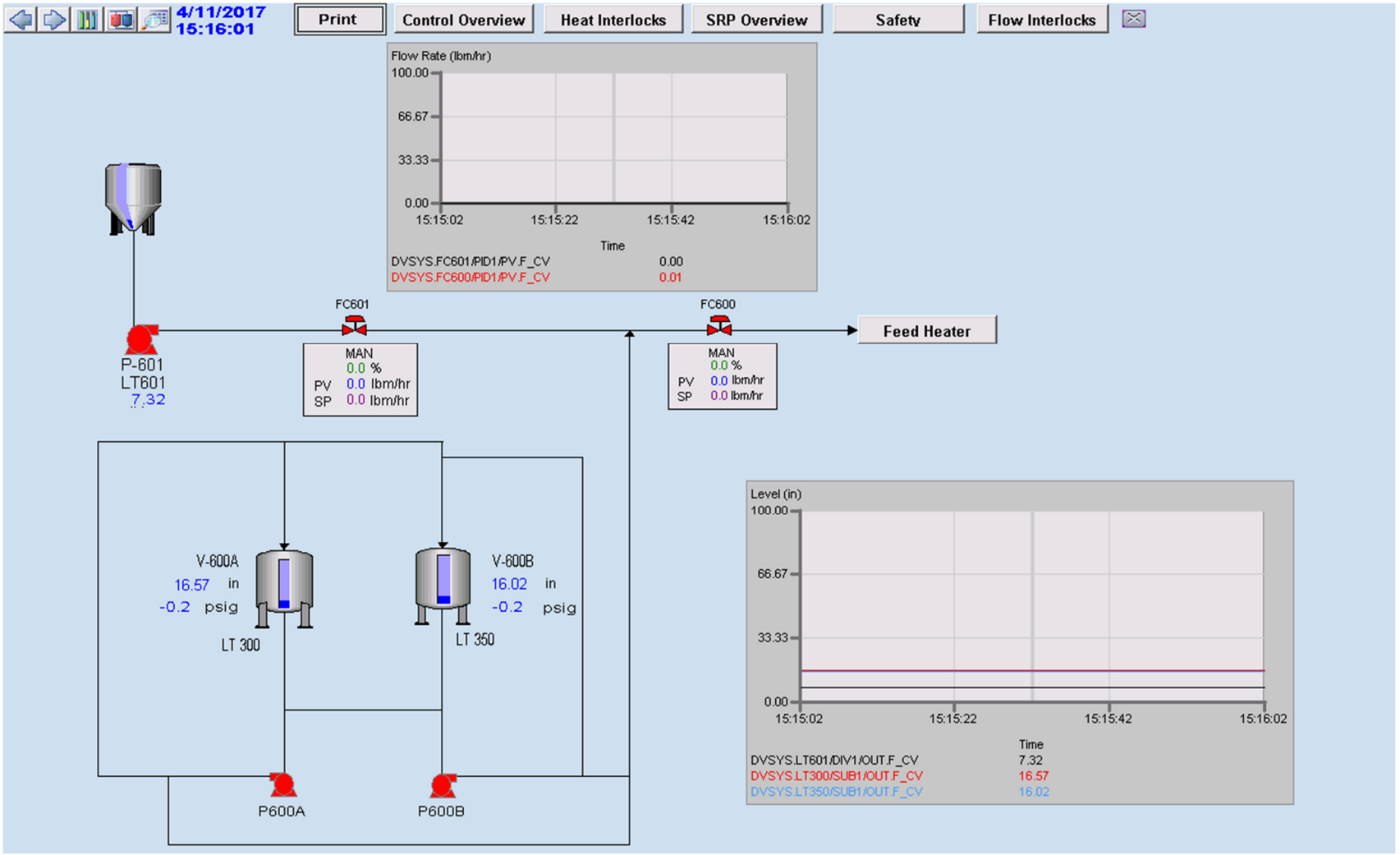

Figure B-11 – Operator screen - Feed

Controller Tuning Parameters

Table B-3. Controller tunings used in DeltaV™

Section	Loop	Parameter	Case [2MP, C6, mX]	Case [2MP, C6, Tol/mX]	Case [2MP, C6/Tol, mX]	Case [2MP/C6, Tol, mX]	
						Run 1	Run 2
Feed	FC601	GAIN	N/A	0.5	N/A	0.5	0.5
		RESET	N/A	10	N/A	10	10
	FC600	GAIN	0.6	0.6	0.6	0.6	0.6
		RESET	2.1	2.1	2.1	2.1	2.1
	TC610	GAIN	1	0.2	0.3	N/A	N/A
		RESET	43	300	450	N/A	N/A
Bottoms	LC602	GAIN	1.08	6	6	6	6
		RESET	283.3	1000	1000	1000	1000
	FC602	GAIN	0.4	0.07	0.07	0.07	0.07
		RESET	5	19.4	19.4	19.4	19.4
	FC606	GAIN	1	1	1	1	1
		RESET	3.5	3.5	3.5	3.5	3.5
	TC6072	GAIN	7.7	2	2	3	3
		RESET	295	600	1200**	1200	1200
Side Draw	LC640	GAIN	3	10	10	10	10
		RESET	182.1	900†	900†	900†	900†
	FC640A	GAIN	0.61	0.61	0.61	0.61	0.61
		RESET	2.2	2.2	2.2	2.2	2.2

Table B-3. continued

Side Draw	FC640B	GAIN	0.53	0.53	0.53	0.53	0.53
		RESET	2	2	2	2	2
	TC640S	GAIN	1.21	1.21	1.21	1.21	1.21
		RESET	163	163	163	163	163
	TC6075	Gain	N/A	N/A	N/A	2	2
		Reset	N/A	N/A	N/A	14400	14400
Top of the Wall	LC630	GAIN	14.09	10	10	10	10
		RESET	133	900*	900*	900*	900*
	TC630S	GAIN	1.18	1.18	1.18	1.18	1.18
		RESET	150	150	150	150	150
	FC630B	GAIN	0.2	0.2	0.2	0.2	0.2
		RESET	2	2	2	2	2
	FC630A	GAIN	0.36	0.5	0.5	0.5	0.5
		RESET	2	2	2	2	2
Overhead	PC615	GAIN	36	36	36	60	120
		RESET	336	336	336	900	1800
	FC603	GAIN	0.38	0.38	0.38	0.38	0.38
		RESET	1.8	1.8	1.8	1.8	1.8
	FC604	GAIN	0.4	0.45	0.45	0.45	0.45
		RESET	6.3	1.9	1.9	1.9	1.9
	LC603	GAIN	10	22	22	22	22
		RESET	130	900	900	900	1800
	TC7079	GAIN	7	7	6	6	6
		RESET	360	360	1200	1200	1200

*15 s filter on level PV

† 10 s filter on level PV

** 30s derivative action

GAS CHROMATOGRAPHY

GC Method

Table B-4 lists the boiling points of all components including the dilutent, methanol. Chemical components for a DWC typically have a wider range of boiling points. A large boiling point range complicates determining an inlet temperature and may require several ramps in oven temperature to avoid long analysis times. Choosing a proper inlet temperature ensures that the sample does not expand beyond the volume of the inlet liner. If that happens, then the entirety of the sample will not reach the detector and area counts may be inconsistent. The oven program was chosen such that the initial oven temperature was slightly lower than lowest boiling point. A component's elution time depends on the temperature of the oven as well as the component's affinity for the column. Temperature ramps and hold times were chosen to decrease the time for one analysis while ensuring proper separation between peaks. Note that the conditions listed in

Table B-5 are those that were entered into the GC. A bubble flowmeter was used to check the carrier gas flow in the instrument. Through this process, it was discovered that the split flow indicator on the instrument was different from the actual flow measured. A split ratio of 20:1 was actually closer to 40:1 and a flow of 1.6 µL/min was closer to 1.0 µL/min through the column.

Table B-4. Component boiling points

Chemical Component	Boiling Point
Methanol	64.5 °C
2-methylpentane	62 °C
Cyclohexane	80.7 °C
Toluene	110 °C
m-Xylene	138 °C

Table B-5. Gas chromatogram conditions

GC Conditions		
Gas Chromatograph	Agilent 6890 with FID	
Column	Rxi-624 Sil MS Column – fused silica, 29M x 0.32 mmID x 1.8µm	
Inject Volume	0.3 µL	
Inlet		
Carrier Gas	Hydrogen	
Heater	120°C	
Pressure	4.16 psi	
Total Flow	38.2 mL/min	
Split Ratio	20:1	
Split Flow	33.6 mL/min	
Column		
Mode	Constant Flow	
H_2 Pressure	4.29 psi	
H_2 Flow	1.6 mL/min	
H_2 Average Velocity	35 cm/s	
Oven Temperature Program		
Oven	Temperature	Hold
Initial	60°C	3.0 minutes
Ramp 1: 20°C/min	100°C	0.5 minutes
Ramp 2: 30°C/min	160°C	1.0 minutes
Total Run Time	8.50 minutes	
Detector (FID)		
Detector Temperature	200°C	
H_2 Flow	40.0 mL/min	
Air Flow	450 mL/min	
N_2 Makeup Flow	40.0 mL/min	

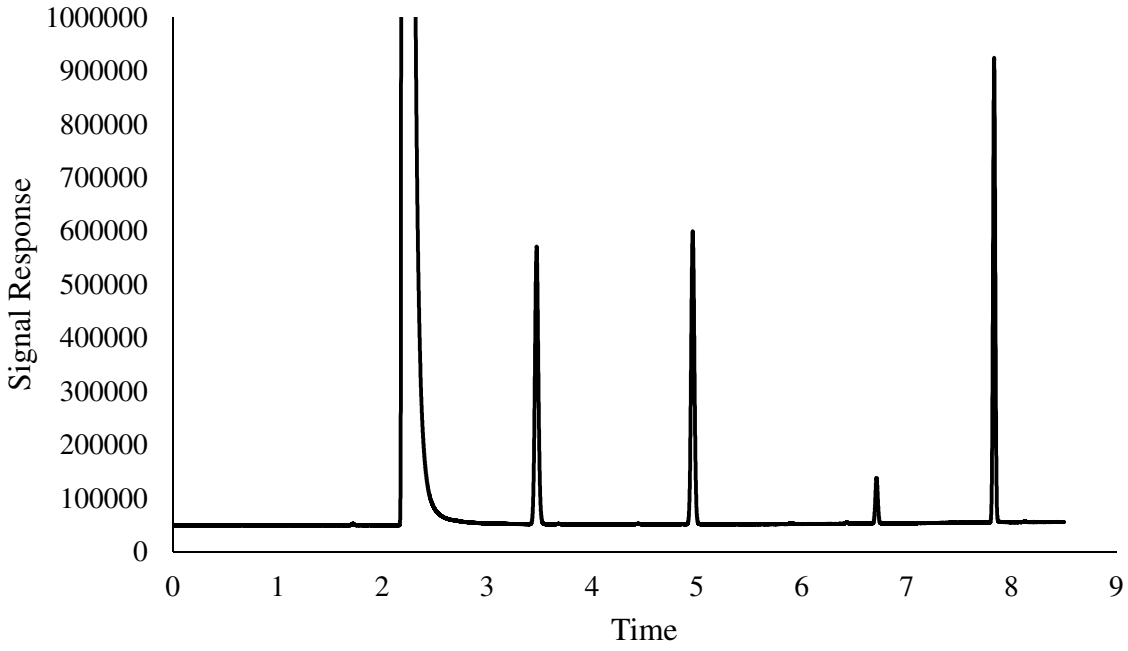

Figure B-12 – Example gas chromatogram from feed sample. Signal response axis was adjusted so that all signals could be seen. Most of the methanol peak has been cut off.

Table B-6. Gas chromatogram elution times

Chemical	Elution Time
Methanol	2.21
2-methylpentane	3.48
Cyclohexane	4.97
Toluene	6.72
m-Xylene	7.84

GC Calibration

The method of relative response factors was used for calibrating the gas chromatogram. Relative response factors are weightings that ensure that all compositions add to 100 percent.[91] Relative response factors could be used for this system because all components were known a priori. The relative response factors were calculated using binary mixtures. One component out of the four, in this case toluene, was chosen to have a relative response factor of 1. The response factors of all other components would therefore be relative to toluene. Binary mixtures using toluene and one other component were created, and samples were injected into and analyzed on the GC multiple times. This was done to ensure reproducibility. The calculated relative response factors were then tested with a four component mixture resembling the process feed. Component

weight percents were calculated as shown in (B-1), where A represents the area counts underneath the peak corresponding to each component.

$$\text{Wt \% 2MP} = \frac{R_{2MP,Tol} \times A_{2MP}}{R_{2MP,Tol} \times A_{2MP} + R_{C6,Tol} \times A_{C6} + R_{Tol,Tol} \times A_{Tol} + R_{mX,Tol} \times A_{2MP}} \quad \textbf{(B-1)}$$

Table B-7. Relative response factors

Chemical	Response Factor
2-methylpentane	0.995
Cyclohexane	0.96
Toluene	1
m-Xylene	1.04

RESULTS

Case [2MP, C6, mX]

The first case conducted on the pilot column was the three component case of 2-methylpentane, cyclohexane, and m-xylene. Though the feed was processed before testing to remove toluene that was originally in the mixture, a residual amount of toluene remained. Most of this toluene was removed as part of the bottoms product. The reported compositions are a result of multiple sample injections on the gas chromatogram.

The control configuration used for this case is shown in Figure 4-3, and the performance of the temperature controllers is shown in Figure B-15 and Figure B-16. Product flow oscillations caused by poor level loop tuning helped lead to the oscillations seen in the temperature controller trends. However, despite these oscillations, the column was able to reach and maintain steady state. As expected from SVD and RGA, the temperature profile was mostly flat through the wall section suggesting a third temperature controller would have little to no impact on the column (Figure B-14).

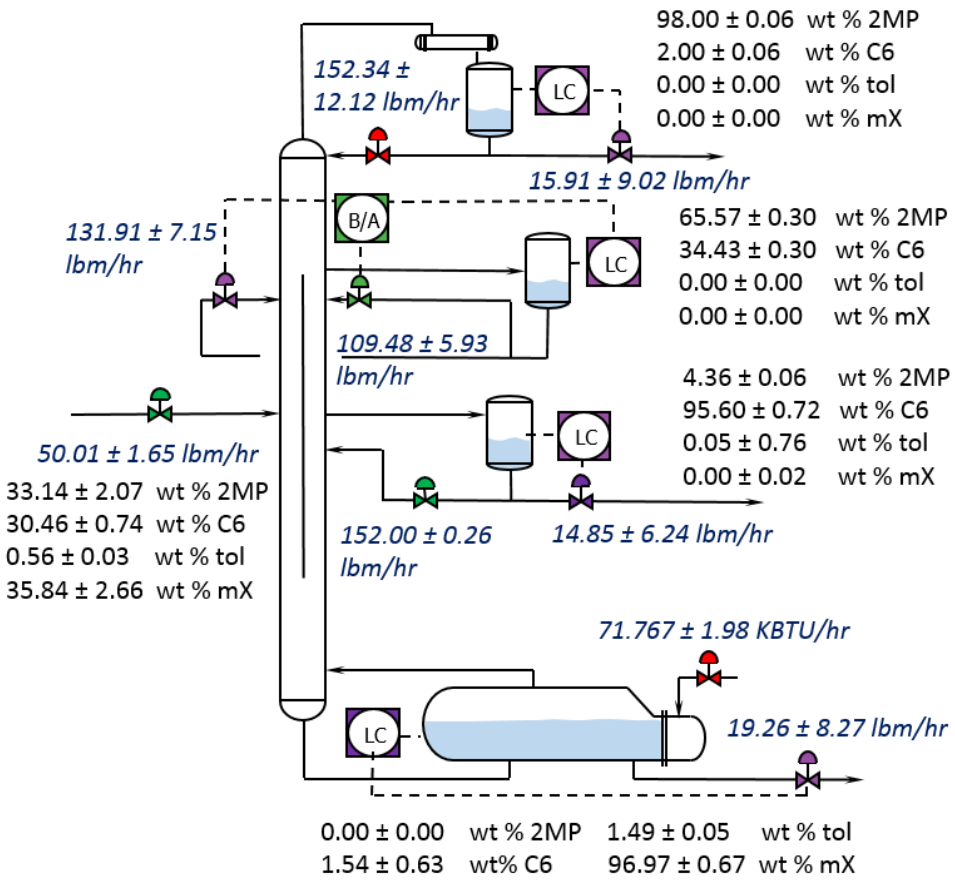

Figure B-13 – Steady state conditions for case [2MP, C6, mX]

Table B-8. Comparison of original model and experimental steady state for [2MP, C6, mX]

Variable	Original Model	Experimental Data	
		Average	Standard Deviation
Product Compositions (wt %)			
Feed			
2MP	32.00	31.14	± 2.07
C6	32.00	30.46	± 0.74
Tol	4.00	0.56	± 0.03
mX	32.00	35.84	± 2.66
Distillate			
2MP	97.50	98.00	± 0.06
C6	2.50	2.00	± 0.06
Tol	0.00	0.00	± 0.00
mX	0.00	0.00	± 0.00

Table B-8. continued

Top of Wall				
	2MP	54.18	65.57	± 0.30
	C6	45.82	34.43	± 0.30
	Tol	0.00	0.00	± 0.00
	mX	0.00	0.00	± 0.00
Side				
	2MP	2.50	4.36	± 0.06
	C6	97.50	95.60	± 0.72
	Tol	0.00	0.05	± 0.76
	mX	0.00	0.00	± 0.02
Bottoms				
	2MP	0.00	0.00	± 0.00
	C6	1.68	1.54	± 0.63
	Tol	0.00	1.49	± 0.05
	mX	98.32	96.97	± 0.67
Material Balance Flows (lbm/hr)				
Feed		50.00	50.01	± 1.65
Distillate		16.66	15.91	± 9.02
Side		16.36	14.85	± 6.24
Bottoms		16.99	19.26	± 8.27
Overhead Reflux	Flow (lbm/hr)	185.74	152.34	± 12.12
	Temperature (°F)	70.00	158.36	± 0.35
Prefrac Reflux	Flow (lbm/hr)	151.41	131.91	± 7.15
	Temperature (°F)	160.00	156.25	± 1.52
Mainfrac Reflux	Flow (lbm/hr)	128.69	109.48	± 5.93
	Temperature (°F)	160.00	153.93	± 1.63
Side Reflux	Flow (lbm/hr)	146.57	152.00	± 0.26
	Temperature (°F)	195.00	182.32	± 1.28
Reboiler Duty (BTU/hr)		69720	71767	± 1980
Ambient Temperature (°F)		80	82.37	± 4.15
Feed Temperature (°F)		195	167.25	± 5.10

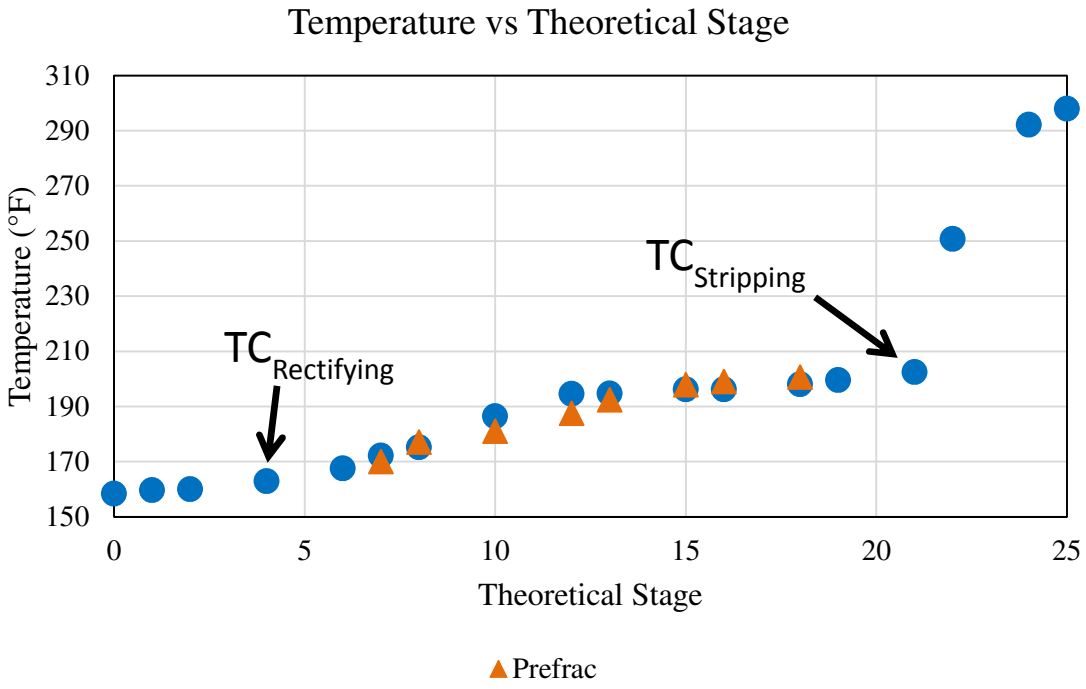

Figure B-14 – Temperature profile for case [2MP, C6, mX]

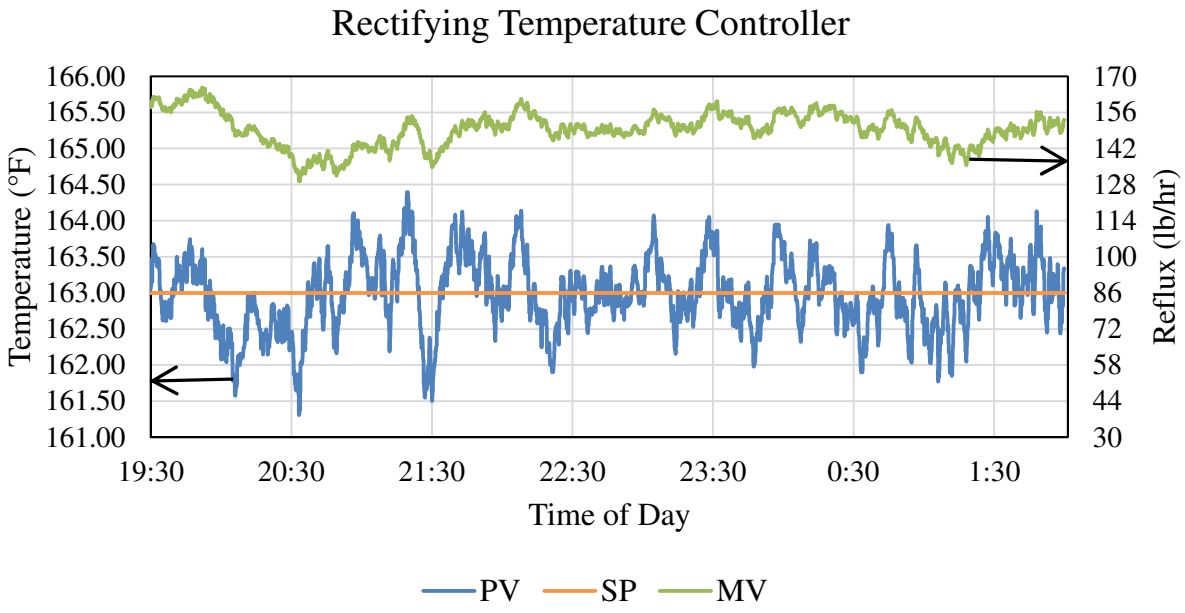

Figure B-15 – Rectifying temperature controller for case [2MP, C6, mX]

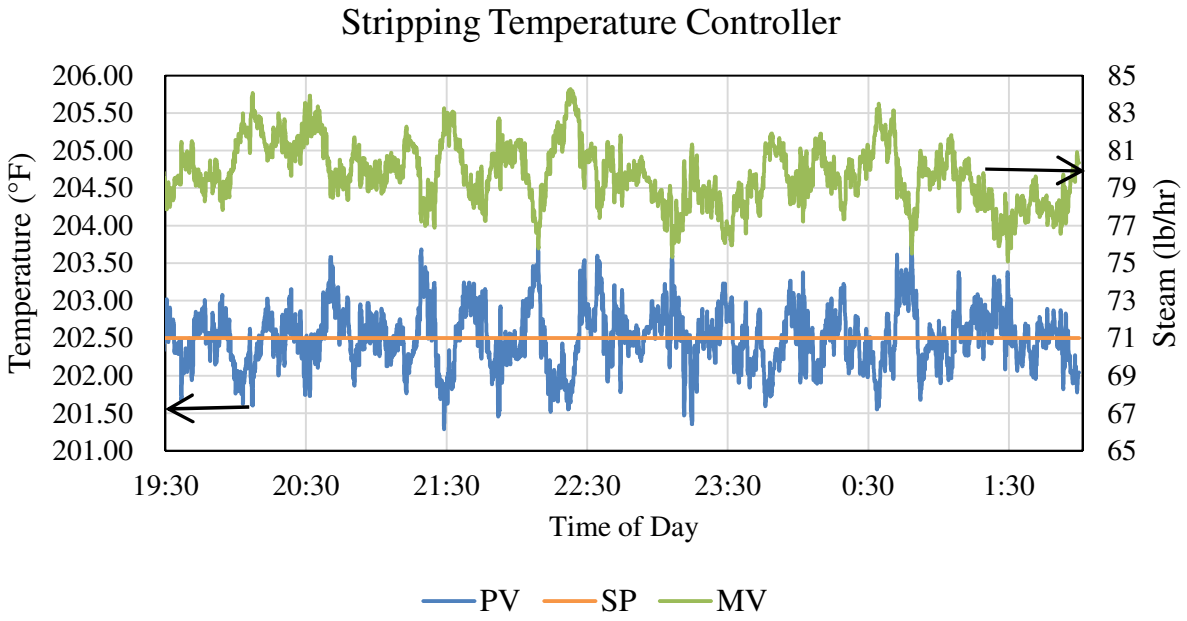

Figure B-16 – Stripping temperature controller for case [2MP, C6, mX]

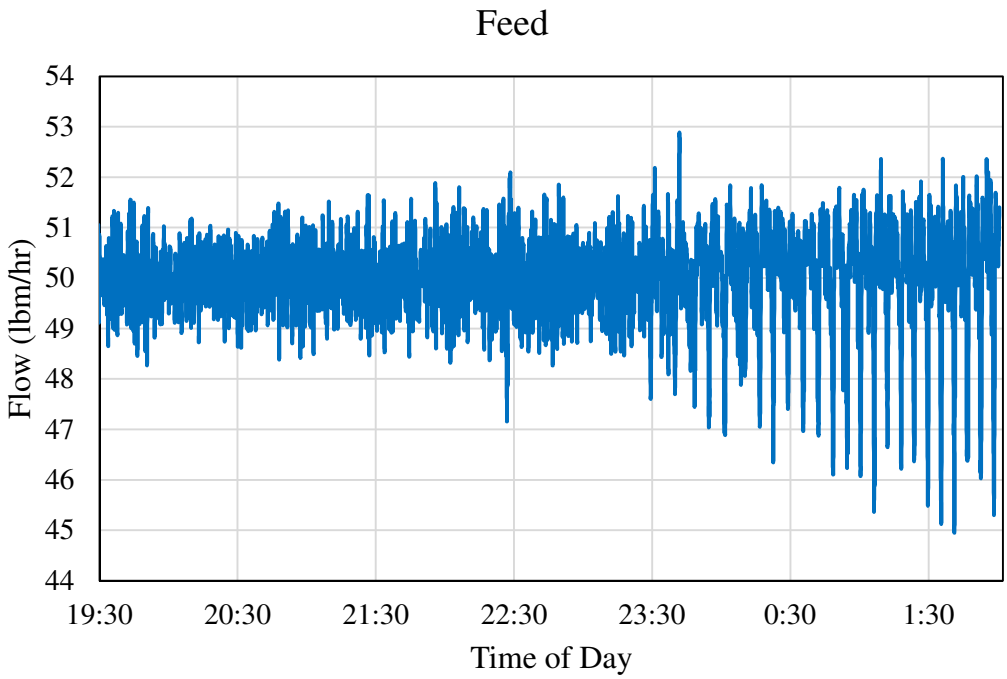

Figure B-17 – Feed flow for case [2MP, C6, mX]

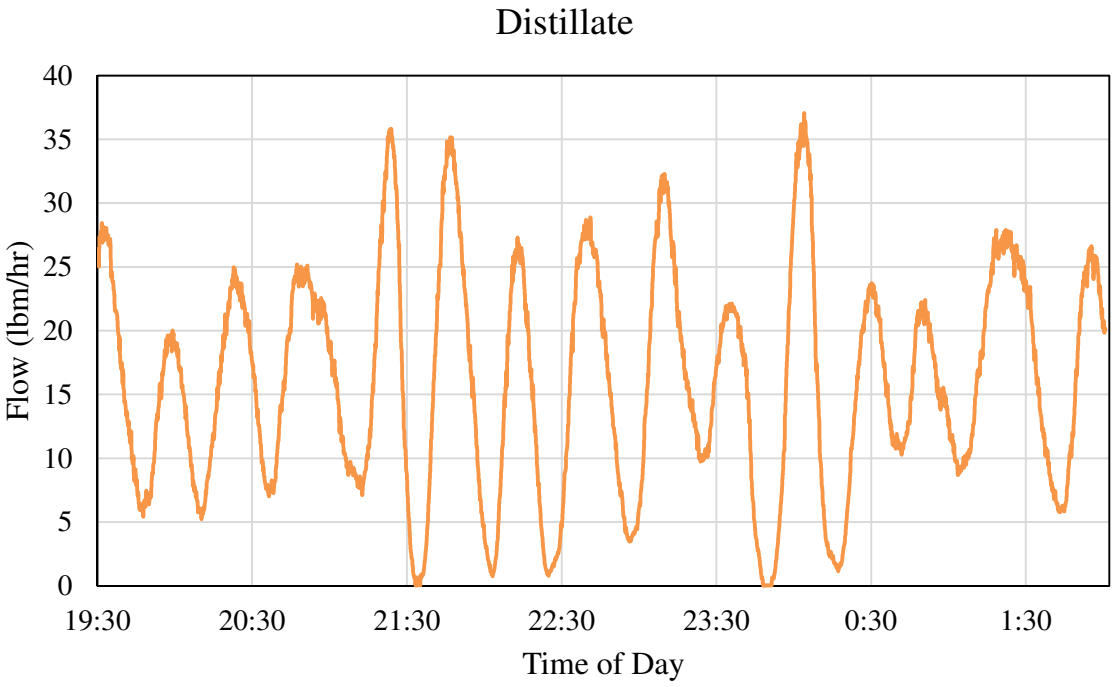

Figure B-18 – Distillate controlling reflux drum level for case [2MP, C6, mX]

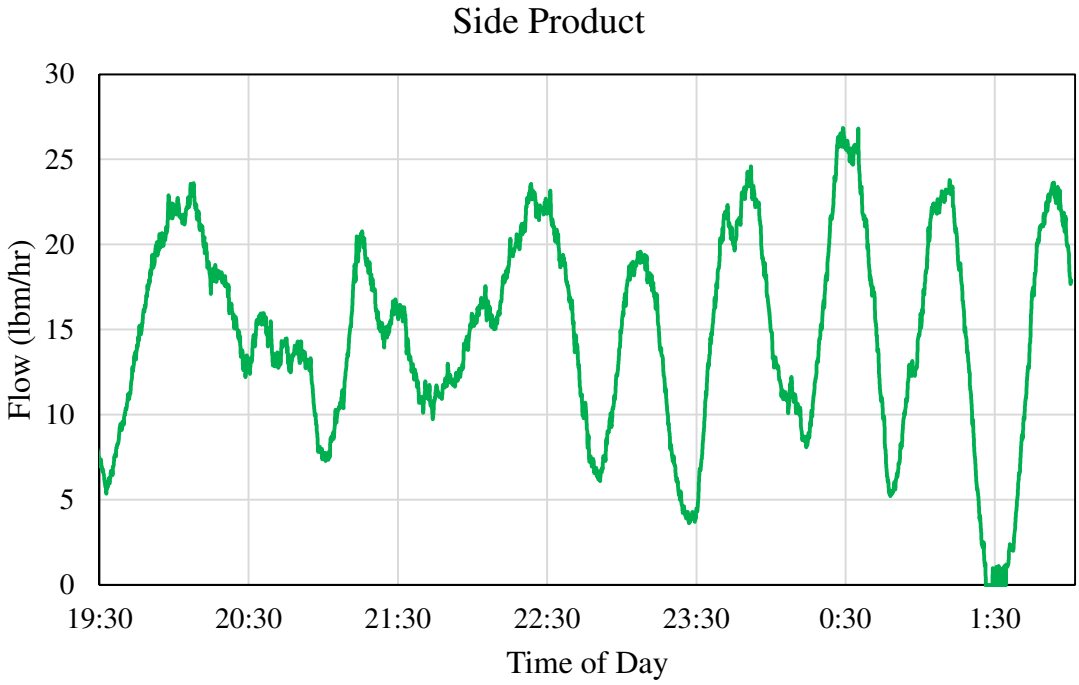

Figure B-19 – Side product flow controlling side tank level for case [2MP, C6, mX]

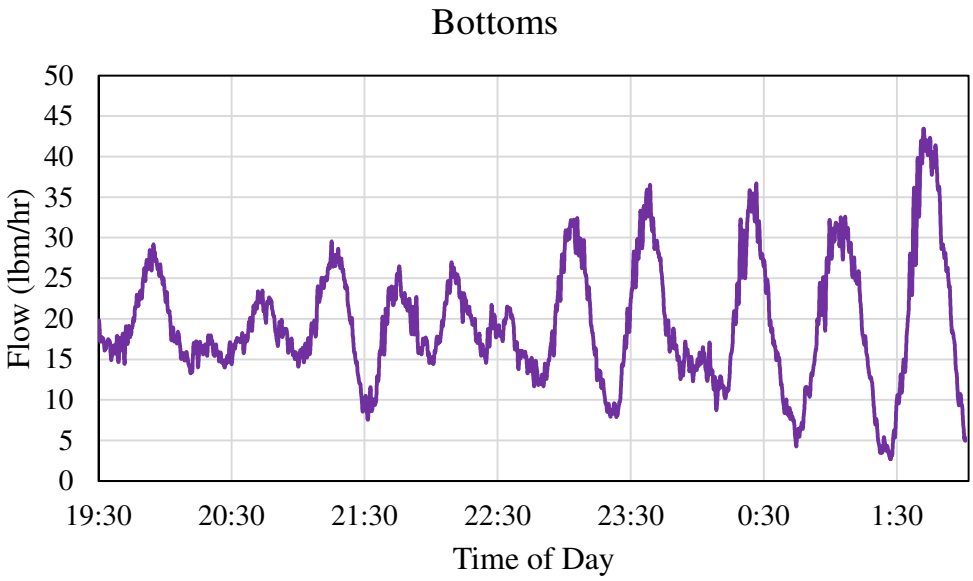

Figure B-20 – Bottoms flow controlling column level for case [2MP, C6, mX]

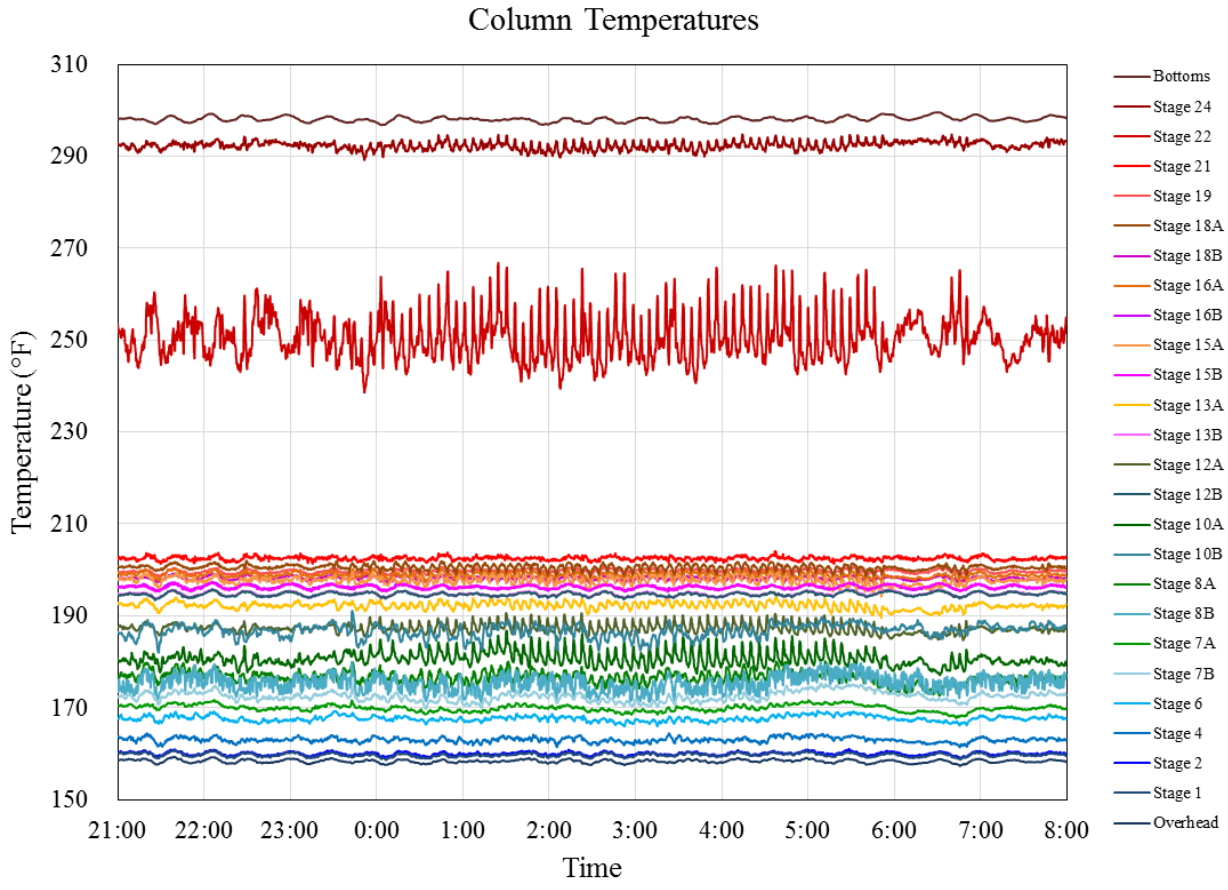

Figure B-21 – Column temperatures for case [2MP, C6, mX]

Transition from Case [2MP, C6, mX] to Case [2MP, C6, Tol/mX]

To operate the four component cases, more toluene needed to be added to the feed. However, before doing so, the setpoints of the wall ratio, rectifying temperature controller, stripping temperature controller, and the side reflux were ramped in DeltaV™ over an hour to their steady state values for the desired four component case (Table B-9). The steady state values were obtained from the dynamic simulation, but the stripping temperature setpoint was later decreased after sample analysis found too much toluene in the sidedraw.

Table B-9. Transition from case [2MP, C6, mX] to case [2MP, C6, tol/mX]

Loop	Initial Value	Final Value	Ramp
Wall Split	0.81	0.96	0.00004167/s
Rectifying Temperature	163°F	166°F	0.000833°F/s
Stripping Temperature	206°F	225°F	0.005278°F/s
Side Reflux	142 lbm/hr	171 lbm/hr	0.00806 lbm/hr/s

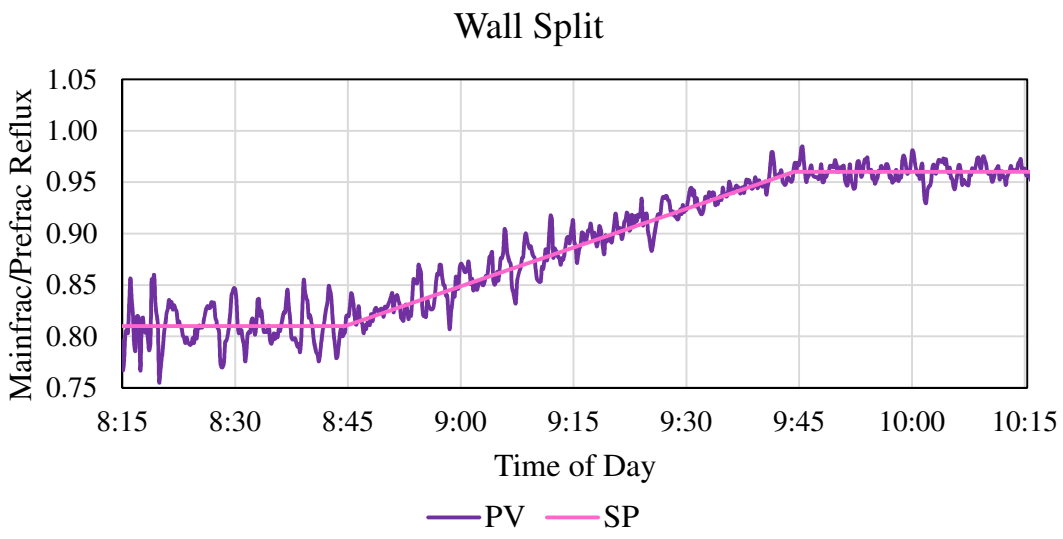

Figure B-22 – Wall split ramp from case [2MP, C6, mX] to case [2MP, C6, Tol/mX]

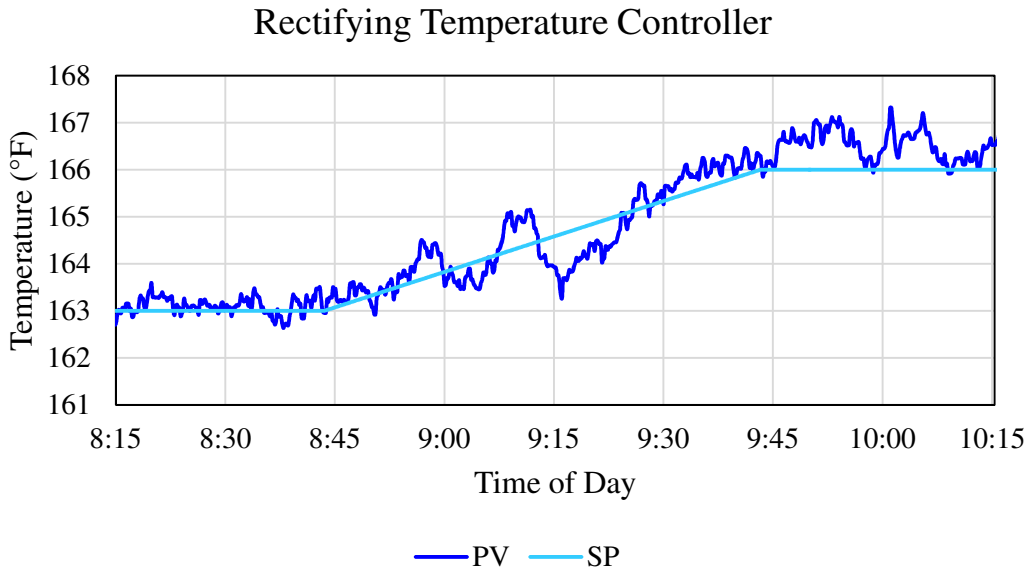

Figure B-23 – Rectifying temperature controller ramp from case [2MP, C6, mX] to case [2MP, C6, Tol/mX]

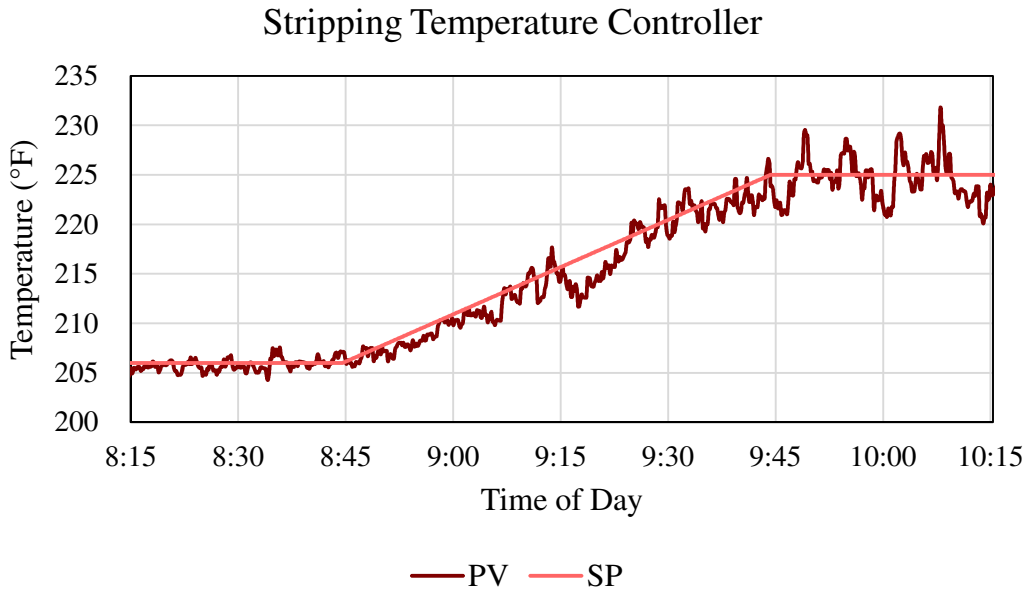

Figure B-24 – Stripping temperature controller ramp from case [2MP, C6, mX] to case [2MP, C6, Tol/mX]

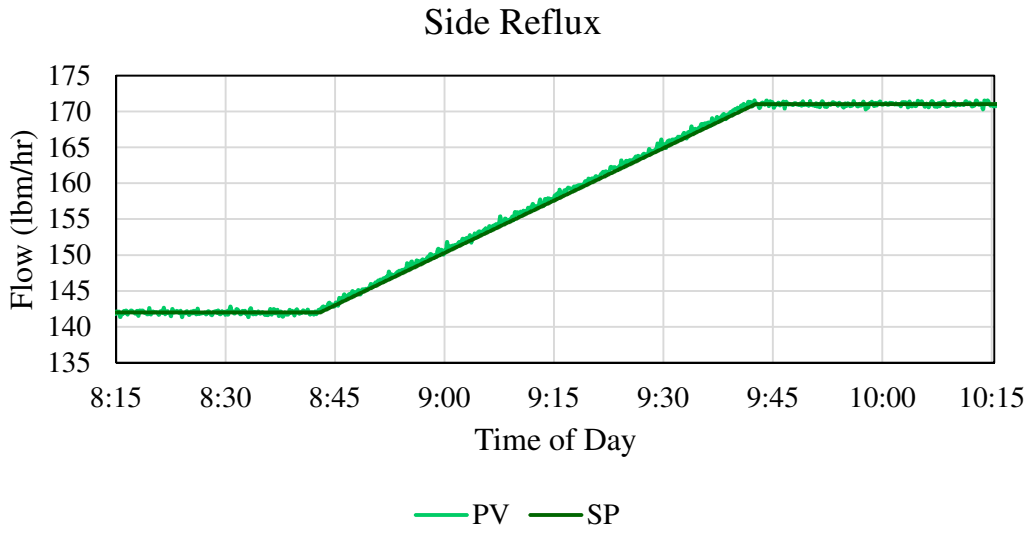

Figure B-25 – Side reflux ramp from case [2MP, C6, mX] to case [2MP, C6, Tol/mX]

After the four loops were at their appropriate setpoints, more toluene was fed to the column (Figure B-26). Even though a toluene feed composition of 4 weight percent was desired, 10 lbm/hr was initially fed to help reach the new steady state faster and to account for the increased inventory of toluene needed in the column and reboiler to achieve the desired compositions. After two hours of feeding roughly 20 weight percent of toluene to the column, the toluene feed was dropped to 2 lbm/hr to reach 4 weight percent feed toluene and to process the remaining feed.

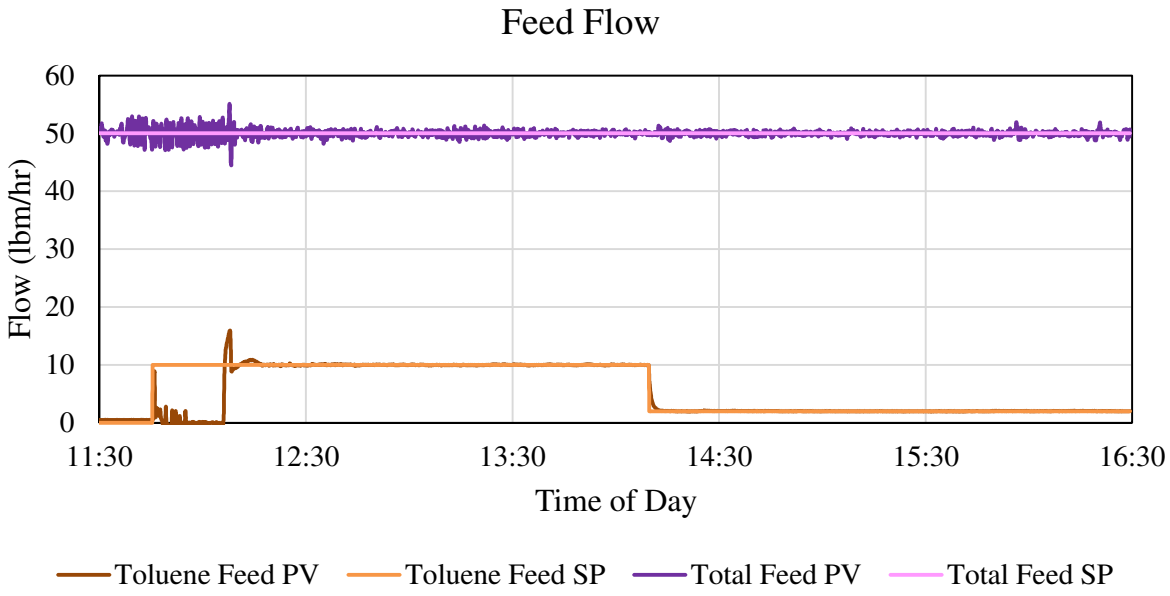

Figure B-26 – Addition of toluene while still feeding 50 lbm/hr total to the column

During the addition of toluene, the rectifying and stripping section temperature controllers maintained setpoint (Figure B-27 and Figure B-28). This maintained the 2-methylpentane/cyclohexane split at the top of the column and the m-xylene/cyclohexane split at the bottom of the column allowing the toluene to become part of the bottoms product.

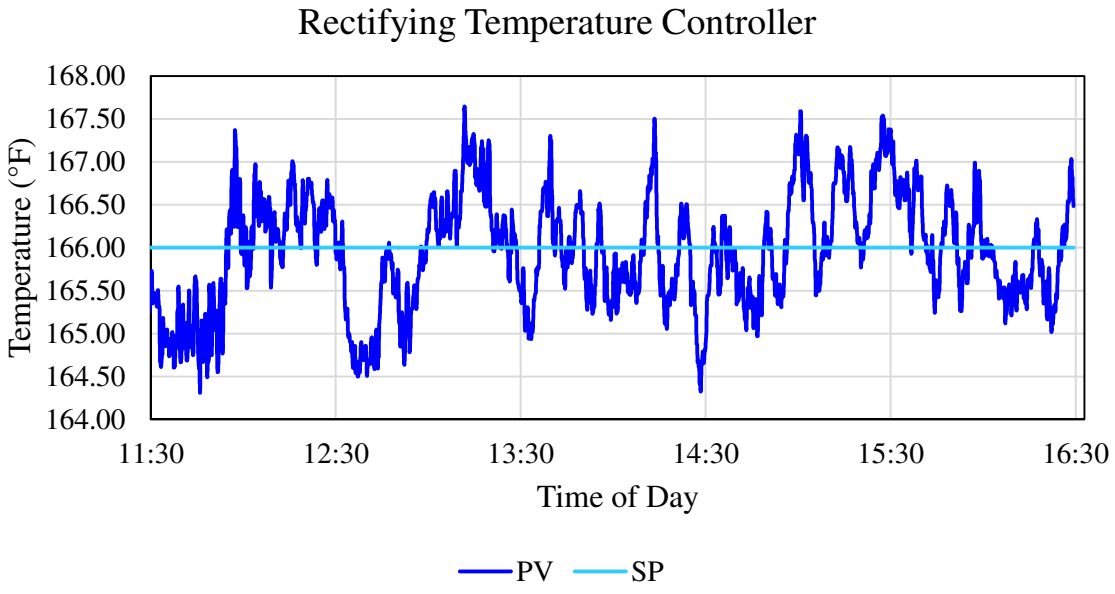

Figure B-27 – Rectifying section temperature controller during the addition of toluene to the feed

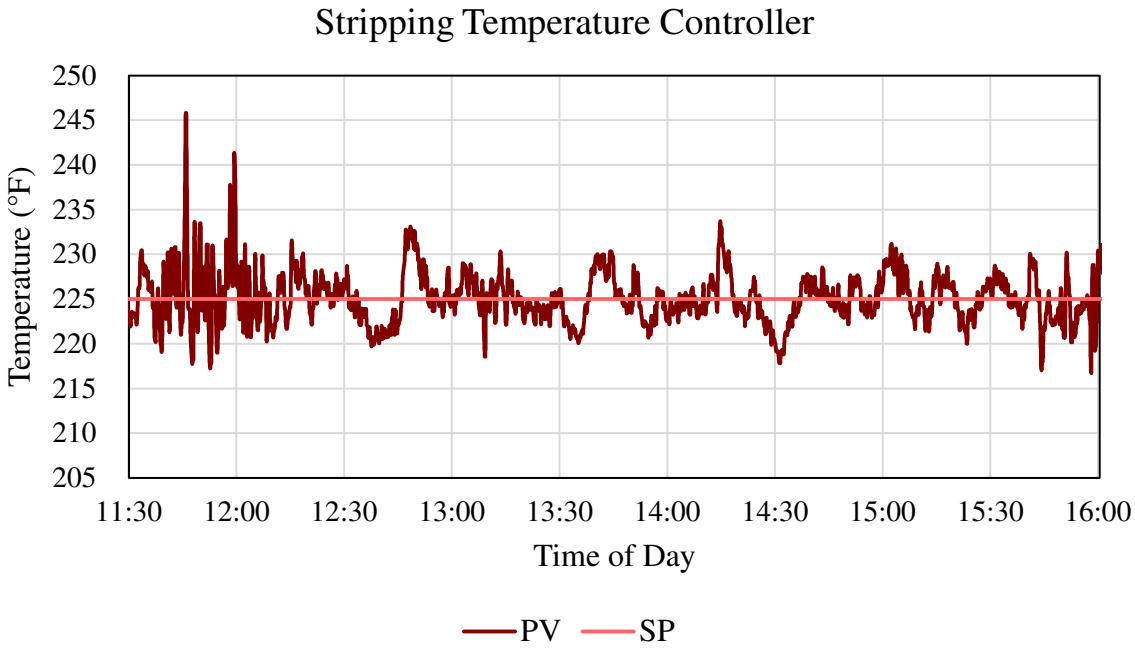

Figure B-28 – Stripping section temperature controller during the addition of toluene to the feed

Since the stripping section temperature controller was at the top of the stripping section close to the bottom of the wall, the toluene increase at the base of the column can be seen in the remaining stripping section temperatures (Figure B-29).

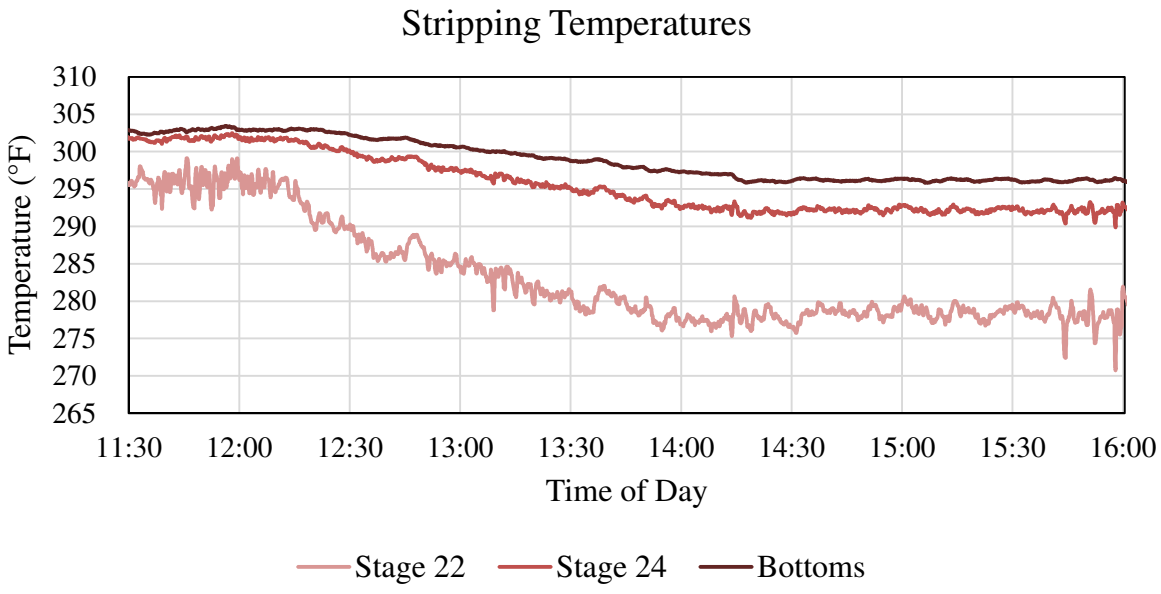

Figure B-29 – Stripping section temperatures (not including control temperature) reflecting the increase of toluene in the bottoms product

Case [2MP, C6, Tol/mX]

Table B-10. Comparison of original model and experimental steady state for [2MP, C6, Tol/mX]

Variable		Original Model	Experimental Data	
			Average	Standard Deviation
Product Compositions (wt %)				
Feed				
	2MP	32.00	31.55	
	C6	32.00	28.25	
	Tol	4.00	4.55	
	mX	32.00	35.65	
Distillate				
	2MP	97.00	96.88	± 0.06
	C6	3.00	3.11	± 0.06
	Tol	0.00	0.00	± 0.00
	mX	0.00	0.01	± 0.01
Top of Wall				
	2MP	48.71	50.62	± 0.30
	C6	51.28	49.38	± 0.30
	Tol	0.01	0.00	± 0.00
	mX	0.00	0.00	± 0.00
Side				
	2MP	2.50	3.61	± 0.06
	C6	97.12	95.91	± 0.72
	Tol	0.38	0.42	± 0.76
	mX	0.00	0.06	± 0.02
Bottoms				
	2MP	0.00	0.00	± 0.00
	C6	0.41	0.57	± 0.63
	Tol	10.77	11.00	± 0.05
	mX	88.82	88.44	± 0.67
Material Balance Flows (lbm/hr)				
Feed		50.00	50.14	± 0.61
Distillate		16.09	15.77	± 3.27
Side		15.90	14.11	± 3.96
Bottoms		18.01	20.16	± 3.80
Overhead Reflux	Flow (lbm/hr)	226.27	172.53	± 6.37
	Temperature (°F)	70.00	73.32	± 0.79
Prefrac Reflux	Flow (lbm/hr)	166.15	134.55	± 3.41
	Temperature (°F)	165.00	160.76	± 0.95

Table B-10. continued

Mainfrac Reflux	Flow (lbm/hr)	159.10	129.16	± 3.29
	Temperature (°F)	165.00	159.28	± 1.03
Side Reflux	Flow (lbm/hr)	170.98	171.00	± 0.21
	Temperature (°F)	180.00	184.21	± 0.83
Reboiler Duty (BTU/hr)		76100	76347	± 2780
Ambient Temperature (°F)		80.00	78.44	± 1.23
Feed Temperature (°F)		195.00	153.85	± 2.55

Case [2MP, C6/Tol, mX]

Table B-11. Comparison of original model and experimental steady state for [2MP, C6/Tol, mX]

Variable	Original Model	Experimental Data	
		Average	Standard Deviation
Product Compositions (wt %)			
Feed			
2MP	32.00	33.61	± 0.27
C6	32.00	30.52	± 0.19
Tol	4.00	3.88	± 0.03
mX	32.00	31.99	± 0.43
Distillate			
2MP	97.00	95.74	± 0.06
C6	3.00	4.26	± 0.06
Tol	0.00	0.00	± 0.00
mX	0.00	0.00	± 0.00
Top of Wall			
2MP	51.61	46.86	± 0.12
C6	48.30	53.06	± 0.12
Tol	0.09	0.08	± 0.01
mX	0.00	0.00	± 0.02
Side			
2MP	1.97	3.66	± 0.06
C6	87.07	84.70	± 0.72
Tol	10.89	11.52	± 0.76
mX	0.07	0.12	± 0.02
Bottoms			
2MP	0.00	0.00	± 0.00
C6	0.00	0.00	± 0.00
Tol	0.37	0.75	± 0.06
mX	99.63	99.25	± 0.06

Table B-11. continued

Material Balance Flows (lbm/hr)				
Feed		50.00	49.99	± 0.55
Distillate		16.13	15.80	± 2.78
Side		17.82	16.62	± 3.64
Bottoms		16.05	17.81	± 3.10
Overhead Reflux	Flow (lbm/hr)	139.26	88.29	± 8.15
	Temperature (°F)	70.00	79.26	± 1.46
Prefrac Reflux	Flow (lbm/hr)	132.27	91.49	± 3.80
	Temperature (°F)	160.00	156.06	± 1.56
Mainfrac Reflux	Flow (lbm/hr)	82.01	73.19	± 3.02
	Temperature (°F)	160.00	151.47	± 1.80
Side Reflux	Flow (lbm/hr)	91.70	129.99	± 0.23
	Temperature (°F)	175.00	184.16	± 1.20
Reboiler Duty (BTU/hr)		62900	66747	± 1514
Ambient Temperature (°F)		80.00	87.30	± 2.83
Feed Temperature (°F)		195	152.25	± 2.07

Transition from Case [2MP, C6/Tol, mX] to Case [2MP/C6, Tol, mX]

The transition from [2MP, C6/tol, mX] to [2MP/C6, tol, mX] was done in steps. First, to push the cyclohexane out of the side product up to the distillate product, the rectifying section temperature controller was taken out of control and the side level control strategy was changed to manipulate the sidedraw reflux. This left the reflux and side product flows in automatic flow control to be gradually decreased over 30 minutes (Table B-12). The reflux was decreased to allow the cyclohexane to reach to distillate (Figure B-30), and the side product flow was decreased to build up toluene in the side product tank (Figure B-31).

Table B-12. First step of transition from case [2MP, C6/Tol, mX] to case [2MP/C6, Tol, mX]

Loop	Initial Value	Final Value	Ramp
Overhead Reflux	123.5 lbm/hr	107 lbm/hr	-0.009167 lbm/hr/s
Side	14.9 lbm/hr	0.2 lbm/hr	-0.008267 lbm/hr/s

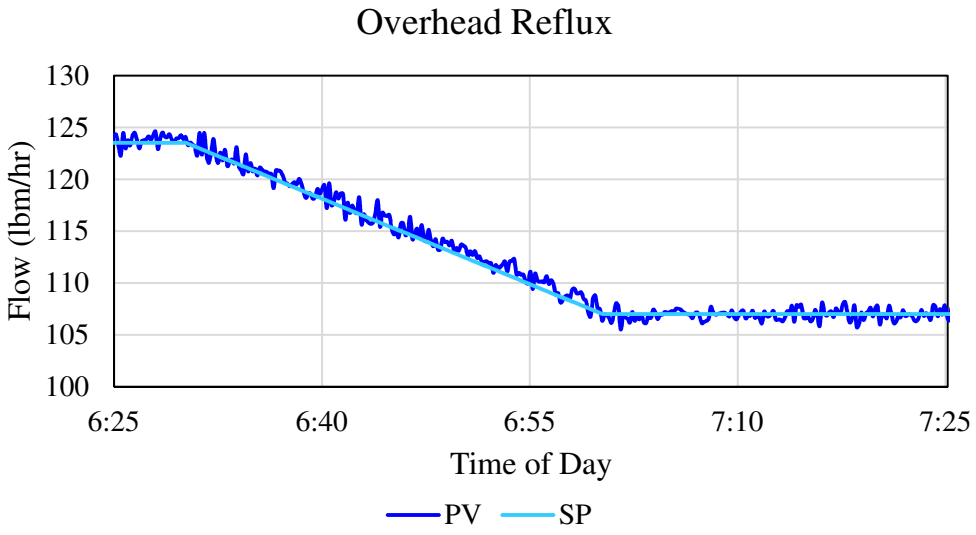

Figure B-30 – First ramp in overhead reflux to transition from case [2MP, C6/Tol, mX] to case [2MP/C6, Tol, mX]

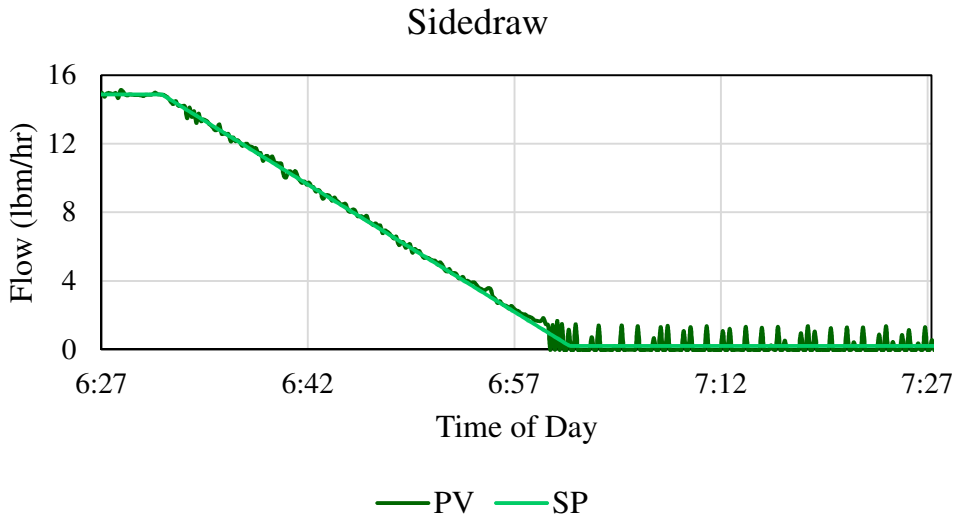

Figure B-31 – Decrease in sidedraw flow to build up toluene in column

The side product tank is operated with approximately three gallons of inventory. Feeding only four weight percent toluene at 50 lbm/hr (2 lbm/hr or 0.0047gpm of toluene) to the column, turning over the side tank composition to pure toluene would have taken a long time. To speed up this process, additional toluene was fed to the column (Figure B-32). After the side product was established as mostly pure toluene, the side product flow was sent back to the toluene tank to maintain the bulk toluene feed composition close to four weight percent.

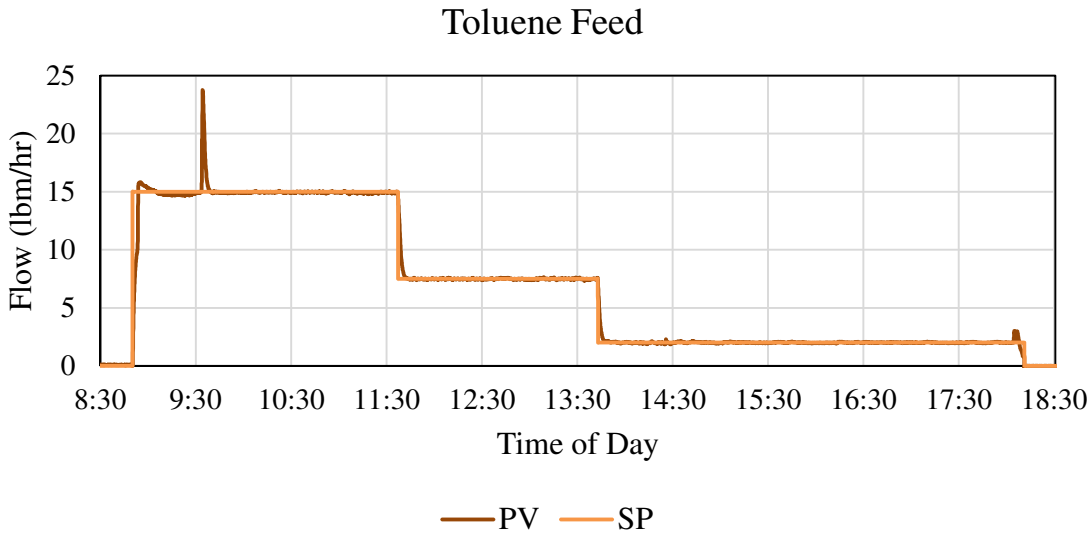

Figure B-32 – Addition of toluene to inventory column during transition from [2MP, C6/tol, mX] to [2MP/C6, tol, mX]

While waiting for the column to reach its new steady state, sensitivity analysis testing was completed on a loosely fitting dynamic model. This model better matched the heat loss to the environment than the model originally used for SVD/RGA and the steady state targets. The sensitivity analysis testing suggested changing the reflux and wall ratio to reach the desired compositions and use less energy. Therefore, a second set of ramps were performed (Table B-13).

Table B-13. Second step of transition from case [2MP, C6/Tol, mX] to case [2MP/C6, Tol, mX]

Loop	Initial Value	Final Value	Ramp
Wall Split	0.80	0.93	0.00013889/s
Overhead Reflux	107 lbm/hr	80 lbm/hr	-0.015 lbm/hr/s

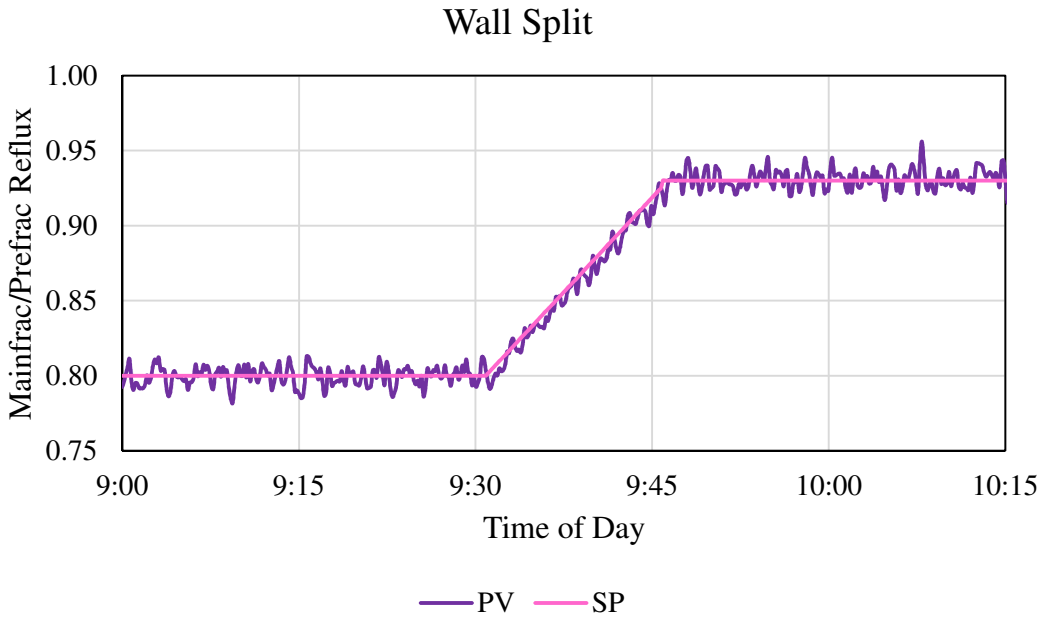

Figure B-33 – Ramp in wall split during transition from [2MP, C6/tol, mX] to [2MP/C6, tol, mX]

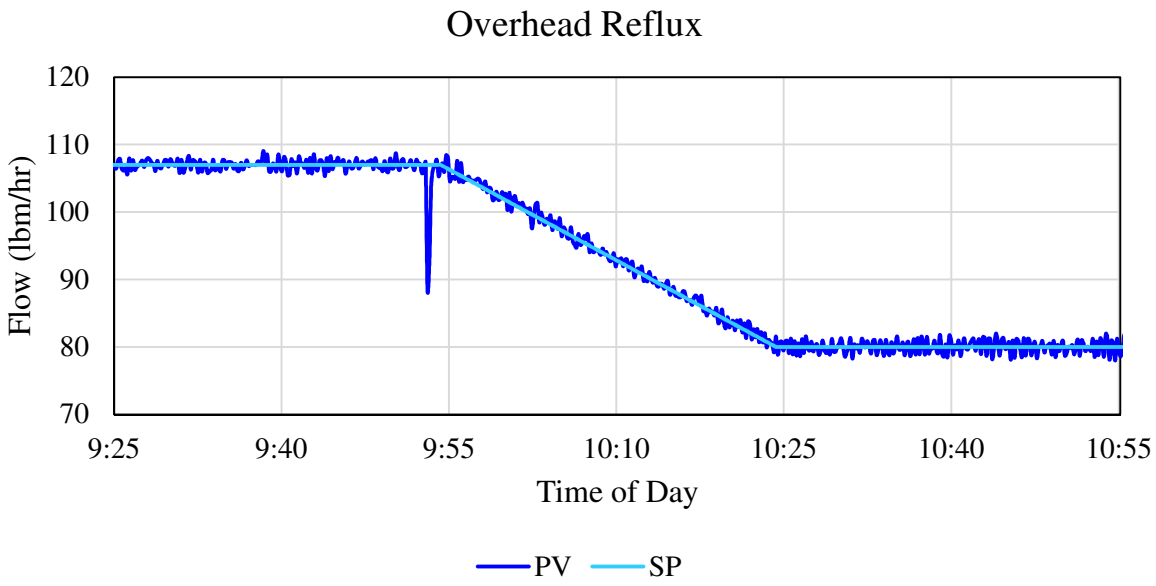

Figure B-34 – Decrease in reflux to allow cyclohexane to move to the distillate product

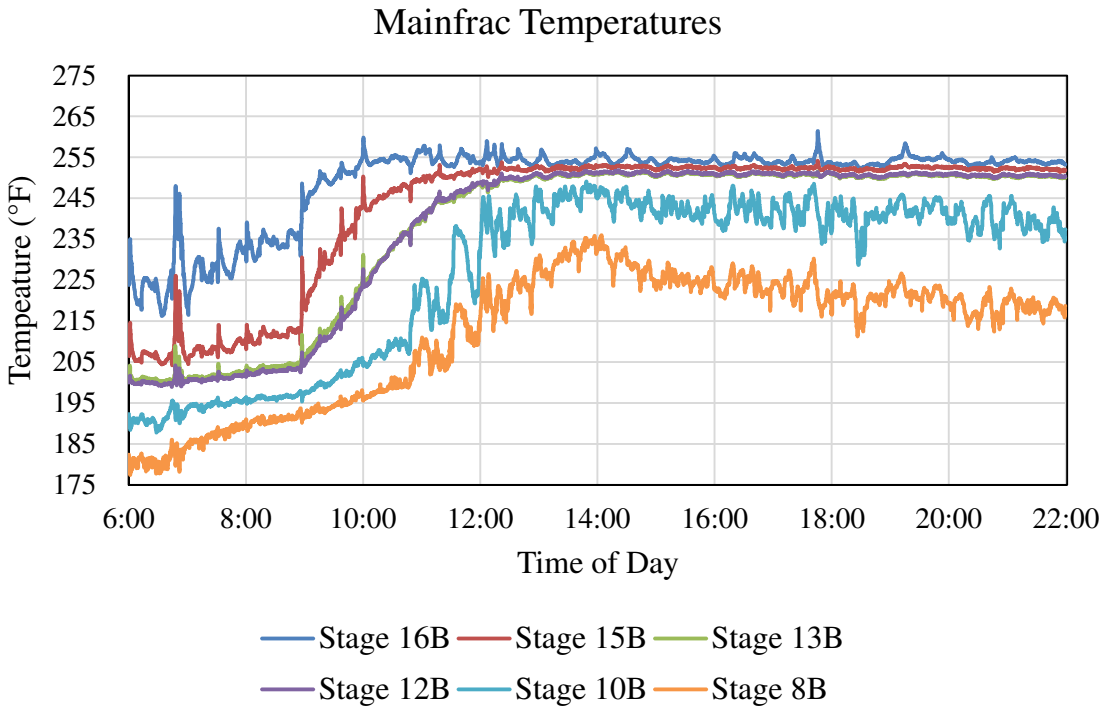

Figure B-35 – Increase in mainfrac temperatures as sidedraw becomes more concentrated in toluene

Case [2MP/C6, Tol, mX] Run 2

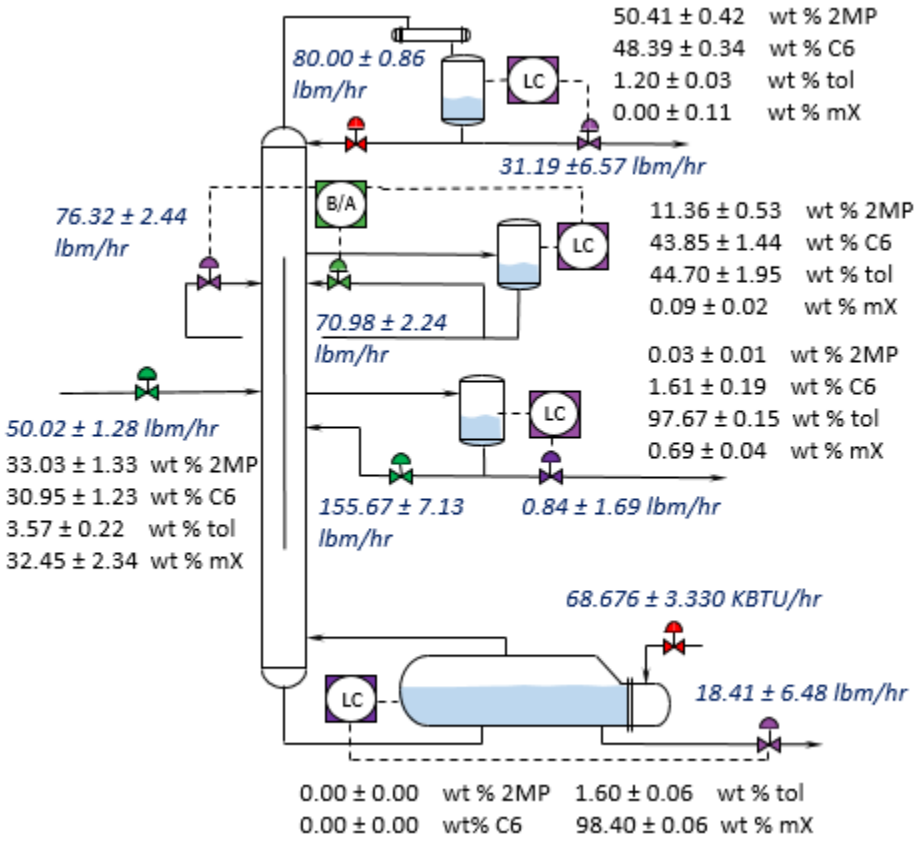

Figure B-36 – Steady state conditions for [2MP/C6, Tol, mX] Run 2. Purple valves are used for level control, green valves are in local automatic flow control, and red valves are manipulated variables for temperature control.

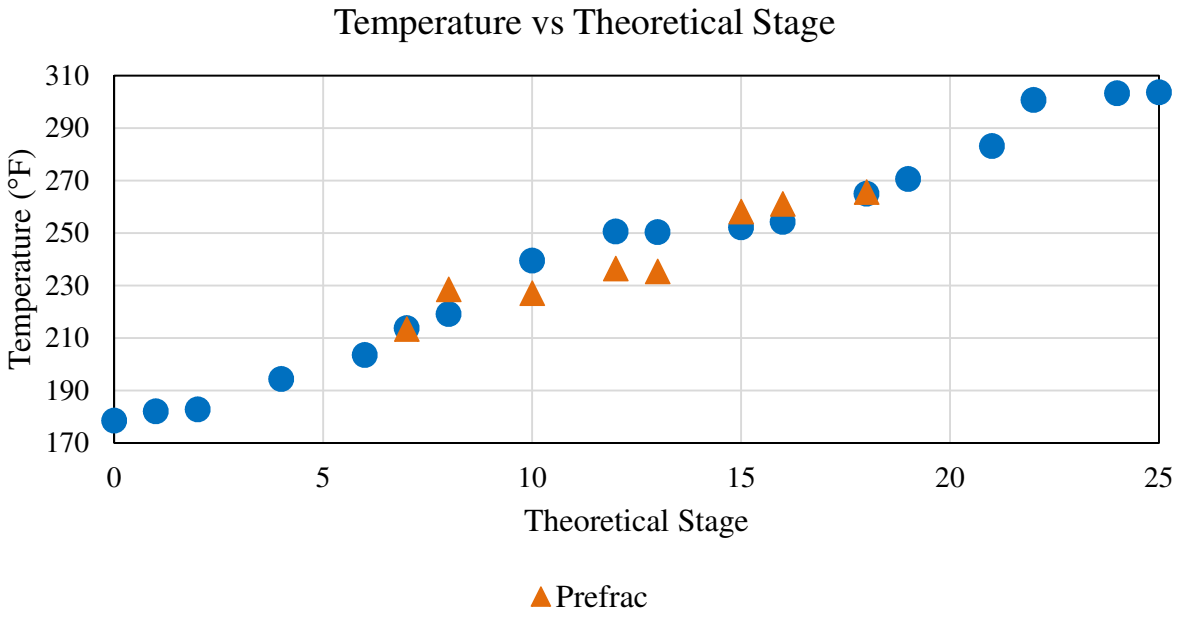

Figure B-37 – Temperature profile for case [2MP/C6, Tol, mX] Run 2

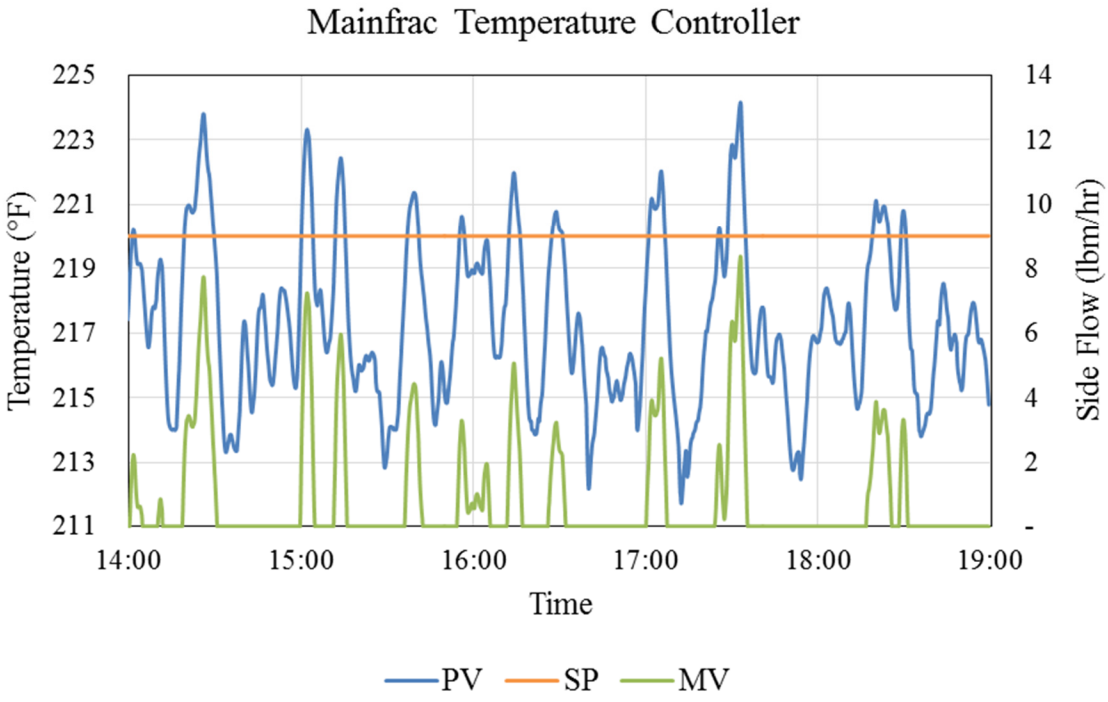

Figure B-38 – Mainfrac temperature controller for case [2MP/C6, Tol, mX] Run 2

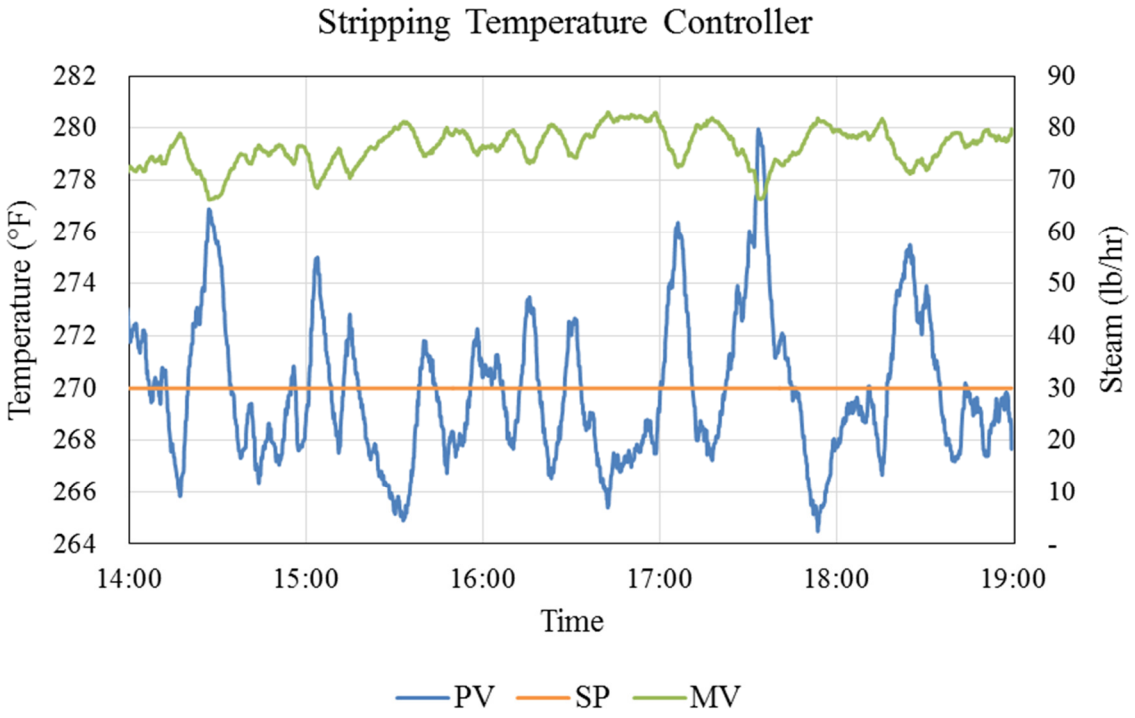

Figure B-39 – Stripping temperature controller for case [2MP/C6, Tol, mX] Run 2

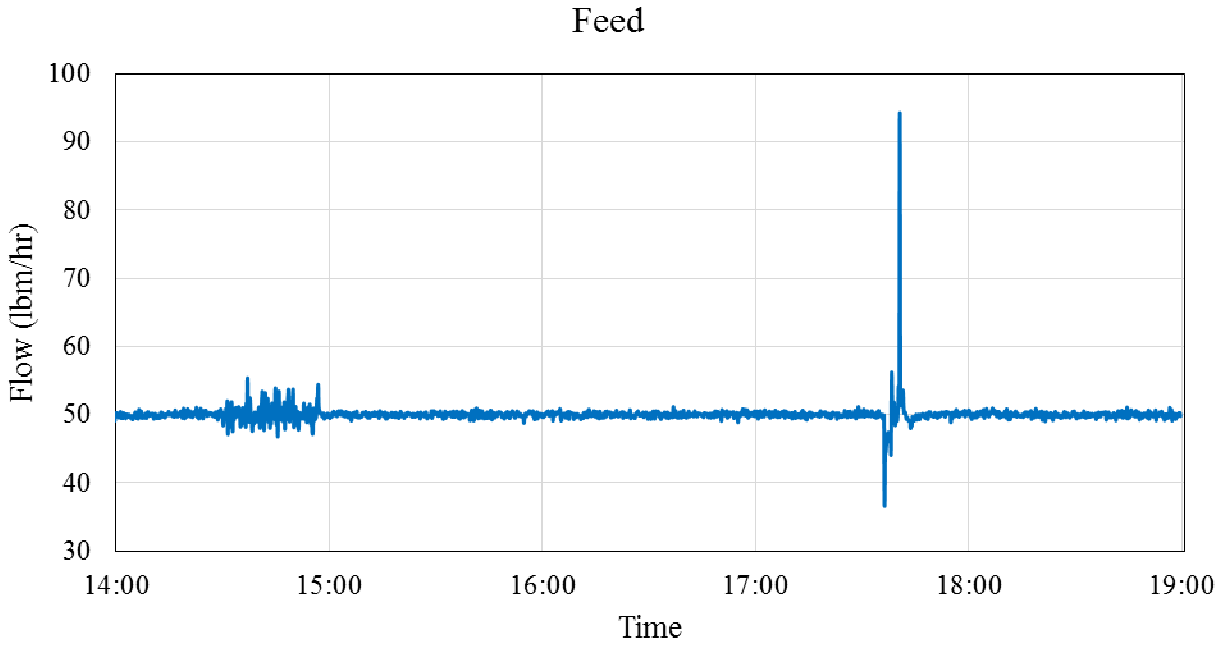

Figure B-40 – Feed flow for case [2MP/C6, Tol, mX] Run 2

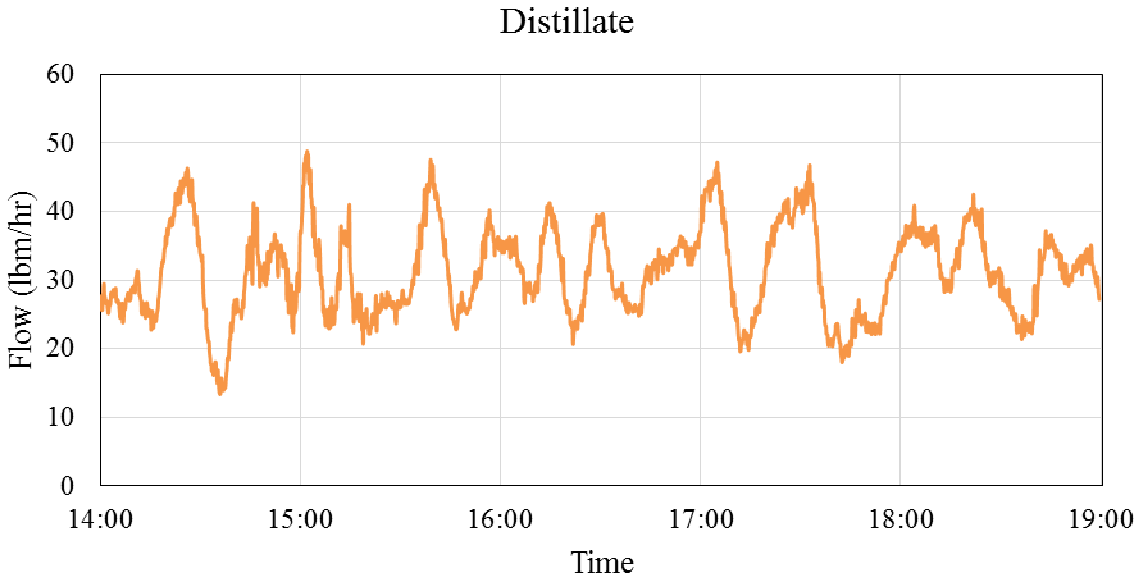

Figure B-41 – Distillate flow controlling reflux drum level for case [2MP/C6, Tol, mX] Run 2

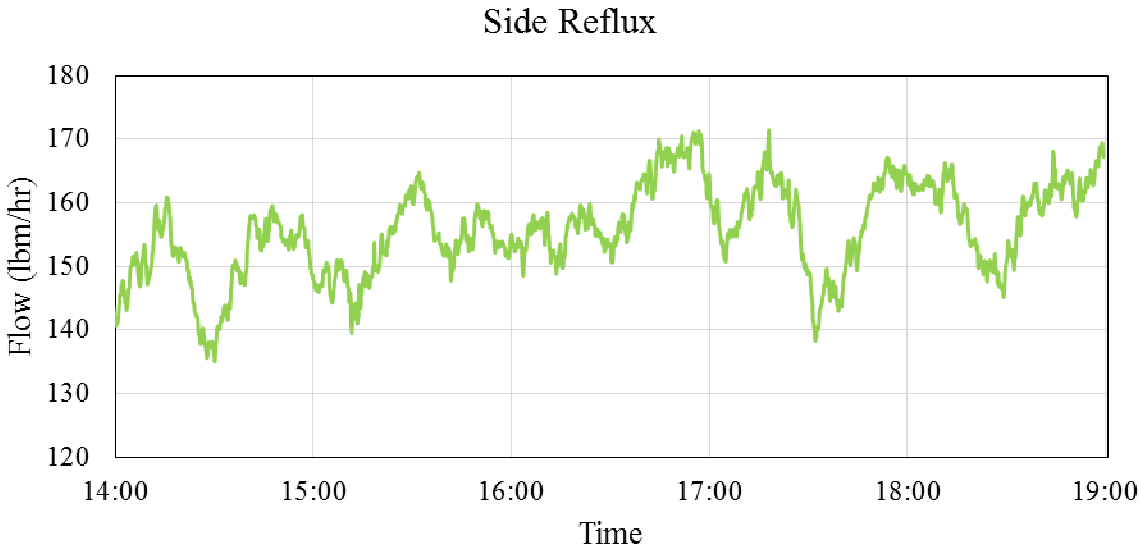

Figure B-42 – Sidedraw reflux flow controlling side product tank level for case [2MP/C6, Tol, mX] Run 2

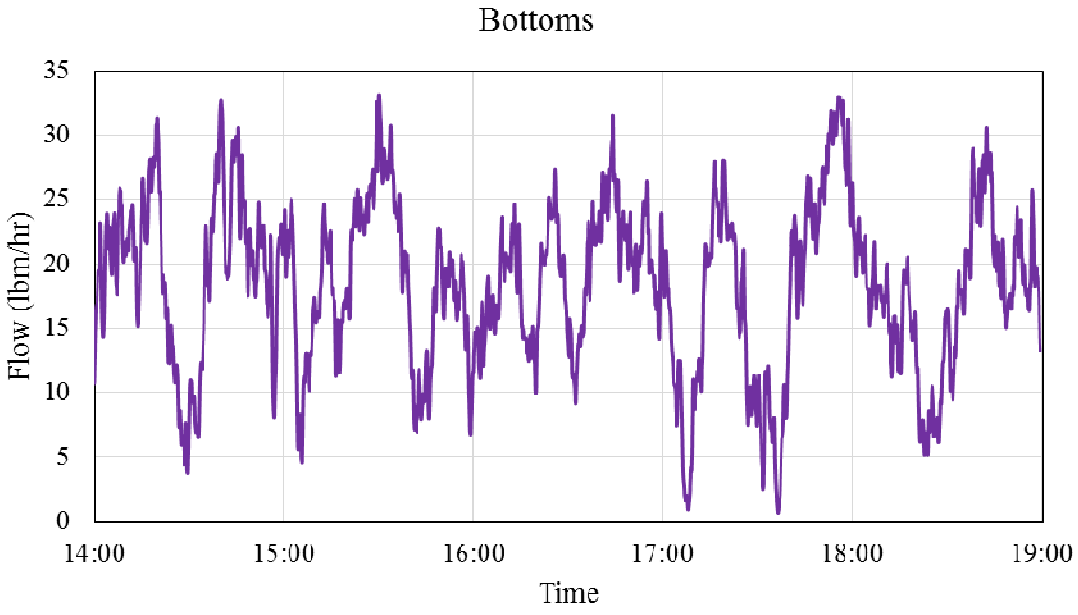

Figure B-43 – Bottoms flow controlling column level for case [2MP/C6, Tol, mX] Run 2

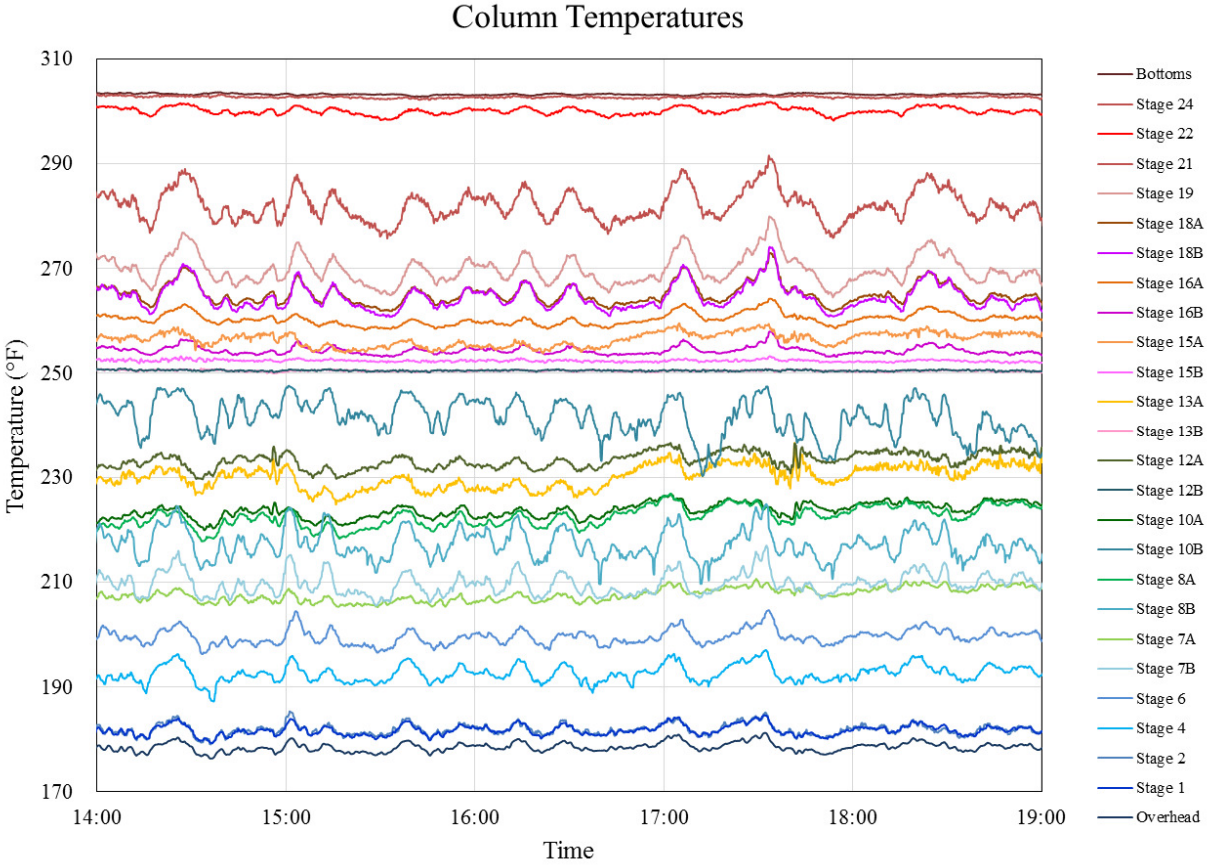

Figure B-44 – Column temperatures for case [2MP/C6, Tol, mX] Run 2

Appendix C: Steady State Data Analysis and Modeling

Feed Composition Analysis Example Calculation

Table C-1 shows samples from a feed batch during [2MP/C6, Tol, mX] run 2. Though not apparent from plotting compositions against time (Figure C-1 and Figure C-2), one of the 22:00 samples is an outlier. This sample is highlighted in red in Table C-1 and circled in Figure C-3.

Table C-1. Feed Samples – red is outlier

Date and Time	2-methylpentane (wt %)	Cyclohexane (wt %)	Toluene (wt %)	m-Xylene (wt %)
7/25/17 19:00	34.25	32.01	3.38	30.35
7/25/17 19:00	34.86	32.59	3.31	29.23
7/25/17 19:00	33.33	31.45	3.45	31.76
7/25/17 22:00	34.17	32.01	3.36	30.47
7/25/17 22:00	33.61	31.45	3.41	31.53
7/25/17 22:00	31.70	30.25	3.60	34.45
7/25/17 22:00	35.34	32.86	3.28	28.53
7/26/17 1:00	34.02	31.91	3.35	30.71
7/26/17 1:00	34.93	32.55	3.31	29.21
7/26/17 1:00	34.40	32.28	3.34	29.98
7/26/17 4:00	33.02	30.72	3.45	32.81
7/26/17 4:00	33.64	31.23	3.38	31.74
7/26/17 4:00	34.33	31.78	3.32	30.57

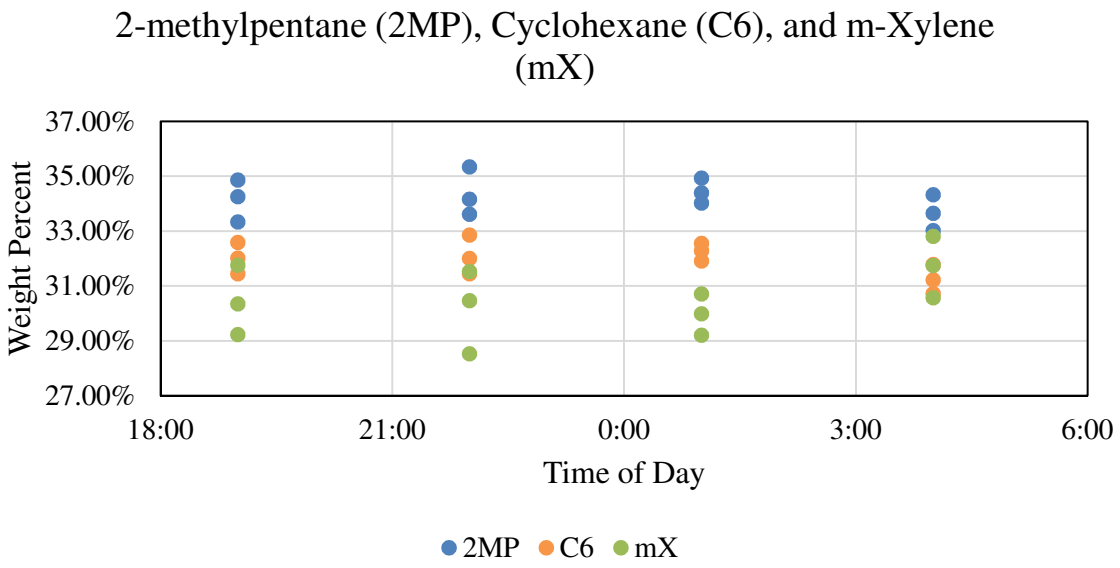

Figure C-1 – Feed samples versus time

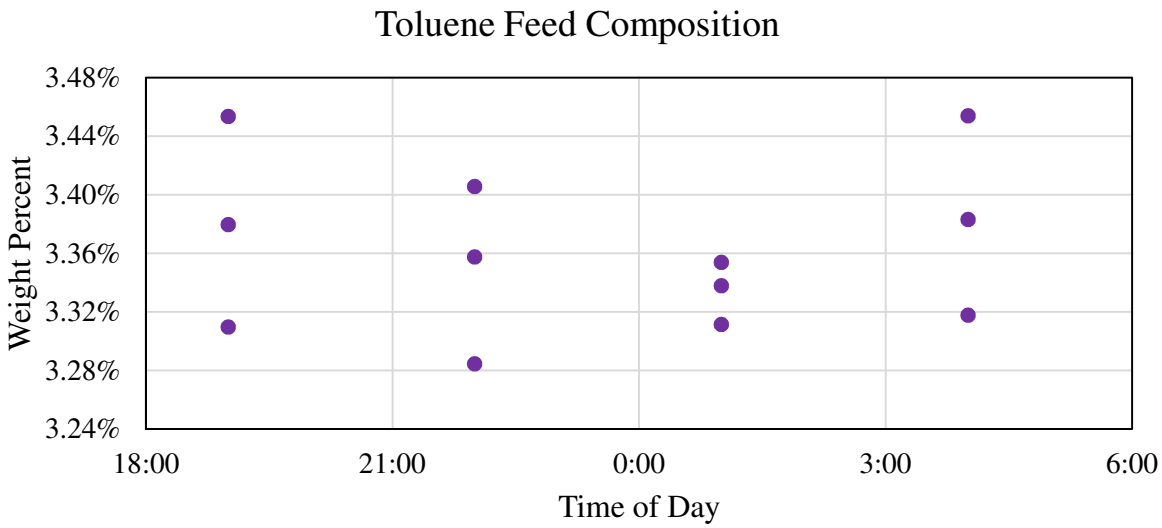

Figure C-2 – Feed samples versus time

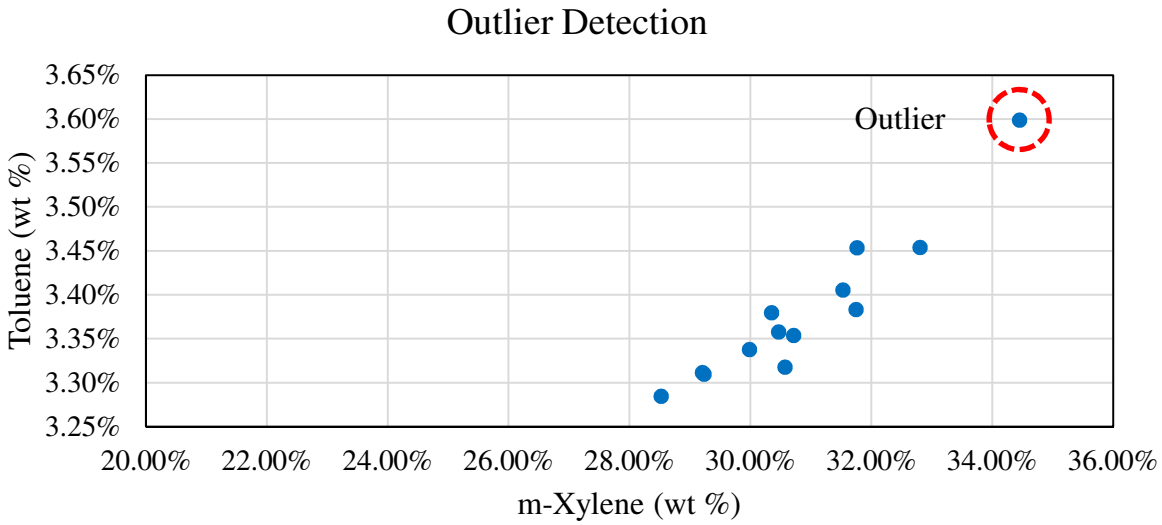

Figure C-3 – Scatter plot revealing an outlier sample (circled)

Table C-2. Comparison of feed averages and standard deviations

		Weight Percent			
		2MP	C6	Tol	mX
Including Outlier	Average	33.97 %	31.78 %	3.38 %	30.87 %
	Standard Deviation	0.91 %	0.72 %	0.08 %	1.54 %
Without Outlier	Average	34.16 %	31.90 %	3.36 %	30.57 %
	Standard Deviation	0.65 %	0.59 %	0.05 %	1.19 %

CLOSING MATERIAL BALANCES EXAMPLE CALCULATION

Example calculation for case [2MP/C6, tol, mX] Run 1

$$Min\ (F - D - S - B)^2 + \sum_{i=2MP}^{mX}(x_{F,i}F - x_{D,i}D - x_{S,i}S - x_{B,i}B)^2$$

Subject to

$$\sum_{i=2MP}^{mX} x_{F,i} = 1$$

$$\sum_{i=2MP}^{mX} x_{D,i} = 1$$

$$\sum_{i=2MP}^{mX} x_{S,i} = 1$$

$$\sum_{i=2MP}^{mX} x_{B,i} = 1$$

0.3193	≤	$x_{F,2MP}$	≤	0.3335
0.3015	≤	$x_{F,C6}$	≤	0.3106
0.0311	≤	$x_{F,tol}$	≤	0.0322
0.3253	≤	$x_{F,mX}$	≤	0.3465
0.5120	≤	$x_{D,2MP}$	≤	0.5204
0.4693	≤	$x_{D,C6}$	≤	0.4760
0.0100	≤	$x_{D,tol}$	≤	0.0107
-0.0002*	≤	$x_{D,mX}$	≤	0.0019
0.0004	≤	$x_{S,2MP}$	≤	0.0006
0.0193	≤	$x_{S,C6}$	≤	0.0230
0.9708	≤	$x_{S,tol}$	≤	0.9738
0.0056	≤	$x_{S,mX}$	≤	0.0064
0.0000	≤	$x_{B,2MP}$	≤	0.0000
0.0000	≤	$x_{B,C6}$	≤	0.0000
0.0127	≤	$x_{B,tol}$	≤	0.0139
0.9861	≤	$x_{B,mX}$	≤	0.9873
49.3291	≤	F	≤	50.6663
26.3142	≤	D	≤	36.1342
0.0000	≤	S	≤	2.7555
11.5390	≤	B	≤	23.3390

Base Conditions		Optimized	
$x_{F,2MP}$	0.3264	$x_{F,2MP}$	0.3238
$x_{F,C6}$	0.3061	$x_{F,C6}$	0.3015
$x_{F,tol}$	0.0317	$x_{F,tol}$	0.0312
$x_{F,mX}$	0.3359	$x_{F,mX}$	0.3435
$x_{D,2MP}$	0.5162	$x_{D,2MP}$	0.5120
$x_{D,C6}$	0.4726	$x_{D,C6}$	0.4760
$x_{D,tol}$	0.0103	$x_{D,tol}$	0.0107
$x_{D,mX}$	0.0008	$x_{D,mX}$	0.0013
$x_{S,2MP}$	0.0005	$x_{S,2MP}$	0.0005
$x_{S,C6}$	0.0211	$x_{S,C6}$	0.0230
$x_{S,tol}$	0.9723	$x_{S,tol}$	0.9708
$x_{S,mX}$	0.0060	$x_{S,mX}$	0.0056
$x_{B,2MP}$	0.0000	$x_{B,2MP}$	0.0000
$x_{B,C6}$	0.0000	$x_{B,C6}$	0.0000
$x_{B,tol}$	0.0133	$x_{B,tol}$	0.0139
$x_{B,mX}$	0.9867	$x_{B,mX}$	0.9861
F	50.00	F	49.69
D	31.22	D	31.43
S	1.25	S	1.00
B	17.44	B	17.26
Objective Function	**0.18**	***Objective Function***	**2.30145E-12**

HEAT TRANSFER COEFFICIENTS

Case [2MP, C6, mX]

Table C-3. Comparison of [2MP, C6, mX] finite reflux data from pilot column (left) and data from Aspen Plus® model with $U_{i,ATM}$ = 9.82 BTU/(hrft^2°F) and U_{WALL} = 0 BTU/(hrft^2°F). Ambient temperature for the pilot data was 82.37 °F.

Variable	Pilot Data		Aspen Plus® $U_{i,ATM}$ = 9.82, U_{WALL} = 0
	Average	Standard Deviation	
Product Compositions (mol %)			
Distillate			
2MP	97.89		98.37
C6	2.11		1.63
Tol	0.00		0.00
mX	0.00		0.00
Top of Wall			
2MP	65.04	± 0.30	64.06
C6	34.96	± 0.30	35.94
Tol	0.00	± 0.00	0.00
mX	0.00	± 0.00	0.00
Side			
2MP	4.20		3.52
C6	95.76		96.44
Tol	0.04		0.04
mX	0.00		0.00
Bottoms			
2MP	0.00		0.00
C6	1.73		1.93
Tol	1.46		1.69
mX	96.81		96.38
Material Balance Flows (lbmol/hr)			
Distillate	0.185		0.185
Side	0.176		0.177
Bottoms	0.183		0.182
Internal Flows			
Overhead Reflux (lbmol/hr)	1.769	± 0.141	1.993
Prefrac Reflux (lbmol/hr)	1.543	± 0.089	1.698
Mainfrac Reflux (lbmol/hr)	1.281	± 0.069	1.389
Side Reflux (lbmol/hr)	1.804	± 0.003	1.563
Reboiler Duty (BTU/hr)	71767	± 1980	71767

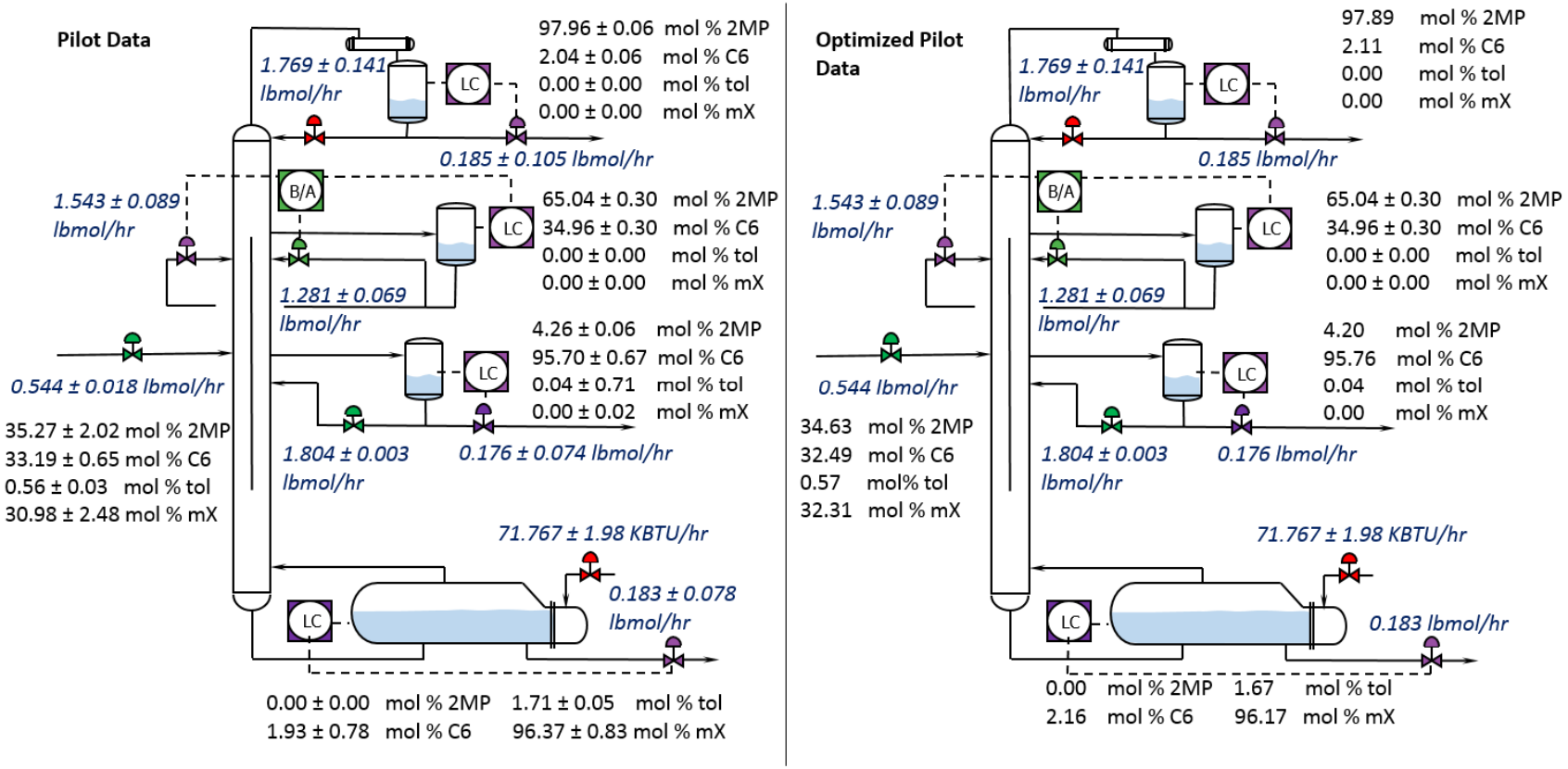

Figure C-4 – Case [2MP, C6, mX] Pilot data vs optimized pilot data

Case [2MP, C6, Tol/mX]

Just as with the three component case, modeling the pilot data with a U_{WALL} of 0 BTU/(hrft^2°F) resulted in a model which overestimated the overhead, prefrac, and mainfrac reflux flows and underestimated the sidedraw reflux (Table C-4). U_{WALL} from case [2MP, C6, mX] resulted in a closer fit. However, all reflux flows were still not within their appropriate standard deviations (Table C-4). To better match the data, U_{WALL} was varied.

Figure C-6 shows the range of wall heat transfer coefficients for which when $U_{i,ATM}$ was 9.82 BTU/(hrft^2°F) and the reboiler duty was 74,200 BTU/hr, the sidedraw reflux and all other reflux flows were within their feasible regions as defined by the standard deviation of the pilot data. The range of feasible wall heat transfer coefficients is 709.54 – 718.9 BTU/(hrft^2°F). Feasible solutions were found for a reboiler range of 73,570 to 74,876.6 BTU/hr. However, changing the reboiler duty and $U_{i,ATM}$ for this particular case led to too many solutions within the flow constraints. Therefore, a reboiler duty of 74,200 BTU/hr was chosen because that value was in the middle of the feasible range.

As with the previous study, compositions were examined to determine the optimal U_{WALL} (Figure C-7 – Figure C-10). Compositions were not matched precisely. However, the heat transfer coefficient which simultaneously matched the reflux flows and provided the best match to the product compositions was chosen. A heat transfer coefficient of 715.26 BTU/(hrft^2°F) was found to provide the best match for all compositions and was therefore chosen as the optimal wall heat transfer coefficient (Figure C-11 and Table C-5). This wall heat transfer coefficient is almost double that found for case [2MP, C6, mX]. This difference can be explained by the assumed area. In determining the overall heat transfer coefficient, a constant fully wetted area was assumed. However, in reality this area may be changing while U_{WALL} is constant.

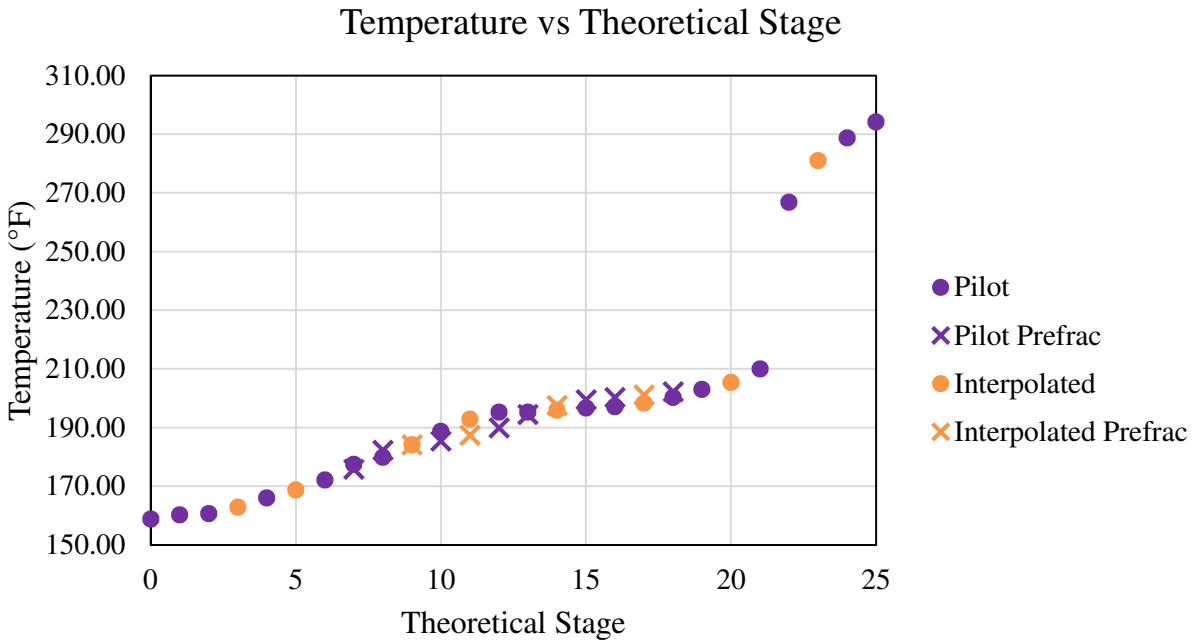

Figure C-5 – Temperature profile for [2MP, C6, tol/mX] finite reflux showing temperatures from experimental data and those interpolated with pchip.

Table C-4. Comparison of [2MP, C6, Tol/mX] finite reflux data from pilot column (left) and data from Aspen Plus® model with U_{WALL} = 0 BTU/(hrft^2°F) (center) and heat transfer coefficients from the three component case (right). Neither of the wall heat transfer coefficients provide a good match. Ambient temperature for the pilot data was 78.44°F.

Variable	Pilot Data		Aspen Plus®	
	Average	Standard Deviation	$U_{i,ATM}$ = 9.82, U_{WALL} = 0	$U_{i,ATM}$ = 9.82, U_{WALL} = 388
Product Compositions (mol %)				
Distillate				
2MP	96.81	± 0.06	97.71	97.64
C6	3.18	± 0.6	2.29	2.36
Tol	0.00	± 0.00	0.00	0.00
mX	0.01	± 0.00	0.00	0.00
Top of Wall				
2MP	50.02	± 0.30	55.90	55.20
C6	49.98	± 0.30	44.10	44.80
Tol	0.00	± 0.00	0.00	0.00
mX	0.00	± 0.00	0.00	0.00

Table C-4. continued

Side				
2MP	3.53	± 0.06	2.62	2.71
C6	96.04	± 0.67	97.00	96.94
Tol	0.39	± 0.71	0.38	0.35
mX	0.05	± 0.02	0.00	0.00
Bottoms				
2MP	0.00	± 0.00	0.00	0.00
C6	0.70	± 0.78	0.65	0.63
Tol	12.44	± 0.05	12.45	12.47
mX	86.85	± 0.83	86.90	86.90
Material Balance Flows (lbmol/hr)				
Distillate	0.183		0.183	0.183
Side	0.167		0.167	0.167
Bottoms	0.193		0.193	0.193
Internal Flows				
Overhead Reflux (lbmol/hr)	2.003	± 0.074	2.133	2.126
Prefrac Reflux (lbmol/hr)	1.580	± 0.040	1.678	1.673
Mainfrac Reflux (lbmol/hr)	1.517	± 0.039	1.612	1.607
Side Reflux (lbmol/hr)	2.029	± 0.002	1.815	1.976
Reboiler Duty (BTU/hr)	76350	± 2780	76350	76350

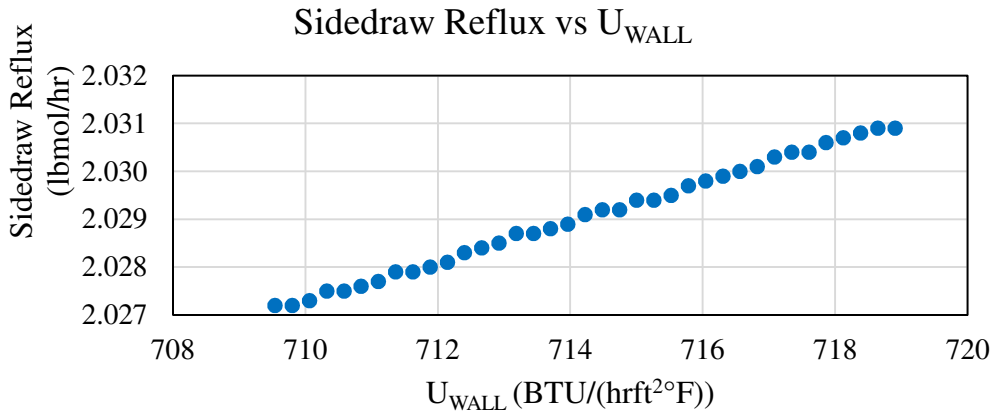

Figure C-6 – Sidedraw reflux versus wall heat transfer coefficient for [2MP, C6, tol/mX] finite reflux with $U_{i,ATM}$ 9.82 BTU/(hrft2°F), constant Q_R, and varying U_{WALL}. Sidedraw reflux and all other reflux values were within their feasible ranges as defined by the standard deviation of the pilot data. Without considering compositions, there is no clear optimal solution. Solutions were feasible for other values of Q_R but were not included here.

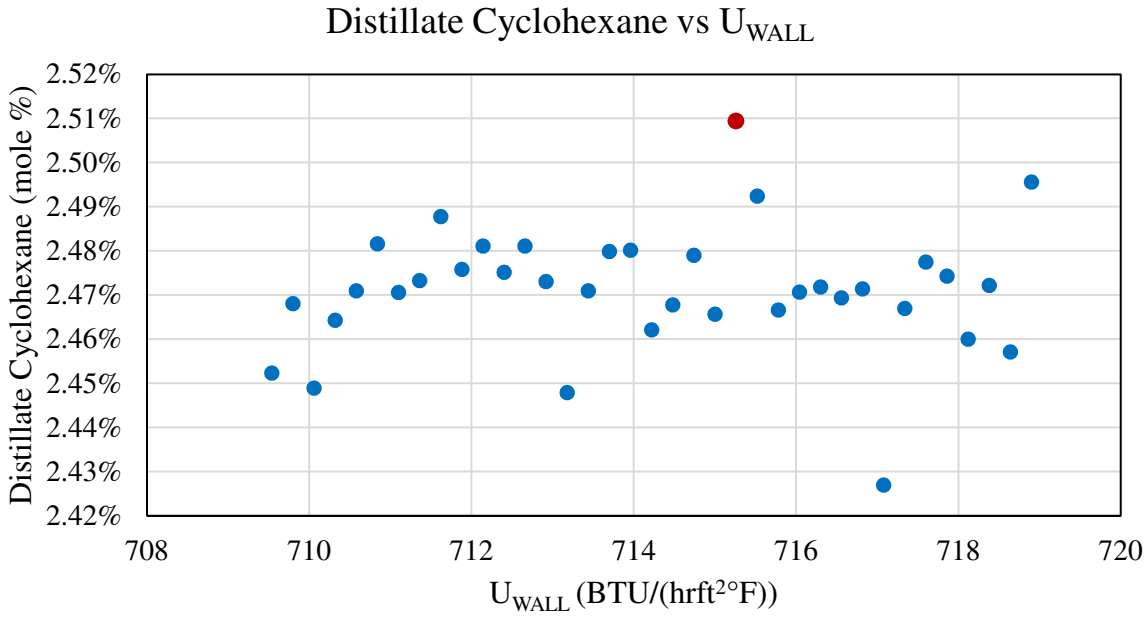

Figure C-7 – Distillate cyclohexane composition vs UWALL for [2MP, C6, tol/mX] finite reflux with $U_{i,ATM}$ 9.82 BTU/(hrft2°F), constant Q_R, and varying U_{WALL}. U_{WALL} of 717.08 BTU/(hrft^2°F) (red) best matches the pilot composition of 3.18 ± 0.06 mole percent cyclohexane.

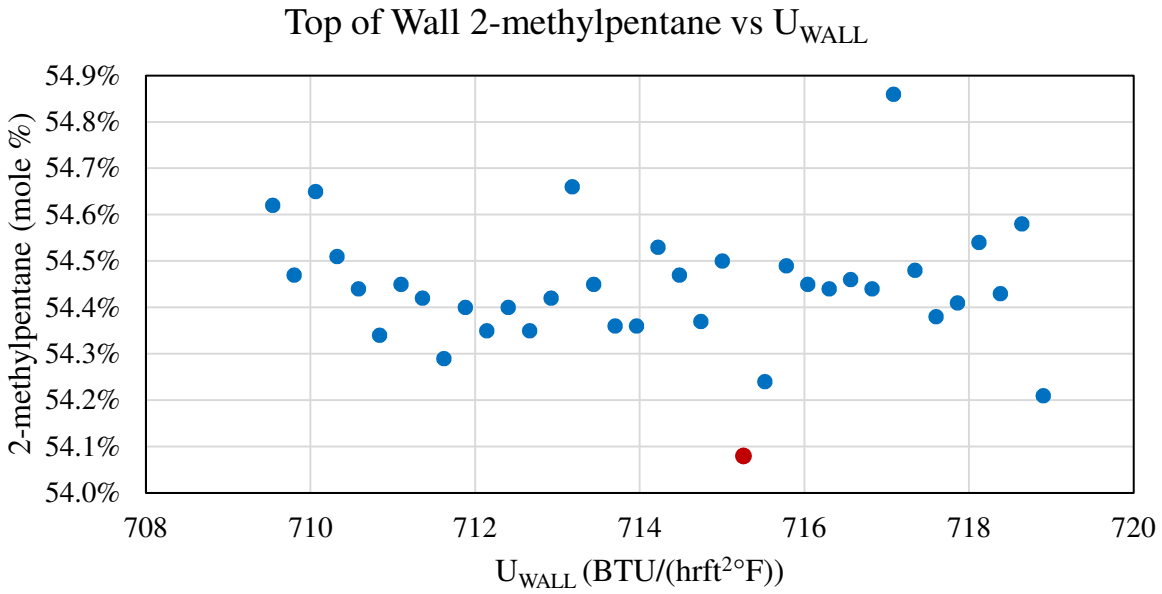

Figure C-8 – Top of wall 2-methylpentane composition vs U_{WALL} for [2MP, C6, tol/mX] finite reflux with $U_{i,ATM}$ 9.82 BTU/(hrft2°F), constant Q_R, and varying U_{WALL}. U_{WALL} of 715.26 BTU/(hrft^2°F) (red) best matches the pilot composition of 50.02 ± 0.30 mole percent 2-methylpentane.

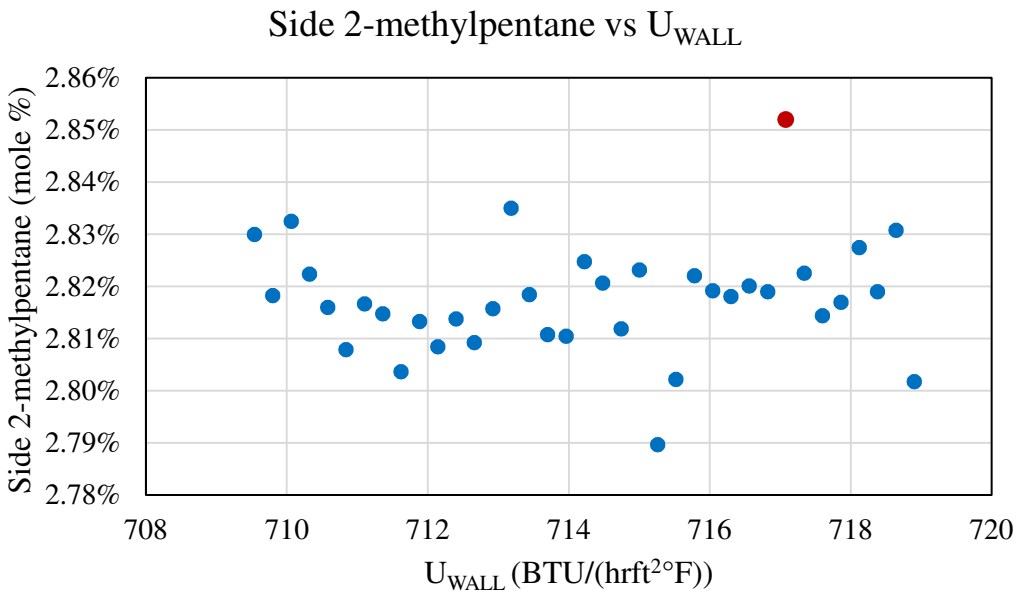

Figure C-9 – Side 2-methylpentane composition vs UWALL for [2MP, C6, tol/mX] finite reflux with Ui,ATM 9.82 BTU/(hrft2°F), constant QR, and varying UWALL. UWALL of 717.08 BTU/(hrft2°F) best matches the pilot composition of 3.53 ± 0.06 mole percent 2-methylpentane.

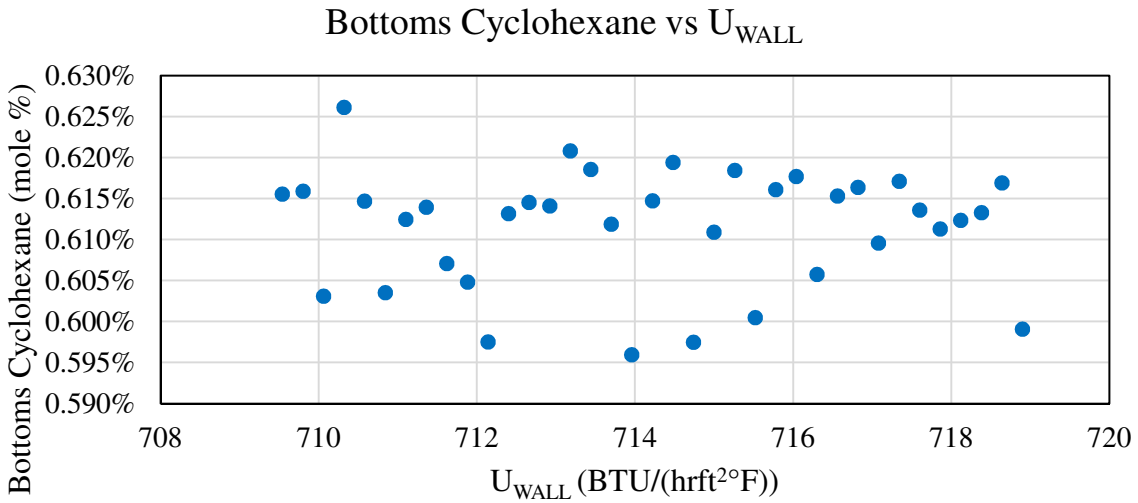

Figure C-10 – Bottoms cyclohexane composition vs U_{WALL} for [2MP, C6, mX] finite reflux with $U_{i,ATM}$ 9.82 BTU/(hrft2°F), constant Q_R, and varying U_{WALL}. U_{WALL} does not have a large effect on bottoms composition. Pilot composition was 0.70 ± 0.76 mole percent.

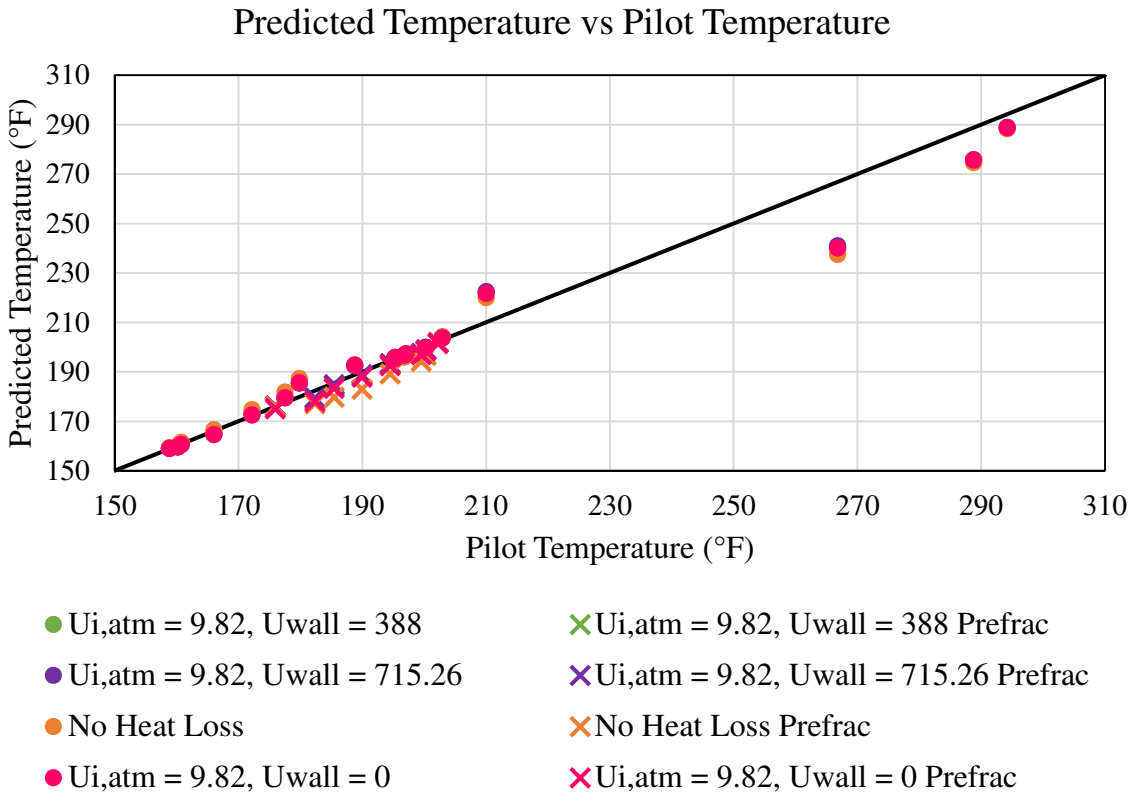

Figure C-11 – Comparison of model and pilot temperatures for [2MP, C6, tol/mX] finite reflux with and without heat loss

Table C-5. Comparison of pilot data, AspenPlus model, and dynamic model for case [2MP, C6, tol/mX]. AspenPlus and the dynamic model use U_{WALL} = 715.26 BTU/(hrft^2°F) and $U_{i,ATM}$ = 9.82 BTU/(hrft^2°F). The dynamic model also accounts for pressure drop.

Variable	Pilot Data		Aspen Plus®	Dynamic Model
	Average	Standard Deviation		
Product Compositions (mol %)				
Distillate				
2MP	96.81	± 0.06	97.49	97.01
C6	3.18	± 0.6	2.51	2.99
Tol	0.00	± 0.00	0.00	0.00
mX	0.01	± 0.00	0.00	0.00
Top of Wall				
2MP	50.02	± 0.30	54.08	49.88
C6	49.98	± 0.30	45.91	50.11
Tol	0.00	± 0.00	0.01	0.01
mX	0.00	± 0.00	0.00	0.00
Side				
2MP	3.53	± 0.06	2.79	3.38
C6	96.04	± 0.67	96.87	96.36
Tol	0.39	± 0.71	0.34	0.26
mX	0.05	± 0.02	0.00	0.00
Bottoms				
2MP	0.00	± 0.00	0.00	0.00
C6	0.70	± 0.78	0.62	0.55
Tol	12.44	± 0.05	12.47	12.55
mX	86.85	± 0.83	86.91	86.90
Material Balance Flows (lbmol/hr)				
Distillate	0.183		0.183	0.183
Side	0.167		0.167	0.167
Bottoms	0.193		0.193	0.193
Internal Flows				
Overhead Reflux (lbmol/hr)	2.003	± 0.074	1.993	2.039
Prefrac Reflux (lbmol/hr)	1.580	± 0.040	1.584	1.604
Mainfrac Reflux (lbmol/hr)	1.517	± 0.039	1.521	1.540
Side Reflux (lbmol/hr)	2.029	± 0.002	2.029	2.191
Reboiler Duty (BTU/hr)	76350	± 2780	74200	74200

Case [2MP, C6/Tol, mX]

When using the atmospheric heat transfer coefficient from [2MP, C6, mX] total reflux and varying the wall heat transfer coefficient, Aspen Plus® simulations crashed before the sidedraw reflux flow matched that from the pilot campaign (Figure C-14). The simulations stopped because the amount of heat loss caused the vapor traffic leaving the upper mainfrac to reach zero. As an alternative approach, wall heat transfer coefficient values from other case studies were used in the simulation and the atmospheric heat transfer coefficient was varied. When the wall heat transfer coefficient was set to 388 BTU/(hrft^2°F) and $U_{i,ATM}$ was varied, the overhead, prefrac, and mainfrac reflux flows were consistently too high. The sidedraw reflux, however, was either too low or within one standard deviation of the experimental value. Therefore, other wall heat transfer coefficients were examined. The wall heat transfer coefficient was set to 222.5 BTU/(hrft^2°F), and $U_{i,ATM}$ and Q_R were changed to match the overhead, prefrac, and mainfrac reflux flows. However, this resulted in the same trend of not matching the prefrac and sidedraw reflux flows simultaneously (Figure C-15). Because flows were not matched using any combination of heat transfer coefficients from previous case studies, both the wall and atmospheric heat transfer coefficients were varied simultaneously. U_{WALL} was changed between 0 and 800 BTU/(hrft^2°F) while $U_{i,ATM}$ was varied between 5 and 12 BTU/(hrft^2°F). The result from this optimization search still provided no feasible solutions (Figure C-16). Although no heat transfer coefficient values were found to match all the reflux flows to their experimental values, including heat transfer in the model still matched the experimental data better than if no heat transfer was included (Figure C-17). Therefore, heat transfer coefficients were still needed. All of the flows and compositions would not match within their ranges, but compositions and flows necessary for control could be prioritized and matched within reason. Because this case was controlled with a temperature controller in the rectifying section, matching the product compositions and therefore the temperature profile in the rectifying section was important. Matching the reflux flow was also important because the reflux was the manipulated variable for the temperature controller. The heat transfer coefficients which matched the distillate 2-methylpentane composition and the overhead, prefrac, and mainfrac reflux flows while maximizing the sidedraw reflux were 11.23 BTU/(hrft^2°F) and 106 BTU/(hrft^2°F), atmospheric and wall respectively.

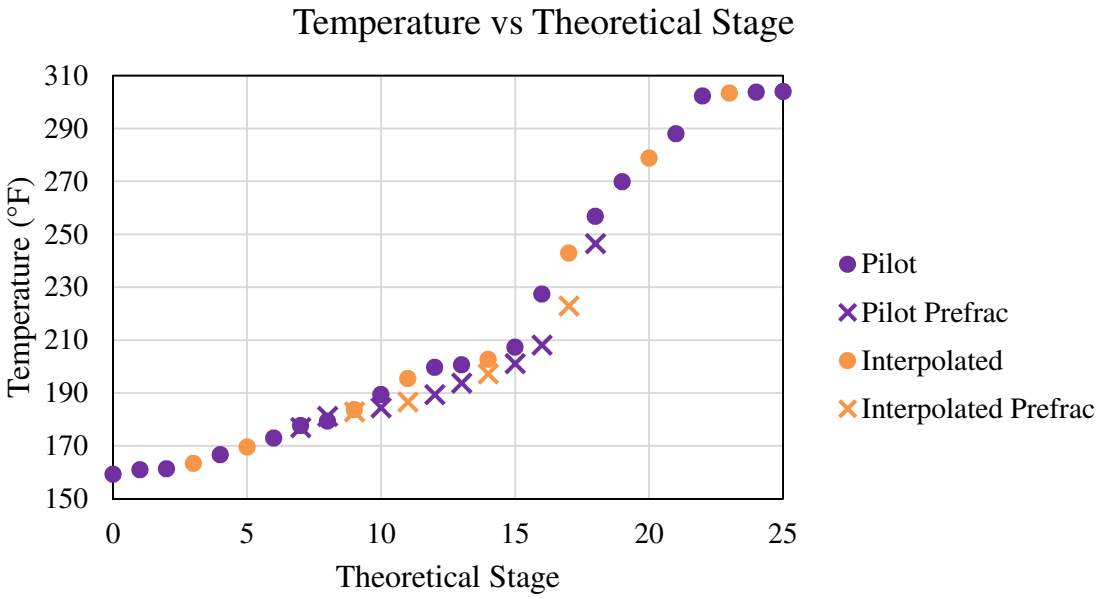

Figure C-12 – Temperature profile for [2MP, C6/tol, mX] finite reflux showing temperatures from experimental data and those interpolated with pchip.

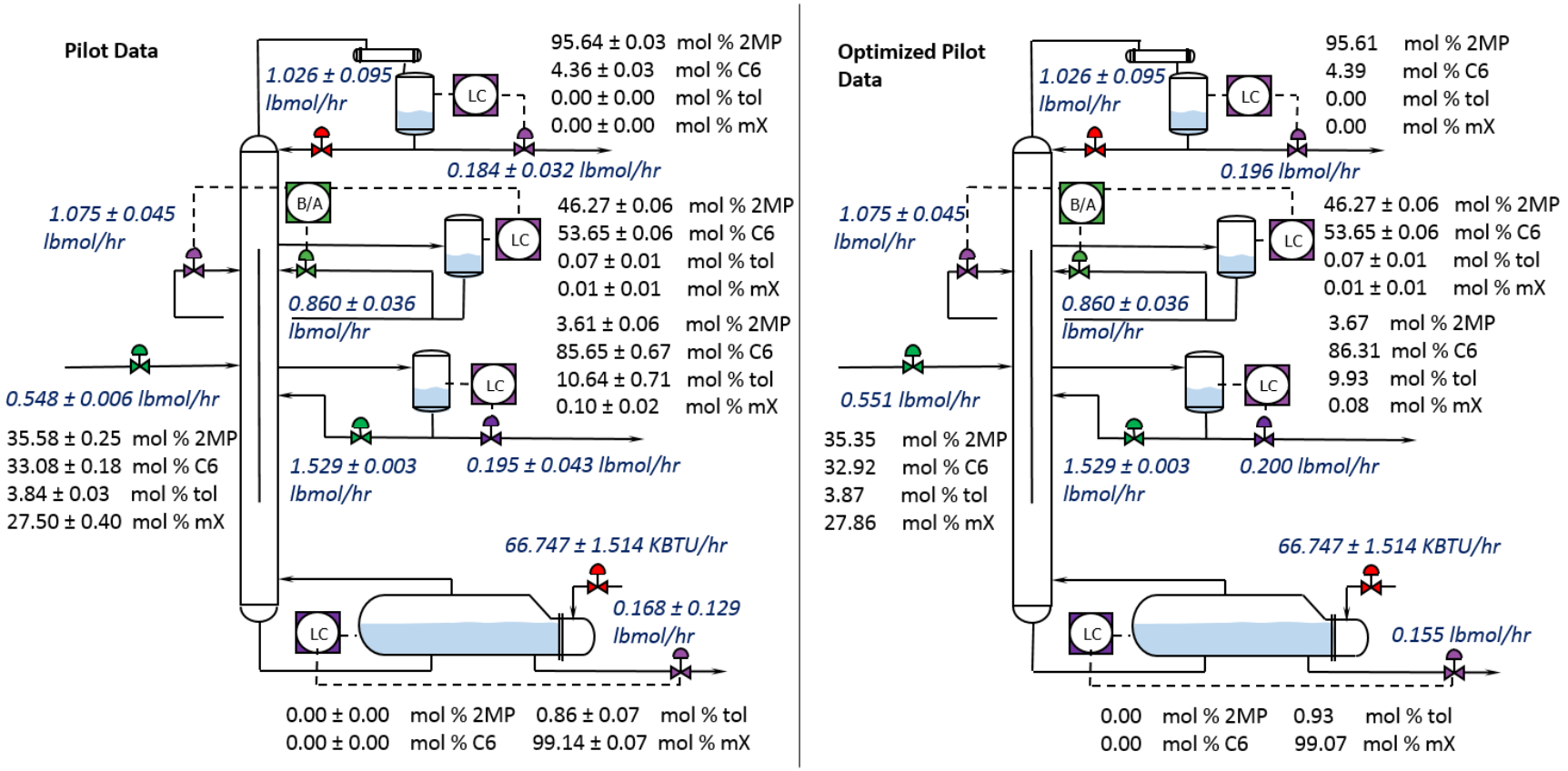

Figure C-13 – Case [2MP, C6/Tol, mX] pilot data vs optimized pilot data

Table C-6. Comparison of [2MP, C6/Tol, mX] finite reflux data from pilot column (left) and data from Aspen Plus® model with U_{WALL} = 0 BTU/(hrft^2°F) (center) and the heat transfer coefficients from case [2MP/C6, Tol, mX] run 2. Neither model matches the pilot data. Ambient temperature for the pilot data was 87.30°F.

Variable	Pilot Data		Aspen Plus®	
	Average	Standard Deviation	$U_{i,ATM}$ = 9.82, U_{WALL} = 0	$U_{i,ATM}$ = 10.78, U_{WALL} = 222.5
Product Compositions (mol %)				
Distillate				
2MP	95.61		96.58	87.38
C6	4.39		3.42	12.60
Tol	0.00		0.00	0.02
mX	0.00		0.00	0.00
Top of Wall				
2MP	46.27	± 0.06	50.06	23.90
C6	53.65	± 0.06	49.83	63.36
Tol	0.07	± 0.01	0.11	12.70
mX	0.01	± 0.01	0.00	0.04
Side				
2MP	3.67		2.74	11.78
C6	86.31		87.21	78.38
Tol	9.93		10.01	9.82
mX	0.08		0.04	0.02
Bottoms				
2MP	0.00		0.00	0.00
C6	0.00		0.00	0.00
Tol	0.93		0.82	1.06
mX	99.07		99.18	98.94
Material Balance Flows (lbmol/hr)				
Distillate	0.196		0.196	0.196
Side	0.200		0.200	0.200
Bottoms	0.155		0.155	0.155
Internal Flows				
Overhead Reflux (lbmol/hr)	1.026	± 0.095	1.389	1.099
Prefrac Reflux (lbmol/hr)	1.075	± 0.045	1.253	1.040
Mainfrac Reflux (lbmol/hr)	0.860	± 0.036	0.984	0.817
Side Reflux (lbmol/hr)	1.529	± 0.003	1.133	1.217
Reboiler Duty (BTU/hr)	66747	± 1514	66747	66747

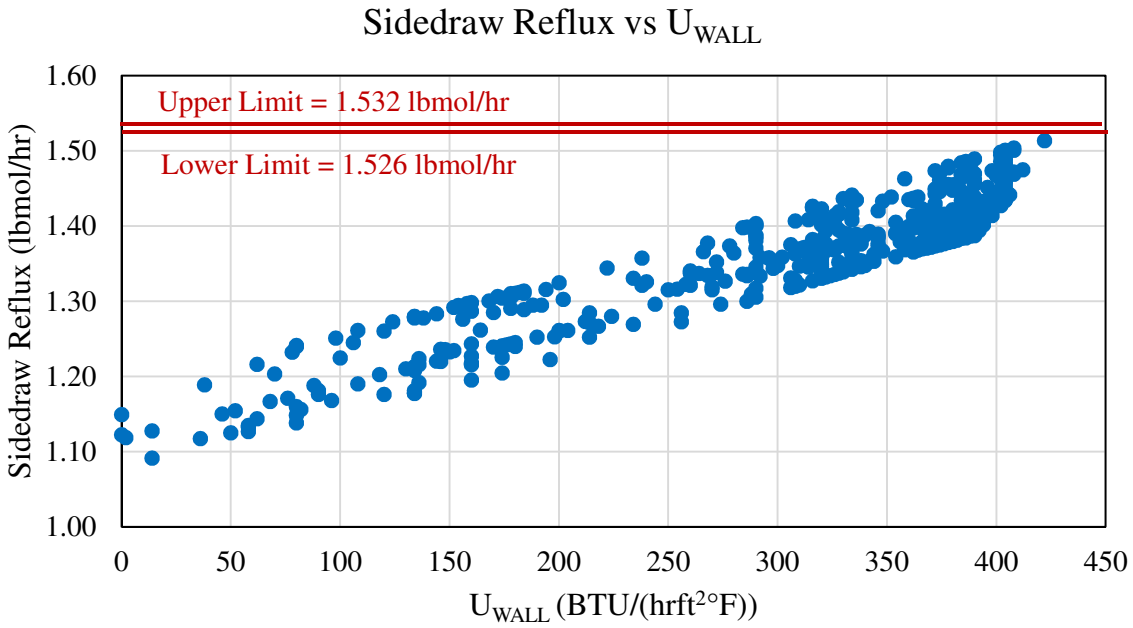

Figure C-14 – Sidedraw reflux versus U_{WALL} for [2MP, C6/tol, mX] finite reflux with $U_{i,ATM}$ of 9.82 BTU/(hrft^2°F) and varying U_{WALL} and Q_R. Simulations stopped around U_{WALL} = 422 BTU/(hrft^2°F) because vapor traffic leaving the upper mainfrac was too low.

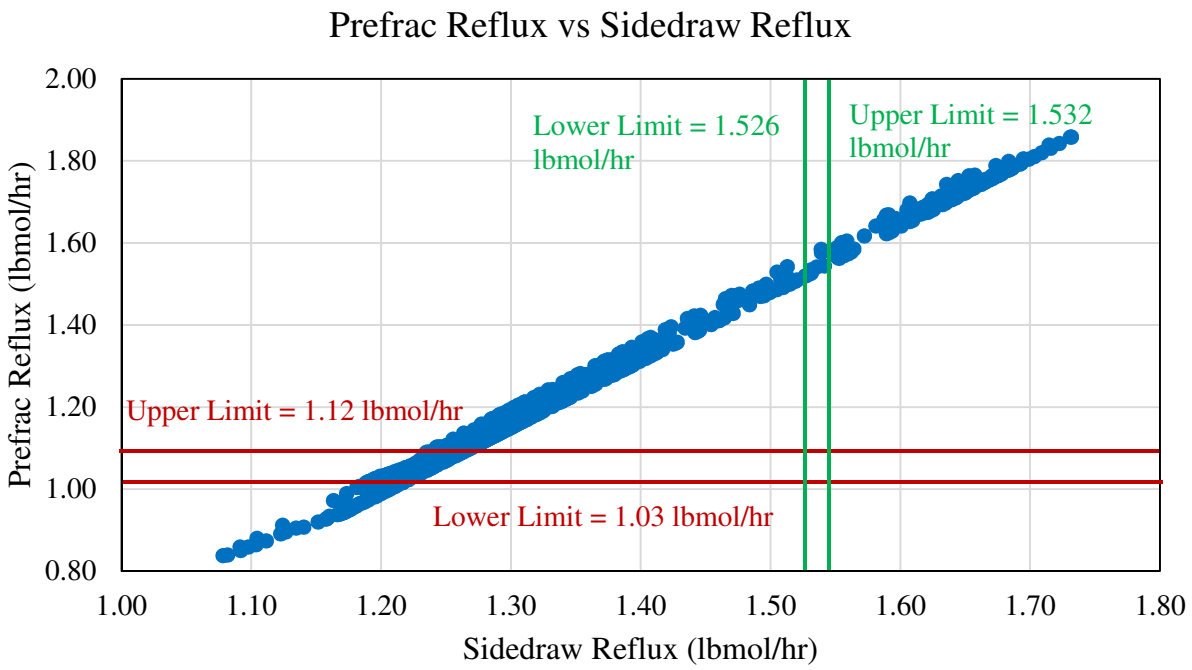

Figure C-15 – Prefrac reflux versus sidedraw reflux for [2MP, C6/tol, mX] finite reflux where $U_{i,ATM}$ was varied and U_{WALL} was 222.5 BTU/(hrft^2°F). Simulations could not satisfy constraints for both flows simultaneously.

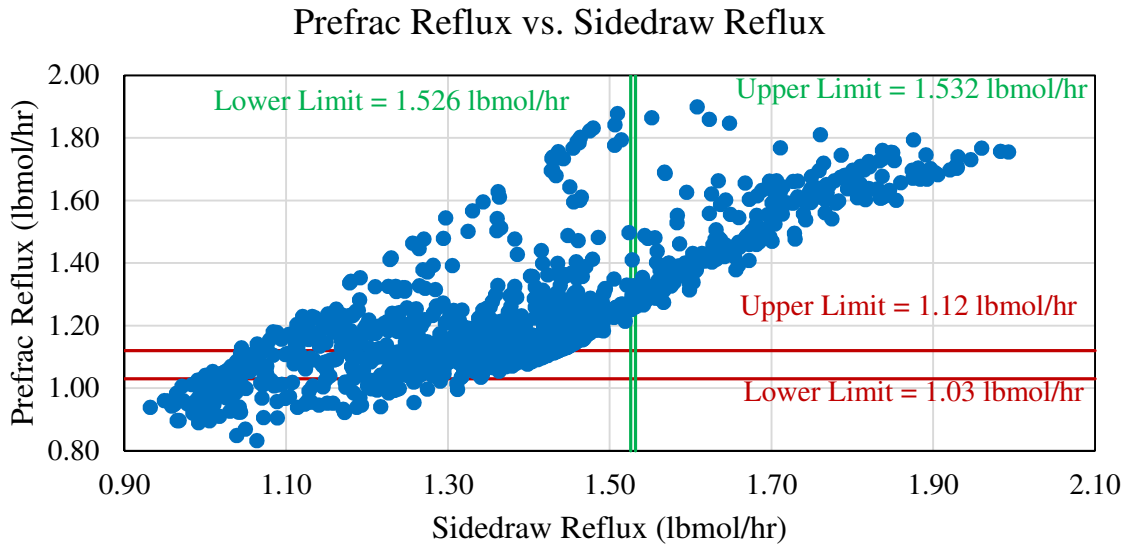

Figure C-16 – Prefrac reflux versus sidedraw reflux for [2MP, C6/tol, mX] finite reflux. Simulations could not satisfy feasibility constraints for both flows at the same time.

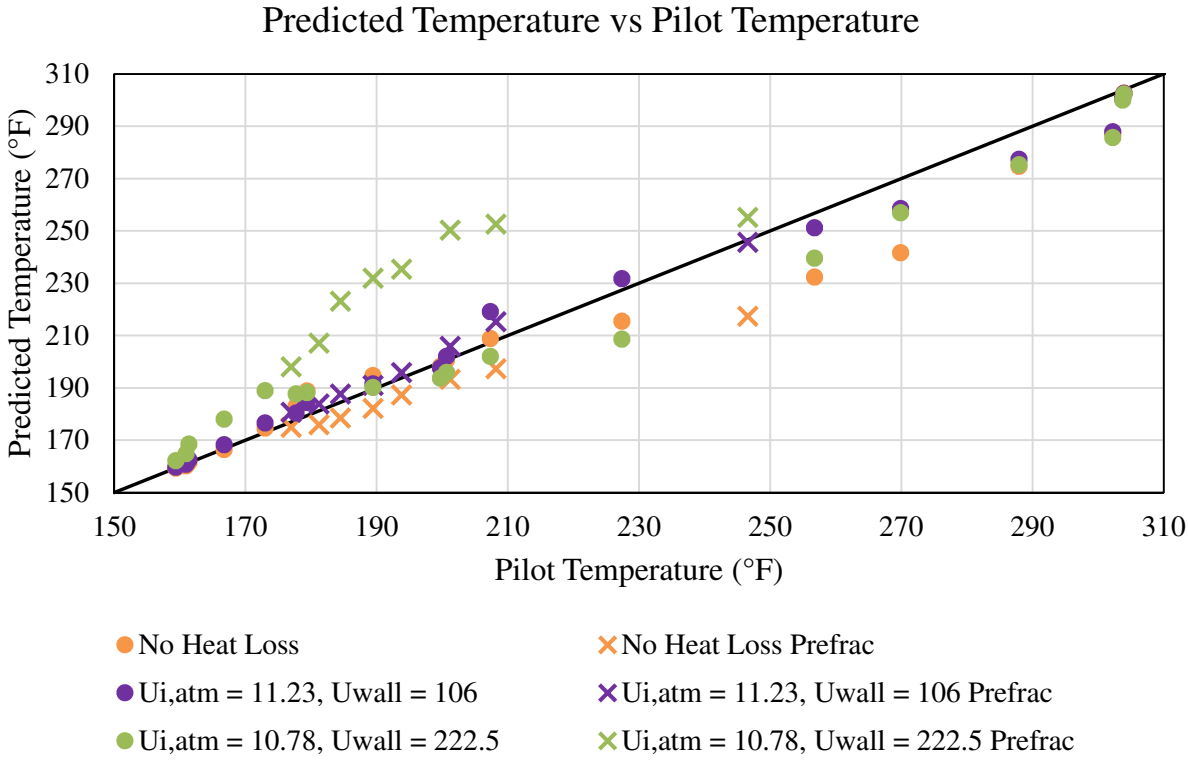

Figure C-17 – Comparison of model and pilot temperatures for [2MP, C6/tol, mX] finite reflux with and without heat loss

Table C-7. Comparison of pilot data, AspenPlus model, and dynamic model for case [2MP, C6/tol, mX]. AspenPlus® and the dynamic model use U_{WALL} = 106 BTU/(hrft^2°F) and $U_{i,ATM}$ = 11.23 BTU/(hrft^2°F). The dynamic model also accounts for pressure drop.

Variable	Pilot Data		Aspen Plus®	Dynamic Model
	Average	Standard Deviation		
Product Compositions (mol %)				
Distillate				
2MP	95.61		95.38	95.57
C6	4.39		4.62	4.43
Tol	0.00		0.00	0.00
mX	0.00		0.00	0.00
Top of Wall				
2MP	46.27	± 0.06	44.94	45.63
C6	53.65	± 0.06	55.01	54.32
Tol	0.07	± 0.01	0.05	0.06
mX	0.01	± 0.01	0.00	0.00
Side				
2MP	3.67		3.92	3.72
C6	86.31		86.06	86.25
Tol	9.93		9.97	9.99
mX	0.08		0.05	0.04
Bottoms				
2MP	0.00		0.00	0.00
C6	0.00		0.00	0.00
Tol	0.93		0.85	0.84
mX	99.07		99.15	99.16
Material Balance Flows (lbmol/hr)				
Distillate	0.196		0.196	0.196
Side	0.200		0.200	0.200
Bottoms	0.155		0.155	0.155
Internal Flows				
Overhead Reflux (lbmol/hr)	1.026	± 0.095	1.120	1.128
Prefrac Reflux (lbmol/hr)	1.075	± 0.045	1.096	1.115
Mainfrac Reflux (lbmol/hr)	0.860	± 0.036	0.861	0.892
Side Reflux (lbmol/hr)	1.529	± 0.003	1.130	1.143
Reboiler Duty (BTU/hr)	66747	± 1514	67837.1	67837

Case [2MP/C6, Tol, mX] Run 1

When wall heat transfer was not accounted for, the model for [2MP/C6, tol, mX] run 1 overestimated the overhead reflux and underestimated the sidedraw reflux (Table C-8). Using $U_{i,ATM}$ of 9.82 BTU/(hrft^2°F) and varying U_{WALL} produced no feasible designs. Although a wall heat transfer coefficient of 320 to 640 BTU/(hrft^2°F) matched the sidedraw reflux flow, simulations which met the sidedraw reflux requirements did not match the overhead and mainfrac reflux flow rates (Figure C-20 and Figure C-21). This suggested that $U_{i,ATM}$ needed to be changed for this case. Because a U_{WALL} value of 388 BTU/(hrft^2°F) matched the sidedraw reflux and was the same value used for case [2MP, C6, mX], U_{WALL} was set to 388 and $U_{i,ATM}$ was varied. This resulted in a singular feasible $U_{i,ATM}$ value of 10.78 BTU/(hrft^2°F) (Figure C-22 and Table C-9).

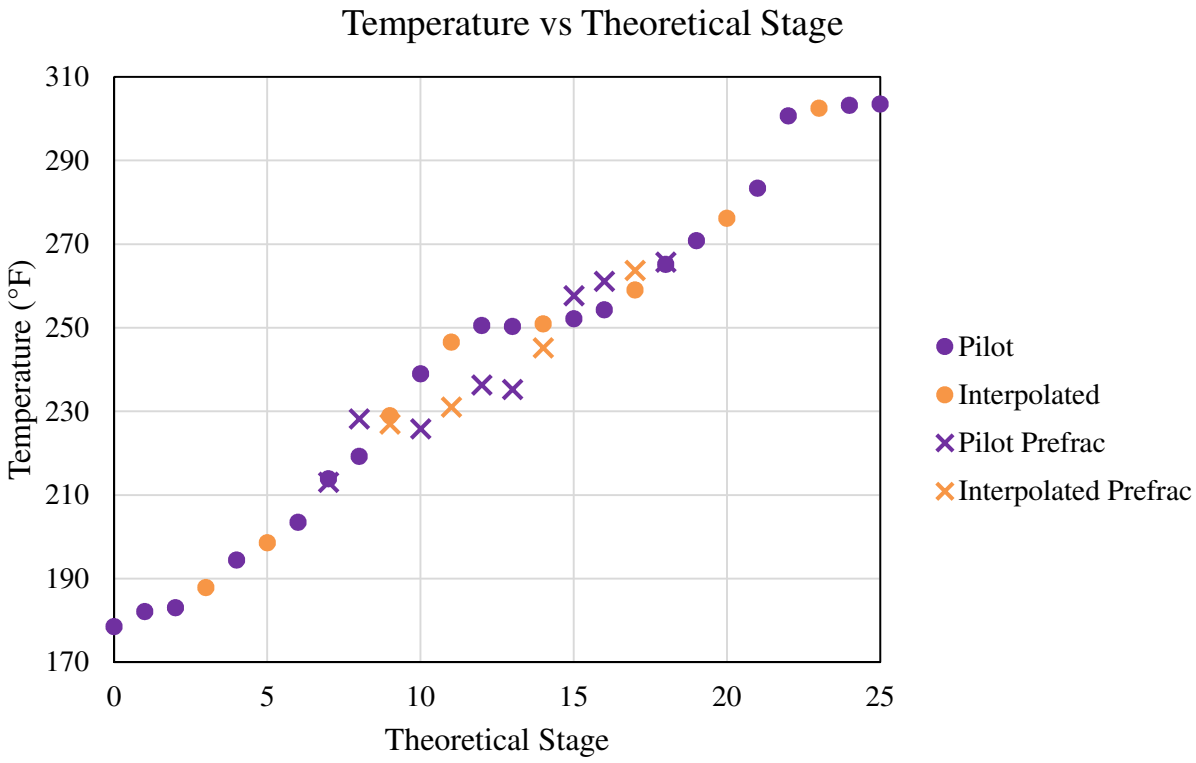

Figure C-18 – Temperature profile for [2MP/C6, tol, mX] finite reflux showing temperatures from experimental data and those interpolated with pchip.

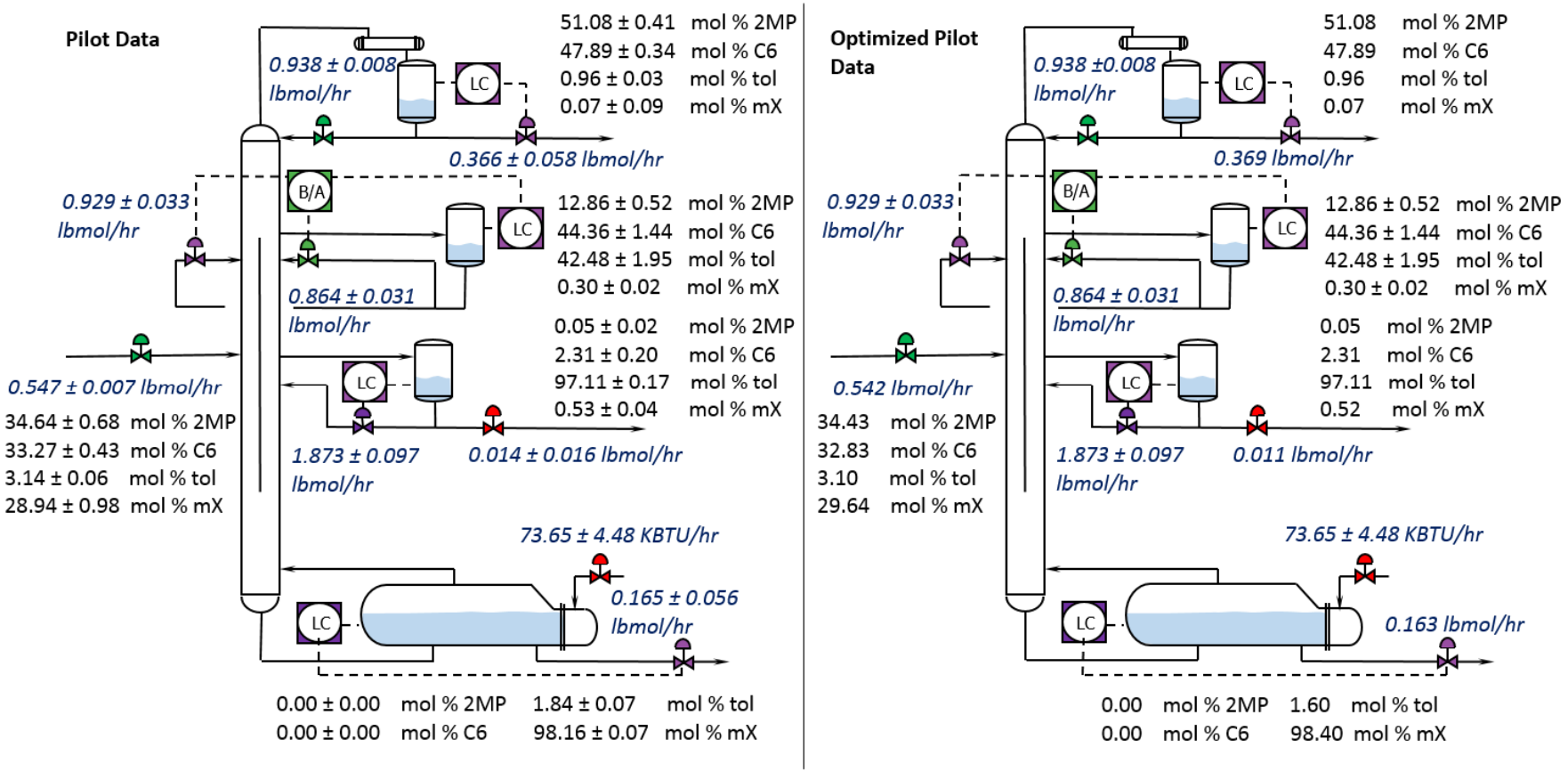

Figure C-19 – Case [2MP/C6, Tol, mX] run 1 pilot data vs optimized pilot data

Table C-8. Comparison of [2MP/C6, Tol, mX] run 1 finite reflux data from pilot column (left) and data from Aspen Plus® model with $U_{i,ATM}$ = 9.82 BTU/(hrft^2°F) and U_{WALL} = 0 BTU/(hrft^2°F) (right). Ambient temperature for the pilot data was 82.87°F.

Variable	Pilot Data		Aspen Plus®
	Average	Standard Deviation	$U_{i,ATM}$ = 9.82, U_{WALL} = 0
Product Compositions (mol %)			
Distillate			
2MP	51.08		50.60
C6	47.89		48.24
Tol	0.96		1.17
mX	0.07		0.00
Top of Wall			
2MP	12.86	± 0.52	8.43
C6	44.36	± 1.44	36.94
Tol	42.49	± 1.95	54.59
mX	0.30	± 0.02	0.04
Side			
2MP	0.05		0.01
C6	2.31		0.15
Tol	97.11		98.16
mX	0.52		1.68
Bottoms			
2MP	0.00		0.00
C6	0.00		0.00
Tol	1.60		1.16
mX	98.40		98.84
Material Balance Flows (lbmol/hr)			
Distillate	0.369		0.369
Side	0.011		0.011
Bottoms	0.163		0.163
Internal Flows			
Overhead Reflux (lbmol/hr)	0.938	± 0.008	0.970
Prefrac Reflux (lbmol/hr)	0.929	± 0.033	0.918
Mainfrac Reflux (lbmol/hr)	0.864	± 0.031	0.848
Side Reflux (lbmol/hr)	1.873	± 0.097	1.321
Reboiler Duty (BTU/hr)	73650	± 4480	73650

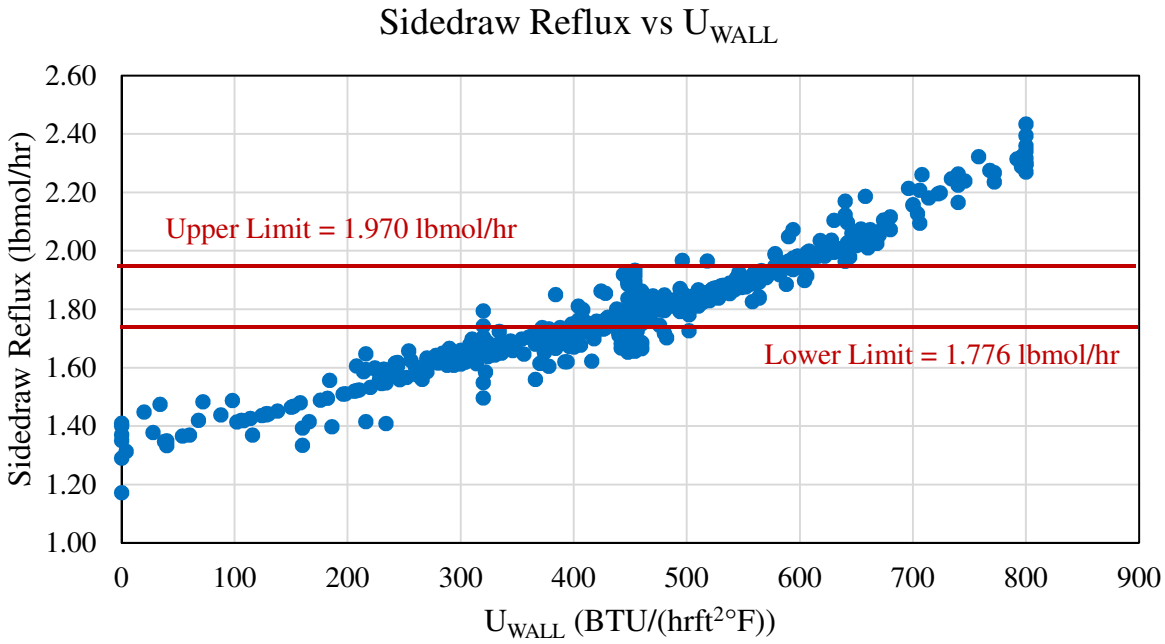

Figure C-20 – Sidedraw reflux versus U_{WALL} for [2MP/C6, tol, mX] finite reflux run 1 with $U_{i,ATM}$ of 9.82 BTU/(hrft²°F). U_{WALL} values between 320 and 640 BTU/(hrft²°F) matched the sidedraw reflux within its constraints. However, simulations could not satisfy feasibility constraints for all reflux flows at the same time.

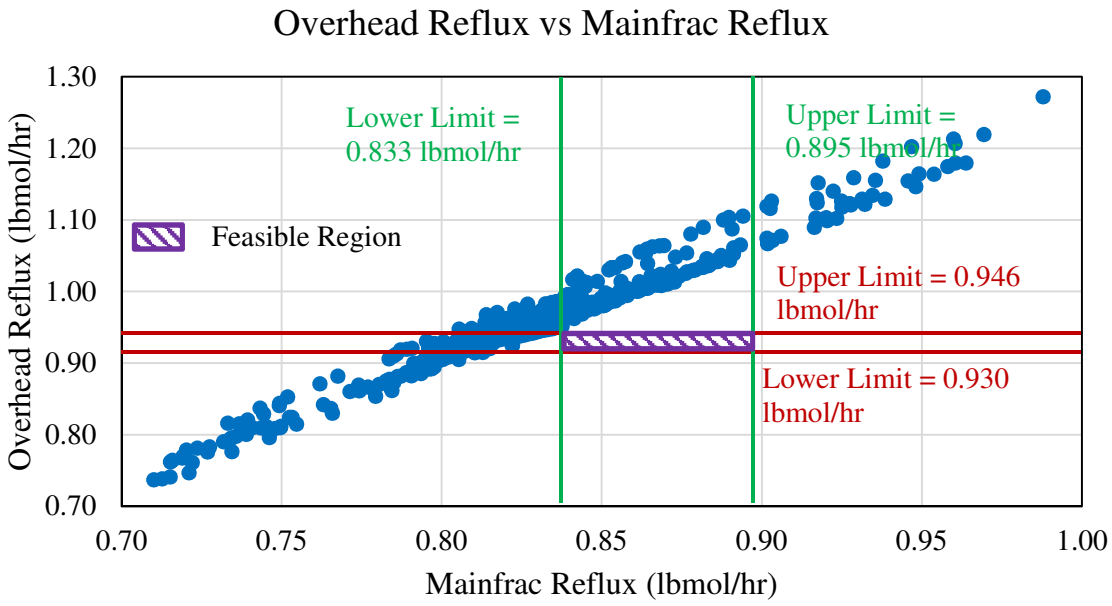

Figure C-21 – Overhead reflux versus mainfrac reflux for [2MP/C6, tol, mX] finite reflux run 1 with $U_{i,ATM}$ of 9.82 BTU/(hrft²°F) and varying U_{WALL} and Q_R. Simulations could not satisfy feasibility constraints for both flows at the same time.

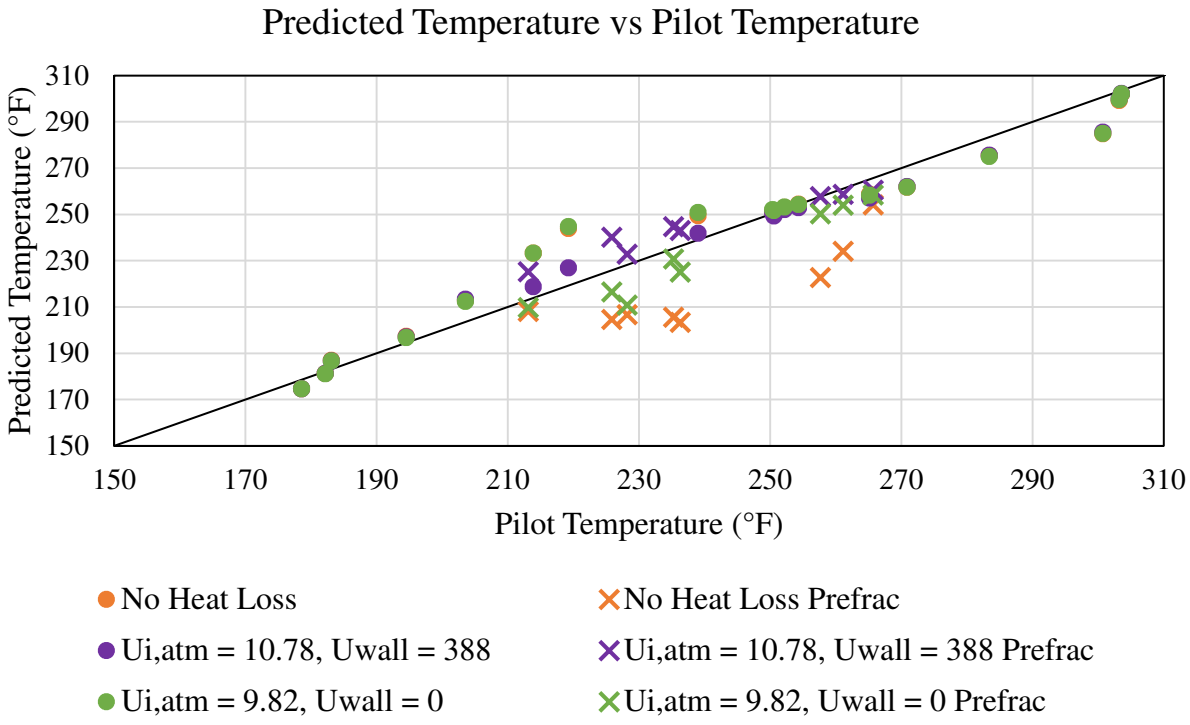

Figure C-22 – Comparison of model and pilot temperatures for [2MP/C6, tol, mX] finite reflux run 1 with and without heat loss

Table C-9. Comparison of pilot data, AspenPlus model, and dynamic model for case [2MP/C6, tol, mX] run 1. AspenPlus and the dynamic model use U_{WALL} = 388 BTU/(hrft^2°F) and $U_{i,ATM}$ = 10.78 BTU/(hrft^2°F). The dynamic model also accounts for pressure drop.

Variable	Pilot Data		Aspen Plus®	Dynamic Model
	Average	Standard Deviation		
Product Compositions (mol %)				
Distillate				
2MP	51.08		50.60	50.60
C6	47.89		48.18	48.22
Tol	0.96		1.22	1.18
mX	0.07		0.00	0.00
Top of Wall				
2MP	12.86	± 0.52	8.26	8.37
C6	44.36	± 1.44	35.59	36.45
Tol	42.49	± 1.95	55.62	54.88
mX	0.30	± 0.02	0.53	0.30
Side				
2MP	0.05		0.05	0.02
C6	2.31		1.92	0.71
Tol	97.11		97.36	98.66
mX	0.52		0.67	0.61
Bottoms				
2MP	0.00		0.00	0.00
C6	0.00		0.00	0.00
Tol	1.60		1.09	1.08
mX	98.40		98.91	98.92
Material Balance Flows (lbmol/hr)				
Distillate	0.369		0.369	0.369
Side	0.011		0.012	0.011
Bottoms	0.163		0.162	0.163
Internal Flows				
Overhead Reflux (lbmol/hr)	0.938	± 0.008	0.945	0.945
Prefrac Reflux (lbmol/hr)	0.929	± 0.033	0.926	0.926
Mainfrac Reflux (lbmol/hr)	0.864	± 0.031	0.854	0.861
Side Reflux (lbmol/hr)	1.873	± 0.097	1.776	1.847
Reboiler Duty (BTU/hr)	73650	± 4480	78130	78130

Case [2MP/C6, Tol, mX] Run 2

Similar to run 1 of [2MP/C6, tol, mX], not including wall heat transfer in the model led to a high reflux flow and a low sidedraw reflux flow (Table C-10). Similarly, using a constant $U_{i,ATM}$ of 9.82 BTU/(hrft^2°F) and varying U_{WALL} resulted in no feasible solutions. Although both the mainfrac and sidedraw reflux constraints could be met simultaneously (Figure C-25), the overhead and prefrac reflux constraints could not (Figure C-26). Using the heat transfer coefficients from run 1 and varying the reboiler duty resulted in simulations which consistently overpredicted the sidedraw reflux value and sometimes matched the other reflux flows (Figure C-27).

Because $U_{i,ATM}$ more greatly impacts the overhead and wall reflux flows and those were feasible, $U_{i,ATM}$ was kept constant and U_{WALL} was varied. This resulted in feasible solutions for wall heat transfer coefficient values between 222.5 and 282.5 BTU/(hrft^2°F) (Figure C-28). The overhead, prefrac, mainfrac, and sidedraw reflux flows were all within their constraints. To determine the optimal wall heat transfer coefficient, the impact of U_{WALL} on the side product toluene composition was examined (Figure C-29). The side product was chosen because the pure product streams for this case study are the side product and the bottoms product. The bottoms product has been shown to not have little correlation with the wall heat transfer coefficient. In addition, the top of the wall composition showed the same trend as that of the side product. A wall heat transfer coefficient of 222.5 BTU/(hrft^2°F) most closely matched the experimental toluene composition of 97.62 mole percent. The heat transfer coefficients of 10.78 BTU/(hrft2°F) and 222.5 BTU/(hrft2°F), atmospheric and wall respectively, provide the closest match to the temperature profile from the pilot data (Figure C-30). Note that a wall heat transfer coefficient of 388 BTU/(hrft2°F) actually predicts a larger temperature difference between the prefrac and mainfrac sections than does the heat transfer coefficient of 222.5 BTU/(hrft2°F). This difference highlights the importance of product composition in determining temperature profiles. More heat transfer across the wall should lead to a lower temperature difference across the wall. However, the large change in compositions at the top of the wall and in the side product (Table C-11) have a larger impact on the column temperature profile than the increase in heat transfer across the wall.

Run 1 and run 2 had the same product distribution and control structure and yet different wall heat transfer coefficients. As stating previously, this could be a result of changes in the heat transfer area that was assumed constant. Due to the lower ambient temperature and therefore higher heat loss to the atmosphere, run 1 had a higher reboiler duty. Therefore there was more liquid

traffic inside the column. The higher liquid flows at the top of the wall could have caused more liquid to coat the wall due to maldistribution within the packing. This increase in heat transfer area is seen as an increase in wall heat transfer coefficient in run 1.

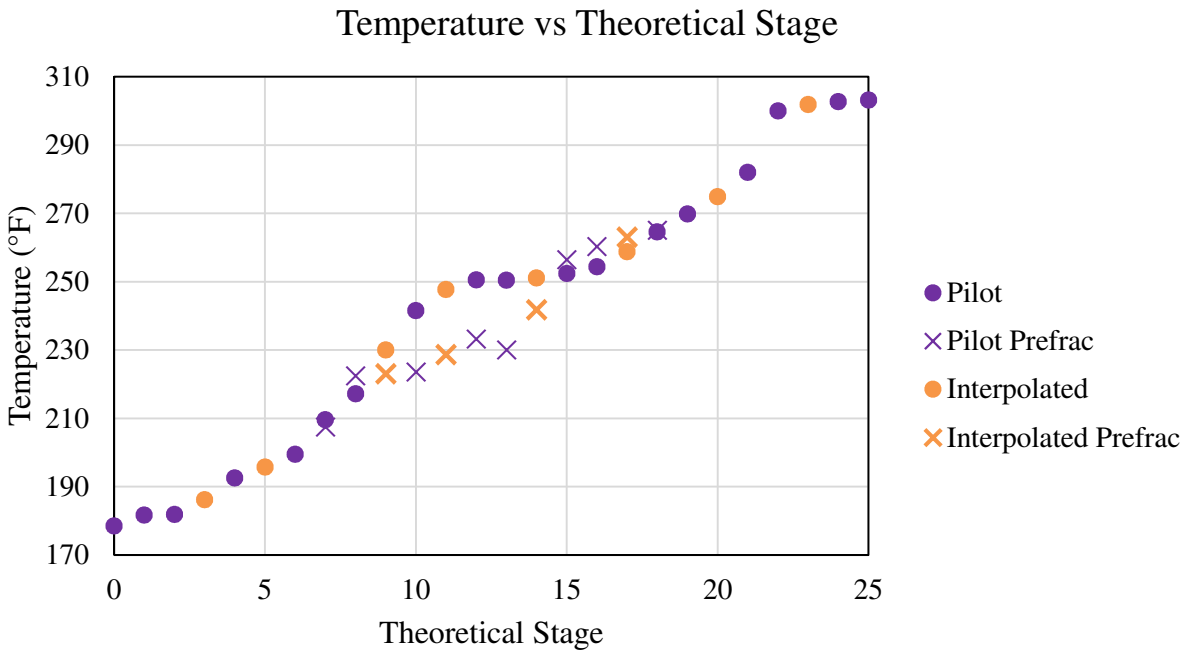

Figure C-23 – Temperature profile for [2MP/C6, tol, mX] finite reflux run 2 showing temperatures from experimental data and those interpolated with pchip.

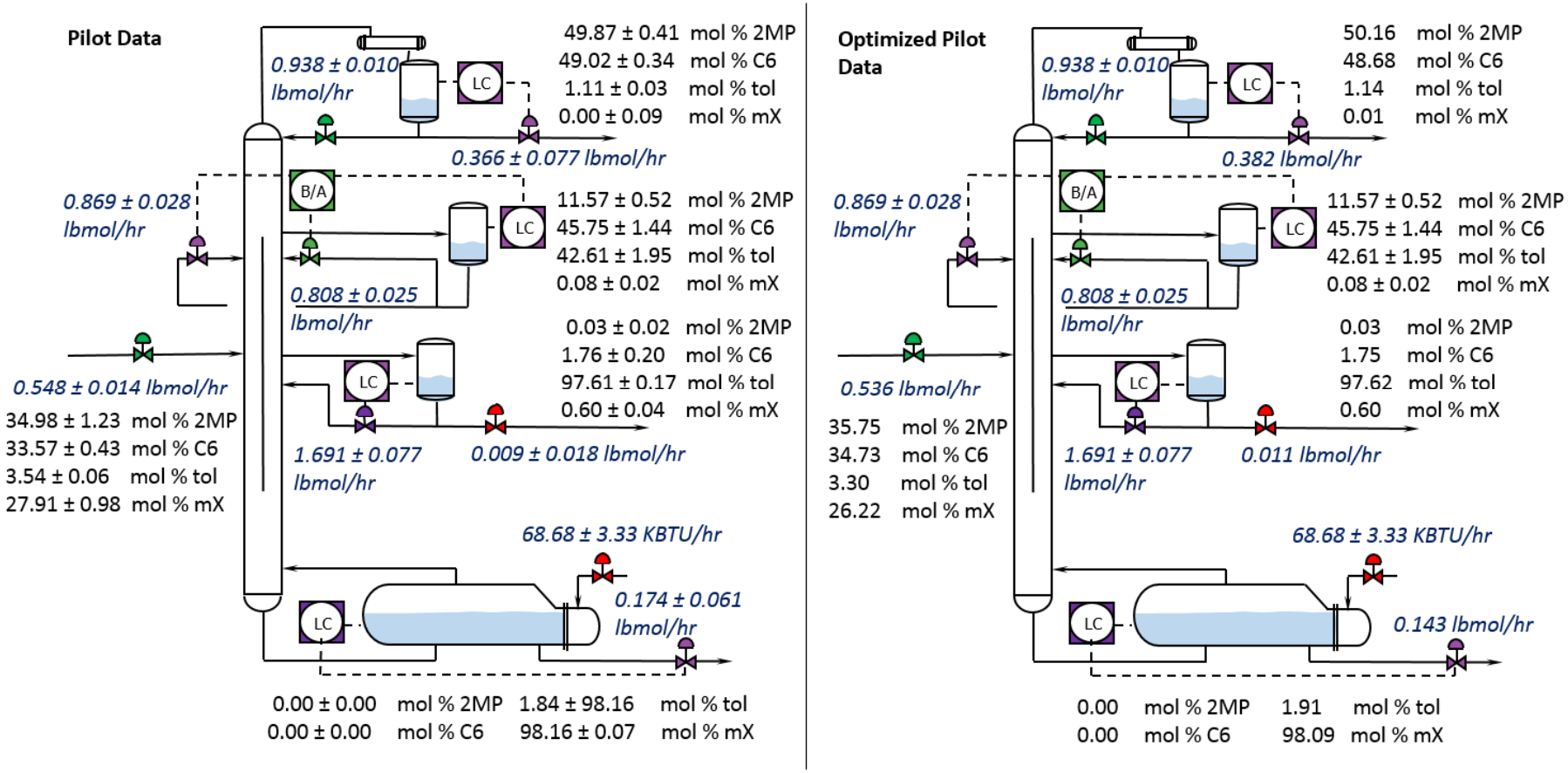

Figure C-24 – Case [2MP/C6, Tol, mX] run 2 pilot data vs optimized pilot data

Table C-10. Comparison of [2MP/C6, Tol, mX] run 2 finite reflux data from pilot column (left) and data from Aspen Plus® model with $U_{i,ATM}$ = 9.82 BTU/(hrft^2°F) and U_{WALL} = 0 BTU/(hrft^2°F) (center) and the heat transfer coefficients from run 1 (right). Neither model matches the pilot data well. Ambient temperature for the pilot data was 99.34°F.

Variable	Pilot Data		Aspen Plus®	
	Average	Standard Deviation	$U_{i,ATM}$ = 9.82, U_{WALL} = 0	$U_{i,ATM}$ = 10.78, U_{WALL} = 388
Product Compositions (mol %)				
Distillate				
2MP	50.16		50.16	50.12
C6	48.68		48.73	47.45
Tol	1.14		1.11	0.03
mX	0.01		0.00	0.00
Top of Wall				
2MP	11.57	± 0.52	9.05	6.54
C6	45.75	± 1.44	39.63	20.41
Tol	42.61	± 1.95	51.29	69.53
mX	0.08	± 0.02	0.03	3.52
Side				
2MP	0.03		0.01	1.40
C6	1.75		0.28	44.00
Tol	97.62		98.31	52.90
mX	0.60		1.40	1.70
Bottoms				
2MP	0.00		0.00	0.00
C6	0.00		0.00	0.00
Tol	1.91		2.01	1.70
mX	98.09		97.99	98.30
Material Balance Flows (lbmol/hr)				
Distillate	0.382		0.382	0.382
Side	0.011		0.011	0.011
Bottoms	0.143		0.143	0.143
Internal Flows				
Overhead Reflux (lbmol/hr)	0.938	± 0.010	0.990	1.030
Prefrac Reflux (lbmol/hr)	0.869	± 0.028	0.869	0.885
Mainfrac Reflux (lbmol/hr)	0.808	± 0.025	0.802	0.817

Table C-10. continued

Side Reflux (lbmol/hr)	1.691	± 0.077	1.227	2.026
Reboiler Duty (BTU/hr)	68680	± 3330	68680	72010

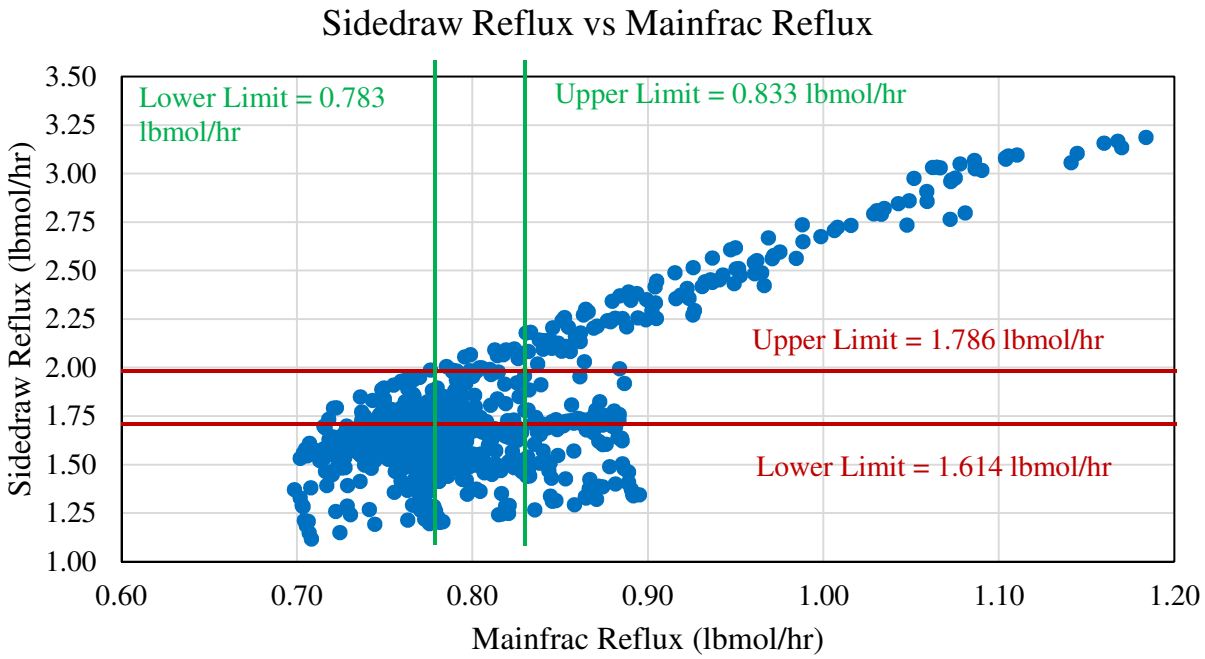

Figure C-25 – Sidedraw reflux versus mainfrac reflux for [2MP/C6, tol, mX] finite reflux run 2 with $U_{i,ATM}$ of 9.82 BTU/(hrft^2°F) and varying U_{WALL} and Q_R. Simulations could satisfy feasibility constraints for both flows at the same time.

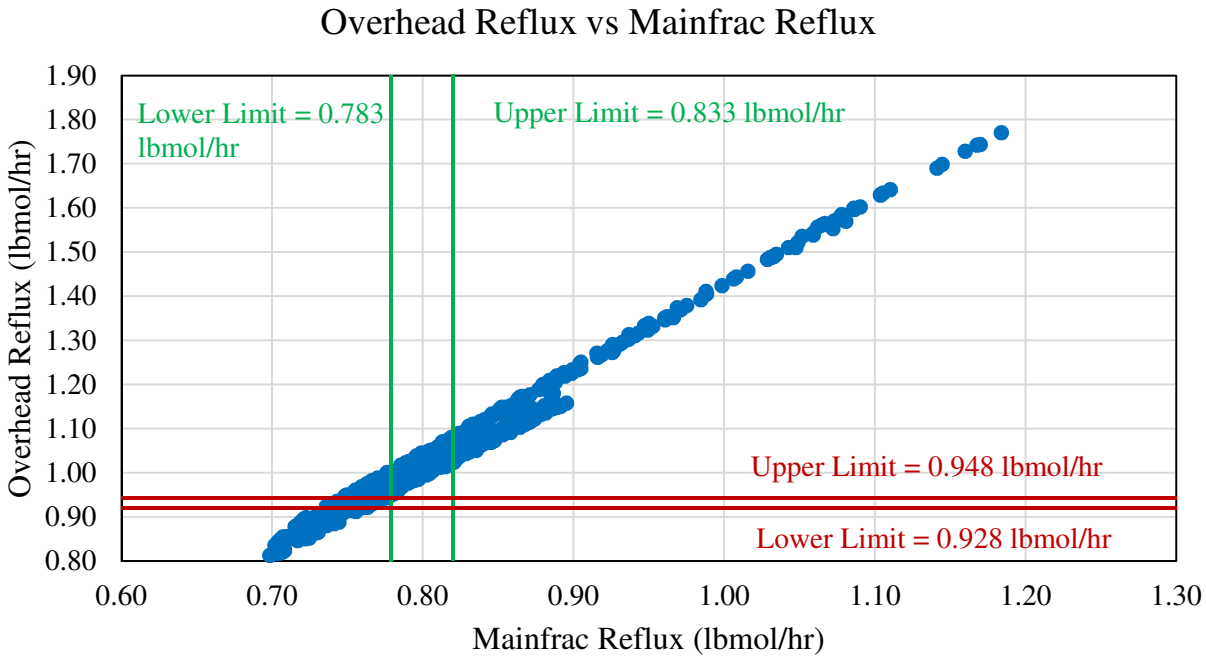

Figure C-26 – Overhead reflux versus mainfrac reflux for [2MP/C6, tol, mX] finite reflux run 2 with $U_{i,ATM}$ of 9.82 BTU/(hrft^2°F) and varying U_{WALL} and Q_R. Simulations could not satisfy feasibility constraints for both flows at the same time.

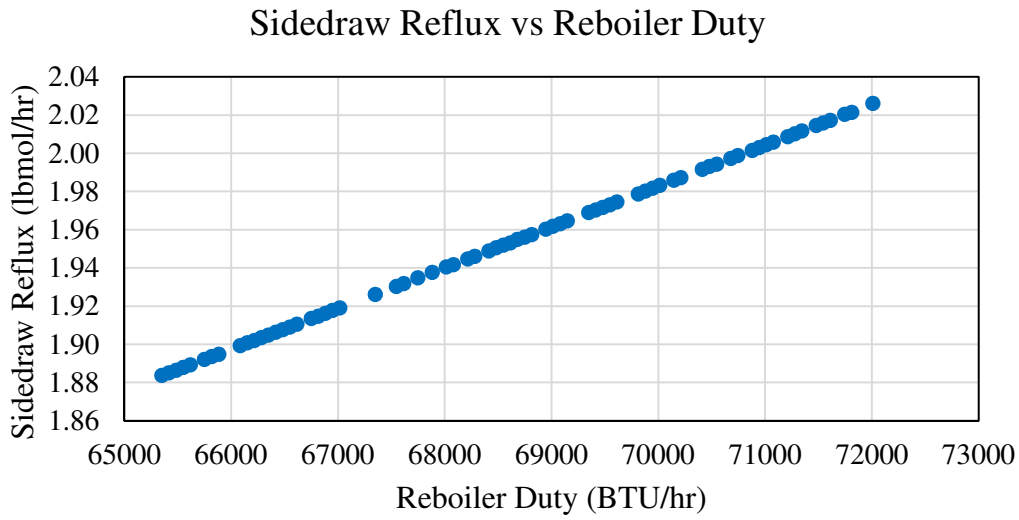

Figure C-27 – Sidedraw reflux versus Q_R for [2MP/C6, tol, mX] finite reflux run 2 for $U_{i,ATM}$ of 10.78 BTU/(hrft^2°F), U_{WALL} of 388 BTU/(hrft^2°F) and varying Q_R. The feasible region for sidedraw reflux is 1.614 – 1.768 lbmol/hr.

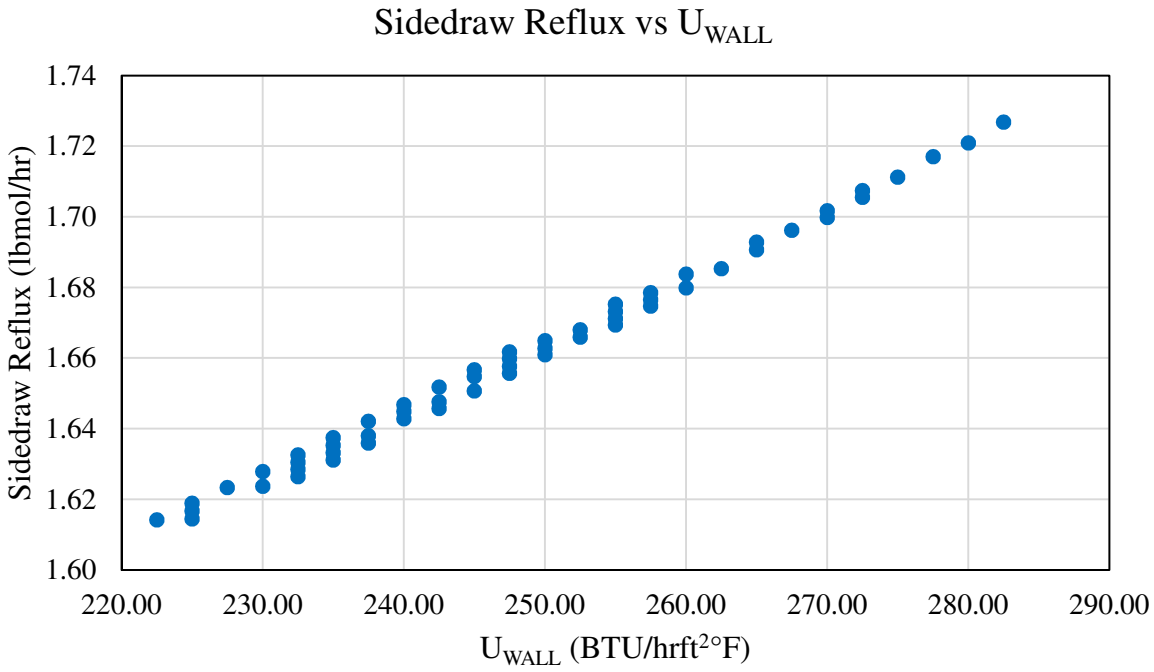

Figure C-28 – Sidedraw reflux versus U_{WALL} for [2MP/C6, tol, mX] finite reflux run 2 with $U_{i,ATM}$ of 10.78 BTU/(hrft^2°F) and varying U_{WALL} and Q_R. The feasible range for sidedraw reflux is 1.614 – 1.778 lbmol/hr.

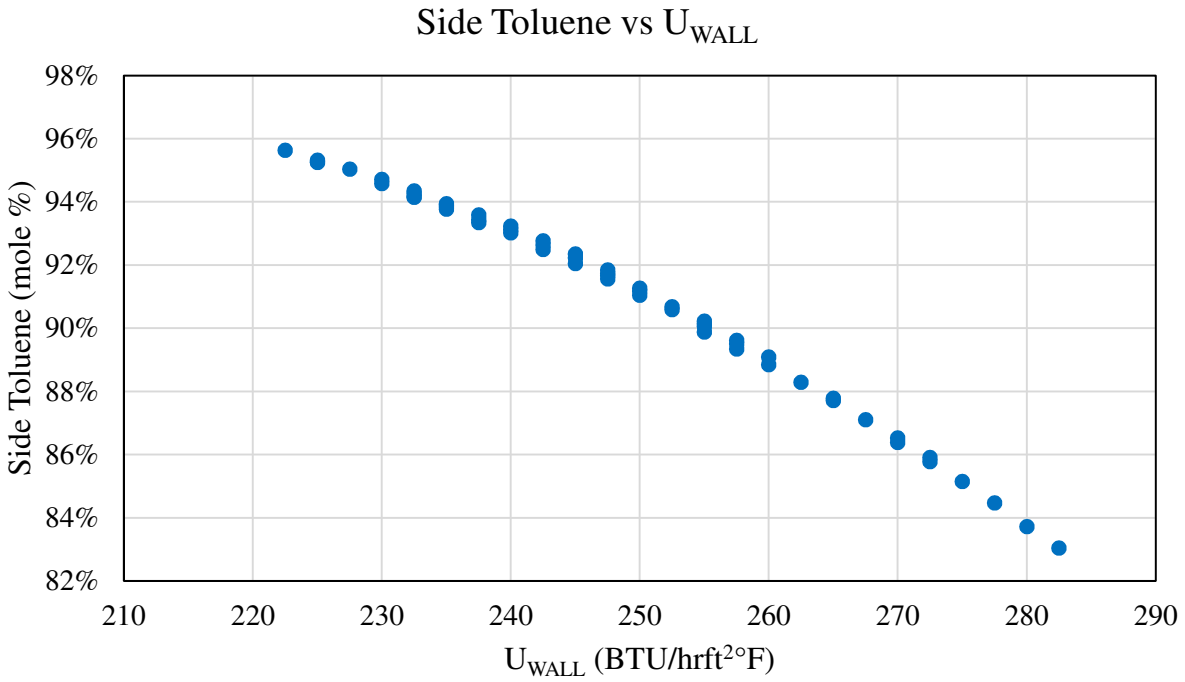

Figure C-29 – Side toluene composition versus U_{WALL} for [2MP/C6, tol, mX] finite reflux run 2. Average side product toluene composition from experiment was 97.62 mole percent.

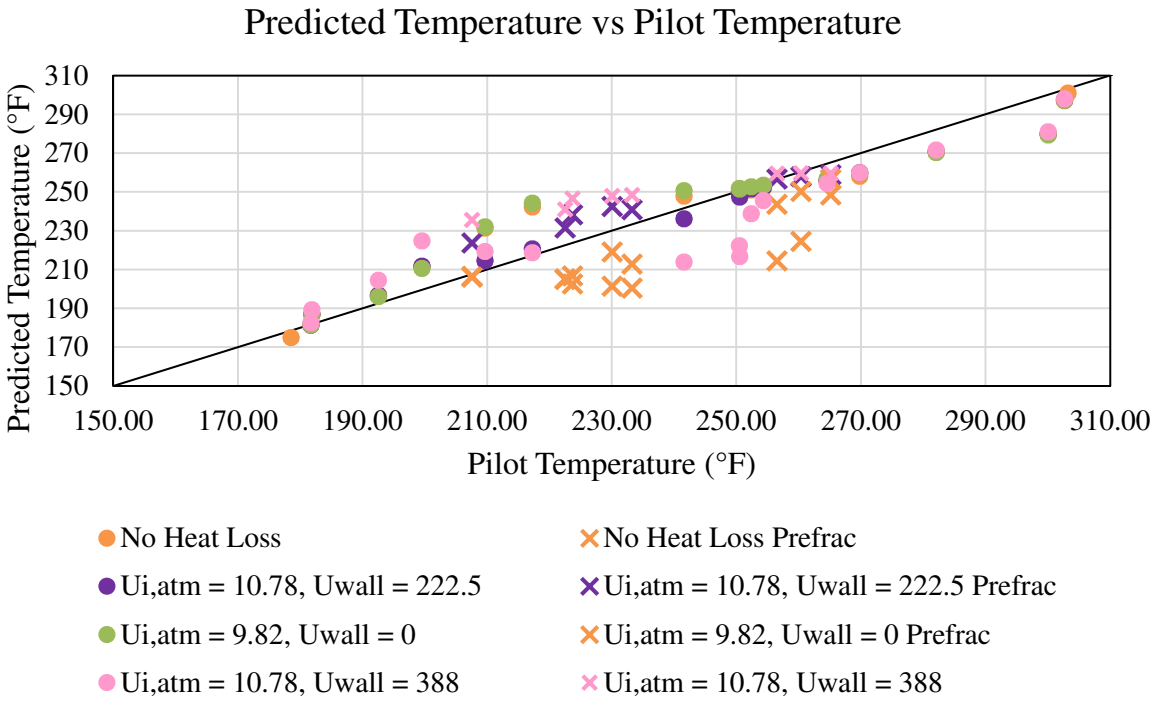

Figure C-30 – Comparison of model and pilot temperatures for [2MP/C6, tol, mX] finite reflux run 2 with and without heat loss

Table C-11. Comparison of pilot data, AspenPlus model, and dynamic model for case [2MP/C6, tol, mX] run 2. AspenPlus and the dynamic model use U_{WALL} = 222.5 BTU/(hrft^2°F) and $U_{i,ATM}$ = 10.78 BTU/(hrft^2°F). The dynamic model also accounts for pressure drop.

Variable	Pilot Data		Aspen Plus®	Dynamic Model
	Average	Standard Deviation		
Product Compositions (mol %)				
Distillate				
2MP	50.16		50.16	50.16
C6	48.68		48.64	48.72
Tol	1.14		1.20	1.12
mX	0.01		0.00	0.00
Top of Wall				
2MP	11.57	± 0.52	8.94	9.12
C6	45.75	± 1.44	37.56	39.37
Tol	42.61	± 1.95	52.97	51.32
mX	0.08	± 0.02	0.53	0.20

Table C-11. continued

Side				
2MP	0.03		0.09	0.02
C6	1.75		3.68	0.72
Tol	97.62		95.64	98.78
mX	0.60		0.59	0.48
Bottoms				
2MP	0.00		0.00	0.00
C6	0.00		0.00	0.00
Tol	1.91		1.90	1.89
mX	98.09		98.10	98.11
Material Balance Flows (lbmol/hr)				
Distillate	0.382		0.382	0.382
Side	0.011		0.011	0.011
Bottoms	0.143		0.143	0.143
Internal Flows				
Overhead Reflux (lbmol/hr)	0.938	± 0.010	0.939	0.952
Prefrac Reflux (lbmol/hr)	0.869	± 0.028	0.854	0.863
Mainfrac Reflux (lbmol/hr)	0.808	± 0.025	0.788	0.802
Side Reflux (lbmol/hr)	1.691	± 0.077	1.614	1.627
Reboiler Duty (BTU/hr)	68680	± 3330	72010	72010

Appendix D: DYNAMICS

MODEL TUNING

The dynamic model does not have flow controllers. Instead, these flows changed instantaneously. Therefore, the only tuning changes necessary were the level and temperature controllers. DeltaV™ uses a reset in seconds while the dynamic model uses a reset in minutes. Therefore, the experimental resets were converted to minutes before being placed in the model. The gain in DeltaV™ has units of percent output/percent measurement (output being the manipulated variable and measurement or input being the controlled variable). However, the model gain has engineering units. The controller input and output ranges were used to convert between the two, and an example calculation for TC6072 is shown in (D-1.

$$Gain_{Model} = 3 * \frac{144^{lb}/_{hr}}{100\ \%} * \frac{100\ \%}{400°F} = 1.08 \text{ lb/hr/°F} \quad \textbf{(D-1)}$$

Table D-1. Comparison of Experimental and Model Tuning

Section	Loop	Experimental				Model	
		Gain	Reset	Input Range	Output Range	Gain	Reset
Bottoms	LC602	6	1000	30	200	40	16.7
	TC6072	3	1200	400	144	1.08	20
Side Draw	LC640	10	900	41.1	300	73	15
	TC6075	2	14400	400	300	1.5	240
Top of Wall	LC630	10	900	42.28	500	118	15
Overhead	LC603	22	900	50	100	44	15

COMPARISON OF PILOT DWC AND MODEL BEFORE DISTURBANCE

Table D-2. Comparison of Experimental and Model before Disturbance

Variable		Pilot Data		Dynamic Model
		Average	Standard Deviation	
Product Compositions (mol %)				
Distillate				
2MP		50.64		50.92
C6		48.17		48.41
Tol		1.16		0.67
mX		0.04		0.00
Top of Wall				
2MP		12.80	± 0.52	10.23
C6		43.77	± 1.44	52.09
Tol		43.30	± 1.95	37.54
mX		0.13	± 0.02	0.15
Side				
2MP		0.05		0.04
C6		2.00		1.91
Tol		97.36		97.11
mX		0.59		0.94
Bottoms				
2MP		0.00		0.00
C6		0.00		0.00
Tol		1.55		0.28
mX		98.45		99.72
Material Balance Flows (lbmol/hr)				
Distillate		0.389		0.388
Side		0.011		0.015
Bottoms		0.144		0.143
Internal Flows				
Overhead Reflux	lbmol/hr	0.937	± 0.072	0.939
	Temperature (°F)	76.82	± 0.48	76.82
Prefrac Reflux	lbmol/hr	0.964	± 0.042	0.945
	Temperature (°F)	178.19	± 1.25	178.19
Mainfrac Reflux	lbmol/hr	0.897	± 0.038	0.879
	Temperature (°F)	174.44	± 1.25	174.44
Side Reflux	lbmol/hr	1.958	± 0.112	1.710
	Temperature (°F)	232.73	± 1.27	232.00

Table D-2. continued

Reboiler Duty (BTU/hr)	77486	± 4870	77284
Ambient Temperature (°F)	81.19	± 0.94	81.19

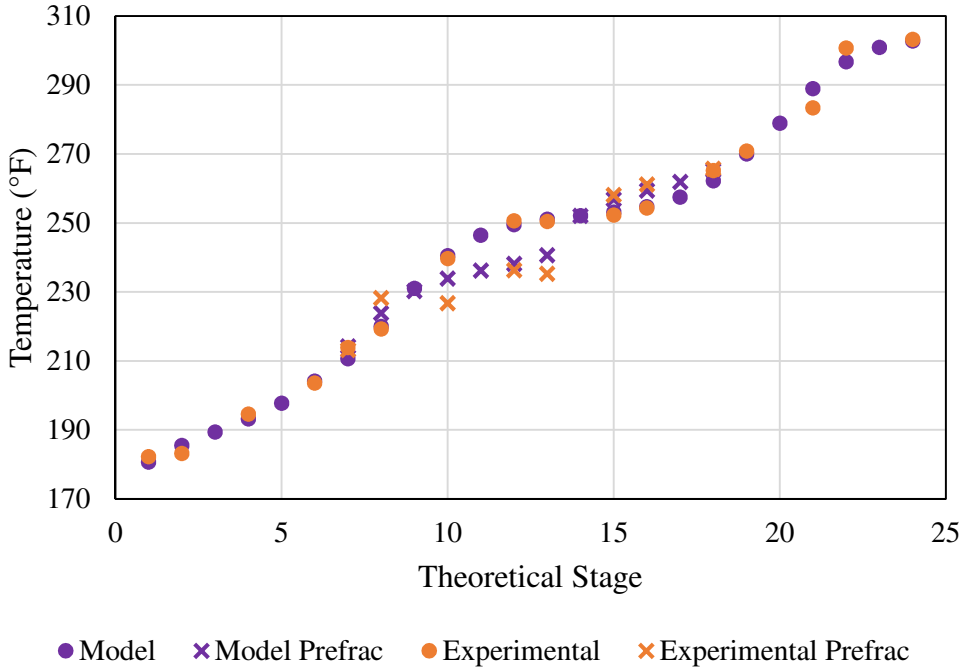

Figure D-1 – Comparison of model and experimental temperature profile at start of disturance

Glossary

2MP = 2-methylpentane

A = area for heat transfer [ft^2]

B = bottoms flowrate [lbm/hr]

C6 = cyclohexane

D = distillate flowrate [lbm/hr]

DCS = distributed control system

DWC = dividing wall column

F = feed flowrate [lbm/hr]

FID = flame ionization detector

GC = gas chromatogram

HETP = height equivalent to theoretical plate [in]

MV = manipulated variable

mX = m-Xylene

NRTL = non-random two-liquid activity coefficient model

PCHIP = piecewise cubic hermite interpolating polynomial

PV = present value of controlled variable or process variable

Q = heat flow ($UA\Delta T$) [BTU/hr]

Q_R = reboiler duty [KBTU/hr]

RGA = relative gain array

RTD = resistance temperature detector

S = side product flowrate [lb/hr]

SHERPA = Simultaneous Hybrid Exploration Robust Progressive Adaptive

SP = setpoint

SVD = Singular Value Decomposition

TMX = temperature multiplexer

Tol = toluene

$U_{i,ATM}$ = atmospheric heat transfer coefficient [BTU/(hrft^2°F)]

U_{WALL} = wall heat transfer coefficient [BTU/(hrft^2°F)]

VLE = vapor-liquid equilibrium

$x_{B,i}$ = mass fraction of component i in the bottoms product

$x_{D,i}$ = mass fraction of component i in the distillate product

$x_{F,i}$ = mass fraction of component i in the feed

$x_{S,i}$ = mass fraction of component i in the side product

Greek Letters

α = relative volatility

ΔT = temperature difference [°F]

Bibliography

(1) Buck, C.; Hiller, C.; Fieg, G. Applying Model Predictive Control to Dividing Wall Columns. *Chem. Eng. Technol.* **2010**, *34* (5), 663–672.

(2) Blevins, T.; Downs, J. J.; Donahue, M. M.; Roach, B. J. Use Model Predictive Control to Achieve Real-Time Management of a DWC. *Hydrocarb. Process.* **2015**.

(3) Rewagad, R.; Kiss, A. Dynamic Optimization of a Dividing-Wall Column Using Model Predictive Control. *Chem. Eng. Sci.* **2012**, *68*, 132–142.

(4) Kumar Dohare, R.; Singh, K.; Kumar, R. Modeling and Model Predictive Control of Dividing Wall Column for Separation of Benzene-Toluene-O-Xylene. *Syst. Sci. Control Eng. Open Access J.* **2015**, *3*, 142–153.

(5) Luyben, W. L. *Practical Distillation Control*; Van Nostrand Reinhold: New York, 1992.

(6) Smith, C. L. *Distillation Control: An Engineering Perspective*; John Wiley & Sons, Inc., 2012.

(7) Skogestad, S. The Dos and Don'ts of Distillation Column Control. *Chem. Eng. Res. Des.* **2007**, *85* (1), 13–23.

(8) Diggelen, R.; Kiss, A.; Heemink, A. Comparison of Control Strategies for Dividing-Wall Columns. *Ind. Eng. Chem. Res.* **2010**, *49*, 288–307.

(9) Luyben, W. Evaluation of Criteria for Selecting Temperature Control Trays in Disillation Columns. *J. Process Control* **2006**, *16*, 115–134.

(10) Lestak, F.; Smith, R.; Dhole, V. Heat Transfer Across The Wall of Dividing Wall Columns. *Trans IchemE* **1994**, *72* (A), 639–644.

(11) Ognisty, T. P.; Manley, D. B. Partitioned Distillation Column. 5709780A, 1998.

(12) Steacy, P. C. Dividing Wall Column Fractionation Tray. US6645350B1, 2003.

(13) Kaibel, G.; Pfeffinger, J.; Stroezel, M. Distillation Column for Separating Liquid Mixtures in Multiple Pure Fractions. EP0640367B1.

(14) Dejanovic, I.; Matijasevic, L.; Halvorsen, I. J.; Skogestad, S.; Jansen, H.; Kaibel, B.; Olujic, Z. Designing Four-Product Dividing Wall Columns for Separation of a Multicomponent Aromatics Mixture. *Chem. Eng. Res. Des.* **2011**, *89*, 1155–1167.

(15) Dwivedi, D.; Halvorsen, I. J.; Skogestad, S. Control Structure Selection for Four-Product Petlyuk Column. *chem. Eng. Process.* **2013**, *67*, 49–59.

(16) Madenoor Ramapriya, G.; Tawarmalani, M.; Agrawal, R. Thermal Coupling Links to Liquid-Only Transfer Streams: A Path for New Dividing Wall Columns. *AIChE J.* **2014**, *60* (8), 2949–2961.

(17) Halvorsen, I. J.; Skogestad, S. Optimal Operation of Petlyuk Distillation: Steady-State Behavior. *J. Process Control* **1999**, *9*, 407–424.

(18) Isopescu, R.; Woinaroschy, A.; Draghicu, L. Energy Reduction in Divided Wall Distillation Column. *REV. CHIM. (Bucure^{o}ti)* **2008**, *59* (7), 812–815.

(19) Brugma, A. J. Process and Device for Fractional Distillation of Liquid Mixtures, More Particularly Petroleum. US 2295256, 1942.

(20) Petlyuk, F. B.; Platonov, V. M.; Slavinskii, D. M. Thermodynamically Optimal Method for Separating Multicomponent Mixtures. *Int. Chem. Eng.* **1965**, *5* (3), 555–561.

(21) Petlyuk, F. B.; Platonov, V. M. Thermodynamically Reversible Multicomponent Distillation. *Khimicheskaya Promyshlennost* **1964**, *10*, 723.

(22) Petlyuk, F. B.; Platonov, V. M.; Avetlyan, V. S. Optimum Arrangements in the Fractionating Distillation of Multicomponent Mixtures. *Khimicheskaya Promyshlennost* **1966**, *42* (11), 865.
(23) Wright, R. O. Fractionation Apparatus. US2471134 A, May 24, 1949.
(24) Glinos, K.; Malone, F. Optimality Regions for Complex Column Alternative in Distillation Systems. *Chem. Eng. Res. Des.* **1988**, *66*.
(25) Triantafyllou, C.; Smith, R. The Design and Optimisation of Fully Thermally Coupled Distillation Columns. *Trans IchemE* **1992**, *70*, 118–132.
(26) Kiss, A.; Bildea, C. A Control Perspective on Process Intensification in Dividing-Wall Columns. *Chem. Eng. Process.* **2011**, *50*, 281–292.
(27) Parkinson, G. Dividing-Wall Columns Find Greater Appeal. *Chem. Eng. Prog.* **2007**, *103* (5), 8–11.
(28) Slade, B.; Stober, B.; Simpson, D. Dividing Wall Column Revamp Optimises Mixed Xylenes Production.
(29) Kiss, A. A.; Suszwalak, D. J.-P. C. Enhanced Bioethanol Dehydration by Extractive and Azeotropic Distillation in Dividing-Wall Columns. *Sep. Purif. Technol.* **2012**, *86*, 70–78.
(30) Bravo-Bravo, C.; Segovia-Hernandez, J. G.; Gutierrez-Antonio, C.; Duran, A. L.; Bonilla-Petriciolet, A.; Briones-Ramirez, A. Extractive Dividing Wall Column: Design and Optimization. *Ind. Eng. Chem. Res.* **2010**, *49*, 3672–3688.
(31) Kiss, A. A.; Nagy, Z. K.; Klein, R.; Findeisen, R. Advanced Control of a Reactive Distillation Column; Elsevier: Bucharest, Romania, 2007.
(32) Ignat, R.; Woinaroschy, A. Dynamic Analysis and Controllability of Dividing-Wall Distillation Columns. *Chem. Eng. Trans.* **2011**, *25*, 647–652.
(33) Sander, S.; Flisch, C.; Geissler, E.; Schoenmakers, H.; Ryll, O.; Hasse, H. Methyl Acetate Hydrolysis in a Reactive Divided Wall Column. *Trans IChemE* **2007**, *85* (A), 149–154.
(34) Mueller, I.; Kenig, E. Y. Reactive Distillation in a Dividing Wall Column: Rate-Based Modeling and Simulation. *Ind. Eng. Chem. Res.* **2007**, *46* (11), 3709–3719.
(35) Halvorsen, I. J.; Dejanovic, I.; Skogestad, S.; Olujic, Z. Internal Configurations for a Multi-Product Dividing Wall Column. *Chem. Eng. Res. Des.* **2013**, *91*, 1954–1965.
(36) Ghadrdan, M.; Halvorsen, I. J.; Skogestad, S. Composition Estimation in Dividing-Wall Columns Using Temperature Measurements. In *James R. Fair Heritage Distillation Conference*; Chicago, Illinois, 2011.
(37) Hernandez, S.; Gudino-Mares, I. R.; Cardenas, J. C.; Segovia-Hernandez, J. G.; Rico-Ramirez, V. A Short Note on Control Structures for Thermally Coupled Distillation Sequences for Four-Component Mixtures. *Ind. Eng. Chem. Res.* **2005**, *44*, 5857–5863.
(38) Baldea, M. From Process Integration to Process Intensification. *Comput. Chem. Eng.* **2015**, *81*, 104–114.
(39) Ehlers, C.; Schröder, M.; Fieg, G. Influence of Heat Transfer Across the Wall of Dividing Wall Columns on Energy Demand. *AIChE J.* **2015**, 1648–1662.
(40) Roach, B. J. A Design Model for Dividing Wall Distillation Columns. PhD Dissertation, The University of Texas at Austin, 2017.
(41) Suphanit, B.; Bischert, A.; Narataruksa, P. Exergy Loss Analysis of Heat Transfer across the Wall of the Dividing-Wall Distillation Column. *Energy* **2007**, *32*, 2121–2134.

(42) Kaibel, G. Distillation Columns with Vertical Partitions. *Chem. Eng. Technol.* **1987**, *10* (1), 92–98.
(43) Niggemann, G.; Fieg, G. Validation of Dividing-Wall Columns Based on Experimental Data and Dynamic Simulations: Pilot-Plant and Production-Scale Columns. *Ind. Eng. Chem. Res.* **2012**, *51* (2), 931–943.
(44) Jing, F.; Yuqi, H.; Chunli, L. Energy-Saving Mechanism in Heat Transfer Optimization of Dividing Wall Column. *Ind. Eng. Chem. Res.* **2013**, *52* (51), 18345–18355.
(45) Dwivedi, D.; Strandberg, J. P.; Halvorsen, I. J.; Preisig, H. A.; Skogestad, S. Active Vapor Split Control for Dividing-Wall Columns. *Ind. Eng. Chem. Res.* **2012**, *51* (46), 15176–15183.
(46) Buck, C.; Hiller, C.; Fieg, G. Decentralized Temperature Control of a Pilot Dividing Wall Column. *Chem. Eng. Process.* **2011**, *50*, 167–180.
(47) Kaibel, G. *European Roadmap of Process Intensification: Heat-Integrated Distillation*; Technology Report 2.1.4; Creatieve Energie; pp 1–13.
(48) Halvorsen, I. J. Minimum Energy Requirements in Complex Distillation Arrangements. Dr.Ing., Norwegian University of Science and Technology: Trondheim, Norway, 2001.
(49) Fidkowski, Z.; Krolikowski, L. Minimum Energy Requirements of Thermally Coupled Distillation Systems. *AIChE J.* **1987**, *33* (4), 643–653.
(50) Agrawal, R.; Fidkowski, Z. Are Thermally Coupled Distillation Columns Always Thermodynamically More Efficient for Ternary Distillations. *Ind. Chem. Eng. Res.* **1998**, *37*, 3444–3454.
(51) King, C. J. Separation Processes. In *McGraw-Hill Chemical Engineering Book Series*; McGraw-Hill Book Company.
(52) Christiansen, A. C.; Skogestad, S. Energy Savings in Complex Distillation Arrangements: Importance of Using the Preferred Separation; Los Angeles, 1997.
(53) Chavez C., R.; Seader, J. D.; Wayburn, T. L. Multiple Steady-State Solutions for Interlinked Separation Systems. *Ind. Eng. Chem. Fundam.* **1986**, *25*, 566–576.
(54) Wolff, E.; Skogestad, S. Operation of Integrated Three-Product (Petlyuk) Distillation Columns. *Ind. Eng. Chem. Res.* **1995**, *34*, 2094–2103.
(55) Stupin, W. J. The Separation of Multicomponent Mixtures in Thermally-Coupled Distillation Systems. PhD Dissertation, University of Southern California, 1970.
(56) Cerda, J.; Westerberg, A. W. Shortcut Methods for Complex Distillation Columns. 1. Minimum Reflux. *Ind. Eng. Chem. Process Des. Dev.* **1981**, *20*, 546–557.
(57) Nikolaides, I. P.; Malone, M. F. Approximate Design and Optimization of a Thermally Coupled Distillation with Prefractionation. *Ind. Eng. Chem. Res.* **1988**, *27*, 811–818.
(58) Fidkowski, Z.; Krolikowski, L. Thermally Coupled System of Distillation Columns: Optimization Procedure. *AIChE J.* **1986**, *32* (4), 537–546.
(59) Carlberg, N. A.; Westerberg, A. W. Temperature-Heat Diagrams for Complex Columns. 3. Underwood's Method for the Petlyuk Configuration. *Ind. Eng. Chem. Res.* **1989**, *28* (9), 1386–1397.
(60) Stichlmair, J. Distillation and Rectification. In *Ullmann's Encyclopedia of Industrial Chemistry*; 1988; Vol. B3, pp 4-31-4–63.

(61) Ling, H.; Luyben, W. New Control Structure for Divided-Wall Columns. *Ind. Chem. Eng. Res.* **2009**, *48*, 6034–6049.
(62) ling, H.; Luyben, W. Temperature Control of the BTX Divided-Wall Column. *Ind. Eng. Chem. Res.* **2010**, *49*, 189–203.
(63) Alstad, V.; Skogestad, S. Null Space Method for Selecting Optimal Measurement Combinations as Controlled Variables. *Ind. Eng. Chem. Res.* **2007**, No. 46, 846–853.
(64) Alstad, V. Studies on Selection of Controlled Variables, Norwegian University of Science and Technology, 2005.
(65) Kiss, A.; Rewagad, R. Energy Efficient Control of a BTX Dividing-Wall Column. *Comput. Chem. Eng.* **2011**, *35* (12), 2896–2904.
(66) Koko, I. O. M.; Barakat, T. A. M. Modelling and Control Analysis Of Dividing Wall Distillation Columns (DWC); University of Khartoum: Friendship Hall Khartoum, 2012; Vol. 1, pp 60–68.
(67) Mutalib, M. I. A.; Zeglam, A. O.; Smith, R. Operation and Control of Dividing Wall Distillation Columns: Part 2: Simulation and Pilot Plant Studies Using Temperature Control. *Chem. Eng. Res. Des.* **1998**, *76* (3), 319–334.
(68) Adrian, T.; Schoenmakers, H.; Boll, M. Model Predictive Control of Integrated Unit Operations: Control of a Divided Wall Column. *Chem. Eng. Process. Process Intensif.* **2004**, *43* (3), 347–355.
(69) Qian, X.; Skogestad, S.; Yuan, X. Comparison of Stabilizing Control Structures for Dividing Wall Columns; Trondheim, Norway, 2016; pp 729–734.
(70) Dwivedi, D.; Halvorsen, I. J.; Skogestad, S. Control Structure Selection for Three-Product Petlyuk (Dividing-Wall) Column. *Chem. Eng. Process. Process Intensif.* **2013**, *64*, 57–67.
(71) Kim, K.; Lee, M.; Park, S. Two-Point Temperature Control Structure Selection for Dividing-Wall Distillation Columns. *Ind. Eng. Chem. Res.* **2012**, *51* (48), 15683–15695.
(72) Niggemann, G.; Hiller, C.; Fieg, G. Experimental and Theoretical Studies of a Dividing-Wall Column Used for the Recovery of High-Purity Products. *Ind. Eng. Chem. Res.* **2010**, *49* (14), 6566–6577.
(73) Mutalib, M. I. A. Operation and Control of the Dividing Wall Column. Doctor of Philosophy, University of Manchester Institute of Science & Technology: Manchester, United Kingdom, 1995.
(74) Serra, M.; Espuna, A.; Puigjaner, L. Control and Optimization of the Divided Wall Column. *Chem. Eng. Process.* **1999**, *38*, 549–562.
(75) Skogestad, S.; Morari, M. Control Configuration Selection for Distillation Columns. *AIchE J.* **1987**, *33* (10), 1620–1635.
(76) Skogestad, S. Dynamics and Control of Distillation Columns: A Tutorial Introduction. *Trans IChemE* **1997**, *75*, 539–562.
(77) Skogestad, S.; Lundstrom, P.; Jacobson, E. W. Selecting the Best Distillation Control Configuration. *AIChE J.* **1990**, *36* (5), 753–764.
(78) Skogestad, S. Dynamics and Control of Distillation Columns - a Critical Survey. *Model. Identif. Control* **1997**, *18* (3), 177–217.
(79) Yi, C. K.; Luyben, W. L. Evaluation of Plant-Wide Control Structures by Steady-State Disturbance Sensitivity Analysis. *Ind. Eng. Chem. Res.* **1995**, *34*, 2393–2405.

(80) Lawson, C. L.; Hanson, R. J. *Solving Least Squares Problems*; Prentice Hall: Englewood Cliffs, New Jersey, 1974.
(81) Noble, B.; Daniel, J. W. *Applied Linear Algebra*; Prentice Hall: Englewood Cliffs, New Jersey, 1977.
(82) Stewart, G. W. *Introduction to Matrix Computations*; Academic Press: New York, New York, 1973.
(83) Moore, C. Application of Singular Value Decomposition to the Design, Analysis, and Control of Industrial Processes. *Am. Control Conf.* **1986**, 643–650.
(84) Seborg, D. E.; Edgar, T. F.; Mellichamp, D. A.; Doyle III, F. J. Chapter 18: Multiloop and Multivariable Control. In *Process Dynamics and Control*; John Wiley & Sons, Inc., 2011; pp 347–353.
(85) Crowe, C. M. Data Reconciliation - Progress and Challenges. *J. Process Control* **1996**, *6* (2/3), 89–98.
(86) Narasimhan, S.; Jordache, C. *Data Reconciliation and Gross Error Detection: An Intelligent Use of Process Data*, 1st ed.; Elsevier, 1999.
(87) Blevins, T.; McMillan, G. K.; Wojsznis, W. K.; Brown, M. W. *Advanced Control Unleashed: Plant Performance Management for Optimum Benefit*; The Instrumentation, Systems, and Automation Society, 2003.
(88) Luyben. *Distillation Design and Control Using Aspen Simulation*.
(89) Chu, K.-T.; Cadoret, L.; Yu, C.-C.; Ward, J. D. A New Shortcut Design Method and Economic Analysis of Divided Wall Columns. *Ind. Eng. Chem. Res.* **2011**, *50* (15), 9221–9235.
(90) Stichlmair, J.; Bravo, J. L.; Fair, J. R. General Model for Prediction of Pressure Drop and Capacity of Countercurre Nt Gas/liquid Packed Columns. *Gas Sep. Prufication* **1989**, *3* (1), 19–28.
(91) McNair, H. M.; Miller, J. M. *Basic Gas Chromatography*, 2nd ed.; 2009.

Vita

Melissa Mary Donahue grew up in Hingham, Massachusetts. She graduated from Hingham High School in 2010 as class valedictorian. She attended the University of Massachusetts Amherst as a Commonwealth College honors student and received the Jack Welch scholarship. While in college, Melissa competed on the varsity rowing team, researched polymer membranes for fuel cell applications, and served multiple positions in Tau Beta Pi. She graduated with a B.S. in chemical engineering summa cum laude in 2014. After college, Melissa entered graduate school at The University of Texas at Austin.

Permanent email: mdonahue@utexas.edu

This dissertation was typed by Melissa Mary Donahue.